Metal borohydrides and derivatives

- synthesis, structure and properties -

Mark Paskevicius,[a] Lars H. Jepsen,[a] Pascal Schouwink,[b] Radovan Černý,[b]

Dorthe B. Ravnsbæk,[c] Yaroslav Filinchuk,[d] Martin Dornheim,[e]

Flemming Besenbacher,[f] Torben R. Jensen[a] *

[a] Center for Materials Crystallography, Interdisciplinary Nanoscience Center (iNANO), and Department of Chemistry, Aarhus University, Langelandsgade 140, DK-8000 Aarhus C, Denmark

[b] Laboratory of Crystallography, DQMP, University of Geneva, 1211 Geneva, Switzerland

[c] Department of Physics, Chemistry and Pharmacy, University of Southern Denmark, Campusvej 55, 5230 Odense M, Denmark

[d] Institute of Condensed Matter and Nanosciences, Université catholique de Louvain, Place L. Pasteur 1, B-1348 Louvain-la-Neuve, Belgium

[e] Helmholtz-Zentrum Geesthacht, Department of Nanotechnology, Max-Planck-Straße 1, 21502 Geesthacht, Germany

[f] Interdisciplinary Nanoscience Center (iNANO) and Department of Physics and Astronomy, DK-8000 Aarhus C, Denmark

* Corresponding author: trj@chem.au.dk

Contents

Abstract

1. Introduction

2. Synthesis of metal borohydrides and derivatives

    2.1 Solvent-based synthesis of monometallic borohydrides

    2.2 Trends in the mechanochemical synthesis of metal borohydrides

    2.3 Trends in the mechanochemical synthesis of metal borohydride-halides

    2.4 Mechanochemical reactions, general considerations

    2.5 Mechanical synthesis in different gas atmosphere

    2.6 Single crystal growth of metal borohydrides

    2.7 Synthesis of metal borohydrides with neutral molecules

3. Trends in structural chemistry of metal borohydrides

    3.1 Monometallic borohydrides, the *s*-block – pronounced ionic bonding

    3.2 Monometallic borohydrides with the *d*- and *f*-block

    3.3 Strongly covalent molecular monometallic borohydrides

    3.4 Bimetallic *s*-block borohydrides

    3.5 Bimetallic *d*- and *f*-block borohydrides

    3.6 Bimetallic *p*-block borohydrides

    3.7 Tri-metallic borohydrides

    3.8 General trends in the structural chemistry of metal borohydrides

    3.9 Comparisons between metal borohydrides and metal oxides

4. Structure of anion substituted metal borohydrides

    4.1 Metal borohydride halides - fully ordered structures

    4.2 Metal borohydride halides - partly ordered structures

    4.3 Metal borohydride halides - fully disordered structures

    4.4 Metal borohydride halides forming solid solutions

    4.5 General trends for halide substitution in metal borohydrides

    4.6 Trends in series of bimetallic borohydride halides

    4.7 Metal borohydride closo-boranes

4.8 Metal borohydride amides

5. Derivatives of metal borohydrides with neutral molecules

5.1 Ammine metal borohydrides

5.2 Hydrazine metal borohydride complexes

5.3 Ammonia borane metal borohydride complexes

5.4 Metal borohydride crystallizing with organic solvents

6. Thermal properties of metal borohydrides

6.1 Thermodynamics of hydrogen release and uptake

6.2 Thermolysis of monometallic borohydrides

6.3 Thermolysis of bi- and trimetallic borohydrides

6.4 Eutectic melting of bi- and trimetallic borohydrides

6.5 Trends in thermal decomposition for metal borohydrides

6.6 The released gas from metal borohydrides, stability of diborane

6.7 Additives to improve reaction kinetics

6.8 Reactive Hydride Composites

6.9 Hydrolysis – decomposition by reaction with water

6.10 Nanoconfinement

7. New properties and future perspectives of metal borohydrides

7.1 Porous metal borohydrides for gas adsorption

7.2 Metal borohydrides as ion conductors

7.3 Metal borohydrides with optical properties

7.4 Metal borohydrides with magnetic properties

7.5 Perspectives for design of novel metal borohydrides

7.6 CO_2-recyling with metal borohydrides

7.7 A possible paradigm shift for solid state hydrogen storage

8. Conclusions

9. Acknowledgements

10. References

Chem Soc Rev

REVIEW ARTICLE



Cite this: *Chem. Soc. Rev.*, 2017, **46**, 1565

Metal borohydrides and derivatives – synthesis, structure and properties

Mark Paskevicius,[a] Lars H. Jepsen,[a] Pascal Schouwink,[b] Radovan Černý,[b] Dorthe B. Ravnsbæk,[c] Yaroslav Filinchuk,[d] Martin Dornheim,[e] Flemming Besenbacher[f] and Torben R. Jensen*[a]

A wide variety of metal borohydrides, MBH_4, have been discovered and characterized during the past decade, revealing an extremely rich chemistry including fascinating structural flexibility and a wide range of compositions and physical properties. Metal borohydrides receive increasing interest within the energy storage field due to their extremely high hydrogen density and possible uses in batteries as solid state ion conductors. Recently, new types of physical properties have been explored in lanthanide-bearing borohydrides related to solid state phosphors and magnetic refrigeration. Two major classes of metal borohydride derivatives have also been discovered: anion-substituted compounds where the complex borohydride anion, BH_4^-, is replaced by another anion, *i.e.* a halide or amide ion; and metal borohydrides modified with neutral molecules, such as NH_3, NH_3BH_3, N_2H_4, *etc.* Here, we review new synthetic strategies along with structural, physical and chemical properties for metal borohydrides, revealing a number of new trends correlating composition, structure, bonding and thermal properties. These new trends provide general knowledge and may contribute to the design and discovery of new metal borohydrides with tailored properties towards the rational design of novel functional materials. This review also demonstrates that there is still room for discovering new combinations of light elements including boron and hydrogen, leading to complex hydrides with extreme flexibility in composition, structure and properties.

Received 27th September 2016

DOI: 10.1039/c6cs00705h

rsc.li/chem-soc-rev

1. Introduction

A wide variety of metal borohydrides have been discovered and characterized during the past few years, revealing an extremely rich chemistry, including fascinating structural flexibility and a wide variety of physical properties to be explored for possible future applications.[1–7] Hydrogen and boron form a variety of molecular compounds, boranes (B_nH_m), which were intensely researched in the 1950's as high energy rocket fuels. Since then, boranes have received significant academic interest, but metal borohydrides appear to have a larger potential for a variety of future applications due to their lower toxicity, lower volatility, and high hydrogen content. Thus, the focus of this review is on the compounds where boron and hydrogen form a negatively charged BH_4^- anion, counterbalanced by metal cations. The boron–hydrogen bond in the complex anion, *e.g.* BH_4^-, is covalent, whereas the coordination to metals in the solid state is more diverse, ranging from ionic to more covalent with well-defined directionality.[8] Two major classes of metal borohydride derivatives have recently been discovered. The first class includes mixed-anion compounds, where the complex anion BH_4^- is substituted by a halide anion or combined with a less similar anion such as an amide or borate.[9–11] The second class includes metal borohydrides coordinated to neutral H-rich molecules, such as NH_3, NH_3BH_3, N_2H_4, *etc.*[6] This review focuses on new trends correlating composition, structure and properties of series of compounds, aiming to provide general knowledge, which contributes to the rational design and discovery of new metal borohydrides and derivatives with tailored properties.

The first homoleptic metal borohydrides $Al(BH_4)_3$, $Be(BH_4)_2$ and $LiBH_4$ were discovered by Schlesinger, Brown and Burg and reported in 1940.[12–14] Schlesinger and Brown discovered uranium borohydride, $U(BH_4)_4$, while working on the Manhattan project during World War II after being assigned with the task of finding volatile uranium compounds for use in the diffusion separation of uranium isotopes.[15] $U(BH_4)_4$ was found to be one of the most

[a] *Center for Materials Crystallography, Interdisciplinary Nanoscience Center (iNANO), and Department of Chemistry, Aarhus University, Langelandsgade 140, DK-8000 Aarhus C, Denmark. E-mail: trj@chem.au.dk*
[b] *Laboratory of Crystallography, DQMP, University of Geneva, 1211 Geneva, Switzerland*
[c] *Department of Physics, Chemistry and Pharmacy, University of Southern Denmark, Campusvej 55, 5230 Odense M, Denmark*
[d] *Institute of Condensed Matter and Nanosciences, Université catholique de Louvain, Place L. Pasteur 1, B-1348 Louvain-la-Neuve, Belgium*
[e] *Helmholtz-Zentrum Geesthacht, Department of Nanotechnology, Max-Planck-Straße 1, 21502 Geesthacht, Germany*
[f] *Interdisciplinary Nanoscience Center (iNANO) and Department of Physics and Astronomy, DK-8000 Aarhus C, Denmark*

volatile uranium compounds known, second only to uranium hexafluoride. Another compound of great importance, $NaBH_4$, was prepared for the first time by Brown and co-workers, during their research for the US Department of Defense, however, their work remained "classified" until 1953.[16] The first application of a metal borohydride as a 'hydrogen carrier' dates back to World War II, when the hydrolysis of a $NaBH_4$ suspension was used for solid state storage of hydrogen for weather balloons. Later, in 1979, Herbert C. Brown was awarded the Nobel Prize in chemistry for his development of boron containing compounds as reducing reagents in organic synthesis, which today still remains the most important use of metal borohydrides. Over the decades many synthesis methods and new compounds have been reported, as borohydrides have constantly remained of interest in organic chemistry.[17] Sodium borohydride was the first member to be structurally investigated in 1947, followed by K, Rb and Cs borohydrides in 1954.[18,19] Titanium borohydride, $Ti(BH_4)_3$, the first genuine transition metal borohydride, was characterized in the gas phase by Dain *et al.* in 1991,[20] while the first full structural characterization of a transition metal borohydride in the solid state, $Mn(BH_4)_2$, was presented in 2009.[21]

During the past decade, metal borohydrides have received significant interest as hydrogen storage materials initiated by investigations of $LiBH_4$.[22–26] Renewable energy sources have been highly sought after due to the ever increasing human energy consumption and made urgent by an increasing awareness of possible climatic changes and healthcare problems associated with the combustion of extreme amounts of fossil fuels.[27,28] Unfortunately, renewable energy is unevenly distributed both over time and geographically, therefore it must be stored in an efficient way.[29] Renewable electricity may be stored directly in lithium based batteries or converted to hydrogen by electrolysis.[30,31] Hydrogen has the highest gravimetric energy content for any known compound, but is a gas at ambient conditions and is therefore



Mark Paskevicius

Mark Paskevicius is a Senior Lecturer in the Fuels and Energy Technology Institute at Curtin University in Australia. He began this position in 2017 after a 3 year research fellowship at Aarhus University in Denmark. His research is focussed on renewable energy storage. He is dedicated to developing new materials for solid-state hydrogen storage to store energy for automotive, stationary and concentrated solar thermal applications. He is also leading research into new solid-state ion conductors for battery applications, focussing on boron-rich materials.



Lars H. Jepsen

Lars H. Jepsen obtained his PhD in chemistry and nanoscience from Aarhus University in 2015 under the supervision of Prof. Torben R. Jensen. Lars' research was focused on synthesis and characterization of boron and nitrogen based complex metal hydrides, including crystal structure determination by combining powder X-ray diffraction, DFT calculations and solid-state NMR spectroscopy. Today Lars works as consultant at the Danish Technological Institute with the aim of supporting Danish and international companies with forefront knowledge and development within materials chemistry.



Pascal Schouwink

Pascal Schouwink obtained his PhD in 2014 at the Laboratory of Crystallography of the Department of Condensed Matter Physics of the University of Geneva, where he explored the functional aspects of complex hydrides using diffraction and different spectroscopies. Following a post doc centered around solid state ionic conductors he joined the École polytechnique fédérale de Lausanne (EPFL) in 2016, where he is responsible for the X-ray diffraction facility of ISIC. His interests concentrate on in situ studies of energy materials using both X-ray and neutron scattering, in particular on polycrystalline materials and thin films.



Radovan Černý

Radovan Černý did his PhD in Solid State Physics at the Charles University, Prague. In 1989 he came to the University of Geneva for a postdoctoral research, and was appointed Lecturer in 1995 and Associated Prof. in 2012. He is interested in the development of powder diffraction methodology, especially ab initio structure solution (computer program Fox), studies of structural defects and structural chemistry of inorganic compounds especially of metal hydrides where his group solved more than 120 crystal structures. Recently he turned his interest in the applied research on complex hydrides from hydrogen storage to solid electrolytes.

This journal is © The Royal Society of Chemistry 2017

difficult to store in an efficient and compact way. This is a fundamental problem associated with the utilization of hydrogen as an energy carrier,[32] which may be solved by the design of novel light weight metal hydrides, such as metal borohydrides.[32–35] Research over the past decade has revealed a range of new light metal borohydrides possessing extremely high hydrogen densities, which may be considered for possible energy storage applications. However, in general, these compounds suffer from poor thermodynamic and kinetic properties, *i.e.* they are often too thermally stable and the hydrogen release and uptake reactions are too slow for practical applications.[5,6,36]

A new approach is to allow multiple hydrides, denoted as reactive hydride composites (RHC), to react during the release of hydrogen to form a different dehydrogenated state. These composites change the hydrogen release pathway and may improve the thermodynamic and kinetic properties, enabling hydrogen release and uptake under more favourable conditions.[37–42] The concept aims to lower the overall reaction enthalpy by introducing extra (endothermic) chemical reaction(s), *i.e.* by utilizing the well-known Hess law from chemistry, also denoted as Medima principles.[43,44]

Composites of two or more metal borohydrides often induce co-melting or eutectic melting.[45] Low temperature melting may reduce the hydrogen release temperature, as observed for $x\mathrm{LiBH_4}$–$(1-x)\mathrm{Mg(BH_4)_2}$, or for preparation of molten metal borohydrides systems for convenient nanoconfinement, *e.g.* in the $0.725\mathrm{LiBH_4}$–$0.275\mathrm{KBH_4}$ with T_m = 105 °C.[46–48] Metal borohydrides with low melting points could allow for fast and convenient re-fuelling of vehicles with similar technology to that known today for liquid fossil fuels.

Metal borohydrides are a multifunctional class of materials that may also be used as fast ion conductors for new types of batteries or for gas adsorption.[3,49] They may also have optical, electronic and magnetic properties and can be used as reducing agents in organic synthetic chemistry.[1,2,17,50] For this reason, mono-, bi- and trimetallic borohydrides have been exposed to intense research efforts to develop new synthesis strategies, perform structural characterization, and investigate physical and chemical properties. In the following, we critically review the progress of metal borohydrides and their derivatives, which may form the basis of future technological applications. The focus of this review is to discover new trends in synthesis, structure and properties and provide perspectives for further research that may act as inspiration for the development of novel materials towards rational materials design.

2. Synthesis of metal borohydrides and derivatives

A number of different synthetic approaches have been developed to prepare new types of metal borohydrides, including anion substitution and the preparation of derivatives including neutral molecules, such as ammonia, hydrazine *etc.* A range of different chemical reactions can be undertaken in different media; and of those, metathesis, *i.e.* double substitution reactions, and addition reactions are the most common. In some cases, more complex or competing reactions are observed. Halide- and solvent-free mono-metallic borohydrides can be obtained using solvent based methods,[51] mechanochemical methods successfully provide numerous bi- and tri-metallic borohydrides,[52] whereas solid–gas reactions are important for the preparation of ammine metal borohydrides.[53,54] Typically, air and moisture sensitive reagents are utilized, which need to be manipulated in a glove box or using standard vacuum and Schlenk techniques in dry and inert atmosphere. In general, metal borohydrides, anhydrous metal halides and many solvents are hygroscopic and readily adsorb water. The hydrates of metal borohydrides containing metals with low electronegativity are often stable at RT but react with water at elevated temperatures and evolve hydrogen. Metal borohydrides of



Dorthe B. Ravnsbæk

Dorthe B. Ravnsbæk is Associate Professor at Department of Physics, Chemistry and Pharmacy at University of Southern Denmark. Her research focuses on synthesis and structure–property relations in novel materials for energy storage – especially rechargeable batteries. She obtained her PhD in Nanotechnology from Aarhus University in 2011 based on her research in synthesis and characterization of multiple novel metal borohydrides. Before joining University of Southern Denmark she spent two years as post doc at Massachusetts Institute of Technology (MIT) specializing in studies of electrode materials for Li-ion batteries especially with focus on operando diffraction studies of battery materials.



Torben R. Jensen

Torben R. Jensen is Professor at Department of Chemistry and iNANO, The Interdisciplinary Nanoscience center at Aarhus University. His research interests focus on synthesis, structural, physical and chemical properties of new inorganic materials and utilisation of synchrotron X-ray radiation for materials characterization. He has published 215 research papers (>5400 citations). Torben received his PhD degree (1999) in materials chemistry at University of Southern Denmark, Odense, and a Doctor of Science degree (DSc in 2014) at Aarhus University. He was awarded a Steno research stipend (2002), a Carlsberg research stipend (2005) by the Carlsberg Foundation and the Science of Hydrogen & Energy prize 2016.

metals with higher electronegativity may adsorb water and react exothermically at RT, releasing hydrogen. Alkali metal borohydrides are stable in basic aqueous solution and *closo*-boranes are stable in neutral and acidic solutions. This section reveals general trends in chemical reactions for the synthesis of different metal borohydrides and their derivatives under different physical conditions. Hydrogen release and uptake reactions in metal borohydrides and synthesis of some of those from the elements are discussed in Section 6.

2.1 Solvent-based synthesis of monometallic borohydrides

The first successful solvent-based synthesis of a metal borohydride was accomplished by Wiberg and Bauer in 1950 by a reaction between diethylmagnesium, $Mg(CH_2CH_3)_2$, and diborane, B_2H_6, in ether.[55] Since diborane is challenging to handle, *i.e.* poisonous, self-igniting and explodes in contact with air or moisture, a borane complex such as triethylamine borane, $(C_2H_5)_3NBH_3$ or dimethylsulfide borane, $(CH_3)_2SBH_3$, is safer and easier to handle. Solvent mediated addition reactions take place between a borane donor and a metal hydride or a metal alkyl compound. The obtained product is commonly a solvate that needs further treatment in order to produce a solvent-free product.[56,57] This approach has provided the first open-structured metal borohydrides, γ-$M(BH_4)_2$, M = Mg or Mn.[3,58] $Ca(BH_4)_2$ can be synthesized in a similar manner from triethylamine borane and CaH_2.[59] Thus, the electron deficient molecule BH_3 can be considered a Lewis acid, which reacts with the Lewis base H^-. Therefore, the reaction is only possible if an ionic or polar covalent metal hydride can be utilised as a reactant.

Metal borohydrides are also often synthesized *via* a quantitative metathesis reaction, illustrated by the preparation of $Al(BH_4)_3$ from aluminum trichloride and lithium borohydride in an organic solvent (*e.g.* toluene).[60]

$$3LiBH_4(s) + AlCl_3(s) \rightarrow Al(BH_4)_3(l) + 3LiCl(s) \quad (2.1)$$

Metal borohydrides and halides often have different solubilities in solvents, allowing for salt-free products to be obtained in high yield. A weakly coordinating solvent that only dissolves the metal borohydride allows for the removal of the metal halide by solvent extraction. The reaction kinetics and yield can be improved by using finely ground reactants with large surface area.

A limitation of solvent-based methods is that the thermodynamically most stable compound is obtained, which is often a monometallic borohydride, typically obtained as a polymorphic pure product. Therefore, reaction mixtures containing two or more metals tend to form mixtures of two or more monometallic borohydrides rather than the bi- or trimetallic borohydrides, which are obtainable through mechanochemical synthesis. Thus, very few bimetallic solvates have been discovered, *e.g.* in diethyl ether, Et_2O, $LiMn(BH_4)_3{\cdot}1/2(Et_2O)$ and $NaMn(BH_4)_3{\cdot}1/2(Et_2O)$.[61] Recently, a new method was developed for the production of bimetallic metal borohydrides using bulky organic cations and weakly coordinating anions.[62,63] The metathesis reaction is carried out in organic solvents, CH_2Cl_2, $CHCl_3$ or toluene, and utilizes precursors such as $[Cat][Zn(BH_4)_3]$ or $[Cat][Y(BH_4)_4]$, where [Cat] symbolizes a bulky cation, *e.g.* $[Ph_4P]^+$ or $[nBu_4N]^+$. The method is also useful for producing less stable bimetallic borohydrides, *i.e.* $LiY(BH_4)_4$, $NaY(BH_4)_4$ or $LiZn_2(BH_4)_5$.[62,63]

The use of dimethyl sulphide, $S(CH_3)_2$, as a co-solvent and extraction solvent has several advantages: (i) the reaction is allowed to proceed faster as the products are being dissolved in $S(CH_3)_2$ as they form, (ii) weak solvent coordination allows for solvent removal at moderate conditions, (iii) the product dissolved in the solvent can readily be separated from the byproducts (*i.e.* LiCl) by filtration. In this manner, the formation of ternary chlorides is avoided, *e.g.* Li- or NaMn-chlorides, or bimetallic borohydrides, previously reported to form mechanochemically from $MnCl_2$ and $LiBH_4$ or $NaBH_4$.[64,65]

Recently, yttrium and gadolinium borohydrides were prepared using dimethyl sulfide as a solvent, providing new solvates as intermediates, $M(BH_4)_3{\cdot}S(CH_3)_2$ (M = Y, La, Ce or Gd), which transform to α-$Y(BH_4)_3$ or $Gd(BH_4)_3$ at $T \sim 140$ °C.[66,67] Other halide-free rare-earth metal borohydrides, $Eu(BH_4)_2$ and $Sm(BH_4)_2$, are prepared by a metathesis reaction of trivalent metal chlorides and $LiBH_4$ in ether, combined with solvent extraction using dimethyl sulfide to remove the halide salts.[68] Donor atoms in solvents typically have increasing strength of coordination in the series S < N < O and are increasing difficult to remove from the metal borohydride products.

2.2 Trends in the mechanochemical synthesis of metal borohydrides

Mechanochemistry is an alternative synthesis approach to bring chemicals together on the atomic scale. Investigations indicate that the induced pressure and reactant composition are of major importance in determining the obtained reaction product.[52] High-energy ball milling induces high pressure and mechanical stress between the reacting materials, which can facilitate chemical reactions, in contrast to traditional solid-state synthesis techniques, which are mainly 'temperature-driven', *i.e.* increasing cation diffusion in the solid state with increasing temperature.[69] Previously, ball milling was mainly aimed at the preparation of alloys and solid solutions of metals, *i.e.* products with statistical distribution of atoms, but now also encompasses the synthesis of ionic, ionic/covalent materials and also organic materials, *i.e.* crystalline materials with ordered distribution of atoms. In some cases, materials can be obtained by mechanochemistry, which apparently cannot be obtained by other means.[52]

High energy mechanochemistry can be very fruitful in the preparation of metal borohydrides where the ball trajectories approach the center of the milling vial, which contrasts grinding mode where the balls follow the circumference of the vial. This treatment maximizes the 'intrinsic pressure' at grain boundaries and limits frictional heating of the sample. Sample heating may be further reduced using pauses during the mechanochemical treatment.[70] Continuous prolonged ball milling may lead to decomposition of the sample, but may also produce new materials, *e.g.* anion-substituted $Na(BH_4)_{1-x}Cl_x$, or nano-sized vanadium boride.[71–73] Mechanochemical synthesis can be performed under a variety of different conditions, *e.g.* at cryogenic conditions, in

 This journal is © The Royal Society of Chemistry 2017

a solvent, or in different gases at elevated pressures (the latter is often denoted reactive ball-milling when the gas takes part in the reaction).[74–77] Hence, mechanochemistry is a versatile technique, which can be used for the preparation of a wide range of materials.[52]

New bi- and trimetallic borohydrides can often be prepared by mechanochemical methods. In cases where pure monometallic borohydrides are available as precursors (*e.g.* prepared by solvent-based methods) addition reactions may be utilized as exemplified by the synthesis of $Cs_2LiY(BH_4)_6$.[78] A major advantage is that a pure product may be obtained.

$$2CsBH_4(s) + LiBH_4(s) + Y(BH_4)_3(s) \rightarrow Cs_2LiY(BH_4)_6(s) \quad (2.2)$$

Monometallic borohydrides may be prepared *via* metathesis reactions, *i.e.* double substitution, usually between a metal halide and a metal borohydride. The reaction scheme (2.3) illustrates the synthesis of $Mn(BH_4)_2$ from $LiBH_4$ and $MnCl_2$.[21,79]

$$MnCl_2(s) + 2LiBH_4(s) \rightarrow Mn(BH_4)_2(s) + 2LiCl(s) \quad (2.3)$$

The drawback is obviously the formation of a mixture of an unwanted metal halide along with the product. The system $ZnCl_2$–MBH_4 (M = Li or Na) can be used to illustrate the complexity of reaction products from mechanochemical synthesis, which may proceed *via* more complex chemical reactions during ball milling.[70]

$$2ZnCl_2(s) + 5LiBH_4(s) \rightarrow LiZn_2(BH_4)_5(s) + 4LiCl(s) \quad (2.4)$$

$$2ZnCl_2(s) + 5NaBH_4(s) \rightarrow NaZn_2(BH_4)_5(s) + 4NaCl(s) \quad (2.5)$$

$$ZnCl_2(s) + 3NaBH_4(s) \rightarrow NaZn(BH_4)_3(s) + 2NaCl(s) \quad (2.6)$$

Reaction schemes (2.5) and (2.6) illustrate that small deviations in the composition of reactants, *e.g.* from (1 : 2.5) to (1 : 3), may lead to significantly different reaction products, both in terms of the stoichiometry and crystal structures, *i.e.* the structures of $NaZn(BH_4)_3$ and $NaZn_2(BH_4)_5$ are significantly different, which may suggest that the synthesis mechanism for these compounds is also different.

Further complications occur due to strong or weak coupling between the chemical reactions that occur during mechanochemical synthesis. Besides the main reaction that forms the product, competing side reactions may also take place, *e.g.* producing bimetallic halides. Sodium chloride produced in reaction (2.5) or (2.6) may further react with the reactant, zinc chloride:

$$ZnCl_2(s) + 2NaCl(s) \rightarrow Na_2ZnCl_4(s) \quad (2.7)$$

Thus, the synthesis of $NaZn_2(BH_4)_5$ only partly proceeds (reaction scheme (2.5)), due to the formation of a stable ternary metal chloride, Na_2ZnCl_4, by a simultaneous and competing reaction (scheme (2.7)). The reaction schemes, (2.5) or (2.6) and (2.7), are weakly coupled shown by the fact that the reaction products contain varying amounts of NaCl, Na_2ZnCl_4, $NaZn_2(BH_4)_5$, and reactants. Thus, reaction schemes (2.5)–(2.7) cannot simply be added to provide a scheme for the total reaction.

Sodium scandium borohydride, $NaSc(BH_4)_4$, can also be prepared mechanochemically and is assumed to follow the metathesis reaction (2.8),[80]

$$ScCl_3(s) + 4NaBH_4(s) \rightarrow NaSc(BH_4)_4(s) + 3NaCl(s) \quad (2.8)$$

However, reaction (2.8) is strongly coupled to the synthesis of a ternary sodium scandium chloride, Na_3ScCl_6 *via* an addition reaction:

$$ScCl_3(s) + 3NaCl(s) \rightarrow Na_3ScCl_6(s) \quad (2.9)$$

Reaction (2.9) is much faster than the formation of the borohydride, $NaSc(BH_4)_4$ (2.8) and these reactions, (2.8) and (2.9) are strongly coupled so they can be added to form an overall reaction (2.10). Therefore, the optimal ratio of reactants $ScCl_3$–$NaBH_4$ to synthesize $NaSc(BH_4)_4$ turns out to be 1 : 2. This mechanochemical synthesis leads to a maximum $NaSc(BH_4)_4$ yield of 22 wt% for a sample with composition (1 : 2) as suggested by reaction (2.10) and not the ratio (1 : 4) suggested in reaction (2.8)

$$2ScCl_3(s) + 4NaBH_4(s) \rightarrow NaSc(BH_4)_4(s) + Na_3ScCl_6(s) \quad (2.10)$$

The above considerations are also valid for synthesis of $KSc(BH_4)_4$, but not for synthesis of $LiSc(BH_4)_4$ where no ternary halide is formed.[70,81]

There is a tendency for more complex chemistry and other chemical reactions to occur when the heavier alkali metals and halides are used as reactants. Mechanochemical synthesis of M_2ZnX_4, M = Li or Na, X = Cl or Br from stoichiometric mixtures of MX and ZnX_2 reveals that reaction times and activation energy decrease as $Li_2ZnCl_4 > Na_2ZnCl_4 > Na_2ZnBr_4$.[82]

The formation of ternary halides can be avoided in the synthesis of trimetallic borohydrides by varying the ratio between borohydrides and halides if at least two reactants are available as mono-metallic borohydrides. While reaction (2.11) produces the ternary salt, Li_2MCl_4, the alternative reaction (2.12) avoids this byproduct formation.[83]

$$15LiBH_4 + 5MCl_2 + 5ZnCl_2 \rightarrow Li_3MZn_5(BH_4)_{15} + 4LiCl + 4Li_2MCl_4 \quad M = Mg \text{ or } Mn \quad (2.11)$$

$$13LiBH_4 + M(BH_4)_2 + 5ZnCl_2 \rightarrow Li_3MZn_5(BH_4)_{15} + 10LiCl \quad (2.12)$$

This observation also suggests that the formation of bimetallic halide salts can be considered a side reaction where the produced metal halide reacts with remaining reactants. In some cases, such side reactions can be suppressed partly or fully by using an excess of metal borohydride reactants, *e.g.* $LiBH_4$, which may shift the reaction equilibrium towards the bi- or trimetallic borohydrides and the monometallic halide, *e.g.* LiCl.

2.3 Trends in the mechanochemical synthesis of metal borohydride-halides

Metal borohydride halides can be prepared with either ordered or disordered crystal structures, where in the latter case solid solutions occur. The system $ZnCl_2$–KBH_4 will be used to illustrate the complexity of the mechanochemical synthesis. Ball milling a

mixture of $ZnCl_2$–KBH_4 (1 : 1) leads to an addition reaction and a single product, $KZn(BH_4)Cl_2$:[84]

$$ZnCl_2(s) + KBH_4(s) \rightarrow KZn(BH_4)Cl_2(s) \qquad (2.13)$$

In this case, there are significant differences between the structures of the reactants and the product. The latter contains a heteroleptic complex ion containing BH_4^- as a ligand, *i.e.* $[Zn(BH_4)Cl_2]^-$ where Zn coordinates to two chloride ions and two hydrogen atoms in η^2-BH_4.[84] This clearly demonstrates that ball milling may initiate complex chemical reactions involving bond breaking and bond formation.[52] In contrast, three novel potassium zinc borohydrides/chlorides are observed in ball-milled KBH_4–$ZnCl_2$ mixtures with molar ratios in the range 1.5 : 1 to 3 : 1, $KZn(BH_4)_3$, $K_2Zn(BH_4)_xCl_{4-x}$ and $K_3Zn(BH_4)_xCl_{5-x}$.[85]

Mechanochemical treatment may also facilitate one solid to dissolve into another, *i.e.* an addition reaction, which leads to formation of a solid solution, *e.g.* formation of a hexagonal solid solution h-$Li(BH_4)_{1-x}Br_x$ where the two anions, BH_4^- and Br^-, are statistically distributed on the same crystallographic position, formed by mechanochemical treatment of $LiBH_4$–LiBr.[86]

In some cases, the crystallinity of the sample and also the overall sample composition may be modified by thermal treatment of the sample. For example, the composition of $NaY(BH_4)_2Cl_2$ changed to $NaY(BH_4)_{1.58}Cl_{2.42}$ at $T = 230$ °C.[87] The rare-earth metals are yet another example: $LiCe(BH_4)_3Cl$ and $LiLa(BH_4)_3Cl$ were prepared by ball milling,[4] whereas $LiGd(BH_4)_3Cl$ only crystallized after heat treatment at $T = 195$ °C.[88] A similar trend is observed for the synthesis of metal borohydride amides *e.g.* $Li_2(BH_4)(NH_2)$, $Li_4(BH_4)(NH_2)_3$, $Na_2(BH_4)(NH_2)$ and $Mg(BH_4)(NH_2)$,[89–91] which are all metal cation conductors. These compounds are formed through ball milling (and annealing) of $M(BH_4)_n$–MNH_2. In this case, NH_2^- does not substitute for BH_4^- to form solid solutions as for Cl^-, instead, new structures are formed with distinct sites for BH_4^- and NH_2^-.

A detailed analysis of the unit cell volumes of $LiBH_4$, KBH_4 and $LiK(BH_4)_2$ indicates that the formation of the bimetallic borohydride is facilitated by a more dense packing as compared to the reactants.[47] Thus, formation of $LiK(BH_4)_2$ is pressure-induced and takes place during ball milling, but not by annealing. This is in agreement with DFT calculations suggesting that $LiK(BH_4)_2$ should decompose to the reactants at ambient conditions.[92] In contrast, the unit cell volumes of the solid solution $Na_{1-x}K_xBH_4$ is larger than the sum of reactant volumes, $(1-x)NaBH_4$–$xKBH_4$.[93] Hence, the formation of $Na_{1-x}K_xBH_4$ is temperature-induced and occurs upon annealing, *i.e.* thermal expansion, but not during ball milling.

2.4 Mechanochemical reactions, general considerations

Table 1 highlights the range of different chemical reactions that are typically observed during the synthesis of metal borohydrides by mechanochemistry. The literature suggests that monometallic borohydrides are more likely to form when $LiBH_4$ is used as the precursor, possibly driven by the formation of the stable halide, LiCl. Furthermore, an excess of $LiBH_4$ may improve the crystallinity of reaction products. The heavier alkali metal borohydrides have a significantly greater tendency to form bimetallic halide salts, $M_xM'X_{x+n}$ *via* addition reactions (the nomenclature is explained in Table 1). Such reactions may occur when LiCl is present together with a heavier metal halide, $M'X_n$ or LiCl may be incorporated into the product producing ordered bimetallic borohydrides chlorides, $LiCe(BH_4)_3Cl$ (except in the case of Li_2CdCl_4 and Li_2MCl_4, M = Mg, Mn). A range of rarer reactions can also be observed, which are considered analogous to the general reactions, (1)–(4) or combinations of those. For example, mono- or bimetallic borohydride chlorides with crystallographically disordered structures *i.e.* $NaY(BH_4)_{1.58}Cl_{2.42}$ can be formed either by substitution (eqn (4)) or complex (eqn (2)) reactions.[87]

Generally, di- and tripositive metal halides, MBH_4–$M'Cl_n$, have very different reactivities and stabilities depending on their metal electronegativity and d-electron configuration. Therefore, different milling times are required to successfully obtain the desired product. For example, synthesis of $MSc(BH_4)_4$ (M = Li, Na or K) occurs by ball-milling MBH_4–$ScCl_3$ (2 : 1) for 120–180 min, while the cadmium borohydrides, α-$Cd(BH_4)_2$, β-$Cd(BH_4)_2$, $KCd(BH_4)_3$ and $K_2Cd(BH_4)_4$ are formed from MBH_4–$CdCl_2$ (M = Li, Na or K) after only 20–30 min mechanochemical treatment. Only the transition metals with d^0, d^5 or d^{10} electron configurations have sufficient stability to allow for mechanochemical preparation.[8] However, transition metal borohydrides, $M'(BH_4)_2$, M′ = Cr^{2+} (d^4), Fe^{2+} (d^6) and Co^{2+} (d^7), were recently prepared in solution at $T < -30$ °C, and stabilised by ammonia–metal coordination, *i.e.* formation of $M'(NH_3)_6(BH_4)_2$ compounds.[94]

2.5 Mechanical synthesis in different gas atmosphere

Solvent-free synthesis of monometallic borohydrides, *e.g.* lithium borohydride, $LiBH_4$, formed in an addition reaction between lithium hydride, LiH, and diborane, B_2H_6 gas at T = 120 °C has recently been demonstrated.[95] The formation of $LiBD_4$ from LiD and B_2D_6 was followed using *in situ* powder neutron diffraction, which reveals that the nucleation of $LiBD_4$ begins at $T \sim 102$ °C, *i.e.* with the formation of the hexagonal polymorph, h-$LiBD_4$. However, the reaction is incomplete and the yield is only ~50% even at elevated temperatures (187 °C)

Table 1 Generalization of chemical reactions observed during mechanochemical synthesis of metal borohydrides from MBH_4–$M'X_n$ reactant mixtures along with selected examples. Nomenclature: X = halide anion, M = alkali metal cation and M′ = di- or tri-positive metal

Reaction type/no.	Reaction
Metathesis/1	$nMBH_4 + M'X_n \rightarrow M'(BH_4)_n + nMX$ Example $2LiBH_4 + MnCl_2 \rightarrow Mn(BH_4)_2 + 2LiCl$
Addition/2	$yMBH_4 + xMX_n \rightarrow M(BH_4)_yX_x$ Example $0.75NaBH_4 + 0.25NaCl \rightarrow Na(BH_4)_{0.75}Cl_{0.25}$
Metathesis-addition/3	$(x+ny)MBH_4 + yM'X_n \rightarrow M_xM'_y(BH_4)_{x+ny} + (ny)MX$ Example $4LiBH_4 + ScCl_3 \rightarrow LiSc(BH_4)_4 + 3LiCl$
Metathesis-addition/4	$M'X_n + nMBH_4 \rightarrow MM'(BH_4)_nX + (n-1)MX$ Example $CeCl_3 + 3LiBH_4 \rightarrow LiCe(BH_4)_3Cl + 2LiCl$

This journal is © The Royal Society of Chemistry 2017

with the product containing small amounts of $Li_2B_{12}H_{12}$. A passivation layer of $LiBH_4$ is suggested to form on the surface of the LiH grains retarding the process.[96,97] Mechanochemical treatment allows for the continuous removal of as-formed borohydride from the surface layer of particles, facilitating a more complete reaction. Diborane gas is produced by heating a ball milled $2.5LiBH_4$–$ZnCl_2$ sample, *i.e.* decomposition of $LiZn_2(BH_4)_5$,[70,96] which is considered a convenient and relatively safe source of diborane as compared to pressurized gas bottles. This new gas–solid mechanochemical synthesis method has also successfully provided other metal borohydrides, such as $Mg(BH_4)_2$, $Ca(BH_4)_2$ and $Y(BH_4)_3$.[97,98] Direct synthesis of α-$Y(BH_4)_3$ by ball milling YH_3 in a B_2H_6 atmosphere gave yields above 75%,[98,99] and ball milling $Y(BH_4)_3$ in B_2H_6 has also led to the discovery of $Y(B_3H_8)_3$ and $Y_2(B_{12}H_{12})_3$, suggesting that higher boranes might also be formed during the decomposition of $Y(BH_4)_3$.[100] These solid–gas reactions can be considered as addition reactions analogous to the solvent-based reactions described above (see Section 2.1). Thus, this analogy suggest that the solvent-free solid–gas reactions are only useful when Lewis base type ionic or polar covalent hydrides, such as LiH, providing an electron-pair donating H^- ion, or BH_4^-, can be utilised as reactants to form a borohydride or higher borane. The solid–gas reactions are promising for extending the series of solvent-free metal boranes.

2.6 Single crystal growth of metal borohydrides

Despite significant efforts, single crystal investigations of metal borohydrides are very scarce. This is mainly due to the complications arising when attempting to grow metal borohydrides by classical solution chemistry. Solvents need to be carefully selected in order to avoid the formation of solvates. Unfortunately, non-coordinating apolar solvents often have low solubility limits. Notably, single crystal studies have been reported on mono-metallic compounds such as $LiBH_4$,[101] $NaBH_4$,[102,103] KBH_4,[104] $Be(BH_4)_2$,[105] $Mg(BH_4)_2$,[106] and $Al(BH_4)_3$,[107] where crystals can be grown from a solution, by annealing the powder, or by recrystallizing from a melt. Techniques involving melting are useful for mono-metallic borohydrides but limited to bi- and trimetallic borohydrides that are sufficiently thermally stable (recall that a high number of these compounds are prepared mechanochemically, stabilized by high pressure rather than elevated temperature). Powder samples of framework-type metal borohydrides produced mechanochemically may, in some cases, be partly dissolved in a suitable solvent and then recrystallized to larger crystals. Single crystals of $KCa(BH_4)_3$ were recently prepared from flux, which can be an eutectically melting mixture of more stable alkali and/or earth alkali metal borohydrides with sufficiently large thermal stability.[108]

Chemical vapour deposition (CVD) was reported as an approach for the crystal growth of $Zr(BH_4)_4$, which is formed by a metathesis reaction of $ZrCl_4$ and $LiBH_4$ during ball milling:[109]

$$ZrCl_4(s) + 4LiBH_4(s) \rightarrow Zr(BH_4)_4(s) + 4LiCl(s) \quad (2.14)$$

The ball milled sample was stored in a vial at −30 °C for 2–4 weeks when transparent single-crystals with a rectangular shape were noticed under the lid, explained by the low sublimation temperature of $Zr(BH_4)_4$ (29 °C) because of its molecular structure.[109] CVD is an elegant method for single crystal growth of metal borohydrides, which may be limited to volatile molecular compounds with low vapour pressures and sublimation temperatures.

The importance of producing single crystal samples stems not only from the fact that physical properties such as ionic conductivity can be highly anisotropic[110] and powder averaging can present problems to such characterizations, but also from the necessity of providing accurate input for theoretical evaluations of hydrogen storage systems.

2.7 Synthesis of metal borohydrides with neutral molecules

Metal borohydrides form complexes with hydrogen-rich nitrogen-based neutral molecules, which can be in the solid state (*e.g.* ammonia borane, NH_3BH_3), liquid state (*e.g.* hydrazine, NH_2NH_2), or gas state (*e.g.* ammonia, NH_3). These compounds are capable of generating large amounts of hydrogen by combining the hydrogen atoms present in the two counterparts. Borohydride complexes with water have similar properties but usually have a lower stability, where the hydrates of sodium,[111] lithium,[112] and calcium[113] are characterized.

Ammonia borane metal borohydride complexes. Ammonia borane metal borohydride complexes are formed by addition reactions between NH_3BH_3 and $LiBH_4$, $Mg(BH_4)_2$, $Ca(BH_4)_2$ and $Al(BH_4)_3$. For the solids $LiBH_4$, $Mg(BH_4)_2$, $Ca(BH_4)_2$ the complexes are prepared by ball-milling.[114,115] Interestingly, the mixture α-$Mg(BH_4)_2$–NH_3BH_3 (1 : 2) converts completely into $Mg(BH_4)_2$-$(NH_3BH_3)_2$ upon ball milling, while $Mg(BH_4)_2(NH_3BH_3)_2$ is not formed when starting from amorphous $Mg(BH_4)_2$ and NH_3BH_3.[115] This is counter-intuitive, since amorphous matter usually has higher reactivity, suggesting that there is a structural relationship allowing the borohydride to coordinate with neutral ligands. Optimal contact between reactants is offered by liquid $Al(BH_4)_3$ at ambient conditions to form single-crystals of $Al(BH_4)_3{\cdot}NH_3BH_3$.[116]

Hydrazine metal borohydrides. Complexes with hydrazine are reported for $LiBH_4$, $NaBH_4$ and $Mg(BH_4)_2$, *e.g.* $LiBH_4{\cdot}NH_2NH_2$. These compounds were synthesized by placing the precursor metal borohydride and hydrazine in different chambers of a sealed system at room temperature.[117] Due to the vapour pressure, hydrazine typically absorbs into the borohydride over the course of hours. Alternatively, the complexes are formed by ball milling solid–liquid mixtures of $M(BH_4)_m$–NH_2NH_2.[118]

Ammine metal borohydrides. Metal borohydrides readily react with ammonia gas in solid–gas reactions forming ammine metal borohydrides, $M(BH_4)_m{\cdot}nNH_3$, except for the heavier alkali metal borohydrides: $NaBH_4$, KBH_4, $RbBH_4$ and $CsBH_4$. However, the first ammine metal borohydrides, *e.g.* $Zn(BH_4)_2{\cdot}4NH_3$, were synthesized in the 1950's by solvent-based methods.[119]

Recent literature reveals that the NH_3/BH_4 ratio (n/m) of ammine metal borohydrides, $M(BH_4)_m{\cdot}nNH_3$, can be efficiently tailored by combining solvent based methods, solid–gas reactions and mechanochemistry. Initially, a metal borohydride is prepared by a solvent-based method or by solvent extraction

of a mechanochemically prepared metal borohydride metal halide mixture, *e.g.* using a weakly coordinating solvent such as dimethyl sulfide, $S(CH_3)_2$. Ammine metal borohydrides may be prepared by passing dry NH_3 gas through the solution of $M(BH_4)_3$ in $S(CH_3)_2$ or by a reaction between dry NH_3 gas and solid $M(BH_4)_3$. Ammonia always coordinates to the metal by a strongly exothermic reaction and cooling is usually needed in order to obtain the metal borohydride containing the highest possible number of ammonia molecules for further synthesis, *e.g.* $M(BH_4)_3{\cdot}7NH_3$, M = Y, Gd or Dy prepared at $T \sim -5$ °C.[53] Synthesis of ammine metal borohydrides in more strongly coordinating solvents, such as THF, is also possible, however, the samples are contaminated by the formation of ammonia borane.[120]

Mechanochemical treatment of the ammine metal borohydride having the highest possible number of ammonia molecules and the corresponding metal borohydride in various ratios is a convenient way to get new ammine metal borohydrides with varying NH_3/BH_4 ratio. This approach is demonstrated for ammine manganese borohydride, $Mn(BH_4)_2{\cdot}nNH_3$ for n = 1, 2, 3 and 6.[54]

$$n\mathrm{Mn(BH_4)_2{\cdot}6NH_3(s)} + (6-n)\mathrm{Mn(BH_4)_2(s)} \rightarrow 6\mathrm{Mn(BH_4)_2{\cdot}}n\mathrm{NH_3(s)} \quad (2.15)$$

3. Trends in structural chemistry of metal borohydrides

The past decade has experienced a major increase in the number of experimental structural studies of novel metal borohydrides, in particular using powder X-ray or neutron diffraction.[121–123] Various equipment has been designed to enable this type of PXD characterization under high gas pressure and temperature.[124,125] The interest in crystal chemistry of metal borohydrides was initiated in the late 1940's by investigations into the most ionic and stable monometallic borohydrides, namely MBH_4, M = Na, K, Rb and Cs.[18,19] Later studies focused on the more challenging molecular, volatile and covalent compounds, *e.g.* $Al(BH_4)_3$, $Zr(BH_4)_4$ and $Hf(BH_4)_4$.[107,126,127] In between these two extremes we find numerous metal borohydrides with framework structures, pronounced bonding directionality and clearly some degree of covalency, *e.g.* $Mg(BH_4)_2$ and $Mn(BH_4)_2$.[3,21,106,128,129] The successful structural analysis of $LiBH_4$ in 2002 was the initiation of this renewed interest in metal borohydrides.[24]

The first bimetallic borohydride, $LiK(BH_4)_2$ was discovered and characterized in 2008.[130] Since then, a rapidly increasing number of bimetallic and also trimetallic[83] borohydrides have been described, often containing complex anions. Some compounds fall within more than one of these categories, for instance, $LiZn_2(BH_4)_5$ contains $[Zn_2(BH_4)_5]^-$ complex anions but can also be considered as being built from interpenetrated frameworks.[70]

Clearly, metal borohydrides exhibit a fascinating and surprisingly versatile crystal chemistry, which the following section will review, highlighting general trends and relationships. Initially, mono-metallic borohydrides will be discussed (Table 2), starting from the simple cubic ionic structures, moving towards more covalent and complex bi- and trimetallic borohydrides (Tables 3 and 4), including framework structures and anionic complexes.

3.1 Monometallic borohydrides, the s-block – pronounced ionic bonding

The alkali metal borohydrides, MBH_4, M = Li, Na, K, Rb and Cs, primarily exhibit ionic bonding and theoretical studies show that there is almost no charge density (<5%) between the M^+ and BH_4^- ions in their structures.[173–176] An experimental charge density investigation of o-$LiBH_4$ reveals transfer of 0.86 ± 0.09 e^- (at 10 and 90 K) from Li to BH_4 in accordance with the ionic structure description.[175]

Lithium borohydride. Four polymorphs of lithium borohydride, $LiBH_4$, have been described and the orthorhombic o-$LiBH_4$ (*Pnma*) structure at ambient conditions is unique.[24] Single crystal XRD investigations of o-$LiBH_4$ at 225 K unambiguously reveal nearly ideal tetrahedral geometry of the BH_4 group, in contrast to more distorted tetrahedra reported in earlier PXD studies.[22,24] Powder neutron diffraction of the triple isotopically substituted o-$^7Li^{11}BD_4$ at 3.5 K reveals boron–hydrogen bond lengths (B–H) of 1.208–1.225 Å, and bond angles (H–B–H) in the range 107.2–111.7°.[177]

Orthorhombic o-$LiBH_4$ transforms to a hexagonal wurtzite-like polymorph h-$LiBH_4$ ($P6_3mc$) at ~110 °C. PND and PXD studies reveal large and anisotropic displacements of hydrogen atoms.[177,178] The observed atomic displacement ellipsoids may indicate orientational disorder in addition to thermal vibrations of the BH_4 group. The large vibrational amplitudes of BH_4 in the hexagonal polymorph agree with an apparent shortening of the B–H bonds to ~1.07 Å. An entropy contribution from this disorder is considered to be a factor in stabilizing the hexagonal structure.[101,178] Two high pressure polymorphs of $LiBH_4$ are also observed at room temperature. One polymorph is observed at a pressure of 1.2–18 GPa, which is pseudo-tetragonal (*Ama*2) with Li tetrahedrally coordinated by four BH_4 groups and the BH_4 groups in a nearly square-planar coordination by four Li atoms.[131] A more complex ordering of the BH_4 groups, showing repulsive interactions, was first suggested in the $\sqrt{2}a \times 2c$ supercell of the *Ama*2 structure theoretically[179] and then shown experimentally.[180] At high pressure a cubic $LiBH_4$ polymorph forms, which is isostructural to cubic $NaBH_4$.[131] In general, the four polymorphs of lithium borohydride primarily show coordination between lithium and the borohydride complex anion by edge sharing, but h-$LiBH_4$ and o-$LiBH_4$ appear to have face sharing for the shortest Li–B contact (2.37 Å). The structural distortions in $LiBH_4$ polymorphs have been analysed by group-theoretical and crystal-chemical considerations revealing the layered structure of $LiBH_4$[181] where the deformation of layers define the structural stability of the observed polymorphs.

The heavier alkali metals. Available p-orbitals and the increasing sizes of heavier alkali metals facilitate the formation of rock salt (NaCl, $Fm\bar{3}m$) type structures of alkali metal borohydrides, MBH_4, M = Na, K, Rb and Cs. Theoretical studies suggest that electron density deformations of the heavier alkali metals may also contribute to the formation of NaCl-type structures.[176] Additional studies at low temperature and high pressures have discovered several other structural polymorphs.[18,19,133,135,182]

 This journal is © The Royal Society of Chemistry 2017

Table 2 Known experimental structures of monometallic borohydrides ordered by cation atomic number

Cation	Polymorph	ρ_m (wt% H)	Stability	Crystal system	Space group	Ref.
Li^+	o-$LiBH_4$	18.5	RT	Orthorhombic	*Pnma*	24
	h-$LiBH_4$		>380 K	Hexagonal	$P6_3mc$	24
	hp1-$LiBH_4$		RT, 1.2–10 GPa	Orthorhombic	*Ama2*	131
	hp2-$LiBH_4$		RT, >10 GPa	Cubic	$Fm\bar{3}m$	131
Be^{2+}	$Be(BH_4)_2$	20.8	RT	Tetragonal	$I4_1/cd$	105
Na^+	α-$NaBH_4$	10.7	RT	Cubic	$Fm\bar{3}m$	19
	lt-$NaBH_4$		<190 K or RT, >6 GPa	Tetragonal	$P4_2/nmc$	132
	hp-$NaBH_4$		>9 GPa	Orthorhombic	*Pnma*	133
Mg^{2+}	α-$Mg(BH_4)_2$	14.9	RT	Hexagonal	$P6_122$	106 and 129
	β-$Mg(BH_4)_2$		RT, metastable, HT polymorph	Orthorhombic	*Fddd*	128 and 134
	γ-$Mg(BH_4)_2$		RT, metastable	Cubic	$Ia\bar{3}d$	3
	δ-$Mg(BH_4)_2$		RT, >2.1 GPa	Tetragonal	$P4_2nm$	3
	ζ-$Mg(BH_4)_2$		~500 K	Hexagonal	$P3_112$	58
Al^{3+}	α-$Al(BH_4)_3$	16.9	150 K	Monoclinic	$C2/c$	107
	β-$Al(BH_4)_3$		195 K	Orthorhombic	$Pna2_1$	107
K^+	α-KBH_4	7.5	RT	Cubic	$Fm\bar{3}m$	19 and 104
	β-KBH_4		<70 K or RT, 3.8–6.8 GPa	Tetragonal	$P4_2/nmc$ $P42_1c$	135 and 136
	γ-KBH_4		RT, >6.8 GPa	Orthorhombic	*Pnma*	136
Ca^{2+}	α-$Ca(BH_4)_2$	11.6	RT	Orthorhombic	*F2dd*	137
	α′-$Ca(BH_4)_2$		>495 K	Tetragonal	$I\bar{4}2d$	137
	β-$Ca(BH_4)_2$		RT, metastable, HT polymorph	Tetragonal	$P\bar{4}$ $P4_2/m$	137 and 138
	γ-$Ca(BH_4)_2$		RT, metastable	Orthorhombic	*Pbca*	139
Mn^{2+}	α-$Mn(BH_4)_2$	9.5	RT	Hexagonal	$P3_112$	21
	γ-$Mn(BH_4)_2$		RT, metastable	Cubic	$Ia\bar{3}d$	58
	δ-$Mn(BH_4)_2$		RT, 1–8 GPa	Tetragonal	$I4_1/acd$	140
	δ′-$Mn(BH_4)_2$		RT, >8 GPa	Orthorhombic	*Fddd*	140
Rb^+	rt-$RbBH_4$	4.0	RT	Cubic	$Fm\bar{3}m$	19
	hp1-$RbBH_4$		RT, 3–12 GPa	Tetragonal	$P4/nmm$	141
	hp2-$RbBH_4$		RT, 12–20 GPa	Orthorhombic	*C222*	141
	hp3-$RbBH_4$		RT, >20 GPa	Tetragonal	$I\bar{4}2m$	141
Sr^{2+}	o-$Sr(BH_4)_2$	6.9	RT	Orthorhombic	*Pbcn*	142
	t-$Sr(BH_4)_2$		>723 K	Tetragonal	$P4_12_12$	143
Y^{3+}	α-$Y(BH_4)_3$	9.1	RT	Cubic	$Pa\bar{3}$	144
	β-$Y(BH_4)_3$		RT, HT polymorph	Cubic	$Fm\bar{3}c$	145
Zr^{4+}	$Zr(BH_4)_4$	10.7	<243 K	Cubic	$P\bar{4}3m$	109 and 127
Cd^{2+}	α-$Cd(BH_4)_2$	5.7	RT	Tetragonal	$P4_2nm$	146
	β-$Cd(BH_4)_2$		>328 K	Cubic	$Pn\bar{3}m$	146
Cs^+	$CsBH_4$	2.7	RT	Cubic	$Fm\bar{3}m$	19
Ba^+	o1-$Ba(BH_4)_2$	4.8	RT	Orthorhombic	*Pnnm*	143
	o2-$Ba(BH_4)_2$		>668 K	Orthorhombic	*Pbcn*	143
	t-$Ba(BH_4)_2$		>718 K	Tetragonal	$P4_12_12$	143
La^{3+}	$La(BH_4)_3$	6.6	RT	Trigonal	$R\bar{3}c$	67
Ce^{3+}	$Ce(BH_4)_3$	6.6	RT	Trigonal	$R\bar{3}c$	67
Sm^{2+}	o-$Sm(BH_4)_2$	4.5	~500 K	Orthorhombic	*Pbcn*	68 and 147
Sm^{3+}	α-$Sm(BH_4)_3$	6.2	RT	Cubic	$Pa\bar{3}$	147
	β-$Sm(BH_4)_3$		RT	Cubic	$Fm\bar{3}c$	147
Eu^{2+}	o-$Eu(BH_4)_2$	4.4	~430 K	Orthorhombic	*Pbcn*	68
	t-$Eu(BH_4)_2$		>668 K	Tetragonal	$P4_12_12$	143
	c-$Eu(BH_4)_2$		>668 K	Cubic	$Fm\bar{3}m$	143
Gd^{3+}	$Gd(BH_4)_3$	6.0	RT	Cubic	$Pa\bar{3}$	144 and 147
Tb^{3+}	$Tb(BH_4)_3$	5.9	RT	Cubic	$Pa\bar{3}$	147
Dy^{3+}	$Dy(BH_4)_3$	5.8	RT	Cubic	$Pa\bar{3}$	144
Ho^{3+}	α-$Ho(BH_4)_3$	5.8	RT	Cubic	$Pa\bar{3}$	148
	β-$Ho(BH_4)_3$		RT	Cubic	$Fm\bar{3}c$	148
Er^{3+}	α-$Er(BH_4)_3$	5.7	RT	Cubic	$Pa\bar{3}$	147
	β-$Er(BH_4)_3$		RT	Cubic	$Fm\bar{3}c$	147
Yb^{2+}	α-$Yb(BH_4)_2$	4.0	RT	Orthorhombic	*F2dd*	149
	β-$Yb(BH_4)_2$		>523 K	Tetragonal	$P\bar{4}$	149 and 150
	γ-$Yb(BH_4)_2$		473–573 K	Orthorhombic	*Pbca*	149 and 150
Yb^{3+}	α-$Yb(BH_4)_3$	5.6	RT	Cubic	$Pa\bar{3}$	150
	β-$Yb(BH_4)_3$		RT, metastable	Cubic	$Pm\bar{3}m$	150
Hf^{4+}	$Hf(BH_4)_4$	6.8	<263 K	Cubic	$P\bar{4}3m$	126
Th^{4+}	$Th(BH_4)_4$	5.5	RT	Tetragonal	$P4_12_12$	151 and 152
U^{4+}	α-$U(BH_4)_4$	5.4	RT	Tetragonal	$P4_12_12$	153
	β-$U(BH_4)_4$		RT	Orthorhombic	*Cmcm*	154
Np^{4+}	$Np(BH_4)_4$	5.5	~130 K	Tetragonal	$P4_2/nmc$	155

Table 3 Known experimental structures of bimetallic borohydrides ordered by cation atomic number of the first cation

Cations		Polymorph	ρ_m (wt% H)	Crystal system	Space group	Ref.
Li^+	K^+	$LiK(BH_4)_2$	10.6	Orthorhombic	*Pnma*	130
Li^+	Rb^+	m-$LiRb(BH_4)_2$	6.6	Monoclinic	*C*2/*m*	156
		o-$LiRb(BH_4)_2$	6.6	Orthorhombic	$Cmc2_1$	156
		h-$Li_2Rb(BH_4)_3$	8.4	Hexagonal	$P6_222$	156
Li^+	Cs^+	o-$LiCs(BH_4)_2$	4.8	Orthorhombic	$Cmc2_1$	156
		h-$Li_2Cs(BH_4)_3$	6.3	Hexagonal	$P6_222$	156
		m-$Li_2Cs(BH_4)_3$	6.3	Monoclinic	*Cc*	156
		m-$LiCs_2(BH_4)_3$	3.8	Monoclinic	*C*2/*c*	156
		o-$Li_3Cs_2(BH_4)_5$	5.6	Orthorhombic	*Fddd*	156
		m-$Li_2Cs_3(BH_4)_5$	4.1	Monoclinic	$P2_1/c$	156
		m-$Li_3Cs(BH_4)_4$	7.6	Monoclinic	$P2_1/c$	156
Li^+	Sc^{3+}	$LiSc(BH_4)_4$	14.5	Tetragonal	$P\bar{4}2c$	81
Li^+	Y^{3+}	$LiY(BH_4)_4$	10.4	Tetragonal	$P\bar{4}2c$	63
Li^+	Yb^{3+}	$LiYb(BH_4)_4$	6.7	Tetragonal	$P\bar{4}2c$	150
Li^+	Lu^{3+}	$LiLu(BH_4)_4$	6.7	Tetragonal	$P\bar{4}2c$	147
Li^+	Zn^{2+}	$LiZn_2(BH_4)_5$	9.5	Orthorhombic	*Cmca*	70, 157 and 158
Li^+	Al^{3+}	$Li_4Al_3(BH_4)_{13}$	17.4	Cubic	$P\bar{4}3n$	159 and 160
	Al^{3+}	$LiAl(BH_4)_4$	17.3	Monoclinic	$P2_1/c$	160
Na^+	Sc^{3+}	$NaSc(BH_4)_4$	12.7	Orthorhombic	*Cmcm*	80
Na^+	Y^{3+}	$NaY(BH_4)_4$	9.4	Orthorhombic	$C222_1$	63 and 161
Na^+	La^{3+}	$NaLa(BH_4)_4$	7.3	Orthorhombic	*Pbcn*	162
Na^+	Yb^{3+}	$NaYb(BH_4)_4$	6.3	Orthorhombic	*Cmcm*	163
Na^+	Zn^{2+}	$NaZn(BH_4)_3$	9.1	Monoclinic	$P2_1/c$	70 and 157
		$NaZn_2(BH_4)_5$	8.8	Monoclinic	$P2_1/c$	70 and 157
Na^+	Al^{3+}	$NaAl(BH_4)_4$	14.7	Monoclinic	*C*2/*c*	160
K^+	Mg^{2+}	$K_2Mg(BH_4)_4$	10.0	Monoclinic	$P2_1/n$	164
		$K_3Mg(BH_4)_5$	9.3	Tetragonal	$P4_2/mbc$ *I*4/*mcm*	164
K^+	Ca^{2+}	lt-$KCa(BH_4)_3$	9.8	Orthorhombic	*Pba*2	1
		ht-$KCa(BH_4)_3$	9.8	Orthorhombic	$Pna2_1$	1
K^+	Sr^{2+}	$KSr(BH_4)_3$	7.1	Orthorhombic	$Pna2_1$	165
K^+	Sc^{3+}	$KSc(BH_4)_4$	11.2	Orthorhombic	*Pnma*	166
K^+	Y^{3+}	o-$KY(BH_4)_4$	8.6	Orthorhombic	*Cmcm*	167
		m-$KY(BH_4)_4$	8.6	Monoclinic	*C*2/*c*	78
K^+	Ce^{3+}	$K_3Ce(BH_4)_6$	7.0	Monoclinic	$P2_1/c$	168
K^+	Gd^{3+}	$KGd(BH_4)_4$	6.3	Monoclinic	$P2_1/c$	50
		$K_2Gd(BH_4)_5$	6.5	Monoclinic	$P2_1/m$	50
		$K_3Gd(BH_4)_6$	6.7	Monoclinic	$P2_1/c$	50
K^+	Ho^{3+}	$KHo(BH_4)_4$	6.1	Orthorhombic	*Cmcm*	148
K^+	Yb^{2+}	lt-$KYb(BH_4)_3$	4.7	Cubic	$P\bar{4}3m$	1
		ht-$KYb(BH_4)_3$	4.7	Orthorhombic	$Pmc2_1$	1
K^+	Yb^{3+}	$KYb(BH_4)_4$	5.9	Orthorhombic	*Cmcm*	163
K^+	Mn^{2+}	$K_2Mn(BH_4)_4$	8.4	Monoclinic	$P2_1/c$	164
		$KMn(BH_4)_3$	8.7	Tetragonal	$P4_2/mbc$	164
K^+	Zn^{2+}	$KZn(BH_4)_3$	8.1	Trigonal	*R*3	85
		$K_2Zn(BH_4)_4$	7.9	Monoclinic	$P2_1/c$	85
		$K_3Zn(BH_4)_5$	7.8	Tetragonal	$P4_2/ncm$	85
K^+	Cd^{2+}	$KCd(BH_4)_3$	6.2	Cubic	$Ia\bar{3}$	146
		$K_2Cd(BH_4)_4$	6.5	Monoclinic	$P2_1/c$	146
K^+	Al^{3+}	$KAl(BH_4)_4$	12.9	Orthorhombic	*Fddd*	169
Rb^+	Mg^{2+}	$Rb_3Mg(BH_4)_5$	5.7	Tetragonal	*I*4/*mcm*	170
Rb^+	Ca^{2+}	lt-$RbCa(BH_4)_3$	7.1	Cubic	$Fm\bar{3}c$	1
		ht1-$RbCa(BH_4)_3$	7.1	Orthorhombic	$C222_1$	1
		ht2-$RbCa(BH_4)_3$	7.1	Tetragonal	*I*4/*mcm*	1
Rb^+	Sr^{2+}	$RbSr(BH_4)_3$	5.6	Orthorhombic	$Pna2_1$	1 and 165
Rb^+	Y^{3+}	o-$RbY(BH_4)_4$	6.9	Orthorhombic	*Pnma*	78
		m-$RbY(BH_4)_4$	6.9	Monoclinic	$P2_1/c$	171
		$Rb_3Y(BH_4)_6$	5.6	Cubic	$Fm\bar{3}$	1 and 78
Rb^+	Ce^{3+}	$Rb_3Ce(BH_4)_6$	5.0	Monoclinic	$P2_1/c$	1
Rb^+	Eu^{2+}	$RbEu(BH_4)_3$	4.3	Orthorhombic	$Pna2_1$	1
Rb^+	Al^{3+}	$RbAl(BH_4)_4$	9.4	Orthorhombic	*Fddd*	160
Cs^+	Mg^{2+}	$CsMg(BH_4)_3$	6.0	Monoclinic	*Cc*	1
		$Cs_3Mg(BH_4)_5$	4.1	Tetragonal	*I*4/*mcm*	170
Cs^+	Ca^{2+}	lt-$CsCa(BH_4)_3$	5.6	Cubic	$Fm\bar{3}c$	1
		ht-$CsCa(BH_4)_3$	5.6	Cubic	$Pm\bar{3}m$	1
Cs^+	Sr^{2+}	$CsSr(BH_4)_3$	4.6	Orthorhombic	$P2_12_12$	1 and 165
Cs^+	Y^{3+}	$CsY(BH_4)_4$	5.7	Tetragonal	$I4_1/a$	171
		$Cs_3Y(BH_4)_6$	4.2	Cubic	$Fm\bar{3}$	1 and 78

This journal is © The Royal Society of Chemistry 2017

Table 3 (*continued*)

Cations		Polymorph	ρ_m (wt% H)	Crystal system	Space group	Ref.
Cs^+	Eu^{2+}	$CsEu(BH_4)_3$	3.7	Tetragonal	$P4/mbm$	1
Cs^+	Gd^{3+}	$Cs_3Gd(BH_4)_6$	3.8	Cubic	$Fm\bar{3}$	1
Cs^+	Mn^{2+}	$CsMn(BH_4)_3$	5.2	Monoclinic	Cc	1
Cs^+	Al^{3+}	ht-$CsAl(BH_4)_4$	7.4	Tetragonal	$I4_1/amd$	160
Cs^+	Pb^{2+}	$CsPb(BH_4)_3$	3.1	Tetragonal	$P4/mbm$	1

Table 4 Known experimental structures of trimetallic borohydrides ordered by cation atomic number of the first cation

Cations			Polymorph	ρ_m (wt% H)	Crystal system	Space group	Ref.
Li^+	K^+	Mg^{2+}	$LiKMg(BH_4)_4$	12.4	Orthorhombic	$Aba2$	172
			$Li_2K_3Mg_2(BH_4)_9$	11.6	Monoclinic	$P2/c$	172
Li^+	K^+	Mn^{2+}	$LiKMn(BH_4)_4$	10.1	Orthorhombic	$Aba2$	172
Li^+	K^+	La^{3+}	$Li_3K_3La_2(BH_4)_{12}$	8.1	Cubic	$Ia\bar{3}d$	168
Li^+	K^+	Ce^{3+}	$Li_3K_3Ce_2(BH_4)_{12}$	8.1	Cubic	$Ia\bar{3}d$	168
Li^+	Rb^+	Mg^{2+}	$LiRbMg(BH_4)_4$	9.2	Orthorhombic	$Aba2$	172
Li^+	Rb^+	Mn^{2+}	$LiRbMn(BH_4)_4$	7.8	Orthorhombic	$Aba2$	172
Li^+	Rb^+	Y^{3+}	$Rb_2LiY(BH_4)_6$	6.8	Cubic	$Fm\bar{3}$	78 and 171
Li^+	Cs^+	Y^{3+}	$Cs_2LiY(BH_4)_6$	5.4	Cubic	$Fm\bar{3}$	78 and 171
Li^+	Cs^+	Ce^{3+}	$Cs_2LiCe(BH_4)_6$	4.8	Cubic	$Fm\bar{3}$	1
Li^+	Cs^+	Gd^{3+}	$Cs_2LiGd(BH_4)_6$	4.7	Cubic	$Fm\bar{3}$	1
Li^+	Mg^{2+}	Zn^{2+}	$Li_3MgZn_5(BH_4)_{15}$	10.2	Hexagonal	$P6_3/mcm$	83
Li^+	Mn^{2+}	Zn^{2+}	$Li_3MnZn_5(BH_4)_{15}$	9.7	Hexagonal	$P6_3/mcm$	83
Rb^+	Mg^{2+}	Ca^{2+}	$RbMg_xCa_{1-x}(BH_4)_3$	—	Orthorhombic	$C222_1$	1

Alkaline earth metal borohydrides. The monometallic alkaline earth metal borohydrides show increasingly covalent and directional bonding with decreasing ionic radius and increasing electronegativity and charge density, in the series, Be > Mg > Ca > Sr > Ba. Indeed, the number of polymorphs (in parentheses) of composition $M(BH_4)_2$ show decreasing trends in the series Mg (7) > Ca (4) > Sr (3) > Ba (4). Porosity in the solid state is also observed in frameworks with the highest covalence, namely α- and γ-$Mg(BH_4)_2$, with 6 and 30% of open space in the structures, respectively.

Strontium and barium borohydride. $Sr(BH_4)_2$ and $Ba(BH_4)_2$ are the most ionic of the alkaline earth metal borohydrides.[142,143] Barium borohydride is synthesised as an orthorhombic polymorph (o1), which transforms to another orthorhombic polymorph (o2) at $T \sim 395$ °C, which is isostructural to o-$M(BH_4)_2$, M = Sr, Sm, Eu.[68,142,143,147] o2-$Ba(BH_4)_2$ transforms to t- and c-$Ba(BH_4)_2$ polymorphs at 445 and 460 °C. Similarly, o-$M(BH_4)_2$, M = Sr, Eu also transform to t- and c-$M(BH_4)_2$ polymorphs upon heating. These polymorphs are structurally related, o1- to $CaCl_2$-type, o- and o2- to α-PbO_2, t- to ht-ZrO_2, and c- to CaF_2.[143] In fact, the $CaCl_2$ structure type is an orthorhombic deformation of the tetragonal rutile type (TiO_2), which is based on *hcp* packing of BH_4^- anions, *i.e.* metal ions placed in octahedral positions. The α-PbO_2 structure is then related to the rutile type by a well-known phase transition which may be induced by applying pressure. The t-polymorph is a superstructure (doubled *c*-axis) of the ht-ZrO_2 type which is a deformation of cubic CaF_2 structure type. The orthorhombic structures of the α-PbO_2-type likely form due to the similar cation sizes, Sm^{2+} (r = 1.22 Å), Eu^{2+} (r = 1.25 Å), Sr^{2+} (r = 1.26 Å), Ba^{2+} (r = 1.42 Å).

Calcium borohydride. Four distinct polymorphs of calcium borohydride, denoted α-, α′-, β- and γ-$Ca(BH_4)_2$, are described, which are structurally related to polymorphs of TiO_2.[183–185] The orthorhombic polymorph, stable at RT, is α-$Ca(BH_4)_2$ ($F2dd$).[137] A second order phase transition at ~220 °C was described as a group–subgroup transition from $F2dd$ to $I\bar{4}2d$ for the polymorphs α- to α′-$Ca(BH_4)_2$.[137] At higher temperatures, the polymorphs α- and α′-$Ca(BH_4)_2$ transform to β-$Ca(BH_4)_2$ with a more complex structure described by two similar models $P4_2/m$[138] and $P\bar{4}$,[137] combining diffraction data and DFT optimization. The β-$Ca(BH_4)_2$ polymorph may have some dynamic motion of the BH_4 groups in the solid state, *e.g.* similar to the high-temperature h-$LiBH_4$ polymorph.[9,101] The high-temperature β-$Ca(BH_4)_2$ polymorph is 4–6% denser than α- and α′-$Ca(BH_4)_2$, and at room temperature it slowly converts back to orthorhombic α-$Ca(BH_4)_2$.[186] Solvent based synthesis methods provide another orthorhombic polymorph, γ-$Ca(BH_4)_2$, which irreversibly transforms to β-$Ca(BH_4)_2$ at $T \sim 320$ °C.[139] The crystal structures of all four $Ca(BH_4)_2$ polymorphs contain calcium cations coordinated by six borohydride anions forming octahedra, which suggests ionic bonding. However, the existence of non-densely packed polymorphs points towards some degree of directionality in the Ca–BH_4 bonding.

Magnesium borohydride. The extreme structural flexibility observed for metal borohydrides is highlighted in magnesium borohydride for which seven very different crystalline polymorphs are known: α-, β-, β′-, ε-, ζ-, γ- and δ-$Mg(BH_4)_2$.[3,106,128,129,134,187–189] The α-$Mg(BH_4)_2$ polymorph crystallizes in a large hexagonal unit cell a = 10.354 and c = 37.055 Å (originally reported in $P6_1$)[190,191] in the symmetry $P6_122$, confirmed by DFT and single-crystal diffraction.[106,192] Analysis of the initial $P6_1$ models shows that the determination of H-atom locations from powder data posed the main problem for identification of the correct symmetry. Solid α-$Mg(BH_4)_2$ contains an unoccupied volume of 6.4% within the structure.[106] These voids are, in principle, large enough

(37 Å^3) to accommodate a small molecule, such as H_2O. The α-polymorph transforms to an orthorhombic β-$Mg(BH_4)_2$ polymorph at $T > 220$ °C, which can be described in a super cell with *Fddd* symmetry, $a = 37.072$, $b = 18.6476$ and $c = 10.9123$ Å.[106,134,190] The high-temperature β-polymorph is ∼3% less dense and contains no unoccupied voids.

Solvent based synthesis using triethylamine borane or dimethyl sulfide borane complexes provide two different crystalline magnesium borohydride solvates.[3,56] The monoclinic solvate structure of $Mg(BH_4)_2{\cdot}1/2S(CH_3)_2$ is a 3D framework containing two Mg sites: one Mg is tetrahedrally coordinated to four BH_4 groups, and the other to four BH_4 groups and one $S(CH_3)_2$ ligand forming a trigonal bipyramid. The $S(CH_3)_2$ ligand can be extracted at moderate conditions ($T < 100$ °C), which provides the highly symmetric cubic structure of γ-$Mg(BH_4)_2$ ($Ia\bar{3}d$) (see Fig. 1), where a single Mg site is tetrahedrally coordinated to the BH_4 groups. The structure has a 3D network of interpenetrated channels and γ-$Mg(BH_4)_2$ is the first hydride to have a large permanent porosity. The empty volume in the structure amounts to ∼33%. The narrowest part of the pore channel is defined by a 5.8 Å distance between hydrogen atoms, but in contrast, a point at (1/8, 1/8, 1/8) in the structure is 3.56 Å away from the nearest H-atom, 4.12 Å from B and 4.82 Å from Mg. The framework topology of γ-$Mg(BH_4)_2$ is isomorphic to both a hypothetical zeolite type polymorph of SiO_2 and to a porous zinc imidazolate framework ZIF-72.[3,193] This is illustrated by the amorphisation of porous γ-$Mg(BH_4)_2$ at RT over time and recrystallization of γ-$Mg(BH_4)_2$ upon heating at $T = 80$ °C. Amorphisation of porous materials, *e.g.* metal organic frameworks (MOF) is a well-known feature, but recrystallization of a porous framework upon heating has possibly not been observed for any other material.[194]

Powder X-ray diffraction experiments conducted at elevated pressures, using diamond anvil cells, reveal extreme collapse of the α- and γ-$Mg(BH_4)_2$ structures upon compression,[195] equating to a ∼20% and ∼44% volume contraction, respectively. The compression of γ-$Mg(BH_4)_2$ displays the largest volume contraction observed, or predicted, for a hydride material. α-$Mg(BH_4)_2$ transforms to a new high pressure polymorph of magnesium borohydride denoted δ-$Mg(BH_4)_2$ at 1.1–1.6 GPa. Whereas highly porous γ-$Mg(BH_4)_2$ transforms to an X-ray amorphous material at 0.4–0.9 GPa and then to crystalline δ-$Mg(BH_4)_2$ at ∼2 GPa. The polymorph δ-$Mg(BH_4)_2$ has a tetragonal structure consisting of two interpenetrated $Mg(BH_4)_2$ frameworks (Fig. 1). Each framework resembles the cristobalite structure (a polymorph of SiO_2), whilst their doubly interpenetrated arrangement has a Cu_2O topology, which is typical for MOFs. This structural organization is stable on compression up to ∼15 GPa, upon decompression to 1 bar, and even on heating up to ∼100 °C at ambient pressure, where it then transforms to α-$Mg(BH_4)_2$.

All experimentally discovered $Mg(BH_4)_2$ polymorphs, and the lowest-energy theoretical structures, contain BH_4 coordinated by two Mg cations *via* opposite tetrahedral edges (η^2) with Mg–B–Mg angles deviating by 3–20° from linearity. The Mg···BH_4 interaction is highly directional and the Mg–BH_4–Mg fragments can be considered fundamental building units in all the structures. Magnesium atoms coordinate four BH_4 tetrahedra in a strongly deformed tetrahedral environment. Interestingly, Mg atoms only form a limited set of MgH_8 polyhedra where only the less uniform Johnson solids are found in the experimental structures.[196] ^{1}H and ^{11}B spin–lattice relaxation NMR studies of the BH_4 reorientational motion support the highly anisotropic BH_4···Mg interaction in α-$Mg(BH_4)_2$.[2] This contrasts the theoretically predicted structures, which always contain MgH_8 cubes.[3] The predicted $Mg(BH_4)_2$ structures also tend to be either highly porous or dense, *e.g.* the low-density $I\bar{4}m2$ ($\rho = 0.56$ g cm^{-3}) and $F222$ ($\rho = 0.54$ g cm^{-3}) structures, containing a single porous framework or a dense, doubly interpenetrated framework $I4_1/amd$ ($\rho = 1.01$ g cm^{-3}). Although these predicted structures are topologically similar to γ- and δ-$Mg(BH_4)_2$ (Fig. 1), they have not yet been observed experimentally.

Both experiments and theoretical predictions suggest vast polymorphism of $Mg(BH_4)_2$. Moreover, all the experimentally observed polymorphs are stable at ambient conditions and in relatively wide temperature and pressure ranges indicating that the reconstruction of strongly bound $Mg(BH_4)_2$ coordination frameworks is kinetically hindered. This may be due to the high stability of the linear Mg–BH_4–Mg units, linking the MgH_8 nodes into various framework structures, similar to partly covalently-bonded MOFs. The stability of $Mg(BH_4)_2$ polymorphs

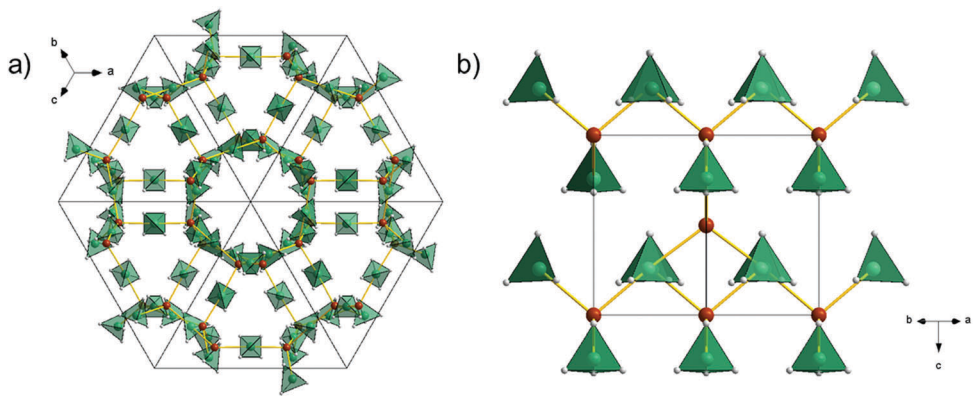


Fig. 1 The crystal structure of (a) porous γ-$Mg(BH_4)_2$, $\rho = 0.550$ g mL^{-1} and (b) the high-pressure δ-$Mg(BH_4)_2$, $\rho = 0.987$ g mL^{-1}.

 This journal is © The Royal Society of Chemistry 2017

may also be related to the relative stability of the MgH_8 polyhedra. Clearly, the BH_4 complexes act as directional ligands, similar to organic ligands ("linkers") with partly covalent coordination to metals in MOFs. The Mg–BH_4 interaction is directional and partly covalent and is essentially the reason for the MOF-like behaviour of $Mg(BH_4)_2$, *i.e.* the rich polymorphism and their relatively high stability, the large pressure-induced volume collapses, the amorphisation under pressure and the surprising recrystallization of porous structures from amorphous material. The unusual crystal chemistry and high structural complexity of $Mg(BH_4)_2$ is the most extreme case for metal borohydrides, but is typical for coordination polymers, such as MOFs.

3.2 Monometallic borohydrides with the d- and f-block

Stable metal borohydrides with the d-block metals can be prepared for metals, which in a low oxidation state, have the d-electron configurations, d^0, d^5 or d^{10}.[8] Scandium borohydride has not yet been obtained in pure form, but a series of alkali scandium bimetallic borohydrides, $MSc(BH_4)_4$, M = Li, Na, K, Rb, Cs are discussed in Section 3.5 of this review. Titanium borohydride, $Ti(BH_4)_3$ with d^1 configuration appears as an exception to this trend, but it is a molecular borohydride (see Section 3.3), with limited stability, decomposing at $T < 0$ °C. Transition metal borohydrides, $M(BH_4)_2$, M = Cr^{2+} (d^4), Fe^{2+} (d^6) and Co^{2+} (d^7) are stable in solution ($T < -30$ °C) but not yet in the solid state at RT.[94]

Yttrium borohydride. $Y(BH_4)_3$, has received significant interest as a hydrogen storage material due to the high gravimetric hydrogen content, $\rho_m(Y(BH_4)_3)$ = 9.07 wt% H_2, and moderate decomposition temperature, $T \sim 270$ °C. $Y(BH_4)_3$ exists as two polymorphs, α- and β-$Y(BH_4)_3$, both stable at ambient conditions.[144,145,197,198] Mechanochemical treatment of $LiBH_4$ and YCl_3 yields α-$Y(BH_4)_3$, and in some cases small amounts of β-$Y(BH_4)_3$. Solvent-based methods may provide a solvate $Y(BH_4)_3S(CH_3)_2$, which transforms to α-$Y(BH_4)_3$ during desolvation at $T \sim 140$ °C.[66] Transformation from α- to β-$Y(BH_4)_3$ is observed when heating in a narrow temperature interval, 190–200 °C, as decomposition begins at higher temperatures.[145,197] The high-temperature polymorph is stable on cooling.

α-$Y(BH_4)_3$ crystallizes in a cubic unit cell a = 10.7445 Å ($Pa\bar{3}$), whilst β-$Y(BH_4)_3$ crystallizes in a slightly larger cubic unit cell a = 11.0086 Å ($Fm\bar{3}c$).[145,197,199] The structure of β-$Y(BH_4)_3$ was initially suggested to be disordered primitive cubic, a = 5.4547 Å ($Pm3m$), based on SR-PXD data, but later defined as ordered in a supercell using powder neutron diffraction data.[145] The major difference between the two powder diffraction patterns is that the strongest reflection in PND data (531), which is the only reflection defining the doubled lattice parameter, is practically invisible in PXD data.[145,197] The cubic framework structures of the two polymorphs are closely related, yttrium being octahedrally coordinated to six BH_4 anions. In β-$Y(BH_4)_3$, the octahedral coordination of Y is regular but is somewhat distorted in α-$Y(BH_4)_3$. The $[Y(BH_4)_6]$ octahedra share corners and coordinate *via* Y–B–Y bridges where BH_4 units share edges (η^2) to yttrium, *i.e.* resulting in a 12-fold coordination of yttrium to hydrogen.[145] Furthermore, the high-temperature β-polymorph structure is 4.6% less dense than α-$Y(BH_4)_3$ and contains relatively large unoccupied voids of 39 Å^3, which are smaller in the low-temperature polymorph. The H···H repulsion seems to be at the origin of the polymorphic transition. The orientation of BH_4 groups in β-$Y(BH_4)_3$ slightly expands the structure and maximizes the H···H contacts, whereas half of the BH_4 complexes in α-$Y(BH_4)_3$ are flipped, allowing for a more densely packed structure, but with shorter H···H contacts (Fig. 2). This situation is somewhat similar to the disordered cubic alkali borohydrides, MBH_4 (M = Na–Cs), where the number of repulsive H···H contacts is minimized *via* a local ordering of the BH_4 groups at low temperatures.[56]

Manganese borohydride. $Mn(BH_4)_2$, (Mn^{2+}, d^5) was the first transition metal borohydride to be described, in 2009, denoted α-$Mn(BH_4)_2$, and is one amongst a total of four manganese borohydride polymorphs known to date.[21,58,140] The polymorph, α-$Mn(BH_4)_2$, was originally prepared mechanochemically from $MnCl_2$ and $LiBH_4$.[200] A different manganese borohydride solvate can be obtained using dimethylsulfide as the solvent, $Mn(BH_4)_2 \cdot 1/2S(CH_3)_2$, which is isostructural to the magnesium analogue, $Mg(BH_4)_2 \cdot 1/2S(CH_3)_2$. Gentle removal of the solvent provides a porous polymorph, γ-$Mn(BH_4)_2$ that is isostructural to the magnesium analogue, γ-$Mg(BH_4)_2$.[58] The unit cell volume of γ-$Mn(BH_4)_2$ is ~8.8% larger than that of the Mg-counterpart,[3] which corresponds well to the radius of Mn^{2+} (r = 0.80 Å) being larger than that of Mg^{2+} (r = 0.71 Å). Furthermore, SR-PXD data[58] indicate one or more unidentified compounds, which may be a manganese analogue of ε-$Mg(BH_4)_2$.[188] Thus, the structural chemistry of manganese borohydride resembles that of the magnesium analogue.

The structure of α-$Mn(BH_4)_2$ contains two independent Mn atoms both surrounded by four BH_4 units in a deformed tetrahedral coordination, whilst each BH_4 is nearly linearly coordinated by two Mn atoms *via* the opposite tetrahedral edges (η^2), exactly as observed for magnesium borohydrides. The structure of α-$Mn(BH_4)_2$ is also isostructural to ζ-$Mg(BH_4)_2$.[58] The structures of α-$Mn(BH_4)_2$

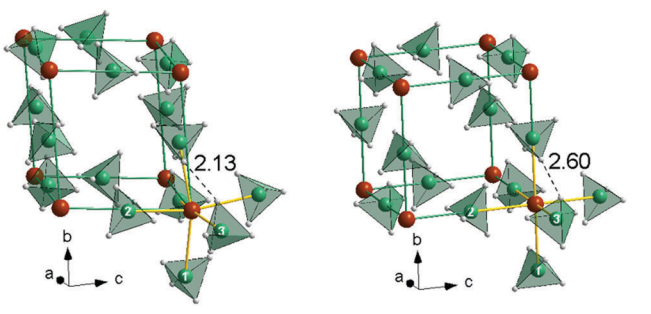


Fig. 2 Fragment (1/8 of the unit cell shown by green lines) of the crystal structure of the low-temperature α-$Y(BH_4)_3$ polymorph (left) and the high-temperature β-$Y(BH_4)_3$ polymorph (right). Both structures are viewed along the same direction of their respective cubic unit cells. While in the low-temperature polymorph the $(BH_4)_6$ octahedron around yttrium is deformed allowing for more efficient packing in the structure but with shorter H···H contacts (given in Å), the same octahedron in the high-temperature polymorph is regular with maximized H···H contacts and a less dense structure. The polymorphic transition is induced by flipping of three BH_4 groups labelled with white numbers.

and α-$Mg(BH_4)_2$ show similarity and both contain similar chiral layers, stacked along the *c*-axis, and rotated by 120° by the 3_1 axis in α-$Mn(BH_4)_2$ and by 60° by the 6_1 axis in α-$Mg(BH_4)_2$. Existence of a solid solution $Mg_xMn_{1-x}(BH_4)_2$ further illustrates the close similarity between manganese and magnesium borohydrides.[65] Similar to α-$Mg(BH_4)_2$, α-$Mn(BH_4)_2$ also has some degree of porosity in the structure and contains isolated voids with an estimated volume of 21 Å^3, occupying 6% of the structure volume.

At pressures above ~1 GPa, α-$Mn(BH_4)_2$ transforms into the high-pressure δ-phase having either $P\bar{4}n2$ or $I4_1/acd$ space group symmetry,[140] the latter shows the same ordering pattern for the BH_4 group as suggested by Yao and Klug for high-pressure $LiBH_4$.[179] δ-$Mn(BH_4)_2$ is quenchable to ambient pressure and shows a volumetric hydrogen density of 125 g H_2 L^{-1} at ambient conditions but turns back into the α-phase on heating to 67–109 °C. At pressure above 8.6 GPa, a δ′-phase with *Fddd* structure forms reversibly.

Cadmium borohydride. $Cd(BH_4)_2$ (Cd^{2+}, d^{10}) is another recently characterized monometallic borohydride with low and high temperature polymorphs, α- and β-$Cd(BH_4)_2$ and a first order polymorphic transition at $T \sim 55$ °C.[146] Both polymorphs consist of two identical interpenetrated three-dimensional frameworks built from Cd coordinated to four BH_4 units by edge sharing (η^2). Each Cd atom is coordinated almost linearly by two BH_4 complexes. The $[Cd(BH_4)_4]$ tetrahedra are slightly distorted in tetragonal α-$Cd(BH_4)_2$ whilst exhibiting ideal tetrahedral geometry in cubic β-$Cd(BH_4)_2$. The cubic β-$Cd(BH_4)_2$ has a Cu_2O-antitype structure with B and Cd on the positions of Cu and O, respectively, while α-$Cd(BH_4)_2$ has a tetragonally distorted structure, identical to the tetragonal high-pressure polymorph of magnesium borohydride δ-$Mg(BH_4)_2$.[3] The parent cubic structure has also been mentioned as a possible high-symmetry polymorph of $Mg(BH_4)_2$.[106,191]

Monometallic rare-earth borohydrides. Synthesis of $La(BH_4)_3$ and $Ce(BH_4)_3$ was initially conducted by mechanochemically facilitated metathesis reactions but without structural characterization.[201,202] A number of other monometallic rare-earth borohydrides are reported, which can be subdivided into two groups, those with oxidation state (III), isostructural to polymorphs of $Y(BH_4)_3$ and those with oxidation state (II), isostructural to $Sr(BH_4)_2$ or $Ca(BH_4)_2$. The later consists of $Sm(BH_4)_2$, $Eu(BH_4)_2$[68] and $Yb(BH_4)_2$ as was mentioned in Section 3.1. Samarium forms monometallic borohydrides both in oxidation state (II) and (III). Mechanochemical treatment of $SmCl_3$ and $LiBH_4$ reveals Bragg peaks corresponding to two primitive cubic unit cells with dimensions a = 11.10 Å ($Pa\bar{3}$) and a = 5.64 Å ($Pm\bar{3}m$).[147] The former is isostructural to α-$Y(BH_4)_3$ and the latter is isostructural to the initially reported structure for β-$Y(BH_4)_3$ from SR-PXD.[197]

Ytterbium reveals a similar structural diversity to samarium, forming borohydrides in both oxidation states (II) and (III), which are isostructural to known structure types.[150,163] In the oxidation state (II), β-$Yb(BH_4)_2$ and γ-$Yb(BH_4)_2$ are isostructural to β-$Ca(BH_4)_2$ and γ-$Ca(BH_4)_2$, respectively. Mechanochemical treatment of $YbCl_3$ and $LiBH_4$ yields α-$Yb(BH_4)_3$ and β-$Yb(BH_4)_3$ that are isostructural to α-$Y(BH_4)_3$ and β-$Y(BH_4)_3$. Erbium borohydride also forms two polymorphs, α-$Er(BH_4)_3$ and β-$Er(BH_4)_3$, isostructural to yttrium borohydride analogues (Fig. 2).

However, the rare-earths gadolinium, terbium and dysprosium each only form one polymorph ($Pa\bar{3}$) $Gd(BH_4)_3$, $Tb(BH_4)_3$ and $Dy(BH_4)_3$, which are isostructural to α-$Y(BH_4)_3$,[144,147] but a high temperature polymorph may also exist for $Gd(BH_4)_3$.[203]

3.3 Strongly covalent molecular monometallic borohydrides

Several monometallic borohydrides appear to have prevailingly covalent bonding and directionality in the M–BH_4 coordination. The first example is beryllium borohydride, $Be(BH_4)_2$, known in one very unique structural form.[105] The tetragonal structure was investigated by single-crystal X-ray diffraction and reveals trigonal-planar coordinated beryllium by three edge-sharing BH_4 groups, *i.e.* beryllium has an unusually high coordination number of six hydrogen atoms in the nearest coordination sphere. Two borohydride complexes are bridging beryllium with linear Be–B–Be geometry and edge sharing (η^2) coordination. Another borohydride anion also coordinates to Be by edge sharing (η^2) but is terminal with two dangling hydrogen atoms. The structure is built from one-dimensional polymeric chains held together by weak interactions. This is illustrated by the fact that beryllium borohydride is reported to have a significant vapour pressure at RT and readily sublimes, which illustrates that there are weak intermolecular interactions and that the polymeric chains dissociate easily. In the gas phase, beryllium borohydride $Be(BH_4)_2$ may be a molecular compound, with face-sharing BH_4 (η^3) and the same coordination of beryllium, CN(Be) = 6. Furthermore, the compound is unusually reactive and pyrophoric due to the characteristic three-centre-two-electron bonds in the Be–H–B contacts,[204] similar to diborane, B_2H_6. $Be(BH_4)_2$ is also extremely poisonous like other beryllium compounds.[105] The highest gravimetric hydrogen density of a metal borohydride is observed for $Be(BH_4)_2$, $\rho_m(Be(BH_4)_2)$ = 20.8 wt% H_2 (Table 2), which also has the second-highest volumetric hydrogen density for metal borohydrides, $\rho_V(Be(BH_4)_2)$ = 127 g H_2 L^{-1}.

The most strongly polarizing cations form molecular monometallic borohydride structures, *e.g.* Ti^{3+}, Al^{3+} with electronegativity $\chi_p \sim 1.5$ and Zr^{4+} and Hf^{4+} with $\chi_p \sim 1.3$. The structures of both zirconium and hafnium borohydride are isostructural molecular metal borohydrides and consist of isolated neutral $M(BH_4)_4$ units (Fig. 3) having low sublimation temperatures, $T_{sub}(Zr(BH_4)_4)$ = 29 °C.[109,126,127] The tetrahedral molecules of Zr and Hf borohydrides are analogous to the methane molecule where each BH_4 complex coordinates *via* face sharing (η^3) to the metal with one dangling hydrogen atom and the solids have primitive cubic unit cells. The experimental structural data clearly supports previous assumptions that solid $Zr(BH_4)_4$ consists of discrete neutral molecules interacting mainly by weak van der Waals and dispersion interactions. The shortest distance between neighbouring molecules in the solid is defined by the intermolecular H···H distances of 2.77 Å. Four hydrogen atoms point towards the center of the unit cell, being responsible for the intermolecular interactions in the crystal structure.[109]

 This journal is © The Royal Society of Chemistry 2017

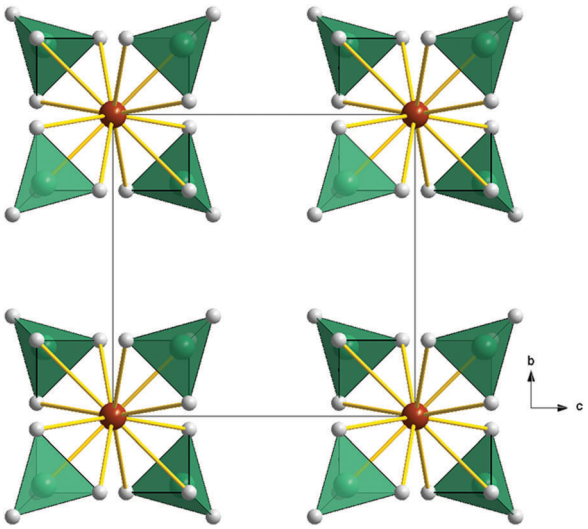


Fig. 3 Illustration of the cubic crystal structure of $Zr(BH_4)_4$.

Aluminum borohydride. Aluminum borohydride is another molecular metal borohydride, consisting of discrete $Al(BH_4)_3$ units, that was characterized in 1997.[107] Aluminum borohydride has a high gravimetric hydrogen content, ρ_m = 16.8 wt% H_2, but is volatile and pyrophoric with a tendency to release diborane at RT and therefore very challenging to handle and utilize in practical applications.[205]

Titanium borohydride. Titanium borohydride, $Ti(BH_4)_3$ is of high interest as the only genuine transition metal borohydride with an open set of d-orbitals (d^1 electron configuration), and despite many published reports on this compound the solid state structure remains unknown.[151,206] However, the gas phase structure has been characterized by electron diffraction,[20] which reveals monomeric $Ti(BH_4)_3$ species with BH_4 face sharing to the metal center (η^3) with an overall C_{3h} symmetry. The tridentate bonding in volatile $Ti(BH_4)_3$ has been confirmed by vibrational spectroscopy[20] and calculated structural optimizations.[207,208] Though following a tridentate coordination-scheme in the gas phase, in some molecular compounds such as $[Li(Et_2O)_2][Ti_2(BH_4)_5(PMe_2Ph)_4]$,[209] titanium centres are bridged by bidentate BH_4 (η^2), thus forming one dimensional chains of linked metal centres. These chains can be considered as dimers $[Ti_2(BH_4)_6]$ being linked by Li, also *via* bidentate BH_4 (η^2). Pronounced aggregation of $Ti(BH_4)_3$ molecules has also been suggested to occur in the solid state for titanium borohydride implying that the predominant species is the dimer $[Ti(BH_4)_3]_2$.[20] Titanium borohydride rapidly decomposes at room temperature but has recently been stabilized through incorporation into a metal–organic framework (MOF).[210]

3.4 Bimetallic s-block borohydrides

The majority of the recently discovered bimetallic borohydrides consist of complex metal borohydride anions counter-balanced by alkali cations. In all these structures the more electronegative metal constitutes the central atom in the complex anion by coordination to a number of borohydride units, as for instance $[Mg(BH_4)_4]^{2-}$. The formation of discrete complex anions can be considered as a consequence of the electronegativity difference between the two metals in the structures, which causes formation of partly covalent bonds between the more electronegative metal and the BH_4 units. This contrasts bi-alkali metal borohydrides where the interaction is rather ionic. Series of bimetallic borohydrides have been discovered and are subdivided here in three groups, those based on s-block metals only, those based on a d- or f-block metals and typically an alkali metal and those based on a p-block metal and an alkali metal. This review focuses on series of compounds in order to aim at analyzing trends in structures and properties.

Bi-alkali metal borohydrides. The first bimetallic borohydride was discovered in 2008, lithium potassium borohydride, $LiK(BH_4)_2$, which has an ionic structure due to similarities in electronegativity of the two metals.[130] Lithium and potassium coordinate to four and seven BH_4 tetrahedra, respectively. The structure can be regarded as built from anionic layers $[Li(BH_4)_2]^-$ cut from an o-$LiBH_4$ framework and intercalated by K^+ cations. The decomposition temperature for this compound is nearly an average of those for the two individual borohydrides.

Sodium potassium borohydride, $NaK(BH_4)_2$, was initially described as a stoichiometric compound,[211] but was later shown to be a solid solution $Na_xK_{1-x}BH_4$, $0 < x < 1$, stable in the temperature range $200 < T < 450$ °C. The solid solution, $Na_xK_{1-x}BH_4$, $0 < x < 1$, is metastable at RT and phase-separates into the monometallic borohydrides at RT within 24 h.[93]

Lithium rubidium and lithium cesium borohydrides. The phase diagram $LiBH_4$–ABH_4 (A = Rb, Cs) has to date revealed ten compounds $Li_iA_j(BH_4)_{i+j}$ (A = Rb, Cs), with i, j ranging between 1 and 3. Amongst these, eight new structure types of homoleptic borohydrides are found. The Li–BH_4 substructure adopts various topologies as a function of the compound's Li content, ranging from one-dimensional isolated chains to three-dimensional networks. The coordination environment around the Li-node is either triangular or tetrahedral in these sublattices, and various compounds of this series contain the rare connectivity of edge-sharing $Li(BH_4)_4$-tetrahedra, following the building principle of $LiKMg(BH_4)_4$,[172] where a charged, layered, honeycomb-like substructure $LiMg(BH_4)_4^-$ is charge-balanced by the larger K^+ counter-cation. Such substructures may suggest that, next to Mg^{2+}, Li^+ may have potential to participate in framework building with the tetrahydroborate anion, BH_4^-, as a linker, if the framework is stabilized by large electropositive counter-cations.

Alkali and alkaline earth bimetallic borohydrides. No bimetallic borohydrides between Li or Na and Mg have been observed. This may be understood when considering the preferred coordination polyhedra of the different cations. (4,4)-Connected tetrahedral Li–Mg frameworks cannot form without countercations, *i.e.* other than as trimetallic borohydrides.[172] Sodium cations are readily accommodated in octahedral coordination but do not adopt higher coordination numbers, which explains why the structural analogues to K–Mg borohydrides do not exist for sodium.

Two bimetallic potassium magnesium borohydrides have been discovered in the KBH_4–$Mg(BH_4)_2$ system, namely $K_2Mg(BH_4)_4$

and $K_3Mg(BH_4)_5$.[164] The structure of $K_2Mg(BH_4)_4$ is isostructural to $K_2Mn(BH_4)_4$ and built from distorted tetrahedral $[Mg(BH_4)_4]^{2-}$ complex anions. The BH_4 anions share an edge with Mg (η^2) similar to all polymorphs of $Mg(BH_4)_2$. Potassium ions form a K_{11} cage (Edshammar polyhedron) around the complex anions. Structural similarities for the series of isostructural bimetallic borohydrides $K_2M(BH_4)_4$ (M = Mg, Mn, Zn, Cd) are discussed later in this section of the review.

The structure of $K_3Mg(BH_4)_5$ is orthorhombic ($P4_2bc$) and has an intriguing nature that can be described as an intergrowth of KBH_4 and $K_2Mg(BH_4)_4$. Interestingly, the BH_4 complexes occur in two different environments, forming complex anions $[Mg(BH_4)_4]^{2-}$ similar to those observed in the structure of $K_2Mg(BH_4)_4$ and with a second boron position only coordinating to potassium. This latter BH_4 is octahedrally coordinated, strongly resembling the local environment of BH_4 in KBH_4, which crystallizes in the rock salt structure as described in Section 3.1. The second component, building up the intergrowth of $K_3Mg(BH_4)_5$, is a bicapped trigonal prism of K_8, surrounding the composite anions of $[Mg(BH_4)_4]^{2-}$ and interconnected *via* common edges.[164]

Alkali metal calcium borohydrides. The heavier alkali metal borohydrides, MBH_4, M = K, Rb and Cs, readily react with calcium borohydride and form perovskite-type metal borohydrides (Fig. 4).[1,193] The compounds all have the same composition $MCa(BH_4)_3$, M = K, Rb, Cs, and each exists in at least two polymorphs, see Fig. 4. Furthermore, a perovskite type solid solution is also described, $RbCa_xMg_{1-x}(BH_4)_3$.[1]

Alkali metal strontium borohydrides. Alkali metal strontium borohydrides are also found to form perovskite-type compounds, $MSr(BH_4)_3$, M = K, Rb, Cs.[165] The alkali-Ca and alkali-Sr borohydrides are the only two series where all three metal cations (K, Rb, Cs) stabilize the perovskite structure type. Interestingly, the Ca-compounds reveal decreasing symmetry across their high temperature polymorphic transitions.[1] In contrast, the Sr-perovskites have increasing symmetry and the ambient temperature Sr-polymorphs are lower in symmetry than their Ca-analogues. This suggests that the Sr cation is too large to stabilize the ideal cubic perovskite type structure, and that the Ba-cation will come to lie outside the stability criteria of this structure type amongst borohydrides.

3.5 Bimetallic d- and f-block borohydrides

Alkali metal scandium borohydrides. The structure of $LiSc(BH_4)_4$ was the first bimetallic borohydride containing discrete anions to be characterized in 2008, while two other members of the series, $NaSc(BH_4)_4$ and $KSc(BH_4)_4$, were described in 2010 (Fig. 5).[80,81,166] Mono-metallic scandium borohydride, $Sc(BH_4)_3$, has not yet been prepared nor structurally characterized. $LiSc(BH_4)_4$ is tetragonal ($P\bar{4}2c$),[81] $NaSc(BH_4)_4$ is orthorhombic (*Cmcm*) with the HT-$CrVO_4$ structure type and $KSc(BH_4)_4$ is also orthorhombic (*Pnma*) but with a $BaSO_4$ type structure.[80,166] Scandium–boron distances and B–Sc–B angles in the tetrahedral geometry of $[Sc(BH_4)_4]^-$ in $NaSc(BH_4)_4$ are relatively regular and resemble the almost ideal tetrahedral $[Sc(BH_4)_4]^-$ anion, found by DFT optimization.[81] The $[Sc(BH_4)_4]^-$ anion is slightly distorted in $KSc(BH_4)_4$ and more deformed in the structure of $LiSc(BH_4)_4$. The Sc–B distances (2.27–2.50 Å) are similar in all three known alkali metal scandium borohydrides and compare well to those in the tetrahedral molecular compounds $Zr(BH_4)_4$ and $Hf(BH_4)_4$.[19,109,126,127] In all three scandium-based compounds, the $[Sc(BH_4)_4]^-$ anion is located inside alkali metal cages, *i.e.* tetragonal Li_8 prisms (all prisms occupied) in $LiSc(BH_4)_4$, slightly deformed trigonal Na_6 prisms (each second prism occupied) in $NaSc(BH_4)_4$ and monocapped trigonal K_7 prisms (all prisms occupied) in $KSc(BH_4)_4$. Note that the Li position is disordered along the *c*-axis in $LiSc(BH_4)_4$ and therefore the exact shape of the Li_8 polyhedra cannot be determined. The primary building principle in $NaSc(BH_4)_4$ and $KSc(BH_4)_4$ consists of packing Na^+/K^+ cations and $[Sc(BH_4)_4]^-$ anions. The BH_4 complex coordinates to Sc by edge sharing (η^2) forming a dominantly covalent bond whereas alkali metal ions tend to coordinate to the complex anions with a dominantly ionic coordination.

Alkali metal yttrium borohydrides. Discrete complex $[Y(BH_4)_4]^-$ ions have been shown to exist in $MY(BH_4)_4$, produced by ball milling $Y(BH_4)_3$–3LiCl mixtures and MBH_4 (M = K, Rb or Cs).[167,171] $KY(BH_4)_4$ is isostructural to $NaSc(BH_4)_4$ (*Cmcm*),[167] whereas $RbY(BH_4)_4$ and $CsY(BH_4)_4$ form unique structures.[171] $RbY(BH_4)_4$ crystallizes in monoclinic unit cell ($P2_1/c$) with a $AgMnO_4$ structure type, which is a deformation of the $BaSO_4$-type structure. There are seven Rb^+ cations located around each $[Y(BH_4)_4]^-$ and seven

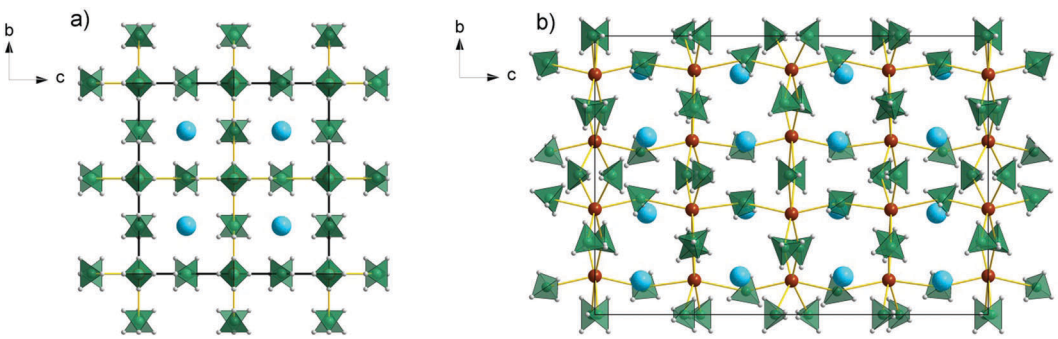


Fig. 4 Crystal structure of (a) the ordered room temperature polymorph of $CsCa(BH_4)_3$ and (b) of the modulated high temperature polymorph of $RbCa(BH_4)_3$. Ca (brown), Rb, Cs (blue), BH_4 (green).

 This journal is © The Royal Society of Chemistry 2017

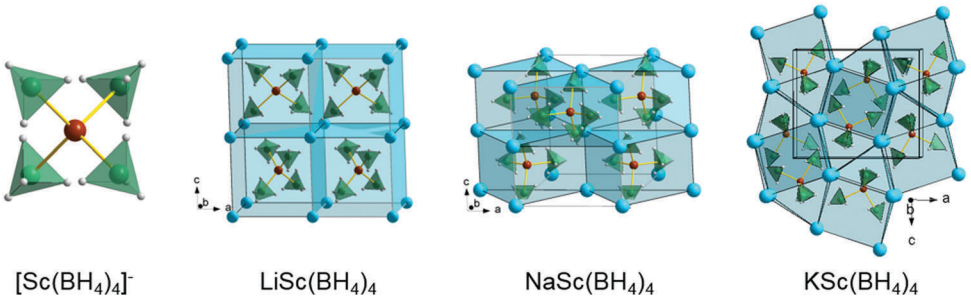


Fig. 5 Tetrahedral complex anion $[Sc(BH_4)_4]^-$, and the packing inside Li_8 square prisms, Na_6 triangular prisms and K_7 mono-capped triangular prisms of respective alkali scandium borohydrides.

$[Y(BH_4)_4]^-$ anions around Rb^+ forming slightly distorted mono-capped trigonal prisms. $CsY(BH_4)_4$ is tetragonal ($I4_1/a$) with a $CaWO_4$-scheelite structure type. Cs^+ is surrounded by eight BH_4 groups forming a distorted dodecahedron (snub disphenoid). While these structures were originally studied on chloride-containing samples, hence the solution of chloride on borohydride sites cannot be excluded, chlorine-free samples later allowed for additional analysis.[78] It was found that $KY(BH_4)_4$ also crystallizes in a monoclinic ($C2/c$) structure with an octahedral coordination of Y, and $RbY(BH_4)_4$ crystallizes in the regular $BaSO_4$ structure type. Double perovskites $A_3Y(BH_4)_6$ (A = Rb, Cs) were also observed.[1] Recently, also $LiY(BH_4)_4$ and $NaY(BH_4)_4$ have been prepared by thermal treatment and the two compounds were found to be isostructural to $LiSc(BH_4)_4$ and $NaSc(BH_4)_4$, respectively.[62,161]

Alkali metal manganese borohydrides. A bimetallic potassium manganese borohydride was synthesized in the KBH_4–$Mn(BH_4)_2$ system, $K_2Mn(BH_4)_4$, which is isostructural to $K_2Mg(BH_4)_4$ and is indexed in a monoclinic cell as discussed above. Structural similarities between the series of isostructural bimetallic borohydrides $K_2M(BH_4)_4$ (M = Mg, Mn, Cd) are discussed later in this section. The decomposition of $K_2Mn(BH_4)_4$ has been shown to generate KBH_4 and a new compound $KMn(BH_4)_3$ identified as a perovskite type metal borohydride.[164] Later, the compound $CsMn(BH_4)_3$ (Cc) was also noticed to have the perovskite type structure.[1]

Alkali metal zinc borohydrides. Several alkali metal zinc borohydrides have been characterized in which zinc coordinates trigonally, in a planar fashion, to three BH_4 units forming complex discrete anions, as for example $MZn(BH_4)_3$ (M = Na or K) containing $[Zn(BH_4)_3]^-$.[70,85] The Zn–BH_4 (η^2) coordination is significantly more directional and covalent in contrast to the alkali metal Na^+ or K^+ coordination. The trigonal coordination in $[Zn(BH_4)_3]^-$ anions in $KZn(BH_4)_3$ is more regular than those in $NaZn(BH_4)_3$. Interestingly, the Zn–B distance of 2.573 Å in $KZn(BH_4)_3$ is similar to the average of the three shortest Zn–B distances of 2.56 Å in $NaZn(BH_4)_3$. In both compounds the $[Zn(BH_4)_3]^-$ anions are located in Na_8 or K_8 cubes and the alkali cations coordinate to six BH_4 units in a trigonal prism. However, the coordination of the BH_4 unit by the cations differs in these two compounds, *i.e.* in $NaZn(BH_4)_3$ the BH_4 units coordinate either almost linearly to one Na and one Zn atom, triangular planar to one Zn and two Na atoms or to one Zn and three Na atoms in a tetrahedral geometry, while in $KZn(BH_4)_3$ only the triangular coordination is observed.

The more zinc-rich alkali zinc borohydrides, $MZn_2(BH_4)_5$ (M = Li or Na) also exhibit similar general structural topologies consisting of two identical interpenetrated three-dimensional frameworks.[70,158] This type of structural topology is common for the coordination polymers involving organic ligands, such as MOFs,[128] however observed for the first time in hydrides in this case. Alternatively, the structures of $MZn_2(BH_4)_5$ (M = Li or Na) can be considered to be built from dinuclear complex ions, $[Zn_2(BH_4)_5]^-$ and alkali metal ions. The $MZn_2(BH_4)_5$ structures reveal strong and directional Zn–BH_4 bonding by edge sharing (η^2) that defines the structural architecture. The Zn atoms in both compounds have a triangular, nearly planar, coordination by three BH_4 groups, similar to Zn in $NaZn(BH_4)_3$ and $KZn(BH_4)_3$. The Li and Na atoms in $LiZn_2(BH_4)_5$ and $NaZn_2(BH_4)_5$ have a saddle-like coordination to four BH_4 units. All BH_4 groups in the $MZn_2(BH_4)_5$ structures are almost linearly coordinated by two metal atoms, either bridging the two zinc atoms in $[Zn_2(BH_4)_5]^-$ or coordinating to one Zn and one M atom. Furthermore, $LiZn_2(BD_4)_5$ has been studied by PND, revising the orientation of one of the BD_4 groups, revealing that the coordination mode for the BD_4 units to both Zn and Li corresponds to the cation$\cdots D_2B$ (η^2) coordination scheme,[158] which is supported by DFT calculations.[157]

Alkali metal cadmium borohydrides. The potassium cadmium borohydride, $KCd(BH_4)_3$, has an interesting 3D polymeric framework topology and contains a complex anion, $[Cd(BH_4)_3]_n^{n-}$ built from corner-sharing $Cd(BH_4)_4$ tetrahedra and $Cd(BH_4)_6$ octahedra. All six BH_4 units in the $[Cd(BH_4)_6]$ octahedra are coordinated almost linearly by another Cd atom from the neighbouring $Cd(BH_4)_4$ tetrahedra, whereas two of the four BH_4 units within the $[Cd(BH_4)_4]$ tetrahedra are terminal. The structure of $KCd(BH_4)_3$ can also be described as a garnet, with K on dodecahedral and octahedral sites, and Cd on octahedral and tetrahedral sites. In contrast, the structure of $K_2Cd(BH_4)_4$ is built from discrete $[Cd(BH_4)_4]^{2-}$ anions counter-balanced by K^+ cations. In the complex anion the Cd atom is coordinated to four BH_4 units in a distorted tetrahedral geometry.[146] The structure of $K_2Cd(BH_4)_4$ resembles that of $MSc(BH_4)_4$ (M = Li, Na and K) and $K_2M(BH_4)_4$ (M = Mg, Mn, Cd) as discussed below.

Electronic and size effects stabilizing tetrahedral complex anions based on bivalent metals. The compounds containing tetrahedral complex anions of the type $[M^{m+}(BH_4)_4]^{(4-m)-}$ (m = 2, 3) are based either on a trivalent cation M such as Sc^{3+}, Y^{3+}, Al^{3+}, Ho^{3+}, Yb^{3+}, Lu^{3+} or on a bivalent cation such as Mg^{2+}, Mn^{2+}, Zn^{2+}, Cd^{2+},

and have already been discussed. Alkali metals often act as counter-cations in these compounds and stabilise the composite anions with a metal center.

The compounds $K_2M(BH_4)_4$ (M = Mg, Mn, Zn, Cd) all represent monoclinically distorted variants of β-K_2SO_4, *i.e.* M and BH_4 occupying the S- and O-positions, respectively and thus replacing the sulphate tetrahedron by a complex anion $[M(BH_4)_4]^{2-}$, with consistently bidentate bonding scheme M···H_2B (η^2). DFT calculations performed on $K_2M(BH_4)_4$ (M = Mg),[164] suggest high stability of the complex anion. DFT structural optimizations reveal that the inner B–H distances are longer than the outer ones, while the H–B–H angle is smaller on the BH_4 edge facing the Mg metal centre.[164] As discussed above, the coordination environment of $[M(BH_4)_4]^{2-}$ is best described as a pentacapped trigonal prism (Edshammar polyhedron, K_{11}), The idealized MK_{11} building block is undistorted in the compound β-K_2SO_4.

Analysis of the relative interatomic distances K–B/M–B in the above mentioned compounds provides some insight to the structural differences caused by differences in metal Pauling electronegativity and ionic radii.[164] A general trend shows that 'the degree of isolation' (*i.e.* the extent to which the crystal should be described on the basis of the complex anion rationalization rather than a framework), as defined by the K-B/M-B ratio, decreases from 1.41 in the Mn compound to 1.11 in the Cd compound.

Interestingly, the volume of the MK_{11} cage, as well as the M–H bonding mode, remain nearly identical, within errors, in $K_2Mg(BH_4)_4$ and $K_2Mn(BH_4)_4$ while the volume of $[M(BH_4)_4]^{2-}$ varies significantly, *i.e.* 7.17 and 7.69 Å^3 for Mn and Mg, respectively (Table 5). This contrasts the fact that the divalent manganese ion, $r(Mn^{2+})$ = 0.80 Å is larger than magnesium $r(Mg^{2+})$ = 0.71 Å. This is attributed to electronic effects, the electronegativity of Mn (1.55) being closer to that of BH_4^- (group electronegativity 2.13) than Mg (1.31), thus driving covalent bonding within the complex anion.[212]

Another compound containing an isolated tetrahedral complex anion is found in this system, $K_3Mg(BH_4)_5$. Bidentate bonding is retained, while the isolation of $[Mg(BH_4)_4]^{2-}$ is increased to 1.45[164] due to the larger coordination polyhedron K_{12}. In this compound, an isolated BH_4 not pertaining to the complex anion, is positionally and orientationally disordered. A repulsive interaction between this BH_4 and the terminal ones of $[Mg(BH_4)_4]^{2-}$ takes place at higher temperatures, ~87 °C, resulting in reorientation of $[Mg(BH_4)_4]^{2-}$ that in turn triggers a symmetry change. Perovskite-type $KMn(BH_4)_3$ forms as a reaction product in the K–Mn system. In the perovskite, Mn is no longer tetrahedrally coordinated, most likely due to enhanced thermal vibration and thus simulated size increase of the metal centre. This phase only exists at high temperatures, which supports this assumption.

Alkali rare-earth bimetallic borohydrides. Significant attention has been devoted to the synthesis and characterization of novel mono- and bimetallic rare-earth based metal borohydrides since the discovery of $LiSc(BH_4)_4$ and $Y(BH_4)_3$ in 2008.[81,144] Rare-earth metal (RE) borohydrides of all rare-earth metals (with the exception of promethium) have been structurally, physically and chemically characterized and many trends in properties appear to follow the size of the rare-earth metal ions, see Table 6. In bimetallic RE-bearing compounds based on Li, the smaller elements: scandium, ytterbium and lutetium crystallize as $LiRE(BH_4)_4$, which are isostructural to $LiSc(BH_4)_4$, whereas the larger elements from lanthanum to samarium all form $LiRE(BH_4)_3Cl$ compounds, which are discussed in Section 4.1. The moderately sized RE metals tend to crystallize with single cation structures similar to α- and β-$Y(BH_4)_3$. The most rich variation of structure types is observed for the stoichiometry $ARE(BH_4)_4$, where A is an alkali metal. Small and medium size RE form different structure types in this manner whilst the large RE do not form structures with this stoichiometry, but instead prefer

Table 5 Comparison of the local environments of the complex tetrahedral anions $[M(BH_4)_4]_2^-$ with M = Mg, Mn, Zn and Cd[164]

Compound	Average M–B (Å)	B–K/M–B (Å)	$V(MK_{11})/V(MB_4)$
$K_2Mg(BH_4)_4$	2.4544(51)	1.41	36.61
$K_2Mg(BH_4)_4$	2.5027(31)	1.38	34.33
$K_2Zn(BH_4)_4$	2.466(17)	1.33	31.85
$K_2Cd(BH_4)_4$	2.881(10)	1.11	24.02
$KSc(BH_4)_4$	2.3204(3)	1.64	31.56
$K_3Mg(BH_4)_5$	2.4369(77)	1.45	38.23 $V(MK_{12})/V(MB_4)$

Table 6 Relationship between the size of a trivalent rare-earth metal cation and the structure type of the corresponding binary and ternary alkali rare-earth metal borohydrides with the composition ABX_4

RE ion	Ion radius (Å)[213]	$LiRE(BH_4)_4$	$NaRE(BH_4)_4$	$KRE(BH_4)_4$	α-$RE(BH_4)_3$	β-$RE(BH_4)_3$	$LiRE(BH_4)_3Cl$	Ref.
Sc^{3+}	0.885	$P\bar{4}2c$ ($CuAlCl_4$)	*Cmcm* (ht-$CrVO_4$)	*Pnma* ($BaSO_4$)				80, 81 and 166
Lu^{3+}	1.001	$P\bar{4}2c$ ($CuAlCl_4$)						147
Yb^{3+}	1.008	$P\bar{4}2c$ ($CuAlCl_4$)	*Cmcm* (ht-$CrVO_4$)	*Cmcm* (ht-$CrVO_4$)	$Pa\bar{3}$ (ReO_3)	$Fm\bar{3}c$ (ReO_3)		150 and 163
Er^{3+}	1.03				$Pa\bar{3}$ (ReO_3)	$Fm\bar{3}c$ (ReO_3)		147
Y^{3+}	1.04	$P\bar{4}2c$ ($CuAlCl_4$)	*Cmcm* (ht-$CrVO_4$)	*Cmcm* (ht-$CrVO_4$) *C2/c* ($LaNbO_4$)	$Pa\bar{3}$ (ReO_3)	$Fm\bar{3}c$ (ReO_3)		62, 78, 144, 145, 167 and 197
Ho^{3+}	1.041			*Cmcm* (ht-$CrVO_4$)	$Pa\bar{3}$ (ReO_3)	$Fm\bar{3}c$ (ReO_3)		148
Dy^{3+}	1.052				$Pa\bar{3}$ (ReO_3)			144
Tb^{3+}	1.063				$Pa\bar{3}$ (ReO_3)			147
Gd^{3+}	1.078			$P2_1/c$ ($LiMnF_4$)	$Pa\bar{3}$ (ReO_3)		$I\bar{4}3m$ (spinel)	50, 88, 144 and 147
Sm^{3+}	1.098				$Pa\bar{3}$ (ReO_3)	$Fm\bar{3}c$ (ReO_3)	$I\bar{4}3m$ (spinel)	147
Nd^{3+}	1.123						$I\bar{4}3m$ (spinel)	147
Pr^{3+}	1.13						$I\bar{4}3m$ (spinel)	147
Ce^{3+}	1.15				$R\bar{3}c$ (ReO_3)		$I\bar{4}3m$ (spinel)	1, 4 and 168
La^{3+}	1.172		*Pbcn*		$R\bar{3}c$ (ReO_3)		$I\bar{4}3m$ (spinel)	88 and 162

This journal is © The Royal Society of Chemistry 2017

to crystallize as double-perovskites with the formula $A_3RE(BH_4)_6$. Different stoichiometries such as $K_2Gd(BH_4)_5$ with square pyramidal and trigonal double pyramidal complex cations have also been observed. As for bivalent RE such as Sm^{2+}, Eu^{2+} and Yb^{2+} they adopt the structures of alkali-earth borohydrides: the one of $Sr(BH_4)_2$ for the larger Sm^{2+} and Eu^{2+} whilst that of $Ca(BH_4)_2$ for the smaller Yb^{2+}.

3.6 Bimetallic p-block borohydrides

Alkali p-block borohydrides. Mechanochemical treatment of $AlCl_3$–$LiBH_4$ and $AlCl_3$–$NaBH_4$ produce chloride containing alkali aluminium borohydrides $Li_4Al_3(BH_4)_{\sim 9}Cl_{\sim 4}$ and $NaAl(BH_4)_{\sim 1}Cl_{\sim 3}$, which are further discussed in Section 4.2.[159,214] The chloride-free synthesis by the spontaneous reaction of aluminium borohydride with alkali borohydrides results in different structures that are, however, based on the same tetrahedral complex anion $[Al(BH_4)_4]^-$ with tridentate binding as seen in the chloride syntheses (with the exception of lithium).[169,205] The reaction between $LiBH_4$ and $Al(BH_4)_3$ produces a framework structure $LiAl(BH_4)_4$ with both cations tetrahedrally coordinated and resembling the framework of RT o-$LiBH_4$. The sodium compound $NaAl(BH_4)_4$ crystallizes with a monoclinic structure that is a deformation of the orthorhombic type ht-$CrVO_4$ also known for $NaSc(BH_4)_4$. Larger alkali metals K and Rb crystallize with the orthorhombic structure type of $TbAsO_4$, observed for potassium for the first time.[160] The larger $CsAl(BH_4)_4$ crystallizes with the $CaWO_4$-scheelite type known from $CsY(BH_4)_4$. Cesium lead borohydride, $CsPb(BH_4)_3$, is hitherto the compound containing the most electronegative metal, $\chi_P = 1.8$, which crystallizes with a perovskite type structure.[1]

3.7 Tri-metallic borohydrides

Trimetallic borohydrides with cation disorder. The first trimetallic homoleptic borohydride compounds, $Li_3MZn_5(BH_4)_{15}$, M = Mg and Mn, were presented in 2013 and are also new cationic solid solutions (see Table 4).[83] The two compounds are isostructural and were structurally investigated using *in situ* SR-PXD and PND, which provides an average view of the structure as hexagonal, a = 15.371, and c = 8.586 Å, ($P6_3/mcm$) for the Mg-compound at RT. Interestingly, DFT optimization suggests locally ordered models in an ortho-hexagonal unit cell, which maximize Mg–Mg separation. Thus, the hexagonal structure observed by diffraction may be a superposition of three such orthorhombic structures in three orientations along the hexagonal c-axis. The framework in $Li_3MZn_5(BH_4)_{15}$ is of the **mco**-topological type, and contains channels built from face sharing $[M(BH_4)_6]$ octahedra with triangularly coordinated lithium occupying the faces, and consists of two interpenetrated frameworks of **tfa**-type (Fig. 6). The framework type is related to bimetallic $LiZn_2(BH_4)_5$ with cation disorder (Li/Mg) on the Li-position. The new borohydrides $Li_3MZn_5(BH_4)_{15}$ are potentially interesting as solid state electrolytes, if the lithium mobility within the octahedral channels is improved by disordering the site *via* heterovalent substitution. The two compounds decompose *via* formation of the more stable mono- and bimetallic borohydrides.[83]

Alkaline earth alkali trimetallic borohydrides. The five trimetallic compounds $ALiM(BH_4)_4$ (A = K or Rb; M = Mg or Mn) and $K_3Li_2Mg_2(BH_4)_9$ represent the first two-dimensional topologies amongst homoleptic borohydrides. The layered substructure is formed from negatively charged Li–Mg 4-connected networks (Fig. 7), which can be rationalized as a honeycomb-like sheet of edge- and corner-sharing tetrahedra. On their basis, the general chemistry of hypothetical, long sought-after, bimetallic Li–Mg borohydrides has been discussed and the results have been put into context with the end-members $Mg(BH_4)_2$ and $LiBH_4$. The crystal structures of these trimetallic compounds reveal interesting structural relationships to aluminosilicates such as $KAlSi_3O_8$ (feldspar) and may be exploited by using them as precursors in an attempt to produce zeolite-like metal borohydrides, since zeolite contains three-dimensional negatively charged Al–Si–O networks, which could be rebuilt by their Li–Mg–BH_4 analogues. The double-sheets found in $K_3Li_2Mg_2(BH_4)_9$ of type $[LiMg(BH_4)_4]^-$ are fragments similar to the structure of β-$Mg(BH_4)_2$ and could provide a new route to design nanoporous open-structured materials with new host–guest adsorption properties.[172]

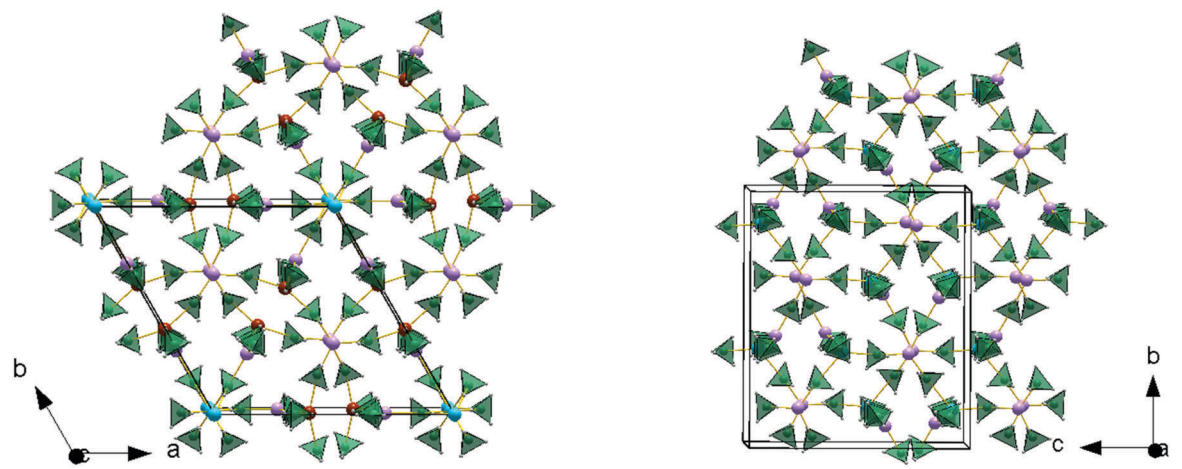


Fig. 6 Structural projections of hexagonal $Li_3MgZn_5(BH_4)_{15}$ along the c_{hex}-axis (left), and of orthorhombic $LiZn_2(BH_4)_5$ along the a_{ortho}-axis (right). A structural fragment with an ideal hexagonal symmetry in $Li_3MgZn_5(BH_4)_{15}$ and pseudo-hexagonal symmetry in $LiZn_2(BH_4)_5$ is clearly visible and underlines the similarity of both structures built from similar frameworks.

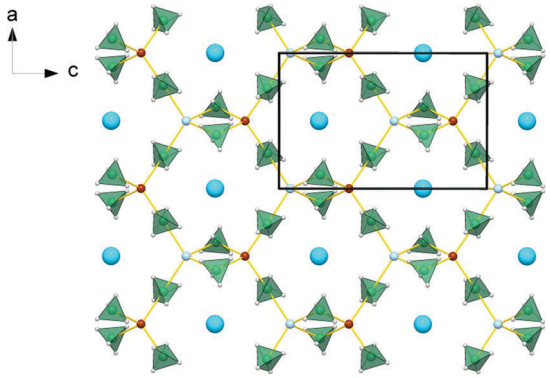


Fig. 7 Honeycomb-like $[LiMg(BH_4)_4]^-$ sheet making up the structure of $ALiMg(BH_4)_4$, with the larger alkali-cation providing the connectivity between adjacent sheets along the crystallographic *b*-axis. A (blue), Li (lavender), Mg (brown), BH_4 (green).

Double perovskite and garnet trimetallic borohydrides. Double perovskites $LiA_2M(BH_4)_6$ have been observed for large alkali metals A = Rb, Cs and M = Y, Ce, Gd while the smaller alkali metal A = K stabilizes the garnet-type structure $Li_3K_3M_2(BH_4)_{12}$ for M = La, Ce.[168]

3.8 General trends in the structural chemistry of metal borohydrides

Metals with increasing Pauling electronegativity have increasing degrees of directionality in the M–BH_4 coordination, in particular alkaline earth and d-block metals, which mostly form framework structures. These structures may have unexpected structural topologies and contain interpenetrated frameworks or some degree of porosity. These metal borohydrides often exist as several polymorphs (metastable in a wide *T* range), with the extreme case of $Mg(BH_4)_2$ showing at least seven polymorphs. These observations highlight the structural flexibility mainly assigned to directionality and some degree of covalence in the M–BH_4 interaction.

The majority of the bimetallic compounds containing an alkali metal and an alkaline earth metal, or a d-block metal, tend to form structures built from discrete composite complex anions formed by a metal and BH_4, which is due to a significant difference in Pauling electronegativity. In all cases, the more electronegative metal coordinates relatively strongly to BH_4 with a dominantly covalent interaction, while the less electronegative metal, usually an alkali, acts as a charge-balancing ion.

The number of BH_4 complexes in the first coordination sphere of metals, in the structures of metal borohydrides, appears to correlate with the ionic radius of the metal, M. As expected, the number of BH_4 complexes increases with the increasing cationic radius of the metal and the number varies from three to thirteen in o-$RbY(BH_4)_4$.[193] In general, the M–BH_4 distances also increase with increasing cationic radii of the metal. The number of BH_4 units coordinating to the same metal vary as shown in Table 7.

3.9 Comparisons between metal borohydrides and metal oxides

Structural relationship between metal borohydrides and metal oxides. This section provides numerous examples of structural similarities of metal borohydrides and metal oxides, which has been reported recently.[193] This similarity may be due to the fact that the tetrahydridoborate, BH_4^-, and the oxide, O^{2-}, anions are isoelectronic, both carrying 10 electrons. However, the main reason is probably due to the fact that both borohydrides and oxides are ionocovalent compounds following similar rules on structure stability such as those dictated by the Pauling rules. The structural similarities are notable for β- and γ-$Mg(BH_4)_2$ where frameworks built from corner-sharing $[Mg(BH_4)_4]$ tetrahedra are related to SiO_2 structure types.[188] Another polymorph, δ-$Mg(BH_4)_2$, was described as a Cu_2O-type framework, *i.e.* as two interpenetrated β-cristobalite-type frameworks (cristobalite is a polymorph of SiO_2). Analogous similarities between the polymorphs of α/α′-, β- and γ-$Ca(BH_4)_2$ and the TiO_2 polymorphs anatase, rutile and brookite, respectively, were also described[185] and are illustrated in Fig. 8. The similarities between borohydride and oxide structures reveal that the homoleptic solid metal borohydrides are, like oxides, structures with partly ionic and partly covalent bonding having different degrees of electron transfer between a metal cation and borohydride anion. Consequently, the Pauling rules[215] can rationalize the crystal structures of borohydrides.[216]

Table 7 Coordination number of metal and ligand in bimetallic compounds. The hapticity, η, is given in the last column if determined by neutron diffraction or periodic DFT calculations

Borohydrides of metal, M′	$r(M'^{n+})$	CN(M′)	$CN(BH_4)$	Hapticity, η $BH_x\cdots M$
Ba	1.38	6	3	—
Sr	1.18	6	3	—
Gd	0.94	5	2, 3, 4	2, 3
Y	0.90	6, 4	2	2, 3
Cd	0.78	4	2, 4	—
Sc	0.75	4	2, 3, 4	3
Zn	0.60	3	2, 3, 4	2

Structural differences between metal borohydrides and oxides. There are differences between the coordination of borohydride, BH_4^-, and oxide, O^{2-}, anions to metal cations, resulting in structural differences between metal borohydrides and oxides. The negative charge of the oxide O^{2-} has twice the charge of the borohydride BH_4^-, which allows for more structural flexibility in oxides, *e.g.* incorporation of metal ions with mixed oxidation states. This can lead to charge-ordering related phenomena such as magnetism or ferroelectricity. The oxide anion also contains electron lone pairs, which decrease the sphericity in case of coordination numbers lower than four. In contrast, the borohydride anion has a more pronounced non-spherical tetrahedral shape. Therefore, metal borohydride crystal structures often have lower symmetry when compared to the symmetry of the related oxides.

Furthermore, the borohydride anion is rather large $r(BH_4^-)$ = 2.03 Å,[19,217] being nearly twice as large as the radius of oxide anion $r(O^{2-})$ = 1.24 or 1.28 Å for tetrahedral or octahedral coordination, respectively. As a consequence, the charge density of the oxide ion is more than eight times larger than that of the borohydride ion. Secondly, the Pauling electronegativity is 3.44 for oxygen and only 2.13 (group electronegativity)[212] for the borohydride anion. This illustrates that the BH_4^- anion is more

 This journal is © The Royal Society of Chemistry 2017

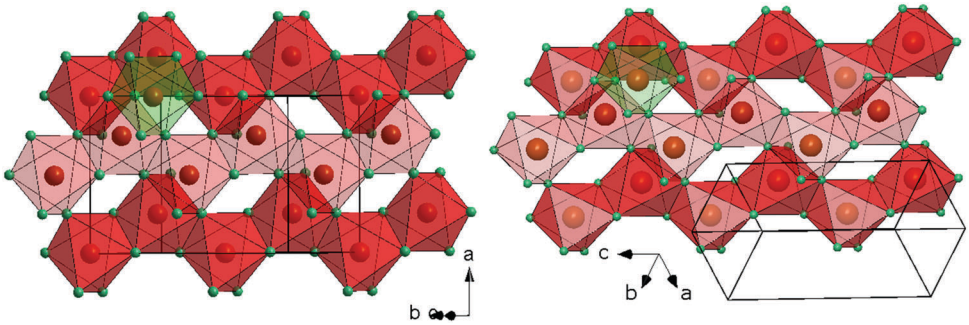


Fig. 8 Stacking of octahedral layers in structures of α-$Ca(BH_4)_2$ (left) and anatase-TiO_2 (right) showing their similarity (hydrogen atoms are omitted for clarity). Octahedral chains in two layers are shown in red and light red. One octahedron from a third layer is shown in green.

reducing than O^{2-}. Therefore, stable oxides are often formed by metal ions with a high oxidation state, small radius and, thus, high charge density. This section shows that the opposite is valid for the metal borohydrides, which are often formed by the larger metal ions with lower oxidation state and lower charge density, *e.g.* potassium tetraoxoferrate(VI), K_2FeO_4 (Fe^{6+}, d^0), is stable at RT whereas $Fe(BH_4)_2$ (Fe^{2+}, d^6) exists in solution at $T < -30$ °C, or stabilized with ammonia at RT as $[Fe(NH_3)_6](BH_4)_2$.[94] Structures of metal oxides are often considered as a close packing of anions with cations filling octahedral or tetrahedral sites. This structural view holds less convincingly for the metal borohydrides, which often have a structural packing deviating significantly from the close packing of anions. This may be ascribed to higher 'softness' and polarizability, which introduces more directionality and covalence in the M–BH_4 bonding compared to metal oxides.[218]

Role of $H^{-}\cdots H^{-}$ interactions. The repulsive $H^{-}\cdots H^{-}$ interaction between neighbouring borohydride groups is another structure-determining parameter. The Switendick limit of 2.1 Å for a minimal H···H distance known from metallic hydrides also seems to hold approximately for borohydrides. An illustrative example of the role of the repulsive H···H interaction is the RT to HT polymorphic transition from α- to β-$Y(BH_4)_3$. While the RT polymorph allows for more dense packing, three H···H distances around each Y are close to Switendick limit of 2.1 Å. The HT β-polymorph is less dense, and by reorientation of three out of six borohydrides in the Y coordination, the shortest H···H distance becomes 2.6 Å (Fig. 2). Interestingly, DFT calculations suggest the HT phase to be the ground state, indicating the overestimation of the H···H repulsion in the calculation. In ReO_3, the oxide equivalent of $Y(BH_4)_3$ is indeed the equivalent to β-$Y(BH_4)_3$, and the oxide equivalent to the RT α-$Y(BH_4)_3$ is obtained by applying the pressure. The flipping of three borohydride groups also straightens the Y–BH_4–Y bridges in the HT-polymorph, which allows maximizing the H···H distances. A similar behaviour was observed for α- and β-$Cd(BH_4)_2$ with a tetrahedral coordination of Cd. While the RT-polymorph is a distorted anti-Cu_2O-type structure, the HT-polymorph crystallizes in the regular cubic anti-Cu_2O type. Whether the flipping of BH_4 groups is at the origin of this phase transformation remains controversial, since the hydrogen positions have not been reliably determined. The repulsive $H^{\delta-}\cdots H^{\delta-}$ interaction is also likely at the origin of the pressure-induced phase transitions in $Mg(BH_4)_2$ and $Mn(BH_4)_2$. These compounds change their structure with pressure from a more porous α- to more dense δ- or δ′-polymorphs, which are also deformation variants of anti-Cu_2O-type.

The repulsive $H^{\delta-}\cdots H^{\delta-}$ interactions are naturally expected to be more pronounced for higher partial hydrogen charges, δ. Indeed, δ varies from −0.86 in o-$LiBH_4$[175] (and even closer to −1 for heavier alkali metals) to values much closer to zero for more covalent borohydrides such as $Mg(BH_4)_2$, where only a partial charge transfer occurs from the metal cation to the BH_4 anion. The limiting case is $Cd(BH_4)_2$, as Cd is the most electropositive metal forming a borohydride at ambient conditions without stabilization by alkali metal ions. The deformations of the Cu_2O-antitype $Mg(BH_4)_2$ and $Cd(BH_4)_2$ with pressure and temperature[3,146] is determined by H···H interactions driven by different values of δ, as well as by different radii of the metal atoms. Thus, the strength of the repulsive H···H interactions depend on the charge transfer from the counter ion and this influences the stability of some polymorphs.

4. Structure of anion substituted metal borohydrides

Metal borohydrides have diverse compositions and rich and fascinating structural chemistry, as discussed in the previous section of this review. The metal borohydrides have been mainly prepared mechanochemically during the past decade, which often produced a variety of metal borohydride halides. Halide substitution in metal borohydrides is a valuable approach for tailoring physical and chemical properties. Metal borohydride halides have either fully ordered, partly ordered or disordered structures (Fig. 9 and Table 8), which is the major focus of this section. Another class of anion substituted metal borohydrides contains both the borohydride, BH_4^-, and the amide, NH_2^-, anions. These boron–nitrogen compounds are also investigated intensively due to their hydrogen storage and ion conductivity properties. In cases where metal borohydrides are contaminated by oxygen containing impurities, *e.g.* water or solvents, they may partly decompose to metal borohydride borates, BO_3^{3-}. Recently, borohydride *closo*-boranes, *i.e.* $B_{12}H_{12}^{2-}$,

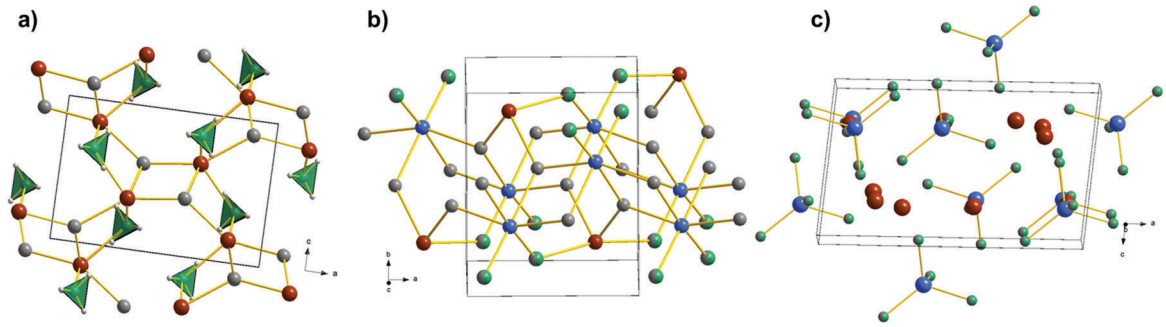


Fig. 9 Crystal structure of (a) fully ordered $Sr(BH_4)Cl$, (b) partly disordered $Y(BH_4)_{2-x}Cl_{2+x}$, and (c) fully disordered $K_2Zn(BH_4)_xCl_{4-x}$. Sr, Na, K (red), Zn, Y (blue) Cl (gray) and B (green).

Table 8 Overview of halide substitution in metal borohydrides

Cation	Composition	Space group	Ref.
Fully ordered structures			
Sr	$Sr(BH_4)Cl$	*Pnma*	142
K, Zn	$KZn(BH_4)Cl_2$	$P2_1/m$	84
Li, La	$LiLa(BH_4)_3Cl$	$I\bar{4}3m$	88
Li, Ce	$LiCe(BH_4)_3Cl$	$I\bar{4}3m$	4
Li, Pr	$LiPr(BH_4)_3Cl$	$I\bar{4}3m$	219
Li, Nd	$LiNd(BH_4)_3Cl$	$I\bar{4}3m$	219
Li, Sm	$LiSm(BH_4)_3Cl$	$I\bar{4}3m$	147
Li, Gd	$LiGd(BH_4)_3Cl$	$I\bar{4}3m$	88
Partly ordered structures			
Ba	o-$Ba((BH_4)_{1-x}Cl_x)_2$	*Pnma*	220
	h-$Ba((BH_4)_{1-x}Cl_x)_2$	$P\bar{6}2m$	220
Na, Y	$NaY(BH_4)_{2-x}Cl_{2+x}$	*P2/c*	87 and 167
Li, Al	$Li_4Al_3((BH_4)_{1-x}Cl_x)_{13}$	$P2_1/c$	159
Na, Al	$NaAl(BH_4)_xCl_{4-x}$	$Pmn2_1$	214
Fully disordered structures			
K, Zn	$K_2Zn(BH_4)_xCl_{4-x}$	$P2_1/n$	85
	$K_3Zn(BH_4)_xCl_{5-x}$	$P4_2/ncm$	85
Li, Yb	$LiYb(BH_4)_{4-x}Cl_x$	$P\bar{4}2c$	81 and 150
Yb	$Yb(BH_4)_{2-x}Cl_x$	*Pbca*	150
Solid solutions			
Li	o-$Li(BH_4)_{1-x}Cl_x$ (RT)	*Pnma*	9
	h-$Li(BH_4)_{1-x}Cl_x$ (HT)	$P6_3mc$	9
	o-$Li(BH_4)_{1-x}Br_x$ (RT)	*Pnma*	86
	h-$Li(BH_4)_{1-x}Br_x$ (HT)	$P6_3mc$	86
	h-$Li(BH_4)_{1-x}I_x$	$P6_3mc$	221
Na	$Na(BH_4)_{1-x}Cl_x$	$Fm\bar{3}m$	222
	$NaB(H_{1-x}F_x)_4$	$Fm\bar{3}m$	223
K	$K(BH_4)_{1-x}Cl_x$	$Fm\bar{3}m$	166
	$KB(H_{1-x}F_x)_4$	$Fm\bar{3}m$	224
Mg	β-$Mg((BH_4)_{1-x}Cl_x)_2$	*Fddd*	225
	β-$Mg((BH_4)_{1-x}Br_x)_2$	*Fddd*	225
Ca	β-$Ca((BH_4)_{1-x}Cl_x)_2$	$P4_2/m$	226 and 227
	tri-$Ca((BH_4)_{1-x}I_x)_2$	$P\bar{3}m_1$	228
	o-$Ca((BH_4)_{1-x}I_x)_2$	*Pnnm*	228
	tet-$Ca((BH_4)_{1-x}I_x)_2$	*I4mm*	228
	β-$Ca((BH_4)_{1-x}I_x)_2$	$P4_2/m$	228

were discovered to host fast ion conduction. These new classes of materials, metal borohydride amides, borates and *closo*-boranes are discussed in the last part of this section.

4.1 Metal borohydride halides – fully ordered structures

Strontium borohydride chloride, $Sr(BH_4)Cl$, is a stoichiometric, ordered compound, which crystallizes in the orthorhombic crystal system at RT (*Pnma*) with the structure type of $Sr(OH)_2$.[142]

Potassium zinc borohydride chloride. The first mixed-anion mixed-cation borohydride, $KZn(BH_4)Cl_2$, characterized in 2010,[84] has a structure with crystallographic sites fully occupied by BH_4^- or chloride anions and consists of isolated heteroleptic $[Zn(BH_4)Cl_2]^-$ anions charge balanced by K^+ cations. The $[Zn(BH_4)Cl_2]^-$ anion is built from Zn in a trigonal-planar orientation to two Cl atoms and one BH_4 unit, similar to zinc in the structures of $NaZn(BH_4)_3$ and $KZn(BH_4)_3$. The BH_4^- complex coordinates to Zn by edge sharing (η^2), which then has coordination number four, CN(Zn) = 4. The potassium atom has an unusual coordination number of eight, with a distorted square antiprismatic coordination, formed by five Cl atoms and three BH_4 groups. In agreement with the high coordination number of K, the K–Cl (3.159–3.66 Å) and K–B (3.274–3.781 Å) distances in $KZn(BH_4)Cl_2$ are slightly longer than in KCl (3.130 Å)[229] and KBH_4 (3.364 Å),[230] where the K^+ ion has an octahedral environment coordinated by six Cl^- or BH_4^-, respectively. This coordination difference underlines that the structure is not directly related to that of KBH_4 and cannot be considered a simple composite of the starting materials.

Lithium rare-earth metal borohydride chlorides. A series of alkali rare-earth metal borohydride chlorides with fully anion-ordered structures, $LiRE(BH_4)_3Cl$, RE = La, Ce, Pr, Nd, Sm or Gd crystallize in cubic unit cells with space group symmetry $I\bar{4}3m$.[4,88,147,219] A combination of X-ray diffraction (SR-PXD), neutron diffraction (PND) and density functional theory (DFT) optimization of structural models reveals that the structure contains isolated tetranuclear anionic clusters $[RE_4Cl_4(BH_4)_{12}]^{4-}$ with a distorted cubane-like RE_4Cl_4 core, known from coordination chemistry.[231] The complex anions $[RE_4Cl_4(BH_4)_{12}]^{4-}$ are charge balanced by discrete Li^+ ions.[4] Each rare-earth metal atom, RE, coordinates to three chloride ions and three borohydride groups forming an octahedron, but the BH_4^- tetrahedra coordinates to the large rare-earth ions by face sharing (η^3). Li^+ ions are disordered, occupying 2/3 of the 12d Wyckoff site, leading to fast lithium ion conduction,[4] further discussed in Section 7. DFT calculations indicate that the structure of $LiCe(BH_4)_3Cl$ is stabilized by entropy, in accordance with the disorder on Li^+ positions.[4,88] This complicated structure type, containing both light and heavy atoms, could not be resolved by any two of the three methods, SR-PXD, PND and DFT calculations, and it was only possible to

 This journal is © The Royal Society of Chemistry 2017

solve with the combined use of all three methods.[4,88] Alternatively, the structure may be rationalized from the borohydride-oxide similarity (Section 3.9) as derived from spinel. If the anions, BH_4^- or Cl^-, are considered to be close packed then rare-earth metals occupy the octahedral sites, and lithium atoms occupy the tetrahedral sites (similar to those in spinel, but in a ratio 1 : 1 instead of 2 : 1 as in spinels).

4.2 Metal borohydride halides – partly ordered structures

Barium borohydride chloride. Mechanochemical treatment of $LiBH_4$–$BaCl_2$ in molar ratios 1 : 1 and 2 : 1 produces two new barium borohydride chlorides with different structures.[220] An orthorhombic chloride-rich compound, o-$Ba(BH_4)_{0.16}Cl_{1.84}$, is obtained using the reactant ratio 1 : 1 and a borohydride-rich hexagonal compound, h-$Ba(BH_4)_{0.85}Cl_{1.15}$, using molar ratio 2 : 1. The structures of o-$Ba(BH_4)_{0.16}Cl_{1.84}$ and h-$Ba(BH_4)_{0.85}Cl_{1.15}$ were described on the basis of SR-PXD data using Rietveld refinement and structural similarities to orthorhombic barium chloride, o-$BaCl_2$ (*Pnma*)[232] and the hexagonal high temperature barium chloride polymorph, h-$BaCl_2$ ($P\bar{6}2m$),[233] respectively. Boron and chlorine atoms occupy the two Cl positions in the $BaCl_2$ polymorphs with the overall occupancy of B and Cl constrained to one. A third anion position in each structure, o-$Ba(BH_4)_{0.16}Cl_{1.84}$ and h-$Ba(BH_4)_{0.85}Cl_{1.15}$, can be regarded as BH_4-free.

Sodium yttrium borohydride chloride. Mechanochemical synthesis produces a mixed-cation mixed-anion borohydride chloride with the ideal composition $NaY(BH_4)_2Cl_2$.[87,167] The compound crystallizes in a polymeric pseudo-orthorhombic unit cell ($P2/c$), only slightly distorted from the orthorhombic metrics (with $\beta = 90^\circ$).[87,167]

However, Rietveld refinements suggest some Cl-substitution on the BH_4 site, resulting in a partly ordered structure with the composition, $NaY(BH_4)_{2-x}Cl_{2+x}$ with $x = 0.21$ at RT.[87] Interestingly, both experimental and theoretical results reveal two anion sites with different sizes in the structural model. The BH_4^- anions clearly have a preference for the larger of the two sites, whereas the chloride anion prefers the smaller, due to the size difference of the two anions, $r(Cl^-) = 1.81$ and $r(BH_4^-) = 2.03$ Å. Both the yttrium and sodium atoms in $NaY(BH_4)_2Cl_2$ have slightly distorted octahedral coordination environments consisting of two BH_4 sites and four Cl atoms for yttrium (*i.e.* $Y(BH_4)_2Cl_4$) and two Cl atoms and four BH_4 sites for sodium atoms (*i.e.* $Na(BH_4)_4Cl_2$). DFT optimization of the experimental structure and Raman spectroscopy suggests that the BH_4 units coordinate by face-sharing (η^3) towards yttrium and by a combination of edge and face-sharing to sodium.[87]

The existence of one larger and one smaller anionic site is analogous to oxides. The structure of $NaY(BH_4)_2Cl_2$ is related to $MgWO_4$, which again is a cation substitution variant of the α-PbO_2 structure. The latter is the structure type observed for $Sr(BH_4)_2$. There is only one anion site in α-PbO_2 but two in $MgWO_4$ with different sizes due to the size difference of the cations, Mg^{2+} and W^{6+}. Interestingly, the cations' coordination number increases from six to seven for the borohydride free compound $NaYCl_4$. However, the triclinic structure of $NaYCl_4$ has similar packing and connectivity of the cation coordination polyhedra as observed for the $MgWO_4$ and $NaY(BH_4)_2Cl_2$ type structures.

Lithium aluminum borohydride chloride. The first example of a bimetallic borohydride based on s- and p-block metals has the ideal composition $Li_4Al_3(BH_4)_{13}$.[159] The structure is built from cationic, $[(BH_4)Li_4]^{3+}$ and a anionic, $[Al(BH_4)_4]^-$, complexes. However, these units are not isolated, *i.e.* the Li–B distances within $[(BH_4)Li_4]^{3+}$ and between the Li atom and B within $[Al(BH_4)_4]^-$ are similar. Hence this structure can be described as a 3D framework. On the other hand, the structure of $Li_4Al_3(BH_4)_{13}$ can be related to that of the anti-Cr_3Si type, by rationalizing it as close packing of complex anions and cations. Detailed structural analysis reveals chloride substitution mainly in the anion-centered complex, $[(BH_4)Li_4]^{3+}$, providing Li–Cl coordination similar to that observed in $LiBH_4$–LiCl solid solutions (see Section 4.4.1).[9,234] Rietveld refinements of SR-PXD data measured for $AlCl_3$–$LiBH_4$ 1 : 4 and 1 : 5 samples reveal the presence of ~27 mol% and ~46 mol% chloride anions in the compositions $Li_4Al_3(BH_4)_{\sim 9.8}Cl_{\sim 3.2}$ and $Li_4Al_3(BH_4)_{\sim 7.5}Cl_{\sim 5.5}$.

Sodium aluminum borohydride chloride. $NaAl(BH_4)_xCl_{4-x}$ with a partly ordered orthorhombic ($Pmn2_1$) structure is also described. The highest yield of $NaAl(BH_4)_xCl_{4-x}$, ~86 mol% together with $NaAlCl_4$, ~14 mol%, was obtained by mechanochemical treatment of a $AlCl_3$–$NaBH_4$ 1 : 1.[214] The structure consists of one Na, one Al, one Cl and two BH_4 sites. There is no indication of any borohydride substitution on the general position occupied by Cl. The borohydride anions appear to prefer two sites with higher local symmetry on the mirror plane. However, Rietveld refinement indicates Cl-substitution on the BH_4 site. The structure contains complex tetrahedral anions of $[Al(BH_4)_xCl_{4-x}]^-$, which form in a relatively narrow composition range $1 < x < 1.43$, counter balanced by Na^+ cations. The highest borohydride content ($x = 1.43$) is obtained from a sample with composition $AlCl_3$–$NaBH_4$ 1 : 3 with relative anion occupancies BH_4^-/Cl^- 0.82/0.18 and 0.61/0.39 on each boron site.[159,214]

Contrary to the complex anions $[M(BH_4)_4]^-$ (M = Mg, Sc, Mn, Cd), $[Zn(BH_4)_3]^-$ and $[Zn_2(BH_4)_5]^-$ the complex anion $[Al(BH_4)_4]^-$ appears to be more difficult to stabilize (see the discussion in Section 3.5), requiring a certain extent of partial substitution of BH_4^- units by the smaller Cl^- ligand.[214]

4.3 Metal borohydride halides – fully disordered structures

Compounds with fully disordered anion positions in the structures have statistical distributions of BH_4 and the heavier halide anion on all anionic sites. The section after this one, 4.4, is devoted to compounds, which may be classified as solid solutions of two compounds.

Potassium zinc borohydride chloride. A fully disordered monoclinic bimetallic borohydride chloride, $K_2Zn(BH_4)_xCl_{4-x}$ ($P2_1/n$) has been identified where all four anionic sites are partly occupied by BH_4^- and Cl^-.[85] The structure of $K_2Zn(BH_4)_xCl_{4-x}$ consists of $[Zn(BH_4)_xCl_{4-x}]^{2-}$ anions with Zn coordinating to four BH_4/Cl groups, forming a somewhat distorted tetrahedron. The compound $K_2Zn(BH_4)_xCl_{4-x}$ is isostructural to the series of bimetallic borohydrides $K_2M(BH_4)_4$, M = Mg, Mn, Cd, discussed in Section 3.5.

In fact, $K_2Zn(BH_4)_xCl_{4-x}$ is a monoclinic distortion of the high temperature K_2ZnCl_4 polymorph observed at $T > 315$ °C with a K_2SO_4 type structure (*Pnma*).[235] Interestingly, the volume per formula unit (*V*/*Z*) for $K_2Zn(BH_4)_{1.47}Cl_{2.53}$ measured at RT is almost identical to that of the high temperature polymorph of K_2ZnCl_4 at 315 °C. This indicates that the unit cell volume expansion caused by the incorporation of BH_4 is similar to the thermal expansion causing the polymorphic phase transformation from the RT polymorph of K_2ZnCl_4 ($Pna2_1$) to the high temperature polymorph (*Pnma*).

$K_3Zn(BH_4)_xCl_{5-x}$ is formed after prolonged ball milling of KBH_4–$ZnCl_2$ (2 : 1).[85] The structure is not fully characterized but may crystallize in the tetragonal space group $P4_2/mbc$ and contains the complex anion $[Zn(BH_4)_xCl_{4-x}]^{2-}$ making it a substitutional and deformation variant of the tetragonal ($I4/mcm$) Cs_3CoCl_5 structure type.

Lithium ytterbium borohydride chloride. The compound $LiYb(BH_4)_{4-x}Cl_x$ can also be formed, which crystallizes in a primitive tetragonal structure with $x \sim 1.0$ ($P\bar{4}2c$), which is isostructural to $LiSc(BH_4)_4$.[81,150] During heating, ytterbium is also reduced, similar to samarium borohydrides, forming $Yb(BH_4)_{2-x}Cl_x$. This compound exists with two different compositions depending on both temperature and synthesis conditions. $Yb(BH_4)_{2-x}Cl_x$, $x = 0.76$, crystallizes in a primitive tetragonal unit cell ($P\bar{4}$), whilst $Yb(BH_4)_{2-x}Cl_x$, $x = 0.3$, crystallizes in a primitive orthorhombic unit cell (*Pbca*).[150]

4.4 Metal borohydride halides forming solid solutions

Compounds with statistically distributed anions in their structures are denoted fully disordered and may be classified as solid solutions of two compounds. This will be further discussed in the following section. Anion substitution is a method for tailoring the properties of known metal borohydrides.[8] Substitution of BH_4^- or H^- by anions with the same charge and comparable size may lead to formation of solid solutions (see Table 9). The first part of this subsection is devoted to investigations regarding substitution of the BH_4^- complex anion with the heavier halides, Cl^-, Br^- or I^-. Fluorine substitution has also been attempted, which is discussed in the end of this section, see Section 4.4.2.

In some cases, full solubility between a metal borohydride and the halide salt can be observed, *e.g.* $Na(BH_4)_{1-x}Cl_x$. General rules for anion substitution are derived from the numerous examples presented in the following section and are described in the end of this section.

4.4.1. Metal borohydride halides, the s-block

Lithium borohydride–lithium chloride. Initially, anion substitution was observed by *in situ* diffraction experiments during heating a sample of $LiBH_4$–LiCl 0.85 : 0.15.[9] Diffraction data suggest that solid LiCl dissolves into the structure of the solid hexagonal polymorph, h-$LiBH_4$, at $T > 110$ °C, obtaining a maximum chlorine substitution of 42 mol%, *i.e.* h-$Li(BH_4)_{0.58}Cl_{0.42}$.[234] The hexagonal solid solution, h-$Li(BH_4)_{0.58}Cl_{0.42}$, obtained using thermal treatment is stable upon cooling to RT, however slow segregation of LiCl is observed and o-$Li(BH_4)_{0.91}Cl_{0.09}$ is obtained after several months.[9,234,237] The mechanism for anion substitution in the system $LiBH_4$–LiCl is described in reaction scheme (4.1), *i.e.* one solid, LiCl, dissolves in another solid, $LiBH_4$.

$$x\mathrm{LiCl} + (1 - x)\mathrm{LiBH_4} \rightarrow \mathrm{Li(BH_4)_{1-x}Cl_x} \qquad (4.1)$$

Lithium borohydride–lithium bromide. The mechanism for anion substitution in $LiBH_4$–LiBr, facilitated by mechanochemical or thermal treatment, has been investigated by *in situ* SR-PXD and the formation of two solid solutions is observed.[86] Mechanochemical treatment, or just hand mixing, of a sample of $LiBH_4$–LiBr leads to formation of a hexagonal solid solution h-$Li(BH_4)_{1-x}Br_x$ with a unit cell volume similar to β-LiBr. This indicates that the first step in the anion substitution process is a dissolution of small amounts of $LiBH_4$ into α-LiBr (β-LiBr and h-$LiBH_4$ are isostructural). Heating the sample to elevated temperatures, $T > 112$ °C, also enables dissolution of LiBr in h-$LiBH_4$ forming a lithium borohydride rich solid solution with unit cell volume similar to $LiBH_4$. Two solid solutions can be observed at $T > 112$ °C and the dissolution process is further accelerated resulting in a single solid solution at elevated temperatures and full solubility in the system $LiBH_4$–LiBr.[86] Cooling such a solid solution of h-$Li(BH_4)_{1-x}Br_x$ should finally lead to crystallization of α-LiBr, o-$Li(BH_4)_{1-x}Br_x$ and/or a hexagonal solid solution h-$Li(BH_4)_{1-x}Br_x$. The composition of the solid solution h-$Li(BH_4)_{1-x}Br_x$ appears to remain constant ($x \sim 0.5$) upon storage at RT for several months, but α-LiBr and presumably amorphous o-$LiBH_4$ are slowly segregated. Bromide substitution stabilizes the hexagonal structure of $LiBH_4$ to RT as a solid solution with composition h-$Li(BH_4)_{0.5}Br_{0.5}$.[86]

Lithium borohydride–lithium iodide. Solid solutions of $Li(BH_4)_{1-x}I_x$ have been obtained by reacting $LiBH_4$ with α-LiI.[221] The substitution process can be induced either by heat treatment at $T \sim 245$ °C or by mechanochemical treatment. *In situ* SR-PXD has demonstrated that anion substitution initially forms two solid solutions, which at elevated temperatures merge into one containing up to 62 mol% LiI. Two solid solutions may occur due to substitution of I^- for BH_4^- in $LiBH_4$ and substitution of BH_4^- for I^- in LiI. The structures of the two solid solutions are identical to the hexagonal structures of h-$LiBH_4$ and β-LiI. The solid solutions of $Li(BH_4)_{1-x}I_x$ have a broader stability range (from RT to the melting at 330 °C) compared to that of both h-$LiBH_4$ and β-LiI.[221]

Sodium borohydride–sodium chloride. The mechanism for anion substitution, facilitated by annealing, was investigated by *in situ* SR-PXD during three consecutive cycles of heating to 300 °C, annealing for 30 min and cooling to RT for a sample of $NaBH_4$–NaCl (1 : 1), see Fig. 10.[222] The unit cell volume of NaCl increases and decreases linearly due to thermal expansion and contraction, respectively (linear thermal expansion coefficients, $\alpha(\mathrm{NaCl}) = 2.562 \times 10^{-4}\ \mathrm{K}^{-1}$ for $T = 32$–300 °C). No changes are observed in the unit cell volume of NaCl before and after the three annealing cycles, *i.e.* no dissolution of $NaBH_4$ into NaCl

Table 9 Ionic radii of selected anions[213,236]

Anion	F^-	H^-	NH_2^-	Cl^-	Br^-	BH_4^-	I^-
Radius (Å)	1.33	1.40	1.68	1.81	1.96	2.03	2.20

 This journal is © The Royal Society of Chemistry 2017

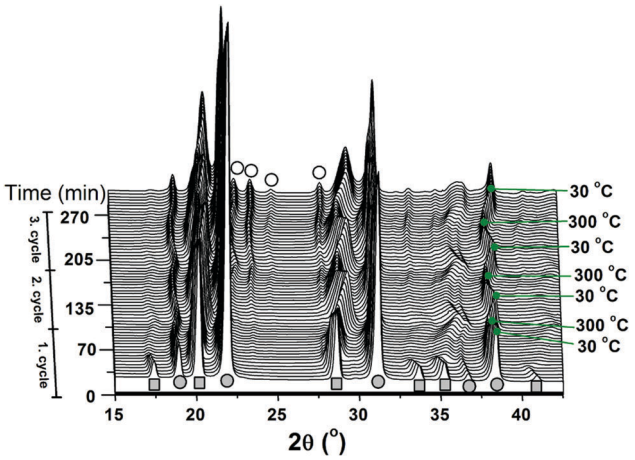


Fig. 10 *In situ* SR-PXD data for BM $NaBH_4$–NaCl (1 : 1) heated from RT–300 °C, kept at 300 °C for 30 min, cooled from 300–30 °C ($\Delta T/\Delta t$ = 10 °C min^{-1}). This is repeated by three cycles. Symbols: ○ NaCl, □ $NaBH_4$ and ○ $NaBO_2$ (λ = 1.072 Å). Adapted with permission from ref. 222. Copyright 2011 Elsevier.

takes place during the short time of the experiment (only 90 min at 300 °C).

At $T \sim 240$ °C the unit cell volume of $Na(BH_4)_{1-x}Cl_x$ decreases rapidly and continues to do so for approximately 20 min. On this time scale the unit cell parameter is found to decrease from 6.2099–6.1295 Å, while the degree of substitution, x changes from approximately 0.15 to 0.50. During the second and third annealing periods at T = 300 °C the unit cell volume of $Na(BH_4)_{1-x}Cl_x$ decreases linearly due to anion substitution. Furthermore, the fact that the decrease in unit cell volume of $Na(BH_4)_{1-x}Cl_x$ is linear upon cooling suggests that NaCl does not segregate from $NaBH_4$ on the time scale of the experiment and the final composition is found to be $Na(BH_4)_{0.43}Cl_{0.57}$.[222]

Dissolution of 10 mol% NaCl into $NaBH_4$, forming $Na(BH_4)_{0.9}Cl_{0.1}$, takes place during relatively mild ball milling, *i.e.* 60 × 2 min with 2 min breaks to restrict sample heating (total BM time 120 min). A higher degree of dissolution of NaCl into $NaBH_4$ is obtained by more harsh BM (*e.g.* 24 h) in some cases combined with sample heating by the reaction heat from decomposition of metal borohydrides. These investigations suggest full solubility in the system $NaBH_4$–NaCl, *i.e.* one solid solution.[71,72] This is expected because NaCl and $NaBH_4$ are both isomorphous. Investigations reveal a linear correlation between the compositions of the solid solutions and the unit cell volume, in agreement with Vegard's law.[71,72,222] Chlorine substitution for the larger iodide anion also occurs readily and stoichiometrically during relatively mild ball milling.

Potassium borohydride–potassium chloride. Anion substitution in potassium borohydride has been observed during the decomposition of $KSc(BH_4)_4$.[166] The mechanochemically produced sample originally contained the three compounds: $KSc(BH_4)_4$, K_3ScCl_6, and KBH_4. The amount of KBH_4 increases during the decomposition of $KSc(BH_4)_4$ in the temperature range 150 to 230 °C and further reacts with K_3ScCl_6 at $T > 230$ °C. The reaction is observed as a continuous change in the position of KBH_4 diffraction peaks toward higher 2θ values, *i.e.*, the unit cell of KBH_4 contracts upon heating. This suggests two simultaneous and coupled chemical reactions taking place. (a) The ternary chloride K_3ScCl_6 reacts with KBH_4 to form potassium chloride, KCl, and possibly also amorphous scandium borides, boron, and/or higher boranes and (b) simultaneously, KCl dissolves in the remaining KBH_4 and forms a solid solution $K(BH_4)_{1-x}Cl_x$ with increasing amounts of KCl, see reaction scheme (4.2).

$$(1 - x)KBH_4 + xKCl \rightarrow K(BH_4)_{1-x}Cl_x \qquad (4.2)$$

Magnesium borohydride–magnesium halide. Anion substitution in $Mg(BH_4)_2$ is observed after annealing a milled mixture of α-$Mg(BH_4)_2$–MgX_2 (X = Cl or Br). The substitution is identified from the shift of Bragg peaks from α- to β-$Mg(BH_4)_2$, *i.e.* anion substitution only occurs in the β-$Mg(BH_4)_2$ polymorph.[225] Structure refinement revealed that unit cell parameters decreased by about 0.1–0.2 Å for β-$Mg(BH_4)_2$ in the mixtures, which corresponds to a volume contraction of the unit cell of about 2%. A combined experimental and theoretical approach for the Cl substitution in $Mg(BH_4)_2$ has shown that the enthalpy gain is more favourable for the β-solid solution than for the α-solid solution.[225]

Calcium borohydride–calcium chloride and bromide. Halide substitution in $Ca(BH_4)_2$–$CaCl_2$ and $Ca(BH_4)_2$–$CaBr_2$ was also investigated.[226,227] Chlorine substitution was not observed after BM of the samples but readily occurs after the transition from α- to β-$Ca(BH_4)_2$ upon heating above ~250 °C. Rietveld analysis of the obtained β-$Ca(BH_4)_{1-x}Cl_x$ phases indicates compositions from x = 0.3 to 0.7 depending on the amount of $CaCl_2$ in the mixtures. No anion substitution with CaF_2 or $CaBr_2$ is observed.[226]

Calcium borohydride–calcium iodide. Anion substitution in the system $Ca(BH_4)_2$–CaI_2 resulted in the formation of three new compounds, which are solid solutions with BH_4^- and I^- anions sharing the same positions in the structures.[228] Sample preparation methods have a significant influence on the reaction pathway. Mechanochemical synthesis (ball milling) mediates a significant degree of dissolution of $Ca(BH_4)_2$ into CaI_2 (~70 mol%) yielding a CaI_2-type trigonal solid solution, tri-$Ca((BH_4)_{1-x}I_x)_2$ ($x \sim 0.7$). Upon heating, tri-$Ca((BH_4)_{0.7}I_{0.3})_2$ transforms to a $CaCl_2$-type orthorhombic structure, o-$Ca((BH_4)_{1-x}I_x)_2$ ($x \sim 0.3$), which is structurally related to β-$Ca(BH_4)_2$. Upon further heating (at 335 °C), the sample partly transforms to a more iodide-rich tetragonal solid solution, tet-$Ca((BH_4)_{1-x}I_x)_2$ ($x \sim 0.6$), with a novel structure type. This compound decomposes to CaHI and CaB_6 (at $T > 345$ °C). Apparently, minor amounts of CaI_2 also dissolve into β-$Ca(BH_4)_2$ forming a solid solution, which is structurally similar to o-$Ca((BH_4)_{1-x}I_x)_2$, *i.e.* β-$Ca((BH_4)_{1-x}I_x)_2$ with $x \sim 0.05$.[228]

4.4.2 Fluoride substitution in metal borohydrides. The smaller halide ion, F^- (1.33 Å), has a similar size to the hydride ion, H^- (1.40 Å) and metal hydrides and fluorides share many properties, *e.g.* the ionic compounds are often found to be isostructural. This suggests that hydrogen and fluorine may substitute for each other in both ionic and covalently bonded compounds.

The most significant difference between the two lies in the electronegativity, which is 2.1 and 4.0 for hydrogen and fluorine, respectively. Therefore, fluorine substitution is expected to lead to significant thermodynamic changes in metal hydrides. The first fluorine-substituted complex hydride was prepared by hydrogenation of the system NaF–Al–H_2, which yielded the complex hydride $Na_3AlH_{6-x}F_x$, *i.e.* fluoride substitution of the complex anion $[AlH_{6-x}F_x]^{3-}$.[238,239] The substitution of fluorine into $NaMgH_3$, forming $NaMgH_2F$, has been shown to stabilize the structure and increase the enthalpy of hydrogen absorption/desorption, a desirable property for concentrating solar thermal energy storage applications.[240]

Fluoride substitution in the BH_4^- complex anion, *i.e.* $H^- \rightarrow F^-$, is also possible. The system $NaBH_4$–$NaBF_4$ provided the first fluorine substituted borohydride, $NaBH_{2.1}F_{1.9}$, observed in a narrow temperature range of 200 to 215 °C by SR-PXD.[223] However, the obtained materials $MB(H_{1-x}F_x)_4$ appear to have relatively low thermal stability and the released hydrogen can be contaminated with significant amounts of boronfluorides and/or borane gases and may lead to the formation of significant amounts of unwanted $M_2B_{12}H_{12}$.[223,241] The system KBH_4–KBF_4 was investigated by solid state ^{11}B and ^{19}F NMR, which appear more consistent with a statistical distribution of fluorine substituted $[B(H,F)_4]^-$ tetrahedra rather than a mix of discreet BH_4^- and BF_4^- tetrahedra.[224]

Hydrogen substitution by fluorine in orthorhombic o-$LiBH_4$ has been investigated with quantum-mechanics calculations aiming to describe thermodynamic properties of $LiB(H,F)_4$ for hydrogen storage applications. Excess enthalpies of the mixed compounds were computed, suggesting that fluorine atoms tend to agglomerate on the same boron atoms rather than be homogeneously dispersed over all the available BH_4 tetrahedra.[242] These data show that, at room temperature, the formation of solid solutions between lithium borohydride and borofluoride is thermodynamically unfavoured, so the fluorine substitution destabilizes the pure hydride.[242]

A number of reactive hydride composites (further discussed in Section 6.8) containing metal fluorides have been successfully hydrogenated and in some cases cycled with hydrogen release and uptake, (CaH_2/CaF_2)–MgB_2,[243,244] Mg–$LiBH_4$ composites catalysed by FeF_3,[245] LiH–LiF–MgB_2 system,[246,247] and $Ca(BH_4)_2$–MgF_2.[248–250] A drawback is the high stability of both ionic metal fluorides MF and molecular covalent borontrifluoride, BF_3.

4.5 General trends for halide substitution in metal borohydrides

Metal borohydrides and the heavier halides. The above Section 4.4 provides a range of examples of halide substitution in stable monometallic alkali and alkaline earth metal borohydrides and some trends in the structural chemistry of anion substitution are observed. Anion substitution by the heavier halides, *i.e.* Cl^-, Br^- or I^-, of borohydrides:

(i) The solid containing the smaller anion tends to dissolve into the compound containing the larger anion, and the structure of the latter tends to be preserved in the obtained solid solution. This trend can be interpreted as a contraction of the structure providing shorter average bond lengths and therefore larger lattice energy.

(ii) Some polymorphs of metal borohydrides are more prone to perform anion substitution than others. This effect is illustrated by the high temperature polymorphs, *e.g.* h-$LiBH_4$, β-$Mg(BH_4)_2$ and β-$Ca(BH_4)_2$, which more readily dissolve solid metal halides into their structures. Investigations using diffraction and solid state MAS NMR reveal that anion substitution is facilitated by structural dynamics and an orientational disorder, *i.e.* entropy effects, in particular related to the BH_4 unit, which possibly make the BH_4 tetrahedra appear more spherical and similar to halides.[177,251]

(iii) In the case where the metal borohydride and the metal halide are isostructural, anion substitution may occur in both compounds, which can lead to two solid solutions. This effect is observed during moderate heat treatment of mechanochemically treated mixtures of various borohydrides and halides, leading to two solid solutions and indicating non-equilibrium conditions. Thus, mechanochemical treatment facilitates formation of the solid solution with volume contraction and moderate heat treatment may facilitate formation of the solid solution with larger volume, as compared to the parent compound, due to thermal expansion. Such binary solid solutions tend to merge to a single solid solution after prolonged heating, *i.e.* a solid solution exists in the full concentration range at higher temperatures (and can be quenched to RT). This is observed for $LiBH_4$–LiBr, $LiBH_4$–LiI and $NaBH_4$–NaCl systems, and notice that β-LiBr, β-LiI and h-$LiBH_4$ and also $NaBH_4$ and NaCl are isostructural.

Reactions during mechanochemical treatment appear to be promoted by elevated pressure, *i.e.* by compression of materials, therefore all anion substitutions obtained by BM appear to follow (i). In contrast, thermal treatment (annealing) tends to facilitate increased mobility, *e.g.* of BH_4^-, and thermal expansion of the structures. Therefore, initially rule (i) appears to be violated in cases where (iii) is valid, but prolonged heating will eventually lead to chemical equilibrium and appear to follow (i), *i.e.* two solid solutions tend to merge to one. In the cases where anion substitution occurs at elevated temperature (ii) the high temperature polymorph is often stabilised to lower temperatures. Here the dissolution of a metal halide at elevated temperatures appears to be a fast process but segregation of the metal halide at lower temperatures is often a slower process.

Thus, in conclusion, anion substitution and anion disorder is a well-known property of metal borohydrides that has been exploited to tailor hydrogen release properties, and more recently to develop ionic conductors. Cation disorder, on the other hand, has not been observed very often, with some examples being, $Mn_{1-x}Mg_x(BH_4)_2$, and $Li_3MZn_5(BH_4)_{15}$, M = Mg and Mn.[65,83] Only very recently have some researchers started to consider the functional design of physical properties by means of cation substitution, which in turn is the most dominant tool to tailor transition metal oxides. Cation disorder may occur for structures containing very large anions dominating structural organization,[4] or when the cations are very similar in size, such as for Mg^{2+} and Mn^{2+} with identical charge and similar ionic radius, $r(Mg^{2+}) = 0.71$ and $r(Mn^{2+}) = 0.80$ Å.[65] However, cation substitution can also occur for cations that have the same preferred coordination sphere such

 This journal is © The Royal Society of Chemistry 2017

as Li^+ and Mg^{2+} that both prefer tetrahedral coordination. Therefore the tri-metallic compound $Li_3MZn_5(BH_4)_{15}$, M = Mg and Mn may be considered as being derived from the bimetallic compound $LiZn_2(BH_4)_5$ by Li–Mg cation substitution.[83]

Fluorine substitution in hydridocomplexes is clearly possible, however the stability of the produced compounds is limited due to the formation of very stable ionic solids or molecular gases. The system Na–Al–F–H can provide the complex $Na_3AlH_{6-x}F_x$, which has a strong tendency to form fully fluorine substituted octahedral complexes $[AlF_6]^{3-}$.[238] Recall the composition of the rather stable mineral cryolite, Na_3AlF_6. The metal borohydride–borofluorides, $NaBH_4$–$NaBF_4$ and KBH_4–KBF_4, provide some new and partly fluorine substituted borohydride complexes, $NaBH_{2.1}F_{1.9}$ built from $[B(H,F)_4]^-$.[223,224] However, their stability is rather limited and these systems have a strong tendency to decompose to significantly more stable ionic metal fluorides or possibly the molecular compound, BF_3.

4.6 Trends in series of bimetallic borohydride halides

In some cases, series of bimetallic alkali metal–d-block metal borohydride halides have been investigated. The monometallic borohydrides are described as two different polymorphs for yttrium and cadmium. The existence of monometallic scandium and zinc borohydrides has been suggested, but they have not been observed experimentally. For the bimetallic systems containing lithium, only cadmium forms a ternary halide, Li_2CdCl_4.[146] For the tri-metallic systems containing lithium, synthesis of $Li_3MZn_5(BH_4)_{15}$ also yields some Li_2MCl_4, M = Mg or Mn.[83] However, ternary halides are formed in most cases for sodium and potassium systems.

The systems MBH_4–$ZnCl_2$ (M = Rb, Cs) and MBH_4–$ScCl_3$ (M = Rb, Cs) remain incompletely characterised due to their complexity. Thus, there is a tendency for more complex structural chemistry, higher numbers of compounds and solid solutions in the phase diagrams and more diverse compositions for heavier alkali metals.

4.7 Metal borohydride *closo*-boranes

There are a few examples of mixed borohydride *closo*-boranes.[1,252] Both $Cs_3BH_4B_{12}H_{12}$ and $Rb_3BH_4B_{12}H_{12}$ were thought to be by-products from the pyrolysis of their respective $B_3H_8^-$ compounds in 1990,[253] which can also be formed as decomposition products from bi- and trimetallic borohydride-perovskites.[78] The compound $Cs_3BH_4B_{12}H_{12}$ was presented in 2003 (see Fig. 11),[254] which can be precipitated from water. This compound crystallizes in a trigonal ($R\bar{3}m$) anti-perovskite structure type, where Cs^+ is considered as a shared vertex of two $[BH_4Cs_6]$ octahedra. Interestingly there is dynamic disorder of the BH_4^- anion at room temperature, whereas a further structural transition is believed to occur near 305 °C, which could involve rotation of the $B_{12}H_{12}^{2-}$ anions. This was also suggested by a more detailed study of the decomposition of borohydride-perovskites, and the symmetry of the high temperature cubic anti-perovskite polymorph was identified as $P23$.[255]

More recently $Na_3BH_4B_{12}H_{12}$ and $(Li_{0.7}Na_{0.3})_3BH_4B_{12}H_{12}$ were synthesized by mechanical milling followed by heat treatment and investigated for their ion conductivity properties.[256] $Na_3BH_4B_{12}H_{12}$ is orthorhombic $Cmc2_1$ and $(Li_{0.7}Na_{0.3})_3BH_4B_{12}H_{12}$ is orthorhombic $Pna2_1$. Filling the interstitial sites of $Na_3BH_4B_{12}H_{12}$ with Li^+ affords $(Li_{0.7}Na_{0.3})_3BH_4B_{12}H_{12}$, where both compounds appear to have ordered $B_{12}H_{12}^{2-}$ and BH_4^- anions, though no conclusions can be drawn on low frequency reorientations.

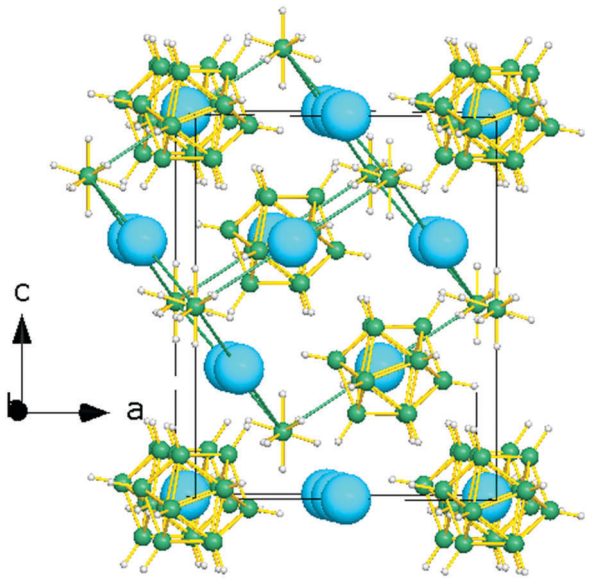


Fig. 11 Room temperature structure ($R\bar{3}m$) of $Cs_3BH_4B_{12}H_{12}$ viewed approximately along the *b*-axis of the hexagonal lattice. The anti-perovskite cubic unit cell of the high temperature polymorph ($P23$) is shown in green. Note the disordered borohydride anion already at room temperature. Cs (blue), B (green) and H (white).

4.8 Metal borohydride amides

The first composite of a metal borohydride and a metal amide, $LiBH_4$–$LiNH_2$ (1 : 2), was reported in 2005[257] with the aim of improving H_2 desorption temperatures, owing to partly negatively and positively charged H atoms present in the composite. In addition, it was shown in 2009 that composites of $LiBH_4$–$LiNH_2$ are good lithium ion conductors.[89] These two factors have inspired research into various other borohydride–amide composites, *e.g.* $Mg(BH_4)_2$–$LiNH_2$[258] and $Mg(BH_4)_2$–$Mg(NH_2)_2$ (see Table 10).[90] As described earlier in Section 4, halides may directly substitute for BH_4^- on the same crystallographic position. On the other hand, due to difference in size and coordination, the complex NH_2^- anion always has unique crystallographic sites compared to BH_4^- in borohydride-amide structures.

The first reported crystal structure of a borohydride–amide was $Li_4(BH_4)(NH_2)_3$, cubic ($I2_13$), with three independent lithium positions that all are coordinated by four ligands, *i.e.* three BH_4^- and one NH_2^-; one BH_4^- and three NH_2^-; and four NH_2^- (Fig. 12).[263,264] The rhombohedral structure ($R\bar{3}$) of $Li_2(BH_4)(NH_2)$ was later determined with two independent lithium positions that are coordinated by three BH_4^- and one NH_2^-; and one BH_4^- and three NH_2^-.[259,260] To our knowledge, the $LiBH_4$–$LiNH_2$ system is unique compared to the other metal borohydride amide systems in the way that new compounds are readily formed by mechanochemical treatment. In all other systems, mechanochemical treatment only leads to physical mixtures of the starting reactants.

Table 10 Overview of reported composites of $M(BH_4)_m$–$M'(NH_2)_m$

M in $M(BH_4)_m$	M′ in $M'(NH_2)_m$	Ratio	Synthesis	Product	Ref.
Li	Li	1 : 1	BM or heat	$Li_2(BH_4)(NH_2)$	259 and 260
Li	Li	1 : 2	BM	$Li_2(BH_4)(NH_2)$ + $Li_4(BH_4)(NH_2)_3$	257, 261 and 262
Li	Li	1 : 3	BM or heat	$Li_4(BH_4)(NH_2)_3$	259, 263 and 264
Na	Na	1 : 1	Heat	$Na_2(BH_4)(NH_2)$	91
Mg	Mg	1 : 1	BM + heat	$Mg(BH_4)(NH_2)$	90
Mg	Li	1 : 1	BM	Mixture of reactants	258
Li	Mg	1 : 1	BM	Mixture of reactants	265
Ca	Li	1 : 1	BM	Mixture of reactants[a]	266 and 267
Ca	Li/Na	1 : 1	BM	Mixture of reactants[a]	268
Ca	Mg/Ca	1 : 2	BM	Amorphous mixture	269

[a] Formation of $MCa(BH_4)_2(NH_2)$ M = Li, Na is proposed.[268]

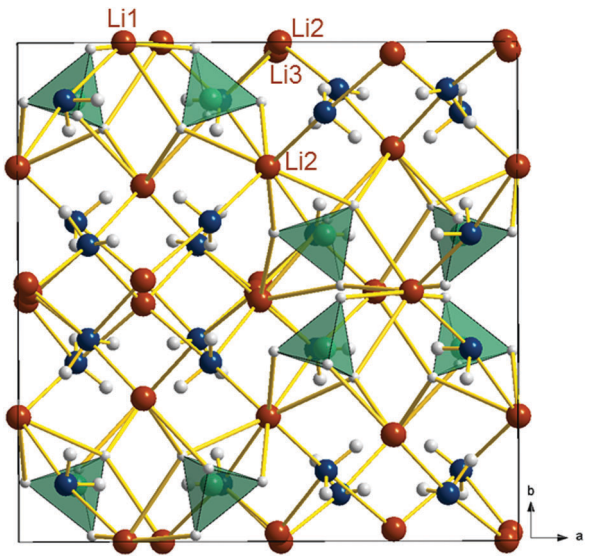


Fig. 12 Crystal structure of $Li_4(BH_4)(NH_2)_3$.[263,264] Remarkably, the crystal structure does not contain dihydrogen bonds, although the substance releases practically pure hydrogen under mild conditions. Li (red), B (green), N (blue) and H (white).

A high temperature polymorph, α-$Na_2(BH_4)(NH_2)$, was prepared by heating $NaBH_4$–$NaNH_2$ to the melting point, 219 °C, for 1 h and subsequently cooling to RT.[91] After longer annealing times (10 days) at lower temperatures, 98 °C, α-$Na_2(BH_4)(NH_2)$ transforms into the low temperature polymorph, β-$Na_2(BH_4)(NH_2)$. The cubic α-$Na_2(BH_4)(NH_2)$ crystallizes in the K_3SO_4F structure type ($Pm\bar{3}m$), whereas β-$Na_2(BH_4)(NH_2)$ has an orthorhombic structure (*Pbcm*). Both structures can directly be derived from the anti-perovskite type structure ABO_3, with the $[BH_4]^-$ and $[NH_2]^-$ moieties in the A and B sites, respectively. The charge balancing Na^+ ions occupy 2/3 of the O positions.

$Mg(BH_4)(NH_2)$ has been prepared by thermal treatment of $Mg(BH_4)_2$–$Mg(NH_2)_2$ at 180 °C.[90] The structure is tetragonal ($I\bar{4}1$) with the Mg^{2+} ions tetrahedrally coordinated by two BH_4^- and two NH_2^- ligands. This material exhibits relatively high Mg^{2+} ion conductivity of 10^{-6} S cm^{-1} at 150 °C.[270]

$LiCa(BH_4)_2(NH_2)$ and $NaCa(BH_4)_2(NH_2)$ are suggested to form by ball milling of $Ca(BH_4)_2$–MNH_2 (M = Li, Na),[268] however, structure determination is not reported.[266,267]

5. Derivatives of metal borohydrides with neutral molecules

Metal borohydrides have diverse compositions with rich and fascinating structural chemistry, which may be further expanded by the inclusion of other negatively charged anions, discussed in the previous sections of this review. Furthermore, a wide range of metal borohydrides containing neutral molecules have been discovered during the past few years that are the topic of the present section. The introduction of nitrogen in metal borohydrides has received significant interest owing to the possible inclusion of dihydrogen bonding *via* partly positively charged hydrogens, *e.g.* $B–H^{\delta-}\cdots{}^{+\delta}H–N$. Dihydrogen bonding is considered a new valuable approach for tailoring a material's physical and chemical properties. A high number of new ammine, NH_3, metal borohydrides have been discovered and trends in composition, structure and properties are first discussed in this section, followed by hydrazine, N_2H_4 and ammonia borane, NH_3BH_3 derivatives. Solvent molecules with nitrogen, oxygen or sulphur as donor atoms may also crystallize with metal borohydrides depending on synthesis conditions.

5.1 Ammine metal borohydrides

Ammine metal borohydrides, $M(BH_4)_m{\cdot}nNH_3$, have been known since the 1950's, but the number of new compounds has increased tremendously during the past ~5 years having received interest as both ammonia and hydrogen stores (Table 11). The number of BH_4^- anions (*m*) in the compounds is fixed and determined by the oxidation state of the metal, whereas the number of NH_3 ligands (*n*) may range from 1 to 8. Compared to the borohydride anions, NH_3 coordinates more strongly and less flexibly to the metal, *i.e.* always *via* an electron pair donated by N, and acts as a terminal ligand.

5.1.1 Mono-metallic ammine metal borohydrides. *Monoammine lithium borohydride*. $LiBH_4{\cdot}NH_3$, is the only reported ammine alkali metal compound stable at RT. Monoammine lithium borohydride crystallizes in an orthorhombic unit cell with symmetry *Pnma*.[271] Each Li atom is tetrahedrally coordinated by three BH_4^- units and one NH_3 molecule, while each BH_4^- unit is linked to three Li atoms and four NH_3 molecules *via* dihydrogen interactions.

Ammine magnesium borohydrides. $Mg(BH_4)_2{\cdot}nNH_3$, are known for n = 1, 2, 3 and 6, while the crystal structure for n = 1 remains

 This journal is © The Royal Society of Chemistry 2017

Table 11 Ammine metal borohydrides, $M(BH_4)_m{\cdot}nNH_3$, with known crystal structures

Compounds	n	Ref.
Mono-metallic		
$LiBH_4{\cdot}nNH_3$	1	271
$Mg(BH_4)_2{\cdot}nNH_3$	1,[a] 2, 3, 6	54, 272 and 273
$Ca(BH_4)_2{\cdot}nNH_3$	1, 2, 4, 6[b]	54 and 274–277
$Sr(BH_4)_2{\cdot}nNH_3$	1, 2, 4[b]	277 and 278
$Al(BH_4)_3{\cdot}nNH_3$	1, 6	279–281
$V(BH_4)_3{\cdot}nNH_3$	3	282
$Cr(BH_4)_2{\cdot}nNH_3$	6[b]	94
$Mn(BH_4)_2{\cdot}nNH_3$	1,[a] 2, 3, 6	54
$Fe(BH_4)_2{\cdot}nNH_3$	6[b]	94
$Co(BH_4)_2{\cdot}nNH_3$	6[b]	94
$Zn(BH_4)_2{\cdot}nNH_3$	2, 4[a]	119 and 283
$Y(BH_4)_3{\cdot}nNH_3$	1, 2, 4, 5, 6, 7	53
$Zr(BH_4)_4{\cdot}nNH_3$	8	284
$La(BH_4)_3{\cdot}nNH_3$	4, 4, 6	285
$Ce(BH_4)_3{\cdot}nNH_3$	4, 4, 5, 6	285
$Gd(BH_4)_3{\cdot}nNH_3$	4, 5, 6, 7	53
$Dy(BH_4)_3{\cdot}nNH_3$	4, 5, 6, 7	53
Bimetallic		
$LiMg(BH_4)_3{\cdot}nNH_3$	2	286
$Li_2Mg(BH_4)_2{\cdot}nNH_3$	6	54 and 287
$Li_2Al(BH_4)_5{\cdot}nNH_3$	6	288
$LiSc(BH_4)_4{\cdot}nNH_3$	4	282
$Li_2Mn(BH_4)_2{\cdot}nNH_3$	6	54
$Li_2Fe(BH_4)_2{\cdot}nNH_3$	6	94
$NaZn(BH_4)_3{\cdot}nNH_3$	2	289
Solid solutions		
$Mn_{1-x}Mg_x(BH_4)_2{\cdot}nNH_3$	6	54
$Co(BH_4)_{2-x}Cl_x{\cdot}nNH_3$	6[b]	94

[a] Detailed crystal structure remains unknown. [b] Unstable at RT.

unknown.[272,273] $Mg(BH_4)_2{\cdot}6NH_3$ is isostructural to $MgCl_2{\cdot}6NH_3$ (if the hydrogen atoms are not considered) and crystallizes in a cubic unit cell ($Fm\bar{3}m$), where Mg is octahedrally coordinated by six NH_3 molecules, forming $[Mg(NH_3)_6]^{2+}$ complexes, while BH_4^- act as counter ions in the crystalline solid.[272] $Mg(BH_4)_2{\cdot}3NH_3$ crystallizes in an orthorhombic unit cell with space group *Pnma*.[54] Here, Mg coordinates to two terminal BH_4^- anions and three NH_3 molecules, forming neutral molecular complexes $[Mg(BH_4)_2(NH_3)_3]$ connected by dihydrogen bonds between $H^{\delta-}$ from BH_4^- and $H^{\delta+}$ from NH_3. Similarly, $Mg(BH_4)_2{\cdot}2NH_3$ forms neutral complexes of $[Mg(BH_4)_2(NH_3)_2]$ where Mg is tetrahedrally coordinated by two BH_4^- anions and two neutral NH_3 ligands.[272]

Ammine calcium borohydrides. $Ca(BH_4)_2{\cdot}nNH_3$, are known for n = 1, 2, 4 and 6, where n = 6 is isostructural to $Mg(BH_4)_2{\cdot}6NH_3$ and consists of octahedral complexes $[Ca(NH_3)_6]^{2+}$ charge balanced by BH_4^-. A monoclinic ($P2_1/c$) $Ca(BH_4)_2{\cdot}4NH_3$ has Ca octahedrally coordinated by four equatorial NH_3 groups and two axial terminal BH_4^- groups forming neutral $[Ca(NH_3)_4(BH_4)_2]$ complexes.[277] The structure is composed of hcp octahedra layers in the *bc*-plane stacked along the *a*-axis in the order AAA, which are connected by dihydrogen bonds. $Ca(BH_4)_2{\cdot}2NH_3$ has an orthorhombic structure (*Pbcn*) in which Ca is coordinated octahedrally by four bridging BH_4^- groups and two terminal NH_3 groups. Ca and the four BH_4^- groups form a 2D layer stacked in the order ABAB.[275] $Ca(BH_4)_2{\cdot}NH_3$ has an orthorhombic unit cell ($Pna2_1$) with Ca octahedrally coordinated by one NH_3 group and five bridging BH_4^- ligands, creating zig-zag chains of edge sharing octahedra running along the *c*-axis forming a 3D network.[274]

Ammine strontium borohydrides. $Sr(BH_4)_2{\cdot}nNH_3$ (n = 1, 2, 4), have been reported with $Sr(BH_4)_2{\cdot}4NH_3$ being isostructural to $Ca(BH_4)_2{\cdot}4NH_3$.[277] $Sr(BH_4)_2{\cdot}2NH_3$ (orthorhombic, *Pnc*2) consists of Sr octahedrally coordinated by four bridging BH_4^- groups in-plane and by two axial NH_3 groups. Similar to $Ca(BH_4)_2{\cdot}2NH_3$, the four BH_4^- groups and the metal create a two-dimensional layer in the *bc*-plane stacked in the sequence AAA along the *a*-axis. The NH_3 groups are terminal ligands pointing between the layers. $Sr(BH_4)_2{\cdot}NH_3$ (orthorhombic, *Pbna*) has Sr coordinated octahedrally by five BH_4^- groups and one NH_3 group similar to Ca in $Ca(BH_4)_2{\cdot}NH_3$.[274] There are two different types of BH_4^- groups in the structure of $Sr(BH_4)_2{\cdot}NH_3$, one BH_4^- is bridging between three Sr atoms by the edge of the tetrahedron (η_2), while one BH_4^- group is bridging two Sr atoms by edge (η_2) and face (η_3) sharing. $Sr(BH_4)_2{\cdot}NH_3$ is a double layered structure in the *ab*-plane, where the identical layers are shifted by an *n*-glide plane. The layers are stacked along the *c*-axis in the sequence ABAB and connected by dihydrogen bonds.

Ammine aluminum borohydride. $Al(BH_4)_3{\cdot}nNH_3$, have been known for n = 1 since 1974,[290] whereas the structure of n = 6 was reported more recently.[281] $Al(BH_4)_3{\cdot}NH_3$ crystallizes in a monoclinic unit cell ($P2_1/n$) and consists of tetrahedral neutral complexes of $[Al(BH_4)_3(NH_3)]$. $Al(BH_4)_3{\cdot}6NH_3$ crystallizes in an orthorhombic unit cell (*Pbcn*) that consists of $[Al(NH_3)_6]^{3+}$ complexes, while BH_4^- act as counter ions in the crystalline solid.

Triammine vanadium borohydride. $V(BH_4)_3{\cdot}3NH_3$, crystallizes in a cubic system ($F23$) and consists of neutral $[V(BH_4)_3(NH_3)_3]$ complexes, where V is octahedrally coordinated.[282]

Hexaammine chromium, iron and cobalt borohydride. $M(BH_4)_2{\cdot}6NH_3$ (M = Cr, Fe, Co) with the metals in the oxidation state (II), are all isostructural and are also isostructural to $M(BH_4)_2{\cdot}6NH_3$ (M = Mg, Ca), *i.e.* consisting of $[M(NH_3)_6]^{2+}$ and $[BH_4]^-$ complexes.[94]

Ammine manganese borohydrides. $Mn(BH_4)_2{\cdot}nNH_3$, are known for n = 1, 2, 3 and 6, while the crystal structure for n = 1 remains unknown, and n = 2, 3 and 6 are all isostructural to the magnesium analogues.[54] Thus, $Mn(BH_4)_2{\cdot}6NH_3$ forms $[Mn(NH_3)_6]^{2+}$ complexes with BH_4^- as counter ions, while $Mn(BH_4)_2{\cdot}3NH_3$ and $Mn(BH_4)_2{\cdot}2NH_3$ contain neutral molecular complexes.

Tetraammine zinc borohydride. $Zn(BH_4)_2{\cdot}4NH_3$ is one of the first reported ammine metal borohydrides, but the crystal structure remains unknown.[119] More recently, $Zn(BH_4)_2{\cdot}2NH_3$, monoclinic ($P2_1$), was discovered and consists of neutral $[Zn(BH_4)_2(NH_3)_2]$ complexes connected by dihydrogen bonds.[283]

Ammine yttrium borohydrides. $Y(BH_4)_3{\cdot}nNH_3$ (n = 1, 2, 4, 5, 6 and 7), form the most extensive ammine metal borohydride series.[53] $Y(BH_4)_3{\cdot}7NH_3$ (orthorhombic, $Pca2_1$) contains cation complexes of Y surrounded by seven NH_3 molecules, forming a monocapped trigonal prism. The $[Y(NH_3)_7]^{3+}$ prisms form a hexagonal pattern in the *ab*-plane, which are stacked in the order ABAB along the *c*-axis. The structure of $Y(BH_4)_3{\cdot}6NH_3$ ($Pa\bar{3}$) is built from Y octahedrally coordinated by six ammonia molecules producing octahedral complexes $[Y(NH_3)_6]^{3+}$. The $[Y(NH_3)_6]^{3+}$

octahedra are ordered in a hexagonal pattern in (111) layers, which are stacked in the sequence ABC along the [111] direction. Compared to the other ammine yttrium borohydrides, $Y(BH_4)_3{\cdot}6NH_3$ has a low density and the BH_4^- may be relatively mobile. $Y(BH_4)_3{\cdot}5NH_3$ has a hexagonal unit cell ($P6_3$) with Y eight-fold coordinated by five NH_3 molecules and three terminal BH_4^- groups in molecular complexes $[Y(NH_3)_5(BH_4)_3]$. The complexes $[Y(NH_3)_5(BH_4)_3]$ are packed in the *ab*-plane in a hexagonal pattern, which are stacked in the order ABAB along the *c*-axis. $Y(BH_4)_3{\cdot}4NH_3$ crystallizes in an orthorhombic unit cell ($Pna2_1$) and Y is seven-fold coordinated by four NH_3 and three BH_4^-, creating neutral molecular complex $[Y(NH_3)_4(BH_4)_3]$. The molecular complexes are packed in *ab*-layers in a hexagonal pattern, which are stacked in the order ABAB along the *c*-axis. $Y(BH_4)_3{\cdot}2NH_3$ (orthorhombic, *Pbca*) with Y^{3+} coordinated to two NH_3 and to four BH_4^- groups in an octahedron, where two of the BH_4^- groups are bridged to other yttrium atoms. Thus, the solid $Y(BH_4)_3{\cdot}2NH_3$ consists of one-dimensional zig-zag ribbons running along the *a*-axis. $Y(BH_4)_3{\cdot}NH_3$ is orthorhombic ($Cmc2_1$) with Y^{3+} coordinated by one NH_3 and five BH_4^- groups, where four of the BH_4^- groups are bridging other yttrium atoms, forming 2D layers stacked in the order ABAB.

Ammine zirconium borohydride. $Zr(BH_4)_4{\cdot}nNH_3$, has the highest number of coordinated NH_3, *i.e.* $n = 8$, and crystallizes in an orthorhombic unit cell (*Pnma*).[284] The structure is built from complex cations $[Zr(NH_3)_8]^{4+}$ charge balanced by BH_4^-.

Ammine lanthanum borohydrides. $La(BH_4)_3{\cdot}nNH_3$ (n = α-4, β-4, 6), have recently been reported.[285] $La(BH_4)_3{\cdot}6NH_3$ crystallizes in an orthorhombic unit cell ($P2_12_12_1$) with La^{3+} coordinated by six NH_3 ligands and two terminal BH_4^- groups, creating a large complex cation $[La(BH_4)_2(NH_3)_6]^+$ that is charged balanced by one BH_4^- (Fig. 13) α-$La(BH_4)_3{\cdot}4NH_3$ and β-$La(BH_4)_3{\cdot}4NH_3$ are, together with the cerium analogues, the only examples of ammine metal borohydrides having two polymorphs. α-$La(BH_4)_3{\cdot}4NH_3$ crystallizes in a monoclinic unit cell ($I2$), where La^{3+} is coordinated by four NH_3 groups and three BH_4^- groups, creating molecular clusters $[La(BH_4)_3(NH_3)_4]$. β-$La(BH_4)_3{\cdot}4NH_3$ are isostructural to $M(BH_4)_3{\cdot}4NH_3$ (M = Y, Gd, Dy).

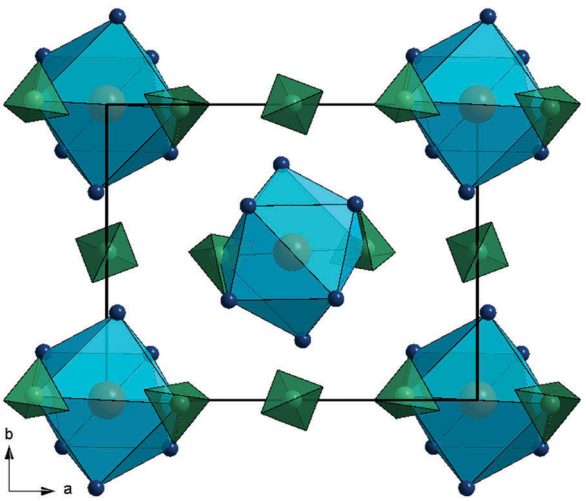


Fig. 13 The structures of $[M(BH_4)_2(NH_3)_6]BH_4$ (M = Ce, La) have two different BH_4^- environments in the same compound.

Cerium lanthanum borohydrides. $Ce(BH_4)_3{\cdot}nNH_3$ (n = α-4, β-4, 5, 6), have been reported.[285] α-and β-$Ce(BH_4)_3{\cdot}4NH_3$ are isostructural to α- and β-$La(BH_4)_3{\cdot}4NH_3$, while $Ce(BH_4)_3{\cdot}5NH_3$ and $Ce(BH_4)_3{\cdot}6NH_3$ are isostructural to $M(BH_4)_3{\cdot}5NH_3$ (M = Y, Gd, Dy) and $La(BH_4)_3{\cdot}6NH_3$, respectively.

5.1.2 Bimetallic ammine metal borohydrides. Seven ammine bimetallic borohydrides have been reported in the scientific literature. Here, NH_3 always coordinates to the metal with the highest charge density, which also has the higher oxidation number, while the metal with lower charge density, typically Li or Na, only coordinate to BH_4^-.

Diammine lithium magnesium borohydride. $LiMg(BH_4)_3{\cdot}2NH_3$, has a hexagonal unit cell ($P6_3$), where Mg is five-fold coordinated and resides in triangular-bipyramidal coordination, with the N atoms located at the axial positions of this polyhedron and the BH_4^- groups at the equatorial positions.[286] Li atoms are located in a triangular antiprism formed by six BH_4^- groups.

Hexaammine dilithium magnesium borohydride. $Li_2Mg(BH_4)_4{\cdot}6NH_3$ (tetragonal, $P4_2/mnm$) is another known ammine bimetallic borohydride based on lithium and magnesium[54,286–291] built from distinct $[Mg(NH_3)_6]^{2+}$ complex ions counter-balanced by one-dimensional $[Li_2(BH_4)_4]_n^{2-}$ polymers.[52,281]

Hexaammine dilithium aluminum borohydride. $Li_2Al(BH_4)_5{\cdot}6NH_3$, was the first ammine bimetallic borohydride reported and reveals a promising hydrogen storage capacity and thermal decomposition temperature.[288] The structure of $Li_2Al(BH_4)_5{\cdot}6NH_3$ is hexagonal ($P\bar{3}c$), where Al is octahedrally coordinated by NH_3 forming complex cations $[Al(NH_3)_6]^{3+}$, as in $Al(BH_4)_3{\cdot}6NH_3$. Li is tetrahedrally coordinated by BH_4^-, and the $Li[BH_4]_4$ tetrahedra are then vertex-linked through three bridging BH_4^- units with the fourth BH_4^- in the *trans* position, leading to the formation of a two-dimensional honeycomb-patterned sheet that spreads along the *ab* plane.

Tetraammine lithium scandium borohydride. $LiSc(BH_4)_4{\cdot}4NH_3$, crystallizes in an orthorhombic unit cell ($Pc2_1n$), where Sc is octahedrally coordinated by three NH_3 ligands and three BH_4^- groups.[282]

Hexaammine dilithium manganese borohydride. $Li_2Mn(BH_4)_4{\cdot}6NH_3$, and hexaammine dilithium iron borohydride, $Li_2Fe(BH_4)_4{\cdot}6NH_3$, are isostructural to $Li_2Mg(BH_4)_2{\cdot}6NH_3$ and consist of $[M(NH_3)_6]^{2+}$ complexes and $[Li_2(BH_4)_4]_n^{2-}$ polymers.[54,94]

Diammine sodium zinc borohydride. $NaZn(BH_4)_3{\cdot}2NH_3$, crystallizes in an orthorhombic unit cell ($P2_1nb$) and consists of large complex bimetallic cations $[NaZn(BH_4)_2(NH_3)_2]^+$ charge balanced by BH_4^-.[289]

5.1.3 Solid solutions of ammine metal borohydrides. Only two solid solutions of ammine metal borohydrides have been reported, which are $Mn_{1-x}Mg_x(BH_4)_2{\cdot}6NH_3$ where the metal cation site is statistically disordered,[54] and $Co(BH_4)_{2-x}Cl_x{\cdot}6NH_3$ where the anion site is partially occupied by Cl^- and BH_4^-.[94] Both $Mn_{1-x}Mg_x(BH_4)_2{\cdot}6NH_3$ and $Co(BH_4)_{2-x}Cl_x{\cdot}6NH_3$ have the cubic symmetry $Fm\bar{3}m$.

5.1.4 Structural trends for ammine metal borohydrides. Ammine metal borohydrides are represented by a range of

 This journal is © The Royal Society of Chemistry 2017

Table 12 Structural trends of ammine mono-metallic and bimetallic borohydrides

M	Composition	Space group	Coordination environment of the metal		Ref.
Structures with one-dimensional chains					
Li	$MBH_4{\cdot}NH_3$	*Pnma*	Li^+: coordinated by one NH_3 and three BH_4^-		271
Y	$M(BH_4)_3{\cdot}2NH_3$	*Pbca*	Y^{3+}: coordinated by two NH_3 and four BH_4^-		53 and 291
Structures with two-dimensional layers					
Ca	$M(BH_4)_2{\cdot}NH_3$	*Pbcn*	Ca^{2+}: coordinated by one NH_3 and five BH_4^-		274
Ca	$M(BH_4)_2{\cdot}2NH_3$	$Pna2_1$	Ca^{2+}: coordinated by two NH_3 and four BH_4^-		275
Sr	$M(BH_4)_2{\cdot}NH_3$	*Pbna*	Sr^{2+}: coordinated by one NH_3 and five BH_4^-		277
Sr	$M(BH_4)_2{\cdot}2NH_3$	*Pnc*2	Sr^{2+}: coordinated by two NH_3 and four BH_4^-		277
Y	$M(BH_4)_3{\cdot}NH_3$	$Cmc2_1$	Y^{3+}: coordinated by one NH_3 and five BH_4^-		53
Structures with neutral molecular complexes					
Mg, Mn	$M(BH_4)_2{\cdot}2NH_3$	*Pcab*	$[M(BH_4)_2(NH_3)_2]$		54 and 272
Mg, Mn	$M(BH_4)_2{\cdot}3NH_3$	*Pnma*	$[M(BH_4)_2(NH_3)_3]$		54
Ca, Sr	$M(BH_4)_2{\cdot}4NH_3$	$P2_1/c$	$[M(BH_4)_2(NH_3)_4]$		277
Al	$M(BH_4)_3{\cdot}NH_3$	$P2_1/n$	$[M(BH_4)_3(NH_3)]$		290
Y, Gd, Dy, Ce	$M(BH_4)_3{\cdot}4NH_3$	$Pna2_1$	$[M(BH_4)_3(NH_3)_4]$		53 and 285
Y, Gd, Dy, Ce	$M(BH_4)_3{\cdot}5NH_3$	$P6_3$	$[M(BH_4)_3(NH_3)_5]$		53 and 285
V	$M(BH_4)_3{\cdot}3NH_3$	*F*23	$[M(BH_4)_3(NH_3)_3]$		282
Zn	$M(BH_4)_2{\cdot}2NH_3$	$P2_1$	$[M(BH_4)_2(NH_3)_2]$		119
Ce, La	$M(BH_4)_3{\cdot}4NH_3$	*I*2	$[M(BH_4)_3(NH_3)_4]$		285
Structures with complex cations and anions					
Mg, Mn, Fe	$Li_2M(BH_4)_4{\cdot}6NH_3$	$P4_2/mnm$	$[M(NH_3)_6]^{2+}$	$[Li_2(BH_4)]_n^{2-}$	54, 94 and 287
Mg, Ca, Mn, Cr, Fe, Co	$M(BH_4)_2{\cdot}6NH_3$	$Fm\bar{3}m$	$[M(NH_3)_6]^{2+}$	BH_4^-	54, 94, 272 and 277
Al	$Li_2M(BH_4)_5{\cdot}6NH_3$	$P\bar{3}c1$	$[M(NH_3)_6]^{3+}$	$[Li_2(BH_4)]_5^{3-}$	288
Al	$M(BH_4)_2{\cdot}6NH_3$	*Pbcn*	$[M(NH_3)_6]^{3+}$	BH_4^-	281
Zn	$NaM(BH_4)_3{\cdot}2NH_3$	$P2_1nb$	$[NaM(BH_4)_2(NH_3)_2]^+$	BH_4^-	289
Y, Gd, Dy	$M(BH_4)_3{\cdot}6NH_3$	$Pa\bar{3}$	$[M(NH_3)_6]^{3+}$	BH_4^-	53
Y, Gd, Dy	$M(BH_4)_3{\cdot}7NH_3$	$Pca2_1$	$[M(NH_3)_7]^{3+}$	BH_4^-	53
Zr	$M(BH_4)_3{\cdot}8NH_3$	*Pnma*	$[M(NH_3)_8]^{4+}$	BH_4^-	284
Ce, La	$M(BH_4)_3{\cdot}6NH_3$	$P2_12_12_1$	$[M(BH_4)_2(NH_3)_6]^+$	BH_4^-	285

different structure types and an overview is provided in Table 12. The structures of magnesium, calcium, strontium, manganese and yttrium borohydride consist of three-dimensional networks of $[M(BH_4)_6]$ octahedra or $[M(BH_4)_4]$ tetrahedra, where each BH_4^- group bridge between two metal atoms with edge (η^2) coordination.[129,137,142,145,197] Introduction of NH_3 molecules interrupts these frameworks. For the series of ammine yttrium borohydrides, the structures vary from two-dimensional layers (n = 1), one-dimensional chains (n = 2), molecular compounds (n = 4 and 5) to those containing large complex cations (n = 6 and 7), see Fig. 14. Similar structural variations appear for the other series of compounds. In general, molecular structures appear when the total number of ligands (NH_3 + BH_4^-) match the preferred coordination number of the cations, *e.g.* $[Mn(BH_4)_2(NH_3)_2]$ and $[Sr(BH_4)_2(NH_3)_4]$. For compounds with higher numbers of coordinated NH_3 molecules, BH_4^- becomes a counter ion, *e.g.* $[Ca(NH_3)_6](BH_4)_2$ and $[Y(NH_3)_n](BH_4)_3$ (n = 6 and 7), whereas one- or two-dimensional structures are formed for compounds with lower numbers of coordinated NH_3 molecules.

The NH_3 coordinated metal cations may be described as complex cations, and the complete structure may be illustrated as a packing of the complex cations (relatively close to being spherical) and borohydride anions. The dihydrogen contacts between them lower the symmetry compared to the simple packing of spheres.

Metal–nitrogen bond distances for selected ammine metal borohydrides plotted as a function of the ionic radius are shown in Fig. 15. As expected, the M–N bond distances increase approximately linearly with increasing ionic radius, and the M–N bond distances do not vary significantly for varying numbers of NH_3 ligands, *e.g.*, the Sr–N bond lengths only varies from 2.69–2.70 Å for $Sr(BH_4)_2{\cdot}nNH_3$ (n = 1, 2 and 4). However, the Zr–N interactions are outliers for this trend with bond

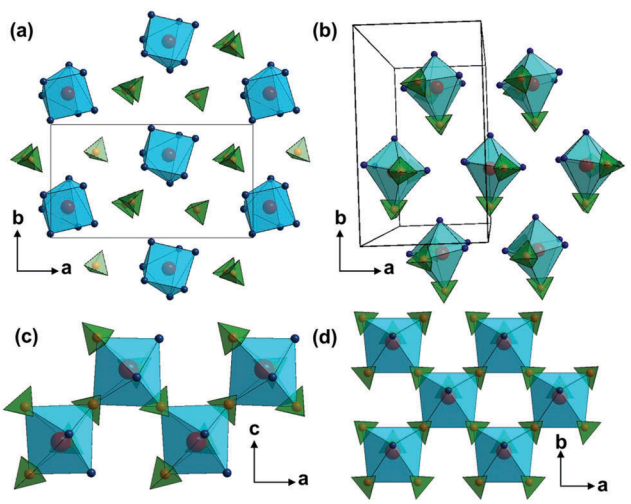


Fig. 14 The four different structure types observed for $Y(BH_4)_3{\cdot}nNH_3$, *i.e.* (a) complex cations (n = 7); (b) molecular compounds (n = 4); (c) one dimensional chains (n = 2); (d) 2D-layered structures (n = 1).

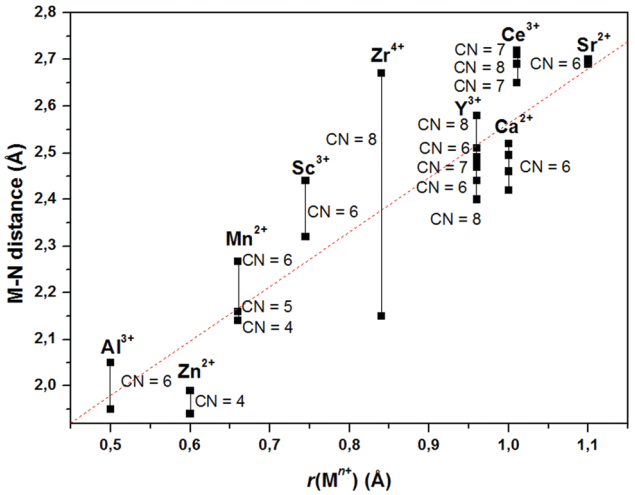


Fig. 15 Metal–nitrogen bond distances for selected ammine metal borohydrides plotted as a function of the ionic radius of the metal. The coordination number (CN) of the metals are provided and represents the number of BH_4^- and NH_3 coordinated to the metal.

lengths ranging 2.15–2.67 Å observed in the $[Zr(NH_3)_8]^{4+}$ side-bicapped trigonal prism for $[Zr(NH_3)_8](BH_4)_4$.[284]

On the other hand, the coordination of BH_4^- tetrahedra to a metal is more flexible, illustrated by the range of M–B distances and varying hapticities from η^0 to η^3 (Fig. 16), *i.e.* BH_4^- can be either a terminal or bridging ligand or act as a counter-ion. As expected, when BH_4^- coordinates to a metal in a partly covalent manner, *i.e.* η^1 to η^3 then bond distances increase for increasing ionic radii of the metal, which is also observed for metal borohydrides.[292] M–B distances substantially increase for decreasing hapticities in the yttrium based series $Y(BH_4)_3{\cdot}nNH_3$: where Y–B is in the range of 4–5 Å when BH_4^- has dominantly ionic interactions with ammine yttrium complexes (η^0) for n = 6, 7 (see Table 13).

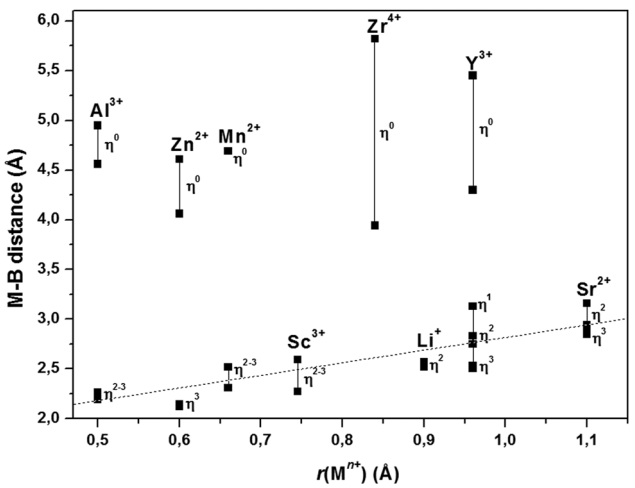


Fig. 16 Metal–boron distances and hapticities (η^x) for selected ammine metal borohydrides plotted as a function of the ionic radius of the metal. Due to the weak scattering of H, hapticities are tentative for structures that are not DFT optimized, *i.e.* $\eta(Al^{3+}) = 2–3$, $\eta(Mn^{2+}) = 2–3$ and $\eta(Sc^{3+}) = 2–3$. The large M–B distances >3.5 occur for BH_4^- acting as a counter anion, η^0.

In ammine bimetallic borohydrides, NH_3 coordinates to the metal with the highest charge density, whereas BH_4^- may coordinate to both metals.

The unit cell volumes per formula unit (V/Z) at RT as a function of the number of NH_3 molecules, n, in the formula unit for $M(BH_4)_m{\cdot}nNH_3$ (M = Ca, Sr, Mn and Y, Fig. 17) reveals an approximately linear relationship for each series. For the manganese-based series, $Mn(BH_4)_2{\cdot}nNH_3$, the slope of the straight line is 34.0 Å^3 per molecule (R^2 = 0.9998) corresponding well to the size of one ammonia molecule, which in solid NH_3 at −80 °C is $V(NH_3)$ = 33.9 Å^3.[293] In order to include $Li_2Mn(BH_4)_4$ in the plot, the volume of two $LiBH_4$ ($V(LiBH_4)$ = 54.2 Å^3)[24] has been subtracted from $V(Li_2Mn(BH_4)_4{\cdot}6NH_3)$, which has a slightly lower V/Z than $Mn(BH_4)_2{\cdot}6NH_3$. Similarly, the DFT optimized structures of $Y(BH_4)_3{\cdot}nNH_3$ increase linearly as a function of n (37.3 Å^3, R^2 = 0.9916), whereas the experimental values deviate slightly from the linear trend.

All ammine metal borohydride structures contain dihydrogen $H^{\delta-}\cdots H^{\delta+}$ contacts between partly positively charged hydrogen, $H^{\delta+}$ bonded to N and partly negatively charged hydrogen, $H^{\delta-}$ bonded to B. The shortest distance, 1.850 Å, between $[Y(NH_3)_7]^{3+}$ and BH_4^- anions is obtained by DFT optimization of $Y(BH_4)_3{\cdot}7NH_3$ determined by X-ray diffraction. However, as discussed in Section 5.1.5, the strength of the dihydrogen bonds do not play a significant role for the composition of the released gases on thermal decomposition.

Structural analogies between ammine metal borohydrides and chlorides or bromides exist, considering only heavier atoms, *i.e.* neglecting hydrogen atoms. For example, $M(BH_4)_2{\cdot}6NH_3$ (M = Mg and Ca) and $MgX_2{\cdot}6NH_3$ (X = Cl and Br) are isostructural, and $Sr(BH_4)_2{\cdot}2NH_3$ and $MCl_2{\cdot}2NH_3$ (M = Ca and Sr) are structurally similar. The borohydride complex, BH_4^-, is a non-spherical anion in contrast to the halide anions; therefore crystal structures of ammine metal borohydrides often have lower symmetry than their halide analogues, as usually observed when comparing metal borohydrides and metal halides. A high degree of structural similarity is observed between compounds with high numbers of coordinated ammonia (n), where both the BH_4^- anion and the halides, X^-, act as counter ions with a predominantly ionic bonding, η^0.

5.1.5 Thermal properties of ammine metal borohydrides. The research of ammine metal borohydrides as potential hydrogen storage materials was initiated by Soloveichik *et al.* in 2008, studying $Mg(BH_4)_2{\cdot}2NH_3$, which mainly releases H_2 upon decomposition, whereas $Mg(BH_4)_2{\cdot}6NH_3$ mainly releases NH_3.[272] Since then, ammine metal borohydrides have attracted attention as promising hydrogen storage materials, *e.g.*, the compounds $Al(BH_4)_3{\cdot}6NH_3$, $Li_2Al(BH_4)_5{\cdot}6NH_3$ and $Zn(BH_4)_2{\cdot}2NH_3$ release 9–12 wt% H_2 in the temperature range 115–170 °C with traces of NH_3.[279,283,288] In comparison, the decomposition of metal borohydrides, $M(BH_4)_m$, below 200 °C is always accompanied by the release of diborane, B_2H_6.

Interestingly, ammine metal borohydrides with low electronegativities (χ_p < 1.6) often display reduced temperatures for gas release when compared to the pure metal borohydride. On the other hand, ammine metal borohydrides with high electronegativities (χ_p > 1.6) are often more thermally stable than

 This journal is © The Royal Society of Chemistry 2017

Table 13 Overview of the coordination of Y, CN(Y), and selected bond lengths for $Y(BH_4)_3{\cdot}nNH_3$.[53] The distances and hapticities (η^x) are obtained from DFT optimized crystal structures with experimental unit cell parameters

	n = 0	n = 1	n = 2	n = 4	n = 5	n = 6	n = 7
CN(Y)[a]	6	6	6	7	8	6	7
CN(Y)[b]	12	12	12	10	8	6	7
Y–N (Å)	—	2.48	2.51	2.44–2.49	2.40–2.58	2.47–2.48	2.47–2.51
Y–B1 (Å)	2.74 (η^2)	2.50 (η^3)	2.53(η^3)	2.80 (η^2)	3.13 (η^1)	5.04 (η^0)	4.30 (η^0)
Y–B2 (Å)	2.75 (η^2)	2.77 (η^2)	2.53(η^3)	2.80 (η^2)		5.15 (η^0)	4.69 (η^0)
Y–B3 (Å)		2.80 (η^2)	2.79 (η^2)	2.83 (η^2)		5.41 (η^0)	4.72 (η^0)
Y–B4 (Å)			2.80 (η^2)			5.45 (η^0)	4.97 (η^0)
Structure type	3D-framework	2D-layers	1D-chains	Molecular	Molecular	Ionic complexes	Ionic complexes

[a] Number of BH_4^- and NH_3 ligands coordinated to Y. [b] Number of H (from BH_4^-) and N (from NH_3) atoms coordinated to Y.

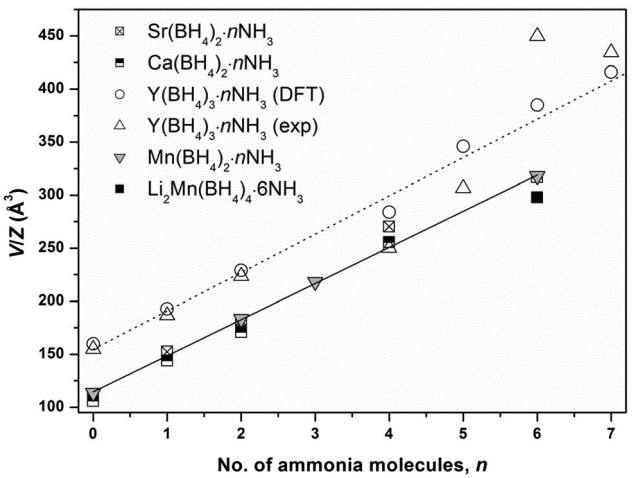


Fig. 17 Unit cell volumes (V) at RT divided by the number of formula units (Z) plotted as a function of the number of ammonia molecules, n, in the formula unit, $M(BH_4)_m{\cdot}nNH_3$. The dashed and solid line correspond to linear fit to the DFT optimized values for $Y(BH_4)_3{\cdot}nNH_3$ and the experimental values for $Mn(BH_4)_2{\cdot}nNH_3$, respectively. The unit cell volume of $Li_2Mn(BH_4)_4{\cdot}6NH_3$ subtracted the volume of two formula units of $LiBH_4$ is also included.

their respective metal borohydride.[54] The stabilization could be due to complex formation in ammine metal borohydrides with high electronegativities ($\chi_P > 1.6$), causing a shielding effect to the metal cation. For example, $Zr(BH_4)_4$ decomposes by sublimation and releases a mixture of B_2H_6 and H_2 at T_{sub} = 29 °C, whereas $[Zr(NH_3)_8](BH_4)_4$ mainly releases H_2 with only impurities of NH_3 at 130 °C.[109,284]

In the literature, H_2 rich (and NH_3 poor) gas streams are often attributed to strong dihydrogen bonds, however, recent experimental results disagree with this hypothesis.[53,54,277] NH_3 is released for $Y(BH_4)_3{\cdot}nNH_3$ (n = 7 and 6), which reveals the strongest dihydrogen bonds (~1.85 Å) among the $Y(BH_4)_3{\cdot}nNH_3$ (n = 7, 6, 5, 4, 2 and 1) compounds. The NH_3/BH_4^- ratios (n/m) also cause higher hydrogen purity for low n/m ratios in some cases, *i.e.* $M(BH_4)_m{\cdot}nNH_3$ (M = Mg, Mn and Y) but not others, *i.e.* $LiBH_4{\cdot}NH_3$, $Ca(BH_4)_2{\cdot}NH_3$ and $Sr(BH_4)_2{\cdot}NH_3$. Therefore, the composition of the released gas depends on two factors:[277]

(i) The stability of the metal borohydride. If the thermal stability of an ammine metal borohydride is similar to or higher than the thermal stability of the corresponding metal borohydride, then H_2 is released. In contrast, NH_3 is released if the thermal stability of the ammine metal borohydride is significantly lower than the corresponding metal borohydride (Fig. 18). $Ca(BH_4)_2{\cdot}nNH_3$ and $Sr(BH_4)_2{\cdot}nNH_3$ clearly become more stable for lower n/m ratios, however, they still decompose at significantly lower temperatures than $M(BH_4)_2$, M = Ca, Sr, and they release NH_3 only. At higher temperatures the remaining $M(BH_4)_2$, M = Ca, Sr, decompose and release hydrogen. Similarly, $Y(BH_4)_3{\cdot}nNH_3$ (n = 7, 6 and 5), release NH_3 at significantly lower temperatures than the decomposition temperature of $Y(BH_4)_3$, $T_{dec}(Y(BH_4)_3)$ ~200 °C, whereas the compounds $Y(BH_4)_3{\cdot}nNH_3$ (n = 4, 2 and 1) release decreasing amounts of NH_3 in the gas mixture consisting of NH_3 and H_2 in the temperature range, T ~ 160–200 °C, approaching $T_{dec}(Y(BH_4)_3)$ ~ 200 °C. Ammine metal borohydrides based on less stable metal borohydrides, *e.g.* M = Al, Zn, Zr and V,[279,280,283,284] do not release pure NH_3 gas, possible because of the lower decomposition temperature of the respective metal borohydrides. Thus, the less stable metal borohydrides react with NH_3 upon decomposition and release H_2 (and in some cases also some NH_3). As an example, $Al(BH_4)_3{\cdot}6NH_3$ releases H_2 and small amounts of NH_3 at ~165 °C, where $Al(BH_4)_3$ is unstable, $T_{dec}(Al(BH_4)_3)$ ~ 25 °C

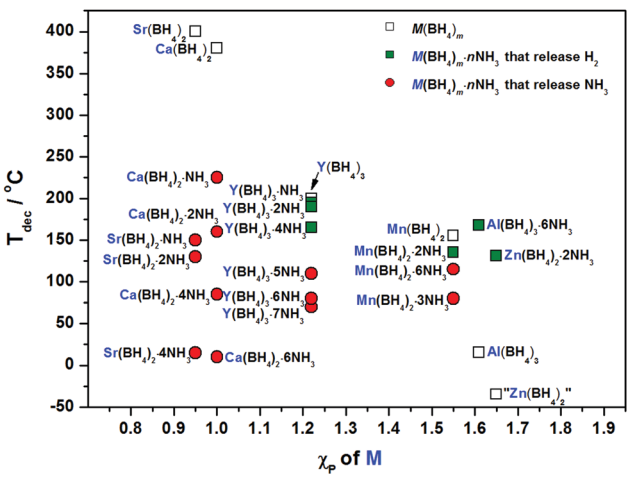


Fig. 18 Decomposition temperatures for selected ammine metal borohydrides and the corresponding metal borohydrides as a function of electronegativity ($Zn(BH_4)_2$ is not experimentally investigated but considered unstable). Ammonia is released when the metal borohydride is more stable than the corresponding ammine metal borohydride (red circle) otherwise hydrogen is released (green square). Adapted with permission from ref. 277. Copyright 2015 John Wiley and Sons.

(Fig. 18).[279] This hydrogen release can be decreased even lower (~120 °C) by encapsulating $Al(BH_4)_3{\cdot}6NH_3$ within a nanoporous polymer.[294]

(ii) The partial pressure of ammonia. In a closed system, the partial pressure of ammonia increases upon ammonia release, $p(NH_3) > 0$, during thermolysis of $LiBH_4{\cdot}NH_3$, $Ca(BH_4)_2{\cdot}nNH_3$ and $Sr(BH_4)_2{\cdot}nNH_3$. At higher temperatures, the released ammonia gas reacts with the metal borohydride, releasing hydrogen exothermically in a solid gas reaction.[275,295]

5.1.6 Mechanism for gas release of ammine metal borohydrides. Hydrogen release from ammine metal borohydrides appears always to be exothermic, which indicates that a chemical reaction is responsible for the gas release. This may suggest that hydrogen is released in an elimination reaction between $H^{\delta+}$ and $H^{\delta-}$. Furthermore, we notice that the thermal stability for ammine metal borohydrides and ammine metal chlorides are similar when comparing the peak temperature of NH_3 release, $T_{dec}(NH_3)$. As examples, $Y(BH_4)_3{\cdot}7NH_3$ ($T_{dec}(NH_3)$ ~ 80 °C) is slightly less stable than $YCl_3{\cdot}7NH_3$ ($T_{dec}(NH_3)$ ~ 100 °C),[291] and $Mg(BH_4)_2{\cdot}6NH_3$ ($T_{dec}(NH_3)$ ~ 150 °C) and $MgCl_2{\cdot}6NH_3$ ($T_{dec}(NH_3)$ ~ 150 °C) have similar thermal stability,[296] whereas $Mn(BH_4)_2{\cdot}6NH_3$ ($T_{dec}(NH_3)$ ~ 130 °C) is slightly more stable than $MnCl_2{\cdot}6NH_3$ ($T_{dec}(NH_3)$ ~ 105 °C).[297] This observation may indicate that the release of ammonia is mainly determined by the strength of the metal–ammonia (M–N) bond in the complex. Thus, the above observations support that there is no direct relation between dihydrogen bond strength, $N{-}H^{\delta+}\cdots{}^{-\delta}H{-}B$, in the solid state and the composition of the released gas. Moreover, hydrogen release from ammine metal borohydrides may in fact be due to a chemical reaction between the proposed intermediate, diborane, B_2H_6, which may take part in the decomposition of metal borohydrides and ammonia released simultaneously or at slightly lower temperatures. We note that diborane release is always suppressed for ammine metal borohydrides as compared to the respective metal borohydrides.

5.2 Hydrazine metal borohydride complexes

Six hydrazine metal borohydride complexes, $M(BH_4)_m{\cdot}nNH_2NH_2$, are known (see Table 14) based on M = Li, Na and Mg, where $LiBH_4{\cdot}NH_2NH_2$ and $LiBH_4{\cdot}2NH_2NH_2$ were first reported in 2012.[118] In 2013 four more hydrazine metal borohydride complexes were reported, *i.e.* $NaBH_4{\cdot}NH_2NH_2$, $Mg(BH_4)_2{\cdot}3NH_2NH_2$, $LiBH_4{\cdot}1/2NH_2NH_2$, $LiBH_4{\cdot}1/3NH_2NH_2$.[117] In contrast to ammonia, NH_3, hydrazine, NH_2NH_2, is a more flexible ligand that can bridge between two metals or be a terminal ligand. The coordination to the metal is always *via* a lone pair donated by a nitrogen atom.

Table 14 Metal borohydride hydrazine complexes with known crystal structures

M in $M(BH_4)_m$	Composition of complex	Symmetry	Ref.
Li	$LiBH_4{\cdot}1/3NH_2NH_2$	Monoclinic, $P2_1$	117
Li	$LiBH_4{\cdot}1/2NH_2NH_2$	Orthorhombic, $P2_12_12_1$	117
Li	$LiBH_4{\cdot}NH_2NH_2$	Monoclinic, Cc	118
Li	$LiBH_4{\cdot}2NH_2NH_2$	Orthorhombic, $Pca2_1$	118
Na	$NaBH_4{\cdot}NH_2NH_2$	Monoclinic, $P2_1/c$	117
Mg	$Mg(BH_4)_2{\cdot}3NH_2NH_2$	Trigonal, $P\bar{3}1c$	117

$LiBH_4{\cdot}NH_2NH_2$ crystallizes in a monoclinic unit cell (Cc) with lithium tetrahedrally coordinated by two BH_4^- and two NH_2NH_2 groups. $LiBH_4{\cdot}2NH_2NH_2$ crystallizes in an orthorhombic unit cell ($Pca2_1$), where lithium coordinates four NH_2NH_2. NH_2NH_2 bridges between two lithium cations forming chain-like cationic complexes $[Li(NH_2NH_2)_4]^+$, which are separated by BH_4^- (see Fig. 19).

$LiBH_4{\cdot}1/2NH_2NH_2$ crystallizes in an orthorhombic unit cell ($P2_12_12_1$) and consists of two-dimensional layers. Li^+ is coordinated by three BH_4^- ligands and one NH_2NH_2 that is bridged to the neighbouring Li^+. There are two types of BH_4^- ligands that both coordinate to Li through the edge (η^2). One BH_4^- is located in the same plane as the Li atoms and coordinates to four Li atoms, while one BH_4^- is positioned slightly above (or below) the plane and coordinates to two Li atoms.

$LiBH_4{\cdot}1/3NH_2NH_2$ crystallizes in a monoclinic unit cell ($P2_1$). Three independent Li atoms are tetrahedrally coordinated, one by four BH_4^- and two by three BH_4^- and one hydrazine molecule. While borohydrides are shared by three or four Li atoms, the hydrazine molecule only bridges two Li atoms. Hence, the resulting 3D framework is rather complex.

$NaBH_4{\cdot}NH_2NH_2$ crystallizes in a monoclinic unit cell ($P2_1/c$). Each Na^+ coordinates to two bridging NH_2NH_2 leading to the formation of $[Na(NH_2NH_2)_2]_n^+$ chains, which are separated by BH_4^- with Na–B distances in the range from 2.97 to 3.05 Å (see Fig. 19).

$Mg(BH_4)_2{\cdot}3NH_2NH_2$ crystallizes in a trigonal unit cell ($P\bar{3}1c$). Each Mg^{2+} is octahedrally coordinated by six NH_2NH_2 forming $[Mg(NH_2NH_2)_6]^{2+}$ complex cations that are charge balanced by BH_4^-.

Generally, the hydrazine metal borohydride complexes have high hydrogen content and also favourable decomposition temperatures, *e.g.* approx. 13.0 wt% H_2 is released from $LiBH_4{\cdot}NH_2NH_2$ at 140 °C in the presence of Fe–B catalysts.[118] However, this leads to the formation of very stable Li_3BN_2 and BN according to reaction scheme (5.1).

$$3(LiBH_4{\cdot}NH_2NH_2)(s) \rightarrow Li_3BN_2(s) + 2BN(s) + N_2(g) + 12H_2(g) \quad (5.1)$$

5.3 Ammonia borane metal borohydride complexes

The first ammonia borane (AB) metal borohydride complexes, $LiBH_4(NH_3BH_3)_{0.5}$ and $Ca(BH_4)_2(NH_3BH_3)_2$ were reported in 2010,[114] whereas other ammonia borane metal borohydride complexes are now reported (Table 15). They are all prepared by mechanochemistry, except for $Al(BH_4)_3(NH_3BH_3)$ (where crystals are formed by reacting liquid $Al(BH_4)_3$ and solid NH_3BH_3) and $Ca(BH_4)_2(NH_3BH_3)$ (that is formed during decomposition of $NH_4Ca(BH_4)_3$). Complex formation is not reported for the more stable ionic alkali metal borohydrides and ammonia borane, but physical mixtures of the reactants are obtained by ball milling with $M(BH_4)_m{-}NH_3BH_3$ (M = Na, K, Rb and Cs).[298] NH_3BH_3 may coordinate to the metal *via* a lone pair donated by nitrogen, *i.e.* act as a terminal ligand; or it may also coordinate to the metal by $H^{\delta}-$ covalently bonded to B, *i.e.* bridge between two metal atoms; or it may even stay isolated from the metal and only coordinate *via* dihydrogen bonds. Ammonia borane complexes

 This journal is © The Royal Society of Chemistry 2017

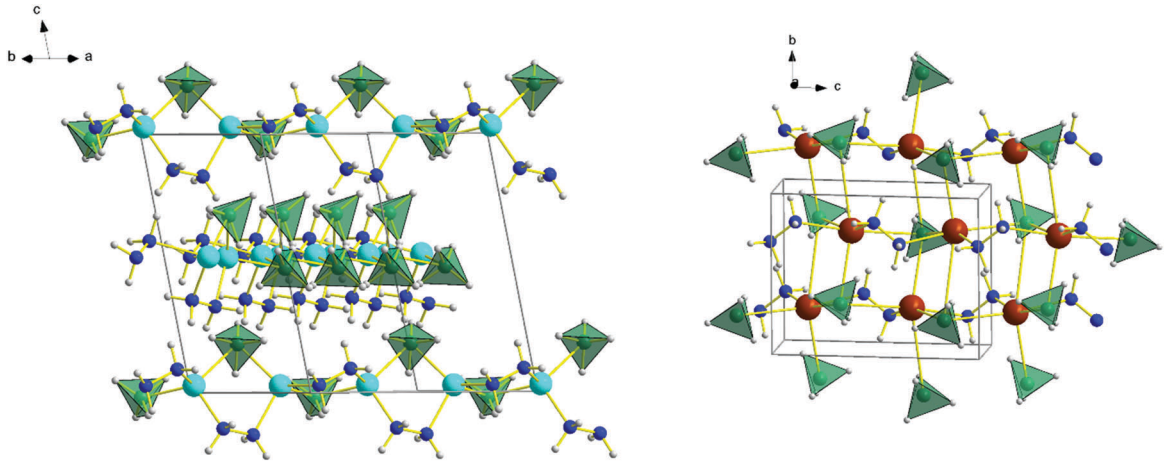


Fig. 19 (left) 1D-chains of $LiBH_4{\cdot}NH_2NH_2$ running along direction [101] in $LiBH_4{\cdot}NH_2NH_2$ and (right) a 3D-framework in $NaBH_4{\cdot}NH_2NH_2$. Li light blue, Na brown, B and BH_4^- tetrahedra green, N blue, H light grey.

Table 15 Metal borohydride ammonia borane complexes

M in $M(BH_4)_m$	Composition of complex	Symmetry	Ref.
Li	$LiBH_4(NH_3BH_3)_{0.5}$	Orthorhombic, *Pnma*	114
Li	$LiBH_4(NH_3BH_3)$	Monoclinic, $P2_1$	301
Mg	$Mg(BH_4)_2(NH_3BH_3)_2$	Orthorhombic, $P2_12_12_1$	115 and 300
Mg	$Mg(BH_4)_2(NH_3BH_3){\cdot}2NH_3$	Tetragonal, *P4bm*	300
Ca	$Ca(BH_4)_2(NH_3BH_3)_2$	Orthorhombic, *Aba2*	114
Ca	$Ca(BH_4)_2(NH_3BH_3)$	Orthorhombic, $P2_1nb$	302
Al	α-$Al(BH_4)_3(NH_3BH_3)$	Monoclinic, $P2_1/c$	116
Al	β-$Al(BH_4)_3(NH_3BH_3)$	Monoclinic, *Cc*	116
Li, Al	$Li_2Al(BH_4)_5(NH_3BH_3)_3{\cdot}6NH_3$	Cubic, *F*23	299

can also be formed from ammine metal borohydrides, resulting in framework structures, *i.e.* $[Al(NH_3)_6][Li_2(BH_4)_5]{\cdot}3NH_3BH_3$ and $[Mg(NH_3)_2(BH_4)_2]{\cdot}NH_3BH_3$ where AB is not coordinated to metal atoms but linked with other hydrogen-containing molecules and ions *via* dihydrogen bonds.[299,300] The hydrogen evolution from these composites is significantly improved compared to the parent compounds containing no ammonia molecules.

The crystal structures of $Mg(BH_4)_2(NH_3BH_3)_2$ and $Al(BH_4)_3(NH_3BH_3)$ both consist of neutral molecular units of $[Mg(BH_4)_2(NH_3BH_3)_2]$ or $[Al(BH_4)_3(NH_3BH_3)]$ coordinated by intermolecular dihydrogen bonds in the solid state (Fig. 20a).[115,116,300] The four other known ammonia borane metal borohydride complexes show strikingly different connectivity, where BH_4^- complexes and NH_3BH_3 molecules act as bridging ligands. The borohydride complexes bridge three lithium and two NH_3BH_3 in the structure

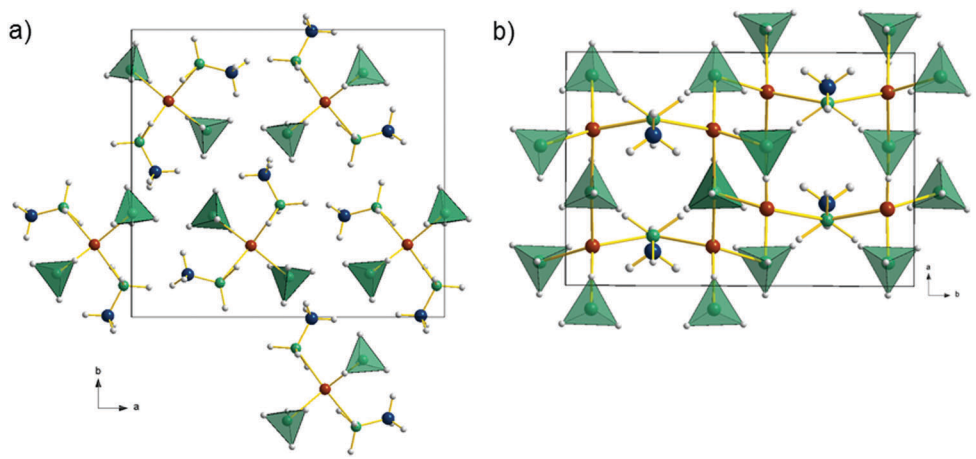


Fig. 20 Crystal structure of (a) molecular $[Mg(BH_4)_2(NH_3BH_3)_2]$ with NH_3BH_3 being a terminal ligand and (b) $LiBH_4(NH_3BH_3)_{0.5}$ which is a 3D framework with bridging NH_3BH_3. Mg (red), B (green), N (blue) and H (white).

of $LiBH_4(NH_3BH_3)_{0.5}$, creating a three-dimensional polymeric framework.[114] The $LiBH_4(NH_3BH_3)$ structure is more complex,[301] containing four independent borohydride anions and four NH_3BH_3 molecules (Fig. 20b). While the borohydride anions coordinate two to four lithium atoms, the NH_3BH_3 molecules act as a terminal ligand or even stay isolated from the metal atoms. In $Ca(BH_4)_2(NH_3BH_3)_2$,[114] the borohydride groups bridge to two metal atoms, forming a two-dimensional square planar net, while the two NH_3BH_3 molecules act as terminal ligands, completing the octahedral coordination of Ca. Another ammonia borane complex, $Ca(BH_4)_2(NH_3BH_3)$, was recently reported, containing just one NH_3BH_3 molecule per unit cell.[302] While structurally related to $Ca(BH_4)_2(NH_3BH_3)_2$, the square planar layers in this net are buckled, and interconnected by a fifth borohydride ligand, which bridges between two Ca atoms. The octahedral coordination polyhedron is again completed by one NH_3BH_3 molecule, which is located in channels formed by the buckled Ca–BH_4 substructure.

5.3.1 Thermal properties of metal borohydride ammonia borane complexes. NH_3BH_3 melts at ~110 °C and releases one equivalent of hydrogen in each of the three decomposition steps, forming polyaminoborane, $[NH_2BH_2]_n$ (90–120 °C), polyiminoborane, $[NHBH]_n$ (120–200 °C) and finally boron nitride, BN (>500 °C).[303–306] In addition, the hydrogen release is accompanied by volatile and toxic by-products, such as B_2H_6 and $B_3N_3H_6$. Generally, the systems $M(BH_4)_m$–NH_3BH_3 (M = Li, Na, K, Mg and Ca) decompose in a similar manner to NH_3BH_3 below 200 °C and do not suppress the release of the toxic gases, as observed for metal amidoboranes, $M(NH_2BH_3)_m$.[114,300,301,307] Thus, it may be concluded that NH_3BH_3 is insufficiently modified in MBH_4–NH_3BH_3 (M = Li, Na, K, Mg and Ca), because NH_3BH_3 maintains its molecular form.[114,308] This is in contrast to metal amidoboranes where one hydrogen atom bonded to N is substituted by a metal atom.[307] $Al(BH_4)_3(NH_3BH_3)$ on the other hand, endothermically releases two moles of H_2 from NH_3BH_3 per Al at 70 °C.[116] Thereby $Al(BH_4)_3(NH_3BH_3)$ differs from pristine ammonia borane, metal amidoboranes and other metal borohydride ammonia borane complexes, and may open up possibilities for reversible hydrogen storage. It was reported that the ability of the strong Lewis acid Al^{3+} to coordinate both the initial hydrogenated species as well as their dehydrogenation products, makes it a good template for chemical transformations involving light chemical and complex hydrides.[309] Therefore the $Al(BH_4)_3(NH_3BH_3)$ system can be used as a model for potentially reversible dehydrogenation of ammonia borane. Both complexes $Mg(BH_4)_2(NH_3BH_3)_2$ and $Al(BH_4)_3(NH_3BH_3)$ melt before decomposition, because of the mononuclear complexes present in the crystal structures and in the melt.[115,116]

5.4 Metal borohydride crystallizing with organic solvents

Solvent based synthesis methods have become more common for the synthesis of metal borohydrides during the past few years as discussed in Section 2 of this review. The solvent may coordinate strongly to the metal borohydride and form a solvate that needs further treatment in order to obtain a solvent-free product. In most cases, the solvent contains a donor atom, O, N or S that coordinates to the metal cation of the borohydride. Selected organic solvents and corresponding solvates are presented in Table 16, including bond lengths between the donor atom and the metal. M–S bonds are generally longer than M–O bonds, suggesting that sulphur based solvents are more easily removed than oxygen based solvents.

Two different structures of metal borohydrides with dimethyl sulfide, $(CH_3)_2S$, are known. The first is the monoclinic structure of $M(BH_4)_2{\cdot}1/2(CH_3)_2S$ (M = Mg, Mn), which is a 3D framework containing two metal atoms: one atom is tetrahedrally coordinated to four BH_4^- groups, and the other to four BH_4^- groups and one $S(CH_3)_2$ ligand to form a trigonal bipyramid.[3,58] Sulfur coordinates relatively weakly to the metal with Mg–S and Mn–S bond lengths being 2.669 and 2.705 Å, respectively. Hence, $S(CH_3)_2$ is easily removed during drying without decomposing $M(BH_4)_2$. Similarly, halide-free and solvent-free yttrium and gadolinium borohydride may be synthesized using dimethyl sulfide with the $M(BH_4)_3{\cdot}S(CH_3)_2$ (M = Y or Gd) solvates as intermediates, which have monoclinic structures ($P2_1/c$).[66]

In $U(BH_4)_4{\cdot}(C_2H_5)_2O$, U is coordinated by four BH_4^- ligands coordinating by edge sharing (η^2), one BH_4^- ligand coordinating by face sharing (η^3) and one O from ether, giving 14 nearest neighbours. Solvent based methods often provide the most thermodynamically stable compound, typically a monometallic borohydride or a solvate, as discussed in Section 2. Thus, very few bimetallic solvates have been discovered, *e.g.* $LiMn_2(BH_4)_5{\cdot}2(C_2H_5)_2O$ and $NaMn_2(BH_4)_5{\cdot}2(C_2H_5)_2O$.[61] Here, Mn is coordinated by four bridging BH_4^- groups, while Li/Na is coordinated tetrahedrally by two BH_4^- groups and two $(C_2H_5)_2O$ ligands Li/Na–O bond lengths ranging from 2.00 to 2.38 Å.

Table 16 Classic organic solvents and selected corresponding solvates

Solvent	Selected solvates	Symmetry	M-donor atom (Å)	Ref.
Dimethyl sulfide/DMS, $(CH_3)_2S$	$M(BH_4)_2{\cdot}1/2(CH_3)_2S$, M = Mg, Mn	Monoclinic, *Cc*	2.67–2.70	3 and 58
	$M(BH_4)_3{\cdot}(CH_3)_2S$ (M = Y or Gd)	Monoclinic, $P2_1/c$	2.89	66
Diethyl ether/Et_2O, $(C_2H_5)_2O$	$U(BH_4)_4{\cdot}(C_2H_5)_2O$	Monoclinic, $P2_1$	2.485	310
	$LiMn_2(BH_4)_5{\cdot}2(C_2H_5)_2O$	Monoclinic, $C2/c$	2.00	61
	$NaMn_2(BH_4)_5{\cdot}2(C_2H_5)_2O$	Monoclinic, *C*2	2.38	61
Tetrahydrofuran/THF, C_4H_8O	$M(BH_4)_2{\cdot}2THF$, M = Sr, Eu, Sm	Monoclinic, $P2_1/c$	2.55–2.62	311–313
Water, H_2O	$NaBH_4{\cdot}2H_2O$	Orthorhombic, *Pbca*	2.38–2.47	103
Ethylenediamine/en, $C_2H_4(NH_2)_2$	$Al(en)(BH_4)_3$	Monoclinic, $P2_1/c$	—	160 and 309
	$Al(en)_3(BH_4)_3{\cdot}en$	Monoclinic, $P2_1/a$	2.00–2.11	314
	$Zn(en)_4(BH_4)_2$	Triclinic, *P*1	—	315
	$Zn(en)_3(BH_4)_2$	Orthorhombic, *Pbca*	—	315

 This journal is © The Royal Society of Chemistry 2017

Similar to the metal borohydrides, THF (C_4H_8O) solvates of $M(BH_4)_2{\cdot}2THF$ are isostructural for M = Sr, Eu, Sm.[311–313] They crystallize in $P2_1/c$ and form one-dimensional chains in which each metal atom is surrounded by four borohydrides and two THF molecules.

Water is a well-known inorganic solvent, but tends to react with metal borohydrides in particular for pH < 7. $NaBH_4{\cdot}2H_2O$ is the first reported metal borohydride hydrate and crystallizes in an orthorhombic unit cell (*Pbca*).[103,111] Na is octahedrally coordinated by four BH_4^- and two H_2O groups that all bridge between two Na atoms. There are three intermolecular $O–H^{\delta+}\cdots{}^{-\delta}H–B$ dihydrogen bonds in the compound in the range 1.77–1.95 Å. Interestingly, $NaBH_4{\cdot}2H_2O$ decomposes upon heating at ~40 °C to $NaBH_4$ and H_2O, which at $T > 40$ °C slowly react to release hydrogen. Thus, the hydrate $NaBH_4{\cdot}2H_2O$ does not directly release hydrogen but decomposes into anhydrous $NaBH_4$ and water. This may be because $NaBH_4$ is stable in basic aqueous solutions. Lithium borohydride also absorbs water, forming $LiBH_4{\cdot}H_2O$.[112,316] Upon thermal treatment, $LiBH_4{\cdot}H_2O$ releases hydrogen at ~65 °C.[316] Calcium borohydride hydrate, $Ca(BH_4)_2{\cdot}H_2O$, has also been reported recently.[113]

6. Thermal properties of metal borohydrides

Metal borohydrides often have a high gravimetric and volumetric hydrogen density and have been of significant interest for many possible applications including solid-state hydrogen storage. However, the reaction mechanisms are often complex and not well understood, showing high kinetic barriers such that decomposition and hydrogen absorption often only occur at elevated temperatures, which hampers technical applications of these materials. Release and uptake of hydrogen can be denoted a chemical reaction involving two-, three- or multiple-phases such as solid–gas, solid–liquid–gas or solid–solid–gas systems. In many cases more than one possible reaction mechanism is involved, which may also change as a function of the physical conditions, *e.g.* partial pressures, temperature and/or stoichiometry of involved starting materials. This section focuses on general aspects regarding reaction mechanisms for hydrogen release and uptake during thermolysis, *i.e.* heating, also denoted pyrolysis, along with different approaches for tailoring and optimization of thermodynamic and kinetic properties. This section reveals that chemical reactions between different hydrides, *i.e.* reactive hydride composites, and additives can provide new perspectives for creating novel hydrogen carrier systems by tailoring physical, chemical, kinetic and thermodynamic properties. Additives have also been investigated along with their possible catalytic properties for hydrogen release and uptake reactions, as well as their function as grain refiners, and as favourable nucleation sites for the formation and decomposition of hydride compounds. Nanoconfinement is another approach that has been tested for its potential to improve both the kinetic and thermodynamic properties of metal borohydrides.

6.1 Thermodynamics of hydrogen release and uptake

There is a close correlation between the temperature of hydrogen release and uptake, at a given equilibrium pressure, and the enthalpy and entropy change for metal borohydrides, similar to metal hydrides. Consider a general reaction where a metal, M, reacts with hydrogen to form a metal hydride according to reaction scheme:

$$M(s) + H_2(g) \leftrightarrow MH_2(s) \tag{6.1}$$

The equilibrium constant for this reaction is,

$$K^{-1} = p(H_2)/p^{\ominus} \quad p^{\ominus} \equiv 1 \text{ bar, standard pressure} \tag{6.2}$$

The Gibbs free energy for the reaction is

$$\Delta G_r = \Delta H_r - T\Delta S_r = -RT\ln K \tag{6.3}$$

where ΔH_r is the change in enthalpy, ΔS_r is the change in entropy, T is the temperature (K), and R = 8.3145 J K^{-1} mol^{-1} H_2. Combining (6.2) and (6.3) gives the van't Hoff equation

$$\ln(p(H_2)/p^{\ominus}) = (RT)^{-1}\Delta H_r - (R)^{-1}\Delta S_r \tag{6.4}$$

A material's hydrogen release temperature is usually given for an equilibrium pressure of $p_{eq}(H_2)$ = 1.0 bar and is often denoted T(1 bar). For this special case, the van't Hoff equation is reduced to:

$$T(1 \text{ bar}) = \Delta H_r/\Delta S_r \tag{6.5}$$

The major contribution to the reaction entropy change, ΔS_r, is from the change in state of hydrogen (from solid to gas phase), $\Delta S^{\ominus}(H_2)$ = 130.7 J $(K\ mol)^{-1}$.[317] Therefore, many metal hydrogen systems, but not all, have $\Delta S_r \sim 130$ J $(K\ mol)^{-1}$. As such, in order to reach an equilibrium pressure of $p(H_2)$ = 1 bar in the temperature range 50 to 200 °C the decomposition enthalpies should be in the range 40–60 kJ mol^{-1} H_2. There is much focus in materials research aimed at identifying hydrides fulfilling this enthalpy range, which corresponds to the operational temperatures for PEM fuel cells.

For the metal borohydrides, however, entropy changes that are significantly different from 130 J $(K\ mol^{-1}\ H_2)$ may be observed due to more complex reaction mechanisms and, in some cases, dynamics in the solid state or liquid–solid transitions. Dynamics such as 'motion' of BH_4^- complex anions may contribute to the entropy of the solid state and a lower than expected entropy of melting.[318] In addition, significantly higher temperatures for hydrogen release and uptake are often observed in order to obtain reasonable reaction kinetics as compared to the ideal temperature dictated by thermodynamics, *e.g.* T(1 bar). This is due to kinetic restraints in the solid state, and therefore a thermodynamic driving force is needed, *i.e.* $T_{dec} > T$(1 bar). A drawback is that higher reaction temperatures often facilitate greater chemical complexity, *e.g.* side-reactions, and also dynamic effects, *e.g.* hydrogen release from high-temperature polymorphs such as h-$LiBH_4$ and, in some cases, hydrogen exchange from a molten phase.

The formation enthalpy, ΔH_f, of metallic hydrides is well defined and exothermic for the stable hydrides. The enthalpy

characterizes the strength of the metal hydrogen bond and is partly determined by the local electron density on the interstitial site where hydrogen is placed.[319–321] The structure of the metallic hydride is often an expanded version of the parent metal structure ($\Delta V \sim$ 10–20%) and may be considered as being derived by hydrogen intercalation.[322] In contrast, the structure of a metal borohydride is much different from the structure of the residue formed by dehydrogenation of the host material. Therefore, the total reaction enthalpy, ΔH_r, for hydrogen exchange of metal borohydrides may be considered a sum of contributions from several partial reactions. Thus, ΔH_r, for metal borohydrides may not directly correlate with the strength of a single covalent boron hydrogen bond. The decomposition enthalpy, ΔH_{dec}, is endothermic and is challenging to measure accurately.[323,324] The decomposition enthalpy may often depend on the method for the measurement and the physical conditions, which may lead to alternative reaction mechanisms or a change of state, such as fusion (*i.e.* then also including ΔH_{fus}). This is further discussed in the following Section 6.2.

The mechanism for hydrogen transport in metallic hydrides, *e.g.* the early transition metal hydrides, is dominated by diffusion of single hydrogen atoms (or partially positively or negatively charged ions) in the solid state.[325] However, more complex transport phenomena may be involved in the hydrogen release and uptake reactions in the solid state of hydrides with ionic and covalent bonds, *i.e.* complex metal hydrides. There are many indications in the literature that relatively stable molecule-like units may participate in hydrogen release and uptake reactions in the solid state of boron, aluminium and nitrogen based complex hydrides, possibly BH_3, AlH_3 or NH_3, which is further discussed in Section 6.6. Thus, the reactions that take place during hydrogen release and uptake in metal borohydrides may be significantly more complex than suggested by eqn (6.1). The thermodynamics of hydrogen release and uptake may be investigated by the Sievert's method by measurement of pressure–temperature–composition (PCT) isotherms. Generally, the published literature suggests increasing difficulty in measuring PCT-isotherms with well-defined plateau pressures for aluminium < nitrogen < boron based hydrides. This may be due to increasing complexity of the involved chemistry, an increasing number of alternative reaction mechanisms, and in some cases, several simultaneous reactions.

6.2 Thermolysis of monometallic borohydrides

Thermolysis denotes the decomposition of a substance upon heat treatment. Monometallic borohydrides may release hydrogen and, in some cases, also diborane during the formation of higher metal boranes, metal borides or even pure boron upon thermolysis, which has been the topic of much research during the past decade. The aim of this section is to provide an overview of some of the general trends that appear in the scientific literature for the thermodynamics of hydrogen release and uptake in selected, well studied, mono-metallic borohydrides. Data collected for the same material with different methods are compared in Table 17. Additives may significantly change the reaction mechanism of decomposition. The addition of small amounts of additives in the range of a few mol% has been considered for possible catalytic effects and is discussed in Section 6.7, whereas larger amounts may react with the metal borohydrides and form reactive hydride composites, see Section 6.8. Physical conditions such as partial pressures and temperatures also influence the mechanism of decomposition *i.e.* the decomposition pathway. The presence of impurities, even in minor quantities, can also influence bubbling and frothing during melting.[45]

Lithium borohydride is the most well investigated metal borohydride regarding the mechanism for hydrogen release and uptake. It undergoes a polymorphic transition from o- to h-$LiBH_4$ at 110 °C and melts at 280 °C.[45] The polymorphic transition and melting events can be associated with minor gas release that is often attributed to impurities, *e.g.* water or oxides, reacting with lithium borohydride.[22,23,45,316,339] Dynamic PCT measurements under constant hydrogen flow provide thermodynamic data *via* the van't Hoff equation for the decomposition reaction, $\Delta H = 74$ kJ mol^{-1} H_2 and $\Delta S = 115$ J K^{-1} mol^{-1} H_2 (see Table 17).[326,331]

Direct decomposition without the presence of intermediate compounds, at elevated temperatures, leads to the production of boron, lithium hydride and release of 13.1 wt% hydrogen, scheme (6.6). Thermodynamic results from calorimetry provide $\Delta H = 66.6$–68.9 kJ mol^{-1} H_2 and $\Delta S = 97.3$–100.2 J K^{-1} mol^{-1} H_2 (see Table 17) for this suggested reaction.

$$LiBH_4(s) \rightarrow LiH(s) + B(s) + 3/2H_2(g) \quad (6.6)$$

Partial dehydrogenation can also occur, forming lithium *closo*-borane, $Li_2B_{12}H_{12}$, *via* less endothermic reactions, scheme (6.7), with a calculated reaction enthalpy of 56 kJ mol^{-1} H_2.[330]

$$LiBH_4(s) \rightarrow 5/6LiH(s) + 1/12Li_2B_{12}H_{12}(s) + 13/12H_2(g) \quad (6.7)$$

Various quantities of hydrogen in the range from 9–14 wt% are reported to be released from $LiBH_4$ under different experimental conditions, *e.g.* 9 wt% H_2 under evolved hydrogen pressure, and 13.8 wt% H is released in flowing He by heating to 600 °C.[22,340] Lithium borohydride has also been decomposed at 600 °C for 5 hours under different partial pressures of hydrogen.[341] Only one-third of $LiBH_4$ transforms to $Li_2B_{12}H_{12}$ at $p(H_2) = 50$ bar and no amorphous boron is observed. In the pressure range, 0.1–10 bar, $LiBH_4$ nearly completely decomposes to $Li_2B_{12}H_{12}$ and amorphous boron. Under these physical conditions (600 °C, 5 h), $LiBH_4$ appears to decompose more efficiently to amorphous boron at lower pressure.[341] Thermolysis of $LiBH_4$ under vacuum at temperatures up to 600 °C is reported to produce LiH, amorphous B (or lithium boride) *via* hydrogen-poor $Li_2B_{12}H_{12-x}$.[342]

The formation of $LiBH_4$ from the elements has also been attempted, which is equivalent to rehydrogenation or reversing reaction (6.6). Amorphous boron is known as a rather inert material with a complex structure of covalently bonded boron that forms a framework containing B_{12} clusters. Lithium hydride is expected to form readily under hydrogen pressure, but further hydrogenation can be very slow until melting, $T_m(LiH) = 689$ °C, which facilitates close contact between the reactants.[343] The kinetics of hydrogen uptake reactions can be

 This journal is © The Royal Society of Chemistry 2017

Table 17 Thermodynamic data for the decomposition of mono-metallic borohydrides

Compound	Proposed reaction	ΔH_{dec} (kJ mol^{-1} H_2)	ΔS_{dec} (J K mol^{-1} H_2)	T_{eq} at 1 bar H_2 (°C)	Method	Notes	Ref.
$LiBH_4$	$LiBH_4 \rightarrow LiH + B + 3/2H_2$	74	115	370	van't Hoff	T = 413–517 °C, PCT under constant gas flow	326
	$LiBH_4 \rightarrow LiH + B + 3/2H_2$	68.9	100.2	415	Calorimetry	—	327 and 328
	$LiBH_4 \rightarrow LiH + B + 3/2H_2$	66.6	97.3	411	Calorimetry	—	317
	$LiBH_4 \rightarrow LiH + B + 3/2H_2$	69.1	—	—	Unreported	—	329
	$LiBH_4 \rightarrow LiH + B + 3/2H_2$	75	—	—	Theoretical	—	330
	$LiBH_4 \rightarrow LiH + B + 3/2H_2$	56	—	—	Theoretical	—	331
	$LiBH_4 \rightarrow 5/6LiH + 1/12Li_2B_{12}H_{12} + 13/12H_2$	56	—	—	Theoretical	—	330
$NaBH_4$	$NaBH_4 \rightarrow Na + B + 2H_2$	108	133	539	van't Hoff	T = 600–700 °C, PCT under constant gas flow	332
	$NaBH_4 \rightarrow NaH + B + 3/2H_2$	89.6	98.6	636	Calorimetry	—	327 and 328
	$NaBH_4 \rightarrow NaH + B + 3/2H_2$	90.2	93.6	691	Calorimetry	—	317
KBH_4	$KBH_4 \rightarrow KH + B + 3/2H_2$	113.9	103.6	826	Calorimetry	—	327 and 328
	$KBH_4 \rightarrow KH + B + 3/2H_2$	112.6	96.9	889	Calorimetry	—	317
$Mg(BH_4)_2$	$Mg(BH_4)_2 \rightarrow MgH_2 + 2B + 3H_2$	39.3	91.3	157	van't Hoff	T = 290–350 °C, PCT under constant gas flow	196
	$Mg(BH_4)_2 \rightarrow MgH_2 + 2B + 3H_2$	57	128	172	van't Hoff	T = 285–360 °C, Stepwise PCT, p = 1–10 bar	333
	$Mg(BH_4)_2 \rightarrow MgH_2 + 2B + 3H_2$	41	—	—	DSC	Multiple backpressure	334
	$Mg(BH_4)_2 \rightarrow MgH_2 + 2B + 3H_2$	40	—	—	Theoretical	—	335
	α-$Mg(BH_4)_2 \rightarrow MgB_2 + 4H_2$	38	—	—	Theoretical	—	336
$Ca(BH_4)_2$	undefined	87	158	278	van't Hoff	T = 356–413 °C, Stepwise PCT, p = 10–60 bar	337
	$Ca(BH_4)_2 \rightarrow 2/3CaH_2 + 1/3CaB_6 + 10/3H_2$	40.6	109.3	98	Theoretical	—	338
	$Ca(BH_4)_2 \rightarrow CaH_2 + 2B + 3H_2$	57.3	105.7	269	Theoretical	—	338
$Y(BH_4)_3$	β-$Y(BH_4)_3 \rightarrow 1/4YH_3 + 3/4YB_4 + 45/8H_2$	22.5	114.4	−76	Theoretical	—	199
	β-$Y(BH_4)_3 \rightarrow 1/2YH_3 + 1/2YB_6 + 21/4H_2$	28.0	116.4	−32	Theoretical	—	199
	β-$Y(BH_4)_3 \rightarrow YH_3 + 3\alpha$-$B + 9/2H_2$	36.2	111.0	53	Theoretical	—	199

increased by thermal treatment of lithium–boron mixtures at 330 and 450 °C in argon, which facilitates the formation of more reactive lithium borides, LiB_3 or Li_7B_6, respectively.[343] The hydrogen uptake reaction has also been investigated by powder neutron diffraction starting with lithium boride.[344] The hydrogen/deuterium absorption starts at ~200 °C with the formation of LiD, and at 350 °C $LiBD_4$ also starts to form. However, under the given experimental conditions, T_{max} = 500 °C, $p(H_2)$ = 180 bar for ~18 hours, a complete reaction was not achieved and LiD remains.[344]

Sodium borohydride, $NaBH_4$, melts at 505 °C, followed by hydrogen release at 534 °C under $p(H_2)$ = 1 bar.[45,332,345] However, hydrogen release can be observed at T ~ 500 °C when measured in helium or argon, p(He, Ar) = 1 bar.[332] Sodium borohydride decomposes to the elements (Na and B), see reaction scheme (6.8), due to the lower stability of NaH, compared to LiH that is formed in the decomposition of $LiBH_4$. Thermal analysis of $NaBH_4$, however, suggests that intermediate compounds may form during the decomposition.[346]

$$NaBH_4(s) \rightarrow Na(l) + B(s) + 2H_2(g) \quad (6.8)$$

Dynamic PCT measurements, under constant hydrogen flow, provide thermodynamic data *via* the van't Hoff equation, ΔH = 108 ± 3 kJ mol^{-1} H_2 and ΔS = 133 ± 3 J K^{-1} mol^{-1} H_2, which corresponds to a decomposition temperature of T_{dec}(1 bar) = 539 °C.[332] These dynamic PCT measurements are conducted at a constant temperature of 600, 650 or 700 °C and the same starting pressure, $p(H_2)$ = 180 bar, with a mass flow controller. The decomposition appears to occur in one step with only one plateau observed on the pressure composition isotherms.[332] The entropic component that is measured with dynamic PCT's (ΔS = 133 J K^{-1} mol^{-1} H_2) is rather high, and much higher than the entropy change measured by calorimetry (ΔS = 93.6–98.6 J K^{-1} mol^{-1} H_2) (see Table 17). It is experimentally important to note the vapour pressure of Na metal is very high (0.1 bar at 675 °C) and this can result in significant Na loss at high temperature, especially under gas flow.[347]

Potassium borohydride melts at 625 °C, followed by hydrogen release near 680 °C with a possible reaction mechanism for decomposition similar to that of $NaBH_4$, scheme (6.8).[33,345] However, increasing evaporation of potassium from the decomposed residue is expected due to the high vapour pressure of potassium (p(K) = 0.4 bar at 672 °C).[348] The high thermal stability of $NaBH_4$ and KBH_4 may be the reason for minimal scientific interest and, as such, the decomposition mechanism remains not well investigated. Although, calorimetry indicates

that the decomposition enthalpy of KBH_4 is high (ΔH = 112.6–113.9 kJ mol^{-1} H_2) (see Table 17), which is favorable for solar thermal applications given adequate kinetics.[349–351]

Magnesium borohydride, $Mg(BH_4)_2$, has received significant interest as a possible hydrogen storage material with a high gravimetric hydrogen content of 14.9 wt% H_2. $Mg(BH_4)_2$ can undergo an array of polymorphic transitions during heating and melting depending on gas partial pressure.[187,188] At elevated hydrogen pressures, $p(H_2) > \sim 1$ bar, decomposition is suppressed and the compound melts.[45] The decomposition mechanism of magnesium borohydride is also quite complex and highly dependent on reaction conditions.[183,187,196,333,352–355] An *in situ* SR-PXD investigation (constant heating, $\Delta T/\Delta t$ = 4 °C min^{-1} in $p(H_2)$ = 1 bar) of γ-$Mg(BH_4)_2$ reveals melting of the β-polymorph at $T \sim 270$ °C and observation of a broad diffraction halo at $d \sim 5.1$ Å.[187] *Ex situ* visual inspection of the melting process reveals a colour change from white to yellow to brown to grey.[187] Magnesium hydride crystallizes from the melt at 320 °C and disappears at 360 °C due to the formation of Mg observed in the temperature range 340–580 °C. Boron containing compounds are not observed until the formation of MgB_2 at 510 °C.[187] Hydrogen release occurs in three steps and the first, 270–325 °C, is assigned to hydrogen release from molten $Mg(BH_4)_2$. The second, 325–360 °C, is assigned to hydrogen release from MgH_2 and the third, 360–410 °C, to remaining non-crystalline boranes, which may also contribute to the second release.[187] Amorphous or nano-crystalline *closo*-borane, $MgB_{12}H_{12}$, has been reported to be a major intermediate product during decomposition of $Mg(BH_4)_2$ in vacuum.[352] However, when $Mg(BH_4)_2$ is decomposed in dynamic vacuum in the temperature range 265 to 400 °C the reaction pathway is different.[356] Here, $Mg(B_3H_8)_2$ was observed as the major decomposition product when $Mg(BH_4)_2$ was heated to 265 °C. Trace amounts of $Mg(B_3H_8)_2$ were observed after heating to 285 °C, and none of the boranes $Mg(BH_4)_2$, $Mg(B_3H_8)_2$ or $MgB_{12}H_{12}$ were observed in samples heated at $T > 285$ °C.[356] Recently, MgB_4H_{10} was also proposed as an intermediate in the decomposition reaction.[355] Lower dehydrogenation temperatures tend to increase the amount of higher boranes and a large quantity of $Mg(B_3H_8)_2$ was obtained after 5 weeks at 200 °C in vacuum.[357] $Mg(B_3H_8)_2$ was converted back to $Mg(BH_4)_2$ after 48 h at 250 °C, $p(H_2)$ = 120 bar.[357] In a similar fashion, a mixture of $Mg(B_3H_8)_2{\cdot}2THF$–MgH_2 (1 : 2) was heated to 200 °C under $p(H_2)$ = 50 bar for 2 h and the product indicated a quantitative conversion to $Mg(BH_4)_2$.[358]

Formation of magnesium borohydride from the elements by hydrogenation has also been conducted but is kinetically slow. Reactive mechanochemistry in a hydrogen atmosphere has been used successfully and ~50% of MgB_2 was hydrogenated to amorphous $Mg(BH_4)_2$ at $p(H_2)$ = 100 bar (ball-milling time up to 100 hours).[359] Magnesium boride, MgB_2, has also been hydrogenated/deuterated at 400 °C and $p(H_2)$ = 800 bar to form β-$Mg(^{11}BD_4)_2$ with a ~43% yield.[134] A higher borohydride yield was found with pre-milled MgB_2 at 400 °C, $p(H_2)$ = 950 bar for 108 h (~75% β-$Mg(BH_4)_2$).[360]

A number of theoretical and experimental studies have been conducted to determine the thermodynamics of decomposition for $Mg(BH_4)_2$ (see Table 17). Theoretical calculations suggest a reaction enthalpy of ΔH = 38–40 kJ mol^{-1} H_2 for reaction (6.9) or (6.10).[335,336]

$$Mg(BH_4)_2 \rightarrow MgH_2 + 2B + 3H_2 \quad (6.9)$$

$$Mg(BH_4)_2 \rightarrow MgB_2 + 4H_2 \quad (6.10)$$

Experimental studies also determine similar enthalpies, with ΔH = 41 kJ mol^{-1} H_2 from a DSC study,[334] and ΔH = 39.3–57 kJ mol^{-1} H_2 from van't Hoff plots.[196,333] The van't Hoff plots were formulated from PCT isotherms in both cases, but the difference in these data could be due to one set of isotherms being measured with constant gas flow and one set being measured stepwise. This variability also demonstrates the difficulty in obtaining accurate thermodynamic data from metal borohydrides.

Calcium borohydride's physical behaviour is similar to $Mg(BH_4)_2$, where a molten phase can be observed near the decomposition temperature, depending on hydrogen backpressure, which is also known to control the decomposition pathway.[45,361] The decomposition pathway is temperature dependent and may proceed through a CaB_2H_6 intermediate to either CaB_6 (320–350 °C) or amorphous boron (400–450 °C).[362,363] Theoretical calculations predict $Ca(BH_4)_2$ decomposition enthalpies to be quantitatively similar to $Mg(BH_4)_2$, where ΔH = 40.6–57.3 kJ mol^{-1} H_2 for decomposition reactions (6.11) or (6.12).[338]

$$Ca(BH_4)_2 \rightarrow 2/3CaH_2 + 1/3CaB_6 + 10/3H_2 \quad (6.11)$$

$$Ca(BH_4)_2 \rightarrow CaH_2 + 2B + 3H_2 \quad (6.12)$$

However, PCT measurements provide much higher thermodynamic quantities with ΔH = 87 kJ mol^{-1} H_2 and ΔS = 158 J K^{-1} mol^{-1} H_2. Here, the entropy is much higher than all other entropies for metal borohydrides (Table 17) including theoretical calculations (ΔS = 105.7–109.3 J K^{-1} mol^{-1} H_2).[338]

Strontium borohydride decomposes at 400 °C and releases H_2.[142,277] Crystalline SrB_6 is observed by *in situ* SR-PXD, which suggests that $Sr(BH_4)_2$ decomposes into SrH_2, SrB_6 and H_2.[165]

Manganese borohydride decomposes at 160 °C with the evolution of hydrogen and large quantities of B_2H_6.[45] For a pure sample of $Mn(BH_4)_2$ (9.5 wt% H_2), a mass loss of 14.8 wt% is observed in the temperature range 125–175 °C.[58] A melting event can also be observed near this temperature but appears to be dependent on hydrogen backpressure and heating rate.[45] Temperature dependent *in situ* SR PXD measured for α-$Mn(BH_4)_2$ reveals that the diffraction peaks disappear and the sample turns X-ray amorphous at 140 °C or 160 °C for $p(Ar)$ = 1 bar and $p(H_2)$ = 10 bar, respectively.[58] The high-pressure polymorph, δ-$Mn(BH_4)_2$, transforms into α-$Mn(BH_4)_2$ during heating in the temperature range 67–109 °C, hence the two polymorphs decomposes similarly.[140]

Yttrium borohydride forms an X-ray amorphous solid above 200 °C and decomposes near 275 °C.[66,98,198,364] When $Y(BH_4)_3$ is decomposed under H_2 back pressure, ranging from $p(H_2)$ = 1–10 bar, $Y(B_3H_8)_3$ is observed as the main intermediate according to scheme (6.13), along with small amounts of $Y_2(B_{12}H_{12})_3$.[100]

$$Y(BH_4)_3(s) \rightarrow 1/3Y(B_3H_8)_3(s) + 2/3YH_3(s) + H_2(g) \quad (6.13)$$

 This journal is © The Royal Society of Chemistry 2017

The ultimate decomposition results in the formation of YH_3, YH_2 and YB_4, but does not reform the borohydride, even under 1550 bar at 300 °C.[66] Theoretical calculations indicate that $Y(BH_4)_3$ is thermodynamically unstable at room temperature with a low decomposition reaction enthalpy ΔH = 22.5–36.2 kJ mol^{-1} H_2.[199]

Cadmium borohydride's low-temperature polymorph α-$Cd(BH_4)_2$ transforms to β-$Cd(BH_4)_2$, by a first order phase transition, at ~55 °C and β-$Cd(BH_4)_2$ decomposes at ~75 °C into metallic Cd and likely a mixture of hydrogen and borane gases according to scheme:[146]

$$\beta\text{-}Cd(BH_4)_2(s) \rightarrow Cd(s) + B_2H_6(g) + H_2(g) \quad (6.14)$$

Molecular metal borohydride. The decomposition mechanism for molecular metal borohydrides, such as $Al(BH_4)_3$, $Ti(BH_4)_3$, or $Zr(BH_4)_4$, remains not fully understood. Apparently these compounds first sublime at low temperatures: around or below 0 °C for $Al(BH_4)_3$[12] and at 29 °C for $Zr(BH_4)_4$.[109,365] In the gas phase all three compounds tend to release diborane *via* polymerization reactions. The spontaneous diborane release from $Al(BH_4)_3$ and $Ti(BH_4)_3$ below room temperature may be responsible for the very aggressive decomposition reactions. The stabilization of $Ti(BH_4)_3$ was recently reported through its confinement within a metal–organic-framework (MOF UiO-66), allowing it to be stored at room temperature for months without decomposition.[210]

6.3 Thermolysis of bi- and trimetallic borohydrides

The thermal decomposition of the metal borohydrides have been shown to occur *via* a wide range of pathways, often in several steps, which may involve simultaneous and, in some cases, coupled chemical reactions. The following focus is on general trends deduced from published literature regarding both the reaction pathways and thermal stability of bi- and trimetallic borohydrides. Their decomposition mechanism is so far defined by one of two schemes:

(i) Stable metal borohydrides that form the bi- and trimetallic borohydride. Here, the bi- and trimetallic borohydride will separate during thermolysis, either splitting into the individual, stable, borohydrides, or possibly melting in an eutectic composition.

For example: $M_xM'_y(BH_4)_z$, M = Li or Na, M′ = K, Rb, Cs are formed from stable metal borohydrides. During heating, the bimetallic compounds phase separate and may form an eutectic melt as described in Section 6.4. $M_xM'_y(BH_4)_z$, (M = Li, Na, K, Rb or Cs, M′ = Mg, Ca or Sr) are formed from stable metal borohydrides. They are observed to decompose *via* the formation of mono-metallic alkali metal borohydrides MBH_4 and alkaline earth metal borohydrides, which decompose individually at higher temperatures.[1,164,165]

(ii) A combination of stable and unstable borohydrides that form the bi- and trimetallic borohydride. In this case, the unstable borohydride is often stabilized by its incorporation into a bi- and trimetallic borohydride, resulting in decomposition at higher than normal temperature. However, the decomposition mechanism is unchanged and the remaining stable metal borohydride will stay intact.

For example: $M_xM'_y(BH_4)_z$, (M = Li, Na, K, Rb or Cs, M′ = Al, Y, Sc, Mn, Zn or Cd), may decompose *via* the formation of mono-metallic alkali metal borohydrides MBH_4 but the remaining part may decompose directly to a metal, hydrogen and diborane.[70,146,159] All the Cd-based borohydrides show low thermal stability. Their decomposition temperatures exhibit the following trend: β-$Cd(BH_4)_2$, ~75 °C < $KCd(BH_4)_3$, ~80 °C < $K_2Cd(BH_4)_4$, ~85 °C, *i.e.* the higher the content of KBH_4 the higher the thermal stability.[146]

6.4 Eutectic melting of bi- and trimetallic borohydrides

Two or more metal borohydrides may be combined as discussed previously in Section 6.3, forming compounds with new compositions and/or structures, *e.g.* a new bimetallic compound $MM'(BH_4)_x$. In some cases a eutectic melting mixture may form, which has been observed in a few cases involving alkali- and alkaline earth-metal borohydrides.[45] For example, $LiBH_4$–MBH_4 systems reveal eutectic melting, M = K, and several new bimetallic compounds for M = Rb or Cs with increasingly complex phase diagrams.[47,156] The formation of an eutectic mixture was observed to cause hydrogen release at lower temperatures during thermolysis, which could be a kinetic effect. However, structural reorganization upon melting may, in principle, result in weakening or strengthening of chemical bonds, which may influence decomposition, *i.e.* a thermodynamic effect. These effects may also influence hydrogen uptake properties. An overview of investigated eutectic mixtures is provided in Table 18.

Lithium borohydride–sodium borohydride. The $LiBH_4$–$NaBH_4$ system shows almost full solubility, *i.e.* a solid solution, $Li_{1-x}Na_xBH_4$, in the temperature range ~110–220 °C with compositions 0.0 < x < 0.9. The lowest melting point is observed for $Li_{0.70}Na_{0.30}BH_4$ at T_{mp} ~ 216 °C.[161,367]

Lithium borohydride–potassium borohydride. The $LiBH_4$–KBH_4 phase diagram reveals a very deep eutectic melting point of T_{mp} = 105 °C (Fig. 21a).[47] Interestingly, a binary stoichiometric compound, $LiK(BH_4)_2$, is formed mechanochemically, not thermally, but separates to the monometallic borohydrides at T > 95 °C. In contrast, the sodium borohydride–potassium borohydride system forms a solid solution upon thermal treatment at ~200 < T < 450 °C. The reason that $LiK(BH_4)_2$ formation is facilitated by compression (mechanochemistry) and $Na_xK_{1-x}(BH_4)$ formation is facilitated by thermal expansion (heating) is due to the volume (V/Z) of the bimetallic compound and solid solution in comparison to their reactants. Compression can form the bimetallic borohydride $LiK(BH_4)_2$ owing to a smaller volume than the reactants, whereas thermal treatment can be used to form a bimetallic borohydride with a larger volume than its reactants, in this case a solid solution, $Na_xK_{1-x}(BH_4)$.[47,93]

Lithium borohydride–magnesium borohydride. The decomposition of the eutectic melting $LiBH_4$–$Mg(BH_4)_2$ system initiates above T_{mp} ~ 180 °C. At 270 °C, a 0.5$LiBH_4$–0.5$Mg(BH_4)_2$ composite releases 7.0 wt% of hydrogen.[45,368] The eutectic system therefore releases hydrogen at significantly lower temperature than the individual lithium and magnesium borohydrides, which occur at ~400 and ~280 °C, respectively.

Lithium borohydride–calcium borohydride. The system $LiBH_4$–$Ca(BH_4)_2$ has been investigated for several compositions using

Table 18 Eutectic melting metal borohydride compositions, melting temperatures for the two individual compounds T_{mp1} and T_{mp2}, melting temperature for the eutectic composition T_{mp}, temperature for major hydrogen release, T_{dec} and morphology of the melt by visual inspection[45]

Eutectic mixture	T_{mp1} (°C)	T_{mp2} (°C)	T_{mp} (°C)	T_{dec} (°C)	Eutectic morphology	Ref.
$0.62LiBH_4$–$0.38NaBH_4$	280	510	215	300	Transparent liquid	366 and 367
$0.725LiBH_4$–$0.275KBH_4$	280	605	105	420	Transparent liquid	47
$0.55LiBH_4$–$0.45Mg(BH_4)_2$	280	280	180	250	Froth	368
$0.7LiBH_4$–$0.3Ca(BH_4)_2$	280	370	200	350	Froth	369
$0.68NaBH_4$–$0.32KBH_4$	510	605	460	465	Dark liquid	93 and 366
$0.45NaBH_4 + 0.55Mg(BH_4)_2$	510	280	205	360	Froth	370

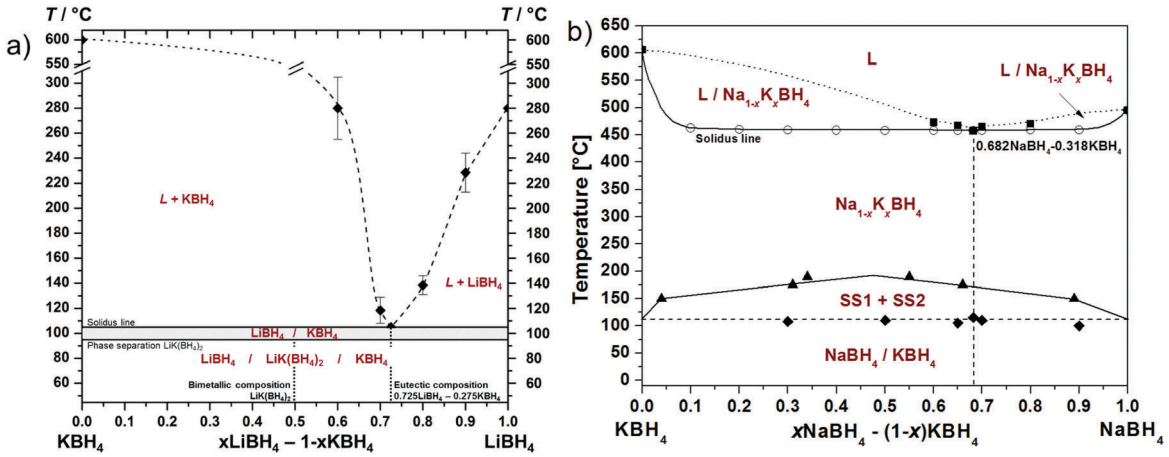


Fig. 21 (a) Binary phase diagram for the $LiBH_4$–KBH_4 system.[47] (b) Binary phase diagram for the $NaBH_4$–KBH_4 system. Adapted with permission from ref. 93. Copyright 2015 American Chemical Society.

DSC, *in situ* SR-PXD, *etc.*[369,371] Interestingly, this composite undergoes eutectic melting with a minimum temperature of $T_{mp} \sim 200$ °C in a relatively wide composition range $0.6 < x < 0.8$.[369,371]

Sodium borohydride–potassium borohydride. The $NaBH_4$–KBH_4 phase diagram (Fig. 21b) reveals full solubility in the entire compositional range $0 < x < 1$ for $Na_{1-x}K_xBH_4$ above 200 °C. The melting point of the solid solution is reduced slightly compared to the individual reactants with a minimum at $T_{mp} \sim 460$ °C for $Na_{0.682}K_{0.318}BH_4$.[93]

Sodium borohydride–magnesium borohydride. The system, $xNaBH_4$–$(1 - x)Mg(BH_4)_2$, x = 0.4–0.5, shows melting/frothing between 205–220 °C.[370] However, the sample does not become a transparent melt. In contrast, no eutectic is observed for $NaBH_4$–$Ca(BH_4)_2$.[370]

6.5 Trends in thermal decomposition for metal borohydrides

Upon heating, stable mono-metallic borohydrides tend to melt and then start to decompose at slightly higher temperatures, see Fig. 22. On the other hand, the less stable molecular metal borohydrides tend to sublime, rather than melt, and decompose in the gas phase. The decomposition products from the group of stable mono-metallic borohydrides appear to change color, morphology, volume *etc.* largely related to the degree of decomposition achieved in each system.[45] Metallic decomposition products are not observed by visual inspection, X-ray diffraction or nuclear magnetic resonance, suggesting that after heating to modest temperatures the products likely remain as metal borohydrides, or form higher metal boranes, metal hydrides, or metal borides. ^{11}B NMR is particularly useful in identifying decomposition products if they are non-crystalline, where diffraction is less useful. The ^{11}B spectra can be used to differentiate between many different metal borohydrides with different cations, due to their varied interactions with the boron nucleus (Fig. 23). Trends in the NMR chemical shifts of borohydrides have been investigated recently.[372] Other spectroscopic methods such as IR and Raman are also useful in characterising crystalline and non-crystalline metal borohydrides, where different bonding environments display characteristic vibrations (Fig. 24). Progress in the spectroscopic understanding of alkali and alkaline earth metal borohydrides, $M(BH_4)_n$ (M = Li, Na, K, Rb, Cs, Be, Mg, Ca) and reactive hydride composites has been recently reviewed.[373–375]

An empirical correlation between the thermal stability, T_{dec}, of metal borohydrides and Pauling electronegativity was first suggested to exist in 1955[391] and has been further investigated theoretically and experimentally by several research groups.[6,392,393] The more stable metal borohydrides tend to follow a linear correlation between the electronegativities and decomposition temperature. This approximation, however, is less pronounced for compounds with higher electronegativities. A comparison of a linear and exponential correlation is shown in the inset in Fig. 22b. The decomposition temperatures, T_{dec}, reported in Fig. 22b are measured by *in situ* SR-PXD or thermal analysis (TGA/DSC) in inert atmosphere, often $p(Ar)$ = 1 bar. In the case of the bimetallic borohydrides, the values for the Pauling

 This journal is © The Royal Society of Chemistry 2017

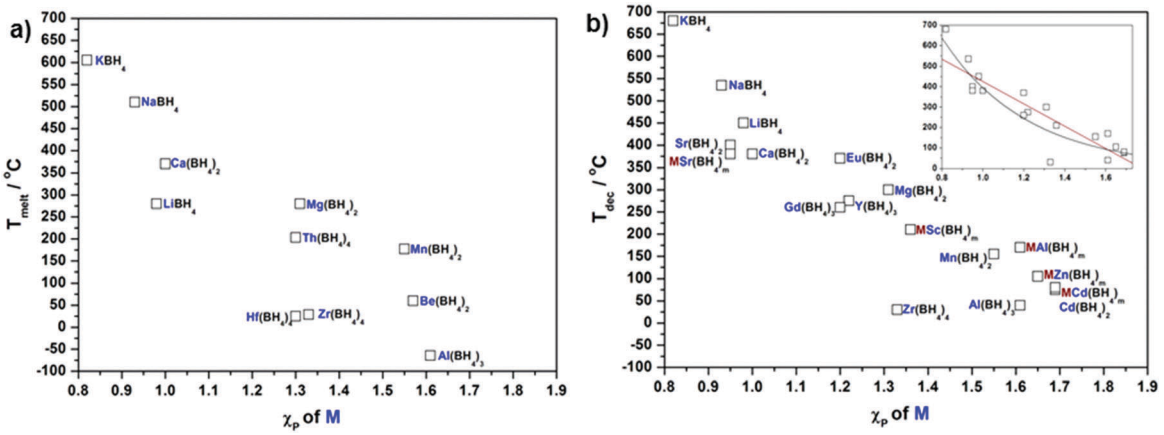


Fig. 22 (a) Experimentally determined melting points for metal borohydrides as a function of the electronegativity of the metal. (b) Experimentally observed decomposition temperatures, T_{dec} for metal borohydrides $M'(BH_4)_n$ and $M_xM'_y(BH_4)_z$ plotted as a function of the electronegativity of the metal, M′. The T_{dec} values refer to the temperature for the maximum gas release and are measured by TGA/DSC or *in situ* SR-PXD at p(He) or p(Ar) = 1 bar. The inset in Fig. 22b reveal a comparison of linear and exponential correlation between observed decomposition temperatures, T_{dec}, as a function of the electronegativity of the metal.

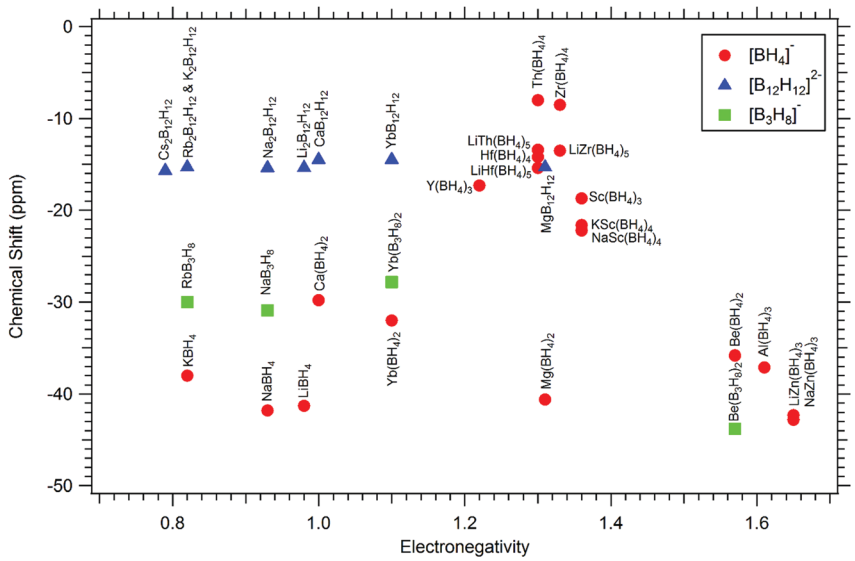


Fig. 23 Experimentally determined ^{11}B NMR chemical shifts of relevant metal borohydride and borane compounds. Bimetallic compounds are presented at the electronegativity of the most electronegative cation.[158,166,197,275,342,376–389]

electronegativities, χ_p, are taken from the more electronegative elements, *i.e.* Sc, Y, Zn, Cd and Al. This approach is justified by the stronger coordination between the more electronegative metal and BH_4, causing the formation of discrete metal borohydride anions (see the discussion in Section 3.8).

The less electronegative metal is often an alkali metal with a dominantly ionic interaction. The validity of this assumption is illustrated by the decomposition of $KCd(BH_4)_3$ to $K_2Cd(BH_4)_4$ and $Cd(BH_4)_2$. The latter immediately decomposes to Cd, H_2 and B_2H_6. Upon further heating, $K_2Cd(BH_4)_4$ decomposes to KBH_4 and $Cd(BH_4)_2$, where the latter again immediately decomposes to Cd, H_2 and B_2H_6.[146] This example illustrates that the more electronegative cation is controlling the stability. Furthermore, metal borohydrides containing complex anions, such as $[Sc(BH_4)_4]^-$, $[Zn_2(BH_4)_5]^-$ and $[Zn(BH_4)_3]^-$ in the compounds $MSc(BH_4)_4$, $MZn_2(BH_4)_5$ and $MZn(BH_4)_3$ reveal only minor variations in the decomposition temperature with changes in alkali metal.[70,166,380] This indicates that the decomposition temperature is specific for these complex anions rather than determined by the overall composition of the compound. This underlines the strong correlation between the decomposition temperature and the electronegativity of the complex-forming metal and the key role of the complex M–BH_4 anions in the structural stability of bimetallic borohydrides.

6.6 The released gas from metal borohydrides, stability of diborane

Materials containing complex ions were overlooked as hydrogen carriers for possible hydrogen storage applications until the late nineties due to their relatively high stability and the fact

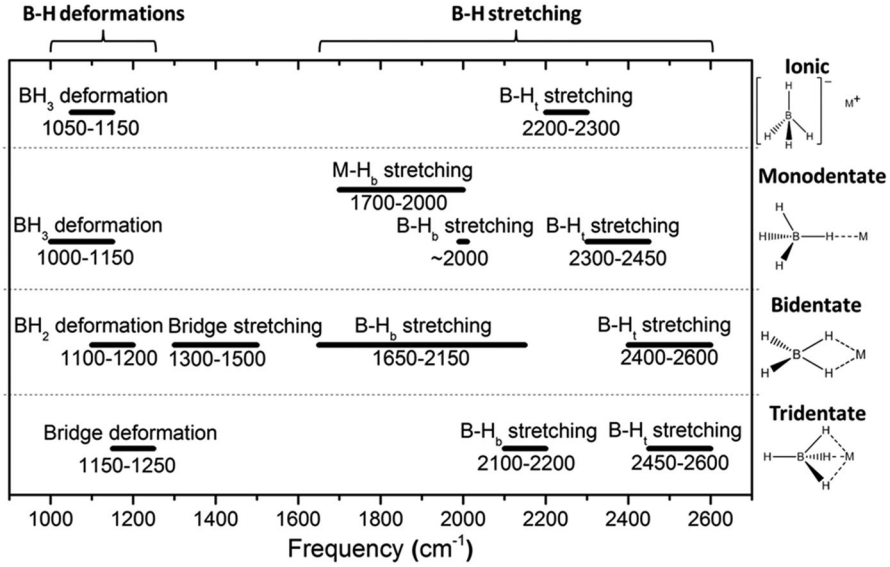


Fig. 24 IR and Raman active fundamental vibrations commonly observed for MBH_4.[390]

that hydrogen uptake only occurs under extreme conditions. A paradigm shift was initiated by the discovery that titanium catalyzed $NaAlH_4$ releases and uptakes hydrogen at moderate conditions,[394] which initiated the research activities in hydrogen storage systems containing complex ions.

The boron, aluminium and nitrogen based complex hydrides, *e.g.* $LiBH_4$, $LiAlH_4$ or $LiNH_2$, contain the complexes, BH_4^-, AlH_4^- or NH_2^-. These complexes form stable crystalline solids with many alkali or alkaline earth metals, which act as counter ions in the solid state. Reversible nitrogen-based complex hydride systems were discovered by Ping Chen *et al.* in 2002 and metal borohydrides were also found to be reversible, albeit under harsh conditions, *e.g.* $LiBH_4$ in 1980.[329,395]

A drawback for these light element complex hydrides, *e.g.* $LiBH_4$, $LiAlH_4$ or $LiNH_2$, appears to be that their neutral counterparts (AH_3) are neutral molecules, BH_3 or NH_3, or metastable solids, AlH_3. In fact, BH_3 is in equilibrium with its dimer, B_2H_6, where the partial pressure of BH_3 is roughly 2×10^{-8} of the pressure of B_2H_6 at room temperature.[396] However, at higher temperature the BH_3 partial pressure is higher, *i.e.* 10^4 times higher at 200 °C than RT, possibly promoting hydrogen release *via* polymerization reactions. Ammonia, NH_3, is a reactive gas at room temperature that liquefies below −33.3 °C at $p(NH_3) = 1$ bar. Ammonia is an industrially useful and energy dense compound (18.6 MJ kg^{-1}), but may be converted to N_2 and H_2 at high temperature, with catalysts, with a $Na/NaNH_2$ cracking system or by the omnipresent NaOH in $NaNH_2$ as shown recently.[397,398] Alane, AlH_3, is a polymeric solid built from octahedra of AlH_6.[399,400] Alane is thermodynamically unstable at room temperature, but is stabilized in the bulk form by surface aluminium oxide layers.[401,402]

There are many indications that these 'molecules' (AH_3) play a crucial role in the mechanism for hydrogen release and uptake in complex hydrides, *e.g.* $LiBH_4$, $LiAlH_4$ or $LiNH_2$. This is exemplified by the fact that the light element complex hydrides can be prepared by a reaction between the 'molecule' and ionic hydrides (mentioned in Section 2.5).[95,403] On the other hand, an ionic hydride, *e.g.* LiH or NaH may also be observed in the dehydrogenated state:

$$AH_3 + LiH \leftrightarrow LiAH_4 \quad A = B, N, \text{ or } Al \qquad (6.15)$$

Lithium borohydride, $LiBH_4$ releases hydrogen at $T > 400$ °C, but was also found to emit diborane at the impurity level.[339] This contrasts with, for example, $Mn(BH_4)_2$, which releases significant amounts of diborane at $T \sim 160$ °C.[58] Thus, metal borohydrides have a tendency to release increasing amounts of diborane when they have lower decomposition temperatures.[97,404] The extreme case is for $LiZn_2(BH_4)_5$ that decomposes at $T \sim 100$ °C and presumably releases a 1 : 1 mixture of hydrogen and diborane due to a reduction of Zn^{2+} to Zn.[70] A similar type of metal ion reduction is also observed for the decomposition of $Cd(BH_4)_2$.[146] Varying mixtures of hydrogen and diborane in the released gas suggests that more than one reaction mechanism is involved. Therefore, the composition of the released gas may depend on physical conditions, such as temperature and hydrogen partial pressure, which may favour a particular competing reaction.

Diborane can react with an ionic hydride and form a metal borohydride *via* a solid–gas addition reaction as shown for lithium borohydride at $T > \sim 120$ °C, reaction scheme (6.16). At slightly higher temperatures, $150 < T < 200$ °C, diborane can further react with lithium borohydride and form metal *closo*-boranes ($M_xB_nH_n$), according to reaction schemes (6.17) and (6.18).[95,252,405]

$$2LiH(s) + B_2H_6(g) \rightarrow 2LiBH_4(s) \qquad (6.16)$$

$$2LiBH_4 + 4B_2H_6 \rightarrow Li_2B_{10}H_{10} + 11H_2 \qquad (6.17)$$

$$2LiBH_4 + 5B_2H_6 \rightarrow Li_2B_{12}H_{12} + 13H_2 \qquad (6.18)$$

Boron chemistry is extremely diverse and all neutral boranes, B_mH_n, can be prepared, directly or indirectly, from diborane with

 This journal is © The Royal Society of Chemistry 2017

the product mainly depending on the temperature and partial pressure of the reactants.[406] Thus, the borane molecule, BH_3, may play an active role for hydrogen release and uptake in metal borohydrides. These arguments may suggest that hydrogen release from metal borohydrides occurs *via* the partial reduction of borane, BH_3, *via* the formation of higher boranes, or complete reduction forming metal borides or amorphous boron. Low total gas pressure may lead to a relatively high partial pressures of diborane, which appears to facilitate the formation of the rather stable metal *closo*-boranes.[361] High partial pressures of hydrogen appear to facilitate the full reduction of BH_3 and the formation of metal borides.

6.7 Additives to improve reaction kinetics

The hydrogen release temperatures of the stable metal borohydrides are usually considered too high for practical applications and catalysis has been widely investigated in an attempt to overcome kinetic barriers and reduce the activation energy for hydrogen release and uptake. The more stable metal borohydrides are of particular interest because they appear to have the potential to release pure hydrogen with no trace of diborane. Small amounts of additives have been sought to act as catalysts and promote both hydrogen release and absorption in metal borohydrides. Additives may also promote the formation of metal borides rather than metal *closo*-boranes, *i.e.* selective formation of a dehydrogenated state that facilitates absorption of hydrogen at more moderate conditions. The present Section 6.7 focuses on smaller quantities of additives investigated for possible catalytic properties and Section 6.8 treats larger amounts of additives that may purposefully react with the metal borohydride to form a reactive hydride composite.

Additive effects for aluminum and magnesium based hydrides. A significant proportion of the research conducted on metal borohydride additives also tends to explore analogies with other hydrides, such as magnesium hydride, MgH_2, and sodium tetrahydrido aluminate, denoted sodium alanate, $NaAlH_4$.[407–410] Catalytic nanoparticles have enabled breakthroughs in low-temperature hydrogen release and uptake in sodium alanate, $NaAlH_4$.[394,411,412] Several metals, such as titanium, scandium or cerium, have been shown to promote both hydrogen release and uptake, undertaking a bifunctional catalytic role.[413] Typically, a transition metal chloride is added to $NaAlH_4$, which then irreversibly reacts, forming inert NaCl and catalytically active Al or Ti–Al nanoparticles, possibly with the catalytically active metal on the surface of $NaAlH_4$.[412,413]

Hydrogen release and uptake in magnesium hydride, MgH_2, has been shown to be promoted by other principles. Alloying effects with other metals such as Al, Cu, or Pd and the formation of $Mg_{17}Al_{12}$, $Mg_2Cu/MgCu_2$, or Mg_6Pd have been shown to influence hydrogen release and uptake.[414–417] Other hydrides may also form and possibly act as an intermediate for hydrogen exchange, *e.g.* formation of Mg_2Ni and Mg_2NiH_4 in MgH_2–Ni samples[418–420] or Mg_2FeH_6 in MgH_2–Fe samples.[421–425] Another mechanism is suggested for the Mg–Nb_2O_5 system where MgH_2 tends to reduce niobium oxide forming a $Mg_{1-x}Nb_xO$ solid solution, which possibly facilitates both hydrogen splitting at the surface as well as hydrogen diffusion through the very inert and dense MgO layer. Because of the high hardness of Nb_2O_5 and other additives these materials have a beneficial effect on the ball-milling process leading to the formation of smaller Mg particles and crystallites, which, in turn, improves kinetics due to surface area or grain boundary area enhancements.[426–429] A significant variety of other additives have been investigated in the MgH_2 system, including metals, intermetallics, oxides, hydrides and halides.[430–432]

Additives for metal borohydrides. The above mentioned examples have been used as inspiration in the exploration of a wide range of additives for hydrogen release and uptake in metal borohydrides. Trends in additive effects may appear when they are grouped into elements, and compounds such as hydrides, borides, oxides and halides. Mainly lithium and magnesium borohydrides have been examined systematically.

Elemental metallic additives. A range of transition metals have been considered as additives in MBH_4 systems, *e.g.* Sc, Ti, V, Cr. Nanoscale transition metal particles are very important in organic chemistry with a long history, involving the chemical transformation of boron compounds, *e.g.* palladium nanoparticles for catalyzed Suzuki–Miyaura cross-coupling reactions, forming new C–C bonds. Homo-coupling reactions can also occur, which form new C–B bonds.[17] For mono-metallic nanoparticles, the activity follows a sequence of Pd > Cu > Ru > Pt.[17]

The adsorption of BH_4^- on the more noble metal surfaces has also been investigated and reveals a weaker interaction with Ag and Au when compared to other noble metals, Pd, Rh, Ru, Pt, Ir and Os. This important result is related to the hydrolysis of borohydrides,[433] which is further discussed in Section 6.9. Metal borohydrides may melt prior to the release of hydrogen, which also increases their reactivity. Gold powder was used as an X-ray standard in a sample of $LiBH_4$, but a reaction took place at $T > T_{mp}(LiBH_4) \sim 290$ °C and a lithium gold alloy formed.[9] A range of metals (Mg, Al, Ti, V, Cr, Sc) have been mixed with $LiBH_4$ in stoichiometric proportions with reported decreases of ~50 °C in its decomposition temperature.[434] However, with high doping levels the entire reaction pathway can be shifted, as in the case of reactive hydride composites, forming alternate reaction products with different reaction thermodynamics.

Elemental non-metallic additives. The addition of excess quantities of amorphous boron to $LiBH_4$ was found to enhance the decomposition process by leading to an alternative reaction mechanism, which reduces the decomposition temperature by $\Delta T \sim 150$ °C and the activation energy by $\Delta E_A \sim 55$ kJ mol^{-1}.[435,436] Pendolino *et al.* propose a reaction of the intermediate $Li_2B_{12}H_{12}$ and B to cause this change in desorption behaviour, by surplus B facilitating faster formation and growth of the solid intermediate by forming a polymer chain or layers with the boron of $B_{12}H_{12}^{2-}$.[436]

Carbon. Carbon has been investigated as an additive to promote hydrogen exchange in metal borohydrides, both theoretically and experimentally. Theoretical modelling suggests that increased curvature of the carbon surface decreases the 'hydrogen removal energy', *i.e.* C_{60} is expected to have a stronger effect in comparison to graphene and graphite.[437] Density functional theory (DFT) was used to evaluate a wide range of chemical reactions suggesting the formation of bimetallic carbides, *e.g.* LiBC in a

reaction between $LiBH_4$ and carbon, which releases 11.95 wt% H_2 with a moderate reaction enthalpy (ΔU_0 = 45.1 kJ mol^{-1} H_2).[438] In a similar manner, the formation of Li_2C_2 was observed in mixtures of $LiBH_4$ with carbon nanotubes, which could be rehydrogenated back to LiH.[439] Another example is the reaction between $LiBH_4$, ScH_2 and C, which is suggested to form ScB_2C and LiH in the decomposed state with a relatively low enthalpy change of $\Delta U_0 \sim$ 52 kJ mol^{-1} H_2.[438] The 'carbon-effect' on metal borohydrides is further discussed in Section 6.10 in regard to nanoconfinement.

Sulphur. The reactions between metal borohydrides and elemental sulfur have been investigated *in situ* during thermal treatment and were found to be highly exothermic (up to 700 J g^{-1}). These reactions are exceptionally rapid and result in the sudden release of substantial quantities of hydrogen gas and should be handled with caution. The metal borohydrides react with molten S at 140, 190 and 180 °C, respectively for $LiBH_4$–S, $NaBH_4$–S and KBH_4–S. Remarkably, $NaBH_4$–S release pure hydrogen, whereas $LiBH_4$–S and KBH_4–S systems also release some H_2S or B_2H_6 gases.[440] The drawback may be the very complex metal sulphur chemistry that results in the formation of multiple complex compounds and intermediates, as observed for the $NaAlH_4$–S system.[441] The reaction between metal borohydrides and sulphur could have implications for their use as solid state electrolytes in Li–S battery applications.

Metal hydrides as additives. Different types of hydrides have also been considered in order to promote hydrogen exchange in metal borohydrides.[434,438,442] Many of these systems alter the decomposition pathway, resulting in altered thermodynamics and are discussed in the following section on reactive hydride composites.

Metal oxides as additives. A variety of metal oxides have also been considered to enhance the hydrogen exchange properties of metal borohydrides. This was initiated by the study of glass powders having an effect on lithium borohydride, *i.e.* $LiBH_4$–SiO_2, which enabled hydrogen release at lower temperatures than observed for pure $LiBH_4$.[22] However, *in situ* diffraction shows an irreversible reaction between SiO_2 and molten $LiBH_4$ at $T > 370$ °C and the formation of orthosilicate, Li_4SiO_4, for small amounts of additive (<10 mol% SiO_2, *i.e.* excess of lithium) and lithium metasilicate (Li_2SiO_3) for larger amounts of additive.[9] The fate of boron remain unclear but the formation of lithium borates may occur.

A minor change in hydrogen release profile for γ-$Mg(BH_4)_2$ with 0.02 mol% TiO_2 and MoO_3 is observed, *i.e.* the DSC events appeared broader and were shifted to slightly lower temperatures (*ca.* 20 °C), as compared to the pure γ-$Mg(BH_4)_2$.[443] A large decrease in the dehydrogenation temperature was found for stoichiometric ratios of $LiBH_4$ with TiO_2 (down to 150 °C), but was due to a redox reaction forming $LiTiO_2$.[444] Several transition metal oxides have also been explored, which have some tendency for release of diborane due to reduction of the metal by BH_4^-, accompanied by the irreversible formation of borates or ternary metal oxides.[445,446]

Metal fluorides as additives. Nickel fluoride, NiF_2, tends to react with γ-$Mg(BH_4)_2$ and form Ni_3B and possibly $Mg(B_3H_8)_2$, which absorbs hydrogen at moderate conditions to form β-$Mg(BH_4)_2$.[447] Similarly, the reaction between $LiBH_4$ and TiF_3 results in an exothermic reaction to form LiF and TiB_2.[448] Borofluorides, $NaBF_4$ and KBF_4, are described in Section 4 and enable fluoride substitution in metal borohydrides to possibly promote the formation of *closo*-boranes during thermolysis. In general, fluorides tend to 'destabilize' the metal borohydride often by promoting irreversible chemical reactions that tend to form stable metal fluorides, *closo*-boranes and possibly diborane gas. Halides of Al, Ti, Zr and Hf may form volatile molecular borohydrides, which then sublime and decompose in the gas phase.

Heavier halides: chlorides, bromides and iodides, as additives. Heavier halides of metals with relatively low electronegativity (*i.e.* alkali- and alkali earth metals) may lead to anion substitution in the metal borohydride, as discussed in Section 4. Anion substitution tends to stabilize the hydrogenated state, and provide hydrogen release at slightly higher temperatures, tending to facilitate the hydrogenation of the sample. Titanium trichloride has a well-documented catalytic effect on the hydrogen release and uptake from $NaAlH_4$[394,413] and appears to decrease the decomposition temperature of $LiBH_4$.[449] A color change from light red/purple to gray/black of a $LiBH_4$–$TiCl_3$ (2 mol%) sample when kept a few hours at RT in an argon-filled glove box indicates that a chemical reaction takes place.[9] This chemical reaction can be suppressed when the sample is kept at low temperatures, *e.g.* $T \sim -35$ °C and *in situ* SR-PXD reveals the formation of LiCl initiated at RT.[9] Thus, the reaction between $LiBH_4$ and $TiCl_3$ results in the formation of $Ti(BH_4)_3$, which decomposes at room temperature by an unknown mechanism.[210] One of the most effective additives was suggested to be $LiBH_4$–0.2$MgCl_2$–0.1$TiCl_3$, which released about 5 wt% H_2 at $T > 60$ °C and absorbed ~4.5 wt% H_2 at T = 600 °C, $p(H_2)$ = 70 bar.[450] The addition of $TiCl_3$ also changes the hydrogen exchange properties for other metal borohydrides, *e.g.* $Mg(BH_4)_2$.[451]

Metal borides as additives. Metal borides are known as inert materials with high melting points that have also been under consideration as additives. Titanium boride, TiB_2, appears to have a limited effect on the decomposition pathway of the $LiBH_4$–1.5Al system, but seems to facilitate the formation of intermediate compounds (*i.e.* Li–Al–B solid solutions) at lower temperatures compared to samples without an additive.[452] Similarly, zirconium boride, ZrB_2, appears to stabilize the hydrogen storage capacity for reactive hydride composites, *e.g.* $LiBH_4$–MgH_2, discussed in the following section, possibly by facilitating nucleation and growth of layered magnesium diboride.[453]

Assessment of additive effects by comparative studies. A series of nickel-based materials, Ni powder (30 nm), Ni_3B, NiF_2 and $NiCl_2$ (2 mol%), have been added to γ-$Mg(BH_4)_2$ and the hydrogen storage properties were evaluated.[447] EXAFS spectra indicate that $NiCl_2$ and NiF_2 react with γ-$Mg(BH_4)_2$ and transform to amorphous nickel boride. The γ-$Mg(BH_4)_2$–NiF_2 sample releases 6.5 wt% gas and the other three samples release 2.7 wt% at moderate conditions, $220 < T < 264$ °C, $10 < t < 60$ h, under static vacuum. Different side-reactions in the fluoride-containing sample may be responsible for the larger gas release. Spectroscopy suggests the formation of $Mg(B_3H_8)_2$ in the decomposed sample due to the relatively low thermolysis temperature. The four

 This journal is © The Royal Society of Chemistry 2017

samples absorb 1–2 wt% H_2 at $210 < T < 262$ °C, $10 < t < 48$ h, and $100 < p(H_2) < 155$ bar.[447]

A series of cobalt-based materials Co_2B, CoF_3, $CoCl_2$ and Co_3O_4 (2 mol%), have been added to γ-$Mg(BH_4)_2$ in a similar manner to the nickel additives.[454] Three full cycles of hydrogen release and uptake were conducted and the first cycle, at $T \sim 286$ °C, $2.6 < p(H_2) < 4$ bar, $10 < t < 40$ h, releases 3.1–4.4 wt% H_2, which is very similar to that of pure γ-$Mg(BH_4)_2$, 4.1–4.2 wt% H_2. Hydrogen absorption was conducted at 280–290 °C at $110 < p(H_2) < 125$ bar. The third cycle releases 1.4–2.0 wt% H_2 and the kinetics for hydrogen release and uptake is similar to pure γ-$Mg(BH_4)_2$.[454]

General discussion of the effect of additives on metal borohydrides. Overall, no real catalyst for B–H bond breaking or formation has been identified. The investigated additives may be divided into either reactive or inert additives. Reactive additives may react irreversibly with metal borohydrides and typically enhance the mass loss from the system in the first hydrogen release cycle. Reactive additives may contain a metal with a relatively high oxidation state and/or electronegativity, which may be reduced during release of diborane and hydrogen. Reactive anions may react irreversibly with the metal borohydride and form metal borates or more stable boranes, *e.g. closo*-borane. Inert additives may be metals or metal borides. However, the latter may have a beneficial effect and facilitate the crystallization of metal borides in the decomposed state. Small amounts of transition metal compounds like VCl_3, $ZrCl_4$ or Zr-isopropoxide added prior to the ball-milling process of reactive hydride composites (discussed in Section 6.8), *e.g.* $2LiBH_4$–MgH_2 have beneficial kinetic effects. The additives may transform to transition metal boride nanoparticles during thermolysis or aggressive ball-milling, which could facilitate the formation of metal borides in the dehydrogenated state and thereby hydrogen absorption.[455]

In most cases, only the first dehydrogenation is investigated, which hampers the distinction between irreversible chemical reactions and possible catalytic effects. Chemical reactions often show a significant enhancement of the first hydrogen release reaction, which may occur with faster kinetics and therefore also at apparently lower temperatures. A disadvantage for the use of volumetric or Sievert's methods for measuring the gas release is that measured changes in pressure is converted to an equivalent amount of hydrogen, which is incorrect if gases other than hydrogen are released. A chemical reaction between a reactive additive and a metal borohydride may often be identified by a mass loss, which scales with the amount of additive. Irreversible chemical reactions will lead to significant losses of the hydrogen storage capacity in the first cycle, illustrating the importance of conducting experimental evaluations over several cycles of hydrogen release and uptake.

The available knowledge on the exact mechanism for hydrogen release/uptake remains limited partly owing to difficulties in determining the decomposition products from metal borohydrides, which are often non-crystalline. In several cases, more than one reaction mechanism for hydrogen exchange is proposed, which may change as a function of the physical conditions, *e.g. p*, *T*, as discussed in Section 6.2. Thus, the rate determining step in the mechanism remain unknown, which also hampers the design of a catalyst.

Another largely overlooked problem is the fact that many metal borohydrides melt before or during hydrogen release. Fusion eliminates the grain structure and reduces the surface area of multicomponent samples. The partly molten state of the metal borohydride – additive system usually has a relatively high viscosity, thus a gas release leads to bubbling, foaming and possible phase segregation, which further limits reversibility and the use of catalysts.

6.8 Reactive hydride composites

Larger amounts of additives may lead to stoichiometric reactions among the components in a system, denoted Reactive Hydride Composites (RHC). P. Chen (China) was first to apply this approach to nitrogen containing systems like $Mg(NH_2)_2$–2LiH.[456] Later the approach was extended to borohydride containing systems by J. J. Vajo (USA), Y. W. Cho (South Korea) and R. Bormann (Germany).[37,39,42] Several systems combining metal borohydrides and magnesium hydride have been studied intensively during the past decade, *e.g.* $LiBH_4$–MgH_2, $NaBH_4$–MgH_2 and $Ca(BH_4)_2$–MgH_2.[37,38,457] A chemical reaction takes place between two or more components during decomposition, which lowers the overall reaction enthalpy (Fig. 25). This concept is analogous to Medima principles applied to d-block metals and the well-known Hess law from chemistry. The gravimetric hydrogen storage capacity is then the weighted average of the individual hydrogen storage capacity of the components of the RHC system.[8] In the following, selected RHC systems are discussed in more detail and Table 19 provides an overview of the thermodynamic data.

Lithium borohydride–magnesium hydride, $2LiBH_4$–MgH_2. The reactive hydride composite lithium borohydride–magnesium

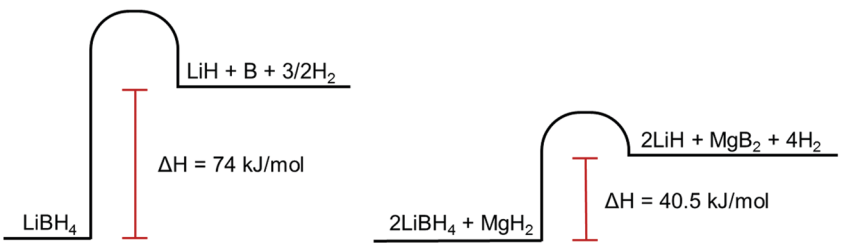


Fig. 25 Schematic illustration of the concept of reactive hydride composites illustrated for $2LiBH_4$–MgH_2.

Table 19 Thermodynamic and hydrogen storage properties of selected reactive hydride systems (RHC) and their components. Selected experimental thermodynamic data for individual components have been included from Table 17

System	ρ_m (wt% H)	ΔH (kJ mol^{-1} H_2)	ΔS (J K^{-1} mol^{-1} H_2)	T_{1bar} (°C)	Onset T_{dec} (°C)	Peak T_{dec} (°C)	Ref.
$LiBH_4$	18.5	74	115	370	280	420–460	45, 326 and 342
$NaBH_4$	10.7	108	133	539	475	510	332 and 458
$Ca(BH_4)_2$	11.6	87	158	278	350	375	45 and 337
MgH_2	7.7	74.1	133.4	282	240	315	323 and 426
$2LiBH_4$–MgH_2	14.4	40.5	81.3	225	300/350	350/420	39
$2NaBH_4$–MgH_2	9.9	64	102	282	280/420	325/470	459–462
$Ca(BH_4)_2$–MgH_2	10.5	—	—	—	270	330	463
$2LiBH_4$–Al	11.4	—	—	—	310	375–410	452 and 464
$2NaBH_4$–Al	7.9	—	—	—	340	500	464
$CaBH_4$–Al	4.9	—	—	—	345	365	464
$4LiBH_4$–MgH_2–Al	12.9	—	—	—	270/370	290/420	465

hydride releases and absorbs hydrogen under less harsh conditions (p, T, t) compared to the individual components. This is due to an exothermic formation of MgB_2 during the endothermic dehydrogenation reaction of the $2LiBH_4$–MgH_2 system, *i.e.* a chemical reaction between $LiBH_4$ and Mg, which leads to hydrogen release, the formation of LiH and a reduction of the total reaction enthalpy, see reaction scheme (6.19). In addition, hydrogen uptake from MgB_2–2LiH occurs at more moderate conditions than for the decomposition products from pure $LiBH_4$, *i.e.* amorphous boron, lithium boride and/or higher boranes like $Li_2B_{12}H_{12}$.[37] This is caused by the open layered structure of MgB_2 as well as the non-covalent bonding between Mg and B in MgB_2.[466] The full reversibility of the $2LiBH_4$–MgH_2 system is reported to only be obtained when the decomposition occurs in a hydrogen back pressure of $p(H_2) \sim$ 1–5 bar, which facilitates the formation of MgB_2 by suppressing the individual decomposition of $LiBH_4$ and MgH_2.[39,467,468]

The phase diagram has recently been investigated for the $2LiBH_4$–MgH_2 system from a comprehensive pressure–composition-isotherm study.[469] It was shown that there is a single equilibrium pressure plateau below 413 °C represented by reaction (6.19a), but there are two plateaus above 413 °C represented by reaction (6.19b). A similar phenomena exists for $NaMgH_2F$.[240]

$$2LiBH_4 + MgH_2 \leftrightarrow 2LiH + MgB_2 + 4H_2 \quad (6.19a)$$

$$2LiBH_4 + MgH_2 \leftrightarrow 2LiBH_4 + Mg + H_2 \leftrightarrow 2LiH + MgB_2 + 4H_2 \quad (6.19b)$$

A calculation of the decomposition enthalpy change yields $\Delta H_{dec} \sim$ 40–46 kJ mol^{-1} H_2, corresponding to T(1 bar) $\sim$ 169 °C.[39,41,469] A similar reaction occurs for a magnesium-rich system, *e.g.* $0.3LiBH_4$–MgH_2 that decomposes to MgB_2 in $p(H_2) > 1$ bar.[470,471] In contrast, the system $LiBH_4$–MgH_2 (0.3 : 1) and (2 : 1) decompose through a different reaction in dynamic vacuum forming α- and β-alloys of Mg_xLi_{1-x}, $x \sim 0.82$ and 0.70, respectively.[470,472] Hydrogen absorption also occurs at rather low pressures and temperatures $p(H_2) < 50$ bar and $T < 300$ °C. These conditions are substantially more favourable than those for $LiBH_4$ and are considered a breakthrough in utilizing borohydrides for reversible hydrogen storage.

The kinetics for hydrogen release and uptake reactions can be significantly enhanced by the addition of suitable additives, *e.g.* small amounts of transition metal compounds like VCl_3, $ZrCl_4$ or Zr-isopropoxide. Initially, the additives have a beneficial effect on the ball-milling process through the reduction of grain and particle sizes and thereby reducing hydrogen diffusion pathways.[455] Further investigations using extended X-ray absorption fine structure (EXAFS), X-ray absorption near edge structure (XANES) and anomalous small angle scattering (ASAXS) measurements indicate the formation of the respective transition metal boride nanoparticles during aggressive ball-milling or subsequent thermolysis.[453,455,473] The transition metal compounds with the best enhancement of reaction kinetics for RHC systems form transition metal borides with small directional and interplanar misfits to MgB_2 by 0.1 and 2.8%. Thus, these transition metal borides may act as favorable heterogeneous nucleation sites for the formation of the MgB_2 during decomposition.[453] Therefore, hydrogen absorption kinetics are significantly faster when compared to RHC without additives. Nanoscale MgH_2 synthesized *via* an organometallic method and used as a starting component appears to suppress the formation of *closo*-boranes, *e.g.* $[B_{12}H_{12}]^{2-}$.[474]

Sodium borohydride–magnesium hydride, $2NaBH_4$–MgH_2. Sodium borohydride readily forms by the hydrogenation of a $2NaH$–MgB_2 composite, see reaction (6.20).[37] The composite $2NaH$–MgB_2 has a calculated gravimetric hydrogen capacity of $\rho_m = 7.8$ wt% H_2, and reaction enthalpy of $\Delta H = 62$ kJ mol^{-1} H_2, corresponding to a decomposition temperature of T(1 bar) = 350 °C.[459] Hydrogenation of the $2NaH$–MgB_2 composite also occurs at low pressure *i.e.* $p(H_2) = 25$ bar ($t = 63$ h) at 400 °C where 6.2 wt% H_2 is absorbed.[475] Hydrogenation starts at $T \sim$ 250 °C but appears to become more complex at lower hydrogen pressures, proceeding *via* an unknown compound and $NaMgH_3$.[475]

$$2NaBH_4 + MgH_2 \leftrightarrow 2NaH + MgB_2 + 4H_2 \quad (6.20)$$

The decomposition pathway of $2NaBH_4$–MgH_2 RHC system appears to be a two-step reaction similar to $2LiBH_4$–MgH_2, see reaction scheme (6.19b). However, the reactivity appears to be lower and some $NaBH_4$ often remains in the sample after the reaction with Mg to form MgB_2.[476]

Calcium borohydride–magnesium hydride, $Ca(BH_4)_2$–MgH_2. The calculated gravimetric hydrogen capacity for the $Ca(BH_4)_2$–MgH_2 system is $\rho_m = 8.3$ wt% H_2 and it shows a complex reaction pathway with a number of intermediates, *e.g.* formation of CaB_6,

 This journal is © The Royal Society of Chemistry 2017

$Ca_4Mg_3H_{14}$ and other Ca–B–H compounds.[338,477–479] The idealized hydrogenation reaction takes place as illustrated in reaction scheme (6.21), which can take place at $p(H_2)$ = 140 bar and T = 250 °C,

$$CaH_2 + MgB_2 + 4H_2 \rightarrow Ca(BH_4)_2 + MgH_2 \quad (6.21)$$

Until now, only partial reversibility has been obtained, however, transition metal-based additives facilitate the formation of MgB_2 in the $Ca(BH_4)_2$–MgH_2 system in a similar way to the $LiBH_4$–MgH_2 system.[250,463]

Lithium borohydride–aluminium, $2LiBH_4$–Al. Access to the hydrogen content of $LiBH_4$ may be facilitated by the addition of a reactive metal, *e.g.* the $2LiBH_4$–Al system. The $2LiBH_4$–Al composite is more prone to rehydrogenation when compared to $LiBH_4$, *e.g.* at T = 400 °C and $p(H_2)$ = 100 bar.[471,480–483] In fact, the $2LiBH_4$–Al, $2NaBH_4$–Al and $CaBH_4$–Al systems can all be hydrogenated under 100 bar at 350–400 °C, but better kinetics are obtained under 600 bar.[464] However, cycling of hydrogen release and uptake in $2LiBH_4$–Al has shown that the system suffers from a significant degradation in hydrogen storage capacity.[452,484,485] The composite $2LiBH_4$–Al has been suggested to release hydrogen in two steps at T < 500 °C represented by reaction schemes:[471,480–483]

$$2LiBH_4(l) + Al(s) \rightarrow AlB_2(s) + 2LiH(s) + 3H_2(g) \quad (6.22)$$

$$LiH(s) + Al(s) \rightarrow LiAl(s) + 0.5H_2(g) \quad (6.23)$$

The enthalpy change for reaction (6.22) is calculated as ΔH = −59.3 kJ mol^{-1} H_2,[486] which corresponds to T(1 bar) = 166 °C.[483] Reactions (6.22) and (6.23) illustrate that the full H_2 capacity of $LiBH_4$ (ρ_m = 18.3 wt% H_2) can be utilized for the composite of $LiBH_4$–1.5Al. However, the addition of Al lowers the gravimetric H_2 capacity of this composite to only ρ_m = 6.5 wt% H_2.

The decomposition of $LiBH_4$–Al results in the formation of LiAl, AlB_2 and $Li_2B_{12}H_{12}$ *via* several reactions and intermediate compounds. Apparently, there is significant formation of $Li_2B_{12}H_{12}$, rather than a diborane release or amorphous boron production.[452] The hydrogen storage capacity reduces significantly over ten cycles of hydrogen release and uptake for the reactive composite $LiBH_4$–1.5Al, see Fig. 26.[452]

Lithium borohydride–sodium alanate composite, $LiBH_4$–$NaAlH_4$. Other metal hydrides have also been explored as possible Al sources, *e.g.* the system, $2LiBH_4$–$NaAlH_4$, ρ_m = 11.9 wt% H_2.[484] However, the samples prepared by ball milling reveal diffraction from both $LiAlH_4$ and $NaBH_4$, due to a metathesis reaction (6.24).[487]

$$LiBH_4(s) + NaAlH_4(s) \rightarrow LiAlH_4(s) + NaBH_4(s) \quad (6.24)$$

Several (coupled) chemical reactions are involved in hydrogen release and uptake. $NaBH_4$ decomposes at a much lower temperature than normal, at ~340 °C, after which some Na vapour is also released due to dynamic vacuum, leaving a LiAl alloy and amorphous boron in the solid state. Sodium borohydride, $NaBH_4$, only partly decomposes to B and NaH at T = 400 °C under $p(H_2)$ ~ 1 bar. The formation of AlB_2 is observed at T = 450 °C along with AlB_x or $Al_{1-x}Li_xB_2$, which stabilizes boron in the solid state. The $LiBH_4$–$NaAlH_4$ system is partially reversible and $LiBH_4$ was rehydrogenated under moderate conditions, T = 400 °C and

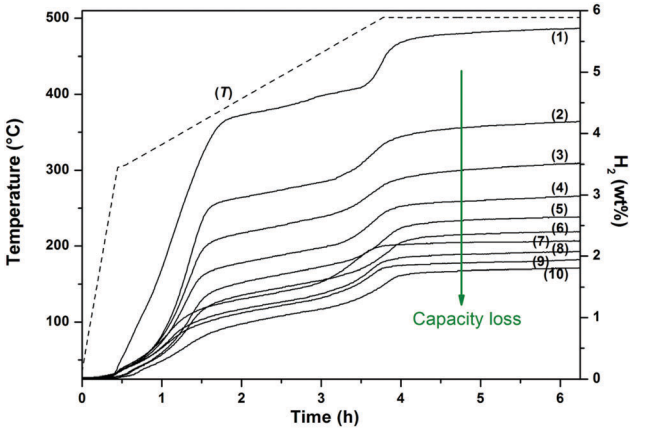


Fig. 26 Sieverts desorption measurements of $LiBH_4$–Al–TiB_2 (39.3, 58.9 and 1.8 mol%). The dashed line is the temperature profile and the ten desorption measurements are numbered (1) to (10). Dehydrogenation was conducted by heating to 300 °C ($\Delta T/\Delta t$ = 10 °C min^{-1}) and subsequently to 500 °C ($\Delta T/\Delta t$ = 1 °C min^{-1}), and then kept at 500 °C for 150 min at $p(H_2)$ ~ 10^{-2} bar. Adapted with permission from ref. 452. Copyright 2013 American Chemical Society.

$p(H_2)$ = 110 bar. During hydrogenation, the diffracted intensity from LiAl decreases at T ~ 200 °C and the formation of LiH and Al is observed, while the consumption of AlB_2 occurs at T ~ 280 °C. Crystalline h-$LiBH_4$ forms upon cooling at T ~ 260 °C. Apparently, the loss of sodium vapour prevents the formation of sodium alanate.[484]

The lithium borohydride–magnesium hydride–aluminium system $LiBH_4$–MgH_2–Al. Several reactive hydride composites (RHC) may also be combined to form more complex systems, *e.g.* the $LiBH_4$–MgH_2 and $LiBH_4$–Al RHC systems are combined to form $LiBH_4$–MgH_2–Al,[465] which has an even lower decomposition temperature *via* another mechanism and results in the formation of $Mg_xAl_{1-x}B_2$ as shown in the idealized reaction scheme:[465]

$$2LiBH_4(s) + xMgH_2(s) + (1 - x)Al(s) \rightarrow 2LiH(s) + Mg_xAl_{1-x}B_2(s) + (4 + x)H_2(g) \quad (6.25)$$

The hydrogen storage capacity of the $LiBH_4$–MgH_2–Al system decreases upon continuous hydrogen cycling (see Table 20). Boron in the hydrogenated sample $4LiBH_4$–MgH_2–Al exists as $Li_2B_{12}H_{12}$ (19.1 mol%) and $LiBH_4$ (80.9 mol%) after three cycles of hydrogen release and uptake, when dehydrogenated in low hydrogen pressure, $p(H_2)$ = 0.15 bar. However, the ratio $Li_2B_{12}H_{12}$–$LiBH_4$ is only 8.7 : 91.3 mol% when the sample is dehydrogenated at $p(H_2)$ = 5.0 bar. For the sample $4LiBH_4$–MgH_2–5Al only 2.4 mol%

Table 20 Molar composition of $LiBH_4$–MgH_2–Al (4 : 1 : 1) and $LiBH_4$–MgH_2–Al (4 : 1 : 5) after three hydrogen release and uptake cycles applying different hydrogen backpressure during desorption[465]

Sample	$p(H_2)$ (bar)	$Li_2B_{12}H_{12}$ (mol%)	$LiBH_4$ (mol%)
$LiBH_4$–MgH_2–Al (4 : 1 : 1)	0.15	19.1	80.9
$LiBH_4$–MgH_2–Al (4 : 1 : 1)	5.0	8.7	91.3
$LiBH_4$–MgH_2–Al (4 : 1 : 5)	0.15	8.0	92.0
$LiBH_4$–MgH_2–Al (4 : 1 : 5)	5.0	2.4	97.6

$Li_2B_{12}H_{12}$ and 97.6 mol% $LiBH_4$ is formed using the higher dehydrogenation partial pressure of hydrogen, $p(H_2)$ = 5.0 bar. These results show that both sample composition and hydrogen partial pressure, *e.g.* $p(H_2) > 1$ bar, during thermolysis is crucial to suppress the formation of more stable *closo*-boranes, $Li_2B_{12}H_{12}$, and thereby preserve the hydrogen storage capacity.

Manganese borohydride–metal hydrides. $Mn(BH_4)_2$ is an interesting candidate for hydrogen storage, owing to its high stability at room temperature, low decomposition temperature of 130–180 °C, high theoretical hydrogen capacity of 9.5 wt% H_2 and the high abundance of manganese in the lithosphere. A drawback for the utilization of $Mn(BH_4)_2$ is that the gas released during decomposition contains high levels of diborane. The mechanism for decomposition remains not fully understood, in particular the possible side reactions that produce diborane.[488] Thus, the hydrogen storage capacity is expected to decrease due to the loss of boron from the system during continued hydrogen release and uptake in manganese borohydride. In the reactive hydride composites, $Mn(BH_4)_2$–MH_x (M = Li, Na, Mg, Ca), the formation of the more stable $M(BH_4)_x$ for M = Li, Na and Ca suppresses the release of diborane and provides a higher hydrogen content in the released gas during the decomposition (Fig. 27).[489]

Bimetallic transition metal hydrides. Reactive hydride composites including Mg_2NiH_4, Mg_2FeH_6 *etc.* have also been explored to promote hydrogen release and uptake in metal borohydrides. The first example was discovered by J. J. Vajo (US, 2010), $LiBH_4$–Mg_2NiH_4, which reversibly stores hydrogen at moderate conditions, $\Delta H = 15.4 \pm 2$ kJ mol^{-1} H_2 and $\Delta S = 62.2 \pm 3$ J K^{-1} mol^{-1} H_2.[490] This is due to the formation of a bimetallic boride in the decomposed state, see reaction (6.26), which also absorbs hydrogen at moderate condition.

$$4LiBH_4 + 5Mg_2NiH_4 \rightarrow 2MgNi_{2.5}B_2 + 4LiH + 8MgH_2 + 8H_2 \quad (6.26)$$

This result suggests that there could be other similar systems because there are numerous complex transition metal hydride anions including $[FeH_6]^{4-}$, $[CoH_5]^{4-}$, and $[NiH_4]^{4-}$.[490–492] The magnesium iron hydride–lithium borohydride system also stores hydrogen reversibly but forms a monometallic boride, FeB, in the decomposed state.

$$2Mg_2FeH_6 + 2LiBH_4 \rightarrow 2LiH + 4MgH_2 + 2FeB + 5H_2 \quad (6.27)$$

The enthalpy change for this system is slightly larger, $\Delta H = 72 \pm 4$ kJ mol^{-1} H_2 and $\Delta S = 147 \pm 7$ J K^{-1} mol^{-1} H_2, and occurs in the temperature range 310–400 °C.[493]

Yttrium hydride. The reactive hydride composite, $4LiBH_4$–YH_3 releases ~7 wt% H_2 at $T \sim 350$ °C following reaction scheme (6.28), which corresponds to a calculated hydrogen content of $\rho_m = 8.5$ wt% H_2.[494]

$$4LiBH_4 + YH_3 \rightarrow 4LiH + YB_4 + 7.5H_2 \quad (6.28)$$

This reaction is reversible at relatively mild rehydrogenation conditions, *e.g.* $T = 350$ °C and $p(H_2) = 90$ bar.[468] Also, a hydrogen pressure of *e.g.* $p(H_2) = 90$ bar facilitates the formation of metal borides during decomposition.[494]

Rare earth metal hydrides are also used as additives, in $6LiBH_4$–MH_2 composites (M = La, Ce), which provide hydrogen release after $LiBH_4$ melting, but below its normal dehydrogenation temperature.[495] PCT measurements performed on $6LiBH_4$–CeH_2 provide thermodynamic data for the decomposition reaction $\Delta H_{dec} = 58 \pm 3$ kJ mol^{-1} H_2 and $\Delta S_{dec} = 113 \pm 4$ J K^{-1} mol^{-1} H_2 corresponding to $T(1\text{ bar}) = 240 \pm 32$ °C.[496] The change in thermodynamics suggests the formation of a reactive hydride composite.

Summary. The concept to lower both the total reaction enthalpy and thus the hydrogen release temperatures of hydride-borohydride mixtures (RHC) is currently working. In some cases, quite astonishing properties are found, such as enhanced absorption kinetics, in spite of a lowered driving force for absorption, however, the progress reached so far is limited. The sorption temperatures are still too high for many technical applications. Less stable borohydrides, decomposing at lower temperatures, show not only the release of hydrogen but also diborane, as mentioned above. To reach a significant breakthrough hydrides and/or reactive additives have to be found that react (reversibly) with the borohydrides at much lower temperatures and thereby capture the boron and prevent the release of diborane or the production of higher boranes.

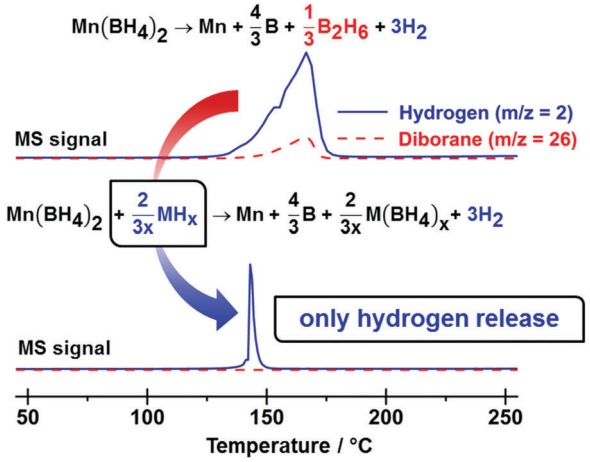


Fig. 27 Mass spectroscopy signal showing hydrogen (m/z = 2) and diborane (m/z = 26) for thermolysis of $Mn(BH_4)_2$ (upper plot) and $Mn(BH_4)_2$–MH_x (M = Li or Na) (lower plot). Adapted with permission from ref. 489. Copyright 2014 American Chemical Society.

6.9 Hydrolysis – decomposition by reaction with water

In an alternative process to thermal decomposition, hydrogen can also be released from hydrides in a reaction with water, denoted hydrolysis.[497] An advantage is that half of the released hydrogen originates from the water and increases the hydrogen capacity of the system.[30,498,499] Sodium borohydride can be stabilized in basic solution with a typical composition of 20% $NaBH_4$ and 1% NaOH (solubility of $NaBH_4$ is 55 g per 100 mL at 20 °C). The hydrolysis reaction is controlled by a catalyst, *e.g.* a late transition metal, such as Ru. The catalytic effect of Pt for the generation of H_2 from BH_4^- hydrolysis was discovered in the early 1960s and this reaction has been extensively investigated on a variety of high-surface area catalysts such as Pt–C.[500]

 This journal is © The Royal Society of Chemistry 2017

DFT calculations indicate that the hydrolysis reaction takes place for BH_4^- co-adsorbed with H_2O on a surface.[433]

The low concentration of $NaBH_4$ reduces the storage capacity of the system to 4 wt% H_2. The product obtained from hydrolysis is sodium metaborate $NaBO_2$ and hydrogen, see reaction (6.29). The concentration of the reactants should be kept sufficiently low in order to prevent precipitation of $NaBO_2$, which may block the catalytic active sites (the solubility of $NaBO_2$ in water is 26 g per 100 mL at 20 °C).[501]

$$NaBH_4(aq) + 2H_2O(l) \rightarrow 4H_2(g) + NaBO_2(s) \quad (6.29)$$

A significant drawback of the hydrolysis approach is that the dehydrogenated product is typically a stable oxide, *e.g.* sodium metaborate $NaBO_2$, with a heat of formation of $\Delta H_f = -1058$ kJ mol^{-1}. The heat of formation for $NaBH_4$, $\Delta H_f = -191$ kJ mol^{-1} is significantly less negative, illustrating that a large amount of energy is required for the preparation of $NaBH_4$ from $NaBO_2$, *e.g.* from a reaction using molten magnesium. Thus, hydrolysis often provides hydrogen at RT, but is considered difficult to reverse because off-board regeneration is needed.[30]

6.10 Nanoconfinement

Nanoparticles may have significantly different properties compared to bulk materials due to (i) increased surface area, (ii) nanoscale diffusion distances, (iii) increased numbers of atoms in the grain boundaries and (iv) intimate contact between different reacting solids, or a melt.[502,503] These nanoscale properties facilitate the release and uptake of hydrogen and enhance reaction kinetics. Thermodynamic properties may also be improved and theoretical studies predict that the increased surface area to bulk volume destabilizes MgH_2 nanoparticles and thereby reduces the reaction enthalpy.[323,503–506] However, thermodynamic improvements are suggested to occur only for MgH_2 nanoparticles with sizes less than ~5 nm, while kinetic enhancement also occurs for larger nanoparticles below ~50 nm.[323,506–508] The most widely used technique for the preparation of hydride nanoparticles is probably mechanochemical treatment, *i.e.* ball milling. In this top-down approach the size of the bulk material is reduced mechanically, in some cases to <100 nm. However, the samples are often contaminated with trace material from the vial and balls,[52] and are challenging to characterize.[509] Furthermore, nanosized particles may grow into larger particles upon continuous hydrogen release and uptake reactions. Nano materials may be directly synthesized and stabilized in a nanoporous scaffold, denoted nanoconfinement, which is discussed below.

Nanoconfinement. The topic for this section is the utilization of nanoporous materials as scaffolds for the preparation and confinement of nanosized metal borohydrides. This bottom-up approach limits the particle size of the borohydride to the pore size of the scaffold material, which allows direct production of smaller particles than mechanically obtainable. Furthermore, particle growth and agglomeration may be hindered by the compartmentalization of nanoparticles within the scaffold material and may also limit the mobility of the decomposition products and keep them in intimate close contact. Thereby, nanoconfinement may improve hydrogen absorption properties of metal hydrides. Phase segregation of decomposition products upon bulk dehydrogenation can limit hydrogen uptake reactions, which can be circumvented with nanoconfinement. A large amount of heat may also be exchanged during hydrogen release and uptake in metal hydrides and heat transport may be a kinetic limiting factor. Metal hydride powders have low thermal conductivities of ~0.1 W m^{-1} K^{-1} in contrast to carbon based support materials, which can have high thermal conductivities, *e.g.* 12–75 W m^{-1} K^{-1} for graphite.[510] Nanoconfined chemistry is receiving increasing general interest and is becoming an important tool within several research areas.[502,511–515] The aim of the following is to highlight selected results obtained by the nanoconfinement of metal borohydrides.

Nanoconfinement of lithium borohydride, $LiBH_4$. Lithium borohydride can be melt infiltrated in ordered mesoporous SiO_2 scaffolds (D_{max} ~ 5–10 nm), *e.g.* at T ~ 295 °C, and high hydrogen pressure, *e.g.* $p(H_2)$ = 100 bar, can suppress a reaction with the scaffold, which would otherwise produce lithium silicates, Li_2SiO_3 or Li_4SiO_4.[516]

Lithium borohydride has a higher stability when nanoconfined in carbon materials and absorbs hydrogen at significantly more mild conditions when compared to bulk $LiBH_4$. Lithium borohydride, solvent infiltrated in mesoporous carbon scaffolds (D_{max} ~ 4 nm), releases hydrogen at T ~ 300 °C.[510] About 70% of the initial hydrogen content is released during the third hydrogen release cycle for $LiBH_4$, confined in microporous activated carbon (D_{avg} < 2 nm), when hydrogen absorption is conducted at $p(H_2)$ = 100 bar, T = 400 °C for two hours. A lower stability of the hydrogen storage capacity is observed for scaffolds with larger pores, *e.g.* carbon aerogel, D_{avg} = 25 nm, where $LiBH_4$ only releases 40% of the initial hydrogen content in the third release cycle. However, the observed increase in hydrogen release and uptake rates with decreasing pore size may be a kinetic effect, which may also contribute to the apparently higher cyclic stability. The hydrogen storage capacity appears to be stabilized and preserved to a higher degree for nanoconfined systems in comparison to bulk systems. This effect may be associated with a different hydrogen exchange mechanism due to the nanoconfinement of reactants and decomposition products, *i.e.* $Li_2B_{12}H_{12}$, $Li_2B_{10}B_{10}$, or LiB_x.[516–519] However, systematic investigation into the effect of varying pore sizes suggests that diborane release and the formation of *closo*-boranes may be reduced using carbon scaffolds with smaller pores.[520]

Nanoconfinement of sodium borohydride, $NaBH_4$. Sodium borohydride has a high decomposition temperature, T_{dec} > 500 °C, with an onset at ~470 °C, which may be reduced to 250 °C upon nanoconfinement in porous carbon. Here, 43% of the hydrogen content is reversible under mild conditions $p(H_2)$ = 60 bar, T = 325 °C for five hours.[521] Encapsulation of $NaBH_4$ nanoparticles by a Ni layer, forming a core shell nanostructure, provides effective nanoconfinement of the molten $NaBH_4$ core and the dehydrogenation products. These nanostructures have high stability and were cycled 5 times with hydrogen release ($p(H_2)$ = 1 mbar) and uptake ($p(H_2)$ = 40 bar) at

T = 350 °C, demonstrating a hydrogen capacity of 5 wt% where *ca.* 80% of the H_2 capacity was exchanged within 1 h.[522]

Nanoconfinement of magnesium borohydride, $Mg(BH_4)_2$. The synthesis of $Mg(BH_4)_2$/carbon nanocomposites from MgH_2 nanoparticles supported on carbon aerogel in a B_2H_6/H_2 atmosphere has been conducted.[523] The nanocomposite exhibits a lower kinetic barrier and a lower peak hydrogen release temperature, T = 160 °C, when compared to bulk $Mg(BH_4)_2$. Furthermore, hydrogen uptake occurs at mild conditions, T = 200 °C and $p(H_2)$ = 80–150 bar.[523] Magnesium borohydride has also been infiltrated into ordered mesoporous carbon (CMK-3) functionalized by Ni nanoparticles (5 wt%).[524] The hydrogen release temperature was significantly decreased with onset at T = 75 °C and peak release at T = 155 °C, compared to 270 °C and >350 °C, respectively, for pure $Mg(BH_4)_2$. Hydrogen release also occurs with faster kinetics in the nanoconfined system.[524]

Lithium–potassium borohydride, $LiBH_4$–KBH_4. Eutectic melting, reactive hydride composites and nanoconfinement all have the potential to improve the reversible hydrogen storage capacity in metal borohydrides. The combined effect of all three methods has been explored in an attempt to improve the lithium–potassium borohydride system, $0.725LiBH_4$–$0.275KBH_4$, which has a low melting temperature T_m = 105 °C.[48] The bulk eutectic mixture and the RHC with magnesium, $LiBH_4$–KBH_4–Mg and $LiBH_4$–KBH_4–MgH_2, have been melt-infiltrated into a nanoporous carbon scaffold. The decomposition of $0.725LiBH_4$–$0.275KBH_4$ (and the RHC) initiates simultaneously with melting at 105 °C, but remains slow until higher temperatures are reached T > 300 °C. Eutectic melting appears to improve the kinetics of the hydrogen de- and absorption, while nanoconfinement lowers the main hydrogen release temperature in the first cycle by up to 200 °C.[48]

Lithium–magnesium borohydride, $LiBH_4$–$Mg(BH_4)_2$. The decomposition of nanoconfined lithium–magnesium borohydride, $Li^{11}BD_4$–$Mg(^{11}BD_4)_2$, was investigated by thermal analysis and small-angle neutron scattering.[525] The dehydrogenation temperature was decreased by up to 60 °C in the nanoconfined system and occurred without the formation of diborane, B_2D_6, or *closo*-boranes, which evolve from the bulk mixture.[525]

Lithium–calcium borohydride, $LiBH_4$–$Ca(BH_4)_2$. Eutectic melting $LiBH_4$–$Ca(BH_4)_2$ has been nanoconfined in different types of carbon scaffolds with surface areas 500 to 2600 $m^2\ g^{-1}$ and pore sizes 5–50 nm. In general, the nanoconfined systems provide faster kinetics and higher stability over several cycles of hydrogen release and uptake, which also occurs at more mild conditions.[369,526–528] Nanoconfined $LiBH_4$–$Ca(BH_4)_2$ in CO_2-activated scaffolds release up to 80 or 73% of the calculated hydrogen content in the second and third hydrogen release cycle, respectively. They can potentially reach hydrogen storage densities in the range ~10–12 wt% H_2 for scaffolds with large pore volumes, 3.1 mL g^{-1}, and large surface areas, 2660 ± 208 $m^2\ g^{-1}$.[527]

Reactive hydride composites, $2LiBH_4$–MgH_2. The first nanoconfined reactive hydride composite (RHC) $2LiBH_4$–MgH_2 was infiltrated in a nanoporous RF-CA scaffold (D_{avg} ~ 21 nm) in an attempt to combine the beneficial effect from nanoconfinement and RHC.[529] The onset temperature for hydrogen release is reduced by 90 °C and the nanoconfined sample desorbed 3.9 wt% H_2 at 390 °C, $p(H_2)$ = 2 bar after 20 h, in accordance with the calculated hydrogen content for the sample of 3.9 wt% H_2. The hydrogen absorption was performed under relatively mild conditions and the fourth desorption released 3.0 wt% H_2, *i.e.* 92 and 74% of the capacity is preserved over three and four cycles, respectively.[529] Similar results were obtained with other methods for infiltration and other scaffold materials.[492,530,531] However, improved capacity as been achieved for $2LiBH_4$–MgH_2 encapsulated within graphene, where an impressive reversible capacity of 8.9 wt% H_2 is reported after 25 cycles at 350 °C.[532]

Functionalization of nanoporous scaffolds may further improve kinetics during hydrogen release and uptake. The stability during cycling was explored for $TiCl_3$,[533] $TiCl_4$[534] and $ZrCl_4$.[535] Several other composites based on lithium borohydride have also been successfully nanoconfined, *e.g.* $2LiBH_4$–$NaAlH_4$,[536] $LiBH_4$–Mg_2NiH_4[537] and $LiBH_4$–$NaBH_4$.[538]

7. New properties and future perspectives of metal borohydrides

Metal borohydrides have diverse compositions with overwhelmingly rich structural chemistry, which has led to new perspectives for the future utilization of this fascinating class of new materials. Furthermore, a wide range of approaches for tailoring the composition and structure of metal borohydrides was discussed in previous sections, along with the effect of additives, reactive hydride composites and nanoconfinement *etc.*, in Section 6. This section provides the state-of-the-art for new perspectives on the utilization of metal borohydrides for practical applications, in addition to those involving their extreme energy densities. This chapter reveals multiple novel properties for metal borohydrides, *e.g.* optical, magnetic, ion or semi conductivity.

7.1 Porous metal borohydrides for gas adsorption

The extreme structural flexibility found for metal borohydrides is highlighted by magnesium borohydride, as described in detail in Section 3.1. The γ polymorph has 33% 'empty space' and a 3D network of interpenetrated channels with pore sizes in the range 5.8–8.8 Å, being the first complex metal hydride with large permanent porosity.[3] Furthermore, it is the first complex metal hydride capable of reversibly adsorbing hydrogen, nitrogen and other small molecules such as CH_2Cl_2. The adsorption of dichloromethane, CH_2Cl_2 is reversible and fast (within minutes), occurring near room temperature with negligible unit cell expansion, forming γ-$Mg(BH_4)_2{\cdot}0.18CH_2Cl_2$. Here, the only host–guest contacts are the dihydrogen bonds $B–H^{\delta-}\cdots{}^{\delta+}H–C$ of 1.9 and 2.0 Å. There are neither substantial guest–guest interactions nor coordination of the guest to the metal atom (Mg···H–C 3.5 Å, Mg···Cl ~ 4 Å). The host–guest interactions illustrate the selectivity of the anionic borohydride groups being capable of binding positively charged moieties. Neutral molecules such as nitrogen (N_2) and hydrogen (H_2) also adsorb in the γ-$Mg(BH_4)_2$ framework at elevated pressure and low temperature. *In situ* SR-PXD data revealed storage capacities of γ-$Mg(BH_4)_2{\cdot}0.63N_2$ at $p(N_2)$ = 30.6 bar and γ-$Mg(BH_4)_2{\cdot}0.80H_2$ at $p(H_2)$ = 105 bar at

 This journal is © The Royal Society of Chemistry 2017

−193 °C. The latter corresponds to a total of 17.4 wt% H_2, including the hydrogen in the framework.[3] Nitrogen or hydrogen molecules are grouped into diffuse rods within the structure, centered around (1/8, 1/8, 1/8) and extended along the cube diagonal (x, x, x), which indicates van der Waals interactions occur between gas molecules and BH_4 groups. The desorption isobars ($p(H_2)$ = 105 bar, $p(N_2)$ = 30.6 bar) indicate that the gas molecules are leaving the framework at relatively high temperatures; desorption of hydrogen starts at −143 °C, with ∼50% H_2 remaining inside the pores at −73 °C. This suggests the potential for efficient hydrogen storage in related materials at moderate temperatures. The isosteric heats of adsorption, Q_{st}, of nitrogen and hydrogen in γ-$Mg(BH_4)_2$ were determined to be: $Q_{st}(N_2)$ ∼ 15 kJ mol^{-1} and $Q_{st}(H_2)$ ∼ 6 kJ mol^{-1} (average value), with Q_{st} > 7 kJ mol^{-1} at a loading of 15 mg H_2 g^{-1}.[3] The latter value is among the highest values measured for MOFs and other porous solids.[539]

The structural similarity between metal borohydride frameworks and covalently bonded metal organic frameworks (MOFs) is illustrated by the significant degree of directionality in the interaction between a metal and the complex borohydride anion. In particular, the same framework topology is observed for both γ-$Mg(BH_4)_2$ and the zinc imidazolate framework ZIF-72,[3,540] and several metal borohydrides have interpenetrated framework structures similar to MOFs, *e.g.* $MZn_2(BH_4)_5$ (M = Li and Na) and $Li_3MZn_5(BH_4)_{15}$ (M = Mg, Mn). Although, there are other borohydrides that mimic the tetrahedral framework of cristobalite, such as δ-$Mg(BH_4)_2$, or α- and β-$Cd(BH_4)_2$. γ-$Mg(BH_4)_2$ shares gas adsorption properties with MOFs and also shares an 'amorphous' to 'crystalline' phase transition at elevated pressures. However, metal borohydride frameworks give rise to specific guest–host interactions with hydridic atoms of the BH_4^- anion, which do not occur in MOFs.

7.2 Metal borohydrides as ion conductors

Hydrides of intermetallic compounds such as $LaNi_5H_6$ have widely been used as electrodes in rechargeable batteries, replacing toxic metal Cd in the Ni–Cd pair. Following the report on the conversion reaction of the redox couple MgH_2/Li[541] many other complex metal hydrides have been studied as battery electrodes.[7,542,543] The use of borohydrides in batteries is very recent, and is actually limited to solid-state electrolytes (Fig. 28). This is despite several reactions having been proposed theoretically by *ab initio* calculations for conversion electrodes in Li-batteries, including a promising reaction, based on $Mg(BH_4)_2$, that results in an enormous theoretical charge capacity of 3969 mA h g^{-1}.[544] The numerous advantages of metal borohydrides as battery materials include their light weight (high charge density), apparent material compatibility with Li and Na electrodes, thermal and electrochemical stability, and easy manufacturing of the electrolyte/electrode interface and thus of the whole battery.

Fast Li-ion conduction in a borohydride was first discovered in the high temperature polymorph h-$LiBH_4$,[545] where conductivities exceeding 2 × 10^{-3} S cm^{-1} above 110 °C (the polymorphic transition temperature) were reported. Since then, several other solid-state metal-borohydride and borohydride-based mixed-anion electrolytes have been developed that exhibit fast Li- and Na-ion conduction.[49]

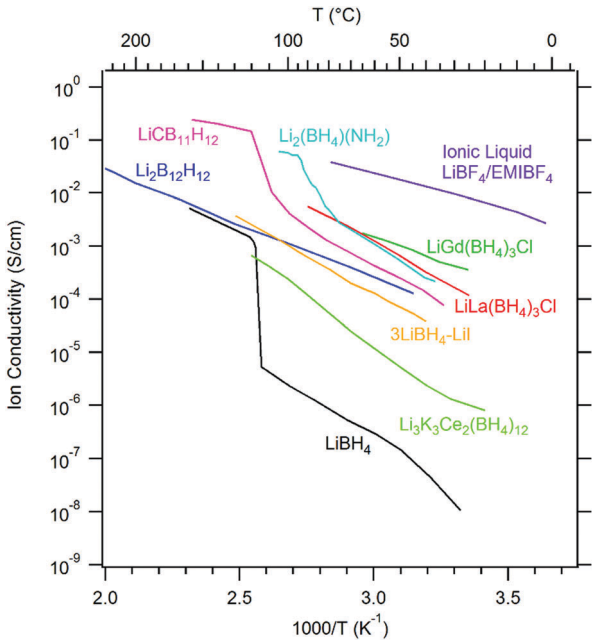


Fig. 28 Li^+ ion conductivity of a range of borohydride-based materials and higher boranes.[88,89,168,546–550]

Lithium borohydride halides as Li-ion conductors. Above the polymorphic transition temperature of 110 °C, the Li ion conductivity of the HT-polymorph h-$LiBH_4$ is three orders of magnitude higher than that of the RT-orthorhombic polymorph, o-$LiBH_4$. It was shown that anion substitution $BH_4^- \leftrightarrow X^-$ (X^- = Halide) stabilizes the h-$LiBH_4$ polymorph down to room temperature, *e.g.* h-$Li(BH_4)_{1-x}I_x$.[551] The RT Li-ion conductivity in the halide stabilized h-$LiBH_4$ reaches 2 × 10^{-5} S cm^{-1}.[550]

Alkali rare-earth spinel-like borohydride halides as Li-ion conductors. Recently, a new series of mixed-cation mixed-anion borohydride chlorides based on rare-earths elements, $LiM'(BH_4)_3Cl$, M′ = La, Gd, and Ce, was discovered using combined mechanochemical synthesis and heat treatment from $M'Cl_3$–$LiBH_4$ (1 : 3) mixtures.[4,88] This growing class of materials has a new structure type and contains isolated tetranuclear anionic clusters $[M_4Cl_4(BH_4)_{12}]^{4-}$ with a distorted cubane M_4Cl_4 core, charge-balanced by Li^+ cations. This compound can also be understood as containing fragments of the spinel structure, *i.e.* $LiCl_4$ tetrahedra and M_4Cl_4 cubane. The Li^+ ions are disordered and occupy 2/3 of the 12d Wyckoff sites and DFT calculations indicate that $LiCe(BH_4)_3Cl$ is stabilized by larger entropy rather than smaller enthalpy. Thus, the structural model and DFT calculations agree well with the very high lithium ion conductivity measured for $LiCe(BH_4)_3Cl$, 1.03 × 10^{-4} S cm^{-1} at T = 20 °C. The other members of this series of isostructural compounds, $LiLa(BH_4)_3Cl$ and $LiGd(BH_4)_3Cl$, also have high Li-ion conductivities at RT and low electronic conductivities, see Table 21. This class of materials, $LiM(BH_4)_3Cl$, holds significant potential in the design of other new ion conductors, which is not yet fully explored. Cation and anion substitution may allow for the preparation of new sodium or magnesium ion conductors.

Table 21 Ion and electronic conductivity at RT and hydrogen storage properties of $LiM(BH_4)_3Cl$, M = La, Ce and Gd[4,88]

Compound	Unit cell a (Å)	ρ (g cm^{-3})	ρ_m (wt%)	ρ_V (kg H_2 m^{-3})	T_{dec} (°C)	Li-ion × 10^{-4} (S cm^{-1})	Electronic·× 10^{-8} (S cm^{-1})
$LiLa(BH_4)_3Cl$	11.7955	1.86	5.36	96.4	260	2.3	1.4
$LiCe(BH_4)_3Cl$	11.7204	2.61	5.33	99.8	260	1.03	—
$LiGd(BH_4)_3Cl$	11.5627	2.16	4.95	102.6	260	3.6	9

Other borohydride-based mixed-anion ion conductors. Some metal amides and imides are good ion conductors, such as lithium imide Li_2NH with an excellent solid-state Li-ion conductivity at RT (2.5 × 10^{-4} S cm^{-1}), but with very low electrochemical stability, 0.7 V.[552] Addition reactions between nitrogen-based compounds and metal borohydrides have therefore been studied, leading to several novel solid state electrolytes such as $Li_2(BH_4)(NH_2)$ and $Li_4(BH_4)(NH_2)_3$[89] with Li-ion conductivities of up to 2 × 10^{-4} S cm^{-1} at RT. The disordered anti-perovskite $Na_2(BH_4)(NH_2)$ was also recently shown to have a Na-ion conductivity of 2 × 10^{-6} S cm^{-1} at RT,[553] and Mg-ion conductivity in tetragonal $Mg(BH_4)(NH_2)$ reaches 1 × 10^{-6} S cm^{-1} at 150 °C.[270]

Alkali rare-earth garnet borohydrides as Li-ion conductors. The oxide-borohydride analogy,[193] is a new tool for the design of novel materials with useful properties, clearly illustrated by the recently discovery of metal borohydride-garnets. Metal borohydride-garnets were synthesized,[168] based on the fact that doped lanthanide-oxide garnets $Li_{3+x}La_3M_2O_{12}$ (where M denotes various metals) are excellent Li-ion conductors.[554] The new metal borohydride garnet analogues, $Li_3K_3Ce_2(BH_4)_{12}$ and $Li_3K_3La_2(BH_4)_{12}$ show high room temperature Li-ion conductivity (3 × 10^{-7} and 6 × 10^{-7} S cm^{-1}). Most importantly, these values are 5 to 6 orders of magnitude above those of undoped metal oxide garnet conductors. The effect of heterovalent cation substitution was investigated as a means of tailoring the ion conductivity. Substitution with divalent Sr^{2+} and Eu^{2+} showed that the Li-ion conductivity can be increased by one order of magnitude in the whole temperature range measured.[168]

Higher-boranes and mixed anion higher borane-borohydrides as Li- and Na-ion conductors. Higher boranes such as $B_{10}H_{10}^{2-}$ or $B_{12}H_{12}^{2-}$ form inorganic salts which, in the case of Na- and Li-based compounds, are good ionic conductors when the cations become disordered in HT-phases,[546,547,555] and are the focus of a recent review.[252] The Na-ion conductivity of $Na_2B_{12}H_{12}$ increases by 3 orders of magnitude between the phase transition from the ordered monoclinic phase to the disordered cubic phase at 256 °C, and reaches a conductivity value of close to 0.1 S cm^{-1}.[546] The concept of anion-mixing was applied to this novel class of solid electrolytes generating $Na_3BH_4B_{12}H_{12}$ and $(Li_{0.7}Na_{0.3})_3BH_4B_{12}H_{12}$, capable of conducting either Na^+ or both Na^+ and Li^+ ions.[256] Unlike order–disorder governed dodeca- and decaboranes the cationic mobility is not entropically activated in $Na_3BH_4B_{12}H_{12}$ and $(Li_{0.7}Na_{0.3})_3BH_4B_{12}H_{12}$, thus a HT phase transition is not required to enable fast ion conduction. $Na_3BH_4B_{12}H_{12}$ reaches RT conductivity values close to 10^{-3} S cm^{-1}. $(Li_{0.7}Na_{0.3})_3BH_4B_{12}H_{12}$, on the other hand, forms only by a reversible chemical reaction at 230 °C, which is accompanied by a dramatic increase in ionic conductivity >10^{-1} S cm^{-1}. Such high temperatures are nevertheless within reasonable limits for large-scale facilities, which operate at over 300 °C in the case of Na–S power grids, for instance.

The paddle-wheel mechanism for ion conduction. Many potential solid-state ionic conductors can be rationally designed from salts containing dynamically disordered complex anions. In such materials, the conduction is not purely vacancy-dependent. The structure typically contains polyanions $[AB_y]^{n-}$ with covalent A–B bonds (*e.g.* PO_4^{3-}, SO_4^{2-} and NO_3^-), where the rotational diffusion of $[AB_y]^{n-}$ promotes cationic conductivity, decreasing the associated activation energy *via* a so-called "paddle-wheel" mechanism.[556] After the first reports on a possible "paddle-wheel" mechanism of the complex anion $[BH_4]^-$ in superionic metal borohydrides,[557–559] it was shown by solid state NMR and quasi-elastic neutron scattering,[560,561] that the high rotational mobility promotes superionicity in the respective materials (Fig. 29). There is also structural evidence for the "paddle-wheel" Ag^+ migration mechanism in $Ag_2B_{12}H_{12}$, where Ag^+ cations can only occupy particular atomic sites in the crystal structure for certain $[B_{12}H_{12}]^{2-}$ anion orientations.[562]

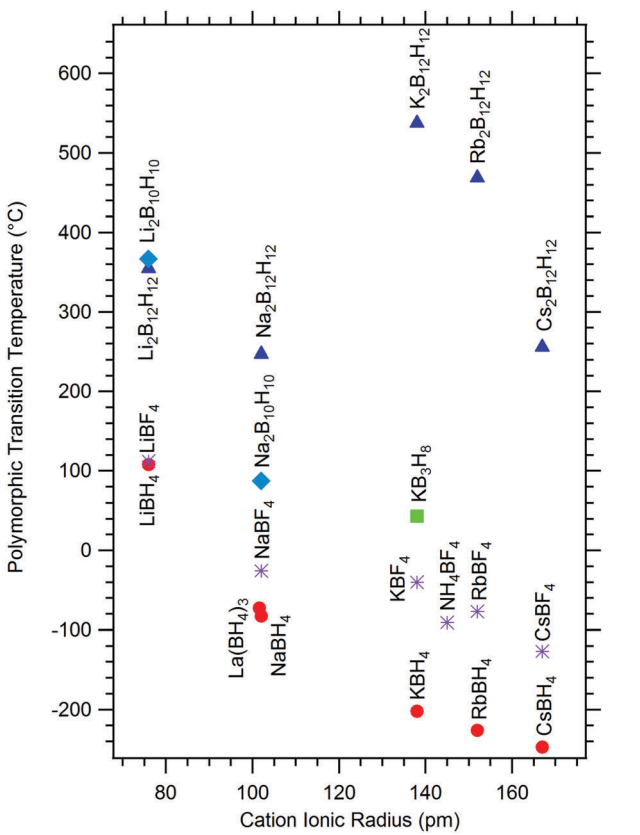


Fig. 29 Polymorphic transition temperatures for fast anion rotational motion in selected boron-based solids.[24,101,132,555,560,563–572]

 This journal is © The Royal Society of Chemistry 2017

7.3 Metal borohydrides with optical properties

Recent reports on perovskite-type borohydrides motivated investigations into lanthanide-luminescence in perovskite and double perovskite host lattices such as $CsCa(BH_4)_3$ or $LiCs_2Y(BH_4)_6$.[1] These systems provided the structural simplicity required in order to study light emission in metal borohydrides, but also enabled tailoring of the emitted spectrum and the efficiency of the light-emitting process in these potential solid-state borohydride phosphors. Very little is known about the Eu(II) luminescence in metal hydrides. Kunkel *et al.* have reported relatively low quantum yields of yellow-red emission in simple binary alkaline earth hydrides $Eu_xM_{1-x}H_2$ (M = Ca, Sr, Ba)[573] as well as in perovskite hosts based on alkali and alkaline earth metals such as $KMgH_3$, $NaMgH_3$ and $LiBa_xSr_{1-x}H_3$,[574] where the emission ranges from yellow to green. While such red-shifts of the Eu(II) emission were explained on the basis of the nephelauxetic effect, in metal borohydrides the bright Eu(II) emission is centred in the blue regime, which is far more common for Eu(II). To our knowledge, the first reports on Eu(II) luminescence in a complex hydride date back only very recently,[313] and is similar to the unsolvated homoleptic borohydrides.[1] These compounds show little concentration quenching and a high quantum yield, rare observations for bulk Eu(II)-based phosphors.

$CsPb(BH_4)_3$ crystallizes in the perovskite type, and is the first borohydride to show a bandgap in the visible light regime, while metal borohydrides commonly are wide gap insulators with band gaps above 5 eV.[1] This material was synthesized in view of the current revolution in photovoltaics, triggered by the hybrid perovskites AMX_3, where A is a bulky organic cation such as CH_3NH_3 or $HC(NH_2)_2$, M is a group IV metal (Pb, Sn, Ge) and X is a halogen. The substitution $X \leftrightarrow BH_4$ may harness alterations to the band gap of the material and hence to the light spectrum that may be harvested by the material.

7.4 Metal borohydrides with magnetic properties

Most physical properties related to magnetism arise from long-range magnetic order, which is dependent on the exchange interaction between magnetic centers, and requires unpaired electrons in open-shell configurations. The interesting transition metals used to generate such ordering are prone to reduction by the borohydride group and hence not stable. Thus, magnetic/electronic correlation has hitherto not been observed in metal borohydrides. Indeed, the only transition metal with an open shell reported amongst borohydrides is Mn, with oxidation state Mn^{2+}. On the other hand, and as shown throughout this review, all di- and many trivalent oxidation states of rare-earth elements form stable borohydride compounds. A series of bimetallic Gd-borohydrides was investigated with the aim of identifying paramagnetic salts and investigating their properties related to the magnetic entropy change $-\Delta S_M$, which is one of the key properties of magnetic refrigerants.[50] Owed to its isotropic f^7 electronic configuration, and hence its large ground state spin multiplicity, most competitive coolers have been based on Gd^{3+}, such as the benchmark material GGG (gadolinium gallium garnet $Gd_3Ga_5O_{12}$).[575] Additionally, a paradigm shift is currently taking place, attempting to develop Mn^{2+}-based materials for sub-Kelvin cooling. Similar to most energy-related materials, restrictions imposed on potential candidates are, in addition to weight and volume, the absence of any long-range ordering down to very low temperatures, in order to replace costly He-3.[576] The mass of the borohydride ligand is close to that of the oxide anion, and hence much lighter than most of the organic ligands employed in MOF materials currently under investigation.[577] The magnetic entropy change per unit mass is thus highly competitive and the recently reported $K_2Gd(BH_4)_5$ reaches values that lie amongst the 5 highest reported to date,[50] and further increases in the magnetic to non-magnetic mass ratio can be expected due to cation substitution $NH_4^+ \leftrightarrow K^+$. Furthermore, many metal borohydrides, both pseudo-binary and -ternary, crystallize in packed structure types derived from *ccp* or *hcp*,[193] which allows sensible values concerning the magnetic entropy change per unit volume. Both pseudo-binary $Mn(BH_4)_2$ as well as Mn-bearing double-salts are stable compounds that are paramagnetic down to at least 2 K and their magnetic refrigeration properties will be investigated in the future. The thermal conductivities of some simple metal borohydrides lie in the range of 2–5 $W\,m^{-1}\,K^{-1}$,[578,579] which is appropriate for the heat transfer in magnetic cooling devices.

7.5 Perspectives for design of novel metal borohydrides

Borohydrides are beginning to play a role as interesting materials in a variety of technical fields. For instance, a semiconducting compound $CsPb(BH_4)_3$ was recently reported,[1] which relates well to the plumbohalides also under investigation for photovoltaics, however, it is not chemically stable for a long time period. Neutron shielding applications were also proposed due to the high absorption cross section of boron (767 barn for natural isotope abundancy).[580] In this context, the energy transfer from the neutron to the material could also be exploited to develop neutron detectors (or scintillators in general) where a luminescent RE-ion emits light upon irradiation of the host, similar to what has been done with borates in the past.

The hydrolysis of metal borohydrides has been investigated since 1953 as a mechanism to quickly generate hydrogen gas from a solid-state storage medium.[581] This research field is still evolving and current research strives for a cost reduction for using hydrolysis as a reversible energy generation and storage system. In a similar manner, metal borohydrides are also investigated as reducing agents in direct borohydride fuel cells.[582] A redox reaction occurs between the borohydride anion itself and an oxidant to generate electricity. These fuel cells offer advantages over traditional fuel cells due to their operating temperatures, voltages, and high power densities. Further reduction reactions have also recently been investigated with the sulfurization of metal borohydrides.[440]

Perovskite-type compounds were briefly discussed in Section 3.4 and 3.5. It was also mentioned that the homopolar dihydrogen contacts between hydridic species pertaining to adjacent BH_4^- ligands generate lattice instabilities. It can be assumed that such close contacts constitute a novel kind of "weak" interaction in perovskites that may be further exploited regarding the stabilization of low symmetries and the possibility of switching between polar bi-stable configurations of the

structure, thus potentially culminating in a novel type of geometric ferroelectricity. From an applied viewpoint, such a scheme would be closely related to the supramolecular ferroelectrics where ferroelectricity arises from various kinds of weak interactions.[583] From a fundamental point of view such hydridic interactions are both highly interesting and timely, forming part of the ever growing family of intriguing weak interactions.[584] Homoleptic metal borohydrides, but also heteroleptic ones, offer a unique opportunity of studying this hydridic interaction, which currently challenges all levels of *ab initio* theory.

Indeed, homo- and heteropolar interactions between protons and hydrides could potentially be meticulously implemented in order to tailor lattice distortions in hybrid organic–inorganic borohydride-based materials. Further means of taking influence on symmetry-determining parameters such as order, polarizability and dipole moments include anion-substitution of the BH_4 group by amides or halides, but also within the BH_4 group by the scheme $H^- \leftrightarrow F^-$. As such, this inorganic family of materials could be placed into the landscape of molecular and supramolecular chemistry. In this context, we could extend the focus from homoleptic metal borohydrides to the heteroleptic compounds, where the tetrahydridoboranate anion may be employed as a hydridic building block in the crystal engineering of molecular and metalorganic compounds.

All in all, this young but vast family of materials offers exotic and enticing new chemistry to materials scientists working in energy-related fields.

7.6 CO_2-recycling with metal borohydrides

Our current energy system is, to a large extent, based on fossil fuels, *i.e.* carbon-based materials, and our energy system is not considered a 'closed materials cycle', because we consume these fuels by combustion on a much faster rate than they are produced by photosynthesis and geological processes. Hence, in order to close the carbon cycle, we must find a route to convert the produced CO_2 into useful fuel. Some metal borohydrides have recently been investigated in this context, of CO_2 capture and recycling. It has been suggested to generate hydrogen by a CO_2-enhanced hydrolysis of KBH_4 where the waste products of fossil fuel combustion, *i.e.* CO_2 and H_2O, can be used in a further cycle for hydrogen production for fuel cells.[585] The proposed reaction results in the formation of a carbonate salt, water and gaseous hydrogen. The porous polymorph γ-$Mg(BH_4)_2$ was also found to have potential in CO_2 recycling where upon CO_2-reduction chemical products such as formate or methoxy-species are produced.[586] Owing to the large specific surface area of γ-$Mg(BH_4)_2$, CO_2 conversion occurs with unprecedented fast kinetics at 30 °C and $p(CO_2)$ = 1 bar. Metal borohydrides with low surface area, such as KBH_4, readily react with CO_2 under mechanochemical conditions at room temperature,[587] yielding mainly formylhydroborates. Whilst, solid–gas reactions in the KBH_4–CO_2 system at high temperature reveal the formation of methanol and methane under water-free conditions.

7.7 A possible paradigm shift for solid state hydrogen storage

The design of a possible successor for liquid fuels like diesel and gasoline faces numerous challenges. About twenty properties need to be optimized simultaneously, which span wide areas including low cost, fast energy recharging, large gravimetric and volumetric energy storage densities, low operation temperature *etc.* This review has illustrated numerous examples of the rational design of novel metal borohydrides with interesting properties, *e.g.* using borohydride–oxide analogies, and also the possibilities of post-modification of the materials, *e.g.* by anion substitution *etc.* Thus, new classes are likely to be discovered in the near future. Two decades ago, alloying metals that reacted with hydrogen to different degrees tended to provide an alloy with intermediate properties. During the past decade, reactive hydride composites were explored, which have an average hydrogen storage capacity compared to the individual components. Recently, the first stabilization of the metastable compound, NH_4BH_4 was discovered by a reaction with the more stable metal borohydride, $Ca(BH_4)_2$. The product, $NH_4Ca(BH_4)_3$, has a different decomposition profile and may be considered as the first member of a larger series of compounds. Notice that, the series BH_4^-, NH_4^+, CH_4 are isoelectronic and the hydrogen density of NH_4BH_4, ρ_V = 157 g H_2 mL^{-1} and ρ_m = 24.5 wt% H_2, is even higher than liquid natural gas, CH_4(l), ρ_V = 137 g H_2 mL^{-1} and ρ_m = 24.8 wt% H_2. Recently, other borane based materials have been discovered, *e.g.* hydrazine bisborane, $BH_3N_2H_4BH_3$.[588]

8. Conclusions

Metal borohydrides have received increasing interest over the past decade with a wide range of new materials discovered. An extremely rich chemistry has been outlined including fascinating structural flexibility and a wide range of elemental compositions. Furthermore, derivatives of metal borohydrides have also been discovered, which strongly contribute to the diverse chemistry. These materials have a wide range of unexpected properties, which may lead to new applications in the future. The systematic work on crystalline metal borohydrides has provided enough results to understand the basic principles which control their crystal structures, and consequently their properties. One of the most important understandings is the description of borohydrides as ionocovalent solids comparable with many other inorganic compounds such as oxides or halides. The crystal chemistry of borohydrides may then be explained by known principles such as Pauling rules, involving the polarisation of the rather soft borohydride anion, various factors based on ionic radii *etc.* A consequences is that the huge crystal chemistry knowledge accumulated for oxides or halides can be now applied to borohydrides in designing new compounds with desired chemical composition, atomic coordination and, in the best case, with desired properties.

This review has outlined trends across the synthetic approaches for metal borohydrides and their halide and neutral molecule complexes, classing reactions into addition, metathesis, or complex metathesis-addition mechanisms. Trends in structural chemistry have also been listed and over 100 compounds are reported for mono-, bi- and tri-metallic borohydrides. Many similarities can be found within certain classes of borohydride, for example those rich in alkali metals, or rare earth metals. The metal borohydride halides

 This journal is © The Royal Society of Chemistry 2017

can also be classed into those compounds that exhibit completely ordered, partly ordered, or completely disordered structures. Many new metal borohydrides have been discovered that are complexed with neutral molecules that can exhibit many interesting properties suitable for technical applications, but have also been shown to influence the decomposition pathway of the parent borohydride. A number of metal borohydrides have been shown to melt individually or in eutectic compositions, but often decompose shortly after in often multi-step pathways that are temperature and pressure dependent. The kinetics of hydrogen release and uptake have typically been poor for metal borohydrides and traditional additives have not been successful in enhancing kinetics, as they have been in many other metal–hydrogen systems. However, techniques including reactive hydride composites and nanoconfinement have offered new possibilities in improving kinetics and thermodynamics of hydrogen release and uptake. The rehydrogenation of metal borohydrides can be performed under more mild conditions by controlling the desorption by-products to restrict the quantity of higher boranes, *i.e.* with lower desorption temperatures or with hydrogen backpressure. Recently, metal borohydrides have been studied for new applications, taking advantage of cation conduction in the solid-state, optical properties, porous structures for gas adsorption, and also magnetic properties.

The knowledge gained mainly during the past decade of research within metal borohydrides is presented in this review, which provides analysis of the trends in synthesis, structure and properties. An overview of the current frontiers of research and new perspectives for the future utilization of this fascinating class of new materials is also provided. A wide range of approaches for tailoring the composition and structure of metal borohydrides is also discussed, which provides new methods for tailoring properties. This is an important step towards rational design of new functional materials. This review also demonstrates that there is still plenty of room for discovering new metal borohydrides since these types of materials have extreme flexibility in composition, structure and properties.

Acknowledgements

The work was supported by the Danish National Research Foundation, Center for Materials Crystallography (DNRF93), The Innovation Fund Denmark (project HyFill-Fast), and by the Danish Research Council for Nature and Universe (Danscatt) and the Danish Council for Independent Research (HyNanoBorN, DFF – 4181-00462). MP acknowledges financial support from The Danish Council for Independent Research for DFF Mobility 1325-00072. We are grateful to the Carlsberg Foundation. This work was partly supported by the Swiss National Science Foundation and Fonds de la Recherche Scientifique – FNRS.

References

1 P. Schouwink, M. B. Ley, A. Tissot, H. Hagemann, T. R. Jensen, Ĺ. Smrčok and R. Černý, *Nat. Commun.*, 2014, **5**, 5706.
2 A. V. Skripov, A. V. Soloninin, O. A. Babanova, H. Hagemann and Y. Filinchuk, *J. Phys. Chem. C*, 2010, **114**, 12370–12374.
3 Y. Filinchuk, B. Richter, T. R. Jensen, V. Dmitriev, D. Chernyshov and H. Hagemann, *Angew. Chem., Int. Ed.*, 2011, **50**, 11162–11166.
4 M. B. Ley, D. B. Ravnsbæk, Y. Filinchuk, Y.-S. Lee, R. Janot, Y. W. Cho, J. Skibsted and T. R. Jensen, *Chem. Mater.*, 2012, **24**, 1654–1663.
5 M. B. Ley, L. H. Jepsen, Y.-S. Lee, Y. W. Cho, J. M. Bellosta von Colbe, M. Dornheim, M. Rokni, J. O. Jensen, M. Sloth, Y. Filinchuk, J. E. Jørgensen, F. Besenbacher and T. R. Jensen, *Mater. Today*, 2014, **17**, 122–128.
6 L. H. Jepsen, M. B. Ley, Y.-S. Lee, Y. W. Cho, M. Dornheim, J. O. Jensen, Y. Filinchuk, J. E. Jørgensen, F. Besenbacher and T. R. Jensen, *Mater. Today*, 2014, **17**, 129–135.
7 A. Unemoto, M. Matsuo and S.-I. Orimo, *Adv. Funct. Mater.*, 2014, **24**, 2267–2279.
8 L. H. Rude, T. K. Nielsen, D. B. Ravnsbæk, U. Bösenberg, M. B. Ley, B. Richter, L. M. Arnbjerg, M. Dornheim, Y. Filinchuk, F. Besenbacher and T. R. Jensen, *Phys. Status Solidi A*, 2011, **208**, 1754–1773.
9 L. Mosegaard, B. Moller, J.-E. Jorgensen, Y. Filinchuk, Y. Cerenius, J. C. Hanson, E. Dimasi, F. Besenbacher and T. R. Jensen, *J. Phys. Chem. C*, 2008, **112**, 1299–1303.
10 M. D. Riktor, Y. Filinchuk, P. Vajeeston, E. G. Bardaji, M. Fichtner, H. Fjellvag and M. H. Sørby, *J. Mater. Chem.*, 2011, **21**, 7188–7193.
11 Y.-S. Lee, Y. Filinchuk, H.-S. Lee, J.-Y. Suh, J. W. Kim, J.-S. Yu and Y. W. Cho, *J. Phys. Chem. C*, 2011, **115**, 10298–10304.
12 H. I. Schlesinger, R. T. Sanderson and A. B. Burg, *J. Am. Chem. Soc.*, 1940, **62**, 3421–3425.
13 A. B. Burg and H. I. Schlesinger, *J. Am. Chem. Soc.*, 1940, **62**, 3425–3429.
14 H. I. Schlesinger and H. C. Brown, *J. Am. Chem. Soc.*, 1940, **62**, 3429–3435.
15 H. I. Schlesinger and H. C. Brown, *J. Am. Chem. Soc.*, 1953, **75**, 219–221.
16 H. I. Schlesinger, H. C. Brown, B. Abraham, A. C. Bond, N. Davidson, A. E. Finholt, J. R. Gilbreath, H. Hoekstra, L. Horvitz, E. K. Hyde, J. J. Katz, J. Knight, R. A. Lad, D. L. Mayfield, L. Rapp, D. M. Ritter, A. M. Schwartz, I. Sheft, L. D. Tuck and A. O. Walker, *J. Am. Chem. Soc.*, 1953, **75**, 186–190.
17 Y. Zhu and N. S. Hosmane, *Coord. Chem. Rev.*, 2015, **293–294**, 357–367.
18 A. M. Soldate, *J. Am. Chem. Soc.*, 1947, **69**, 987–988.
19 S. C. Abrahams and J. Kalnajs, *J. Chem. Phys.*, 1954, **22**, 434–436.
20 C. J. Dain, A. J. Downs, M. J. Goode, D. G. Evans, K. T. Nicholls, D. W. H. Rankin and H. E. Robertson, *J. Chem. Soc., Dalton Trans.*, 1991, 967–977.
21 R. Černý, N. Penin, H. Hagemann and Y. Filinchuk, *J. Phys. Chem. C*, 2009, **113**, 9003–9007.
22 A. Züttel, S. Rentsch, P. Fischer, P. Wenger, P. Sudan, P. Mauron and C. Emmenegger, *J. Alloys Compd.*, 2003, **356–357**, 515–520.

23 A. Zuttel, P. Wenger, S. Rentsch, P. Sudan, P. Mauron and C. Emmenegger, *J. Power Sources*, 2003, **118**, 1–7.
24 J. P. Soulié, G. Renaudin, R. Černý and K. Yvon, *J. Alloys Compd.*, 2002, **346**, 200–205.
25 L. Schlapbach and A. Züttel, *Nature*, 2001, **414**, 353–358.
26 A. Züttel, *Naturwissenschaften*, 2004, **91**, 157–172.
27 J. A. Ritter, A. D. Ebner, J. Wang and R. Zidan, *Mater. Today*, 2003, **6**, 18–23.
28 B. K. Sovacool, *Energy Policy*, 2009, **37**, 1529–1541.
29 D. J. C. MacKay, *Sustainable Energy - Without the Hot Air*, UIT, Cambridge, 2009.
30 M. Felderhoff, C. Weidenthaler, R. von Helmolt and U. Eberle, *Phys. Chem. Chem. Phys.*, 2007, **9**, 2643–2653.
31 M. Fichtner, *J. Alloys Compd.*, 2011, **509**, S529–S534.
32 J. M. Pasini, C. Corgnale, B. A. van Hassel, T. Motyka, S. Kumar and K. L. Simmons, *Int. J. Hydrogen Energy*, 2013, **38**, 9755–9765.
33 S. i. Orimo, Y. Nakamori, J. R. Eliseo, A. Zuttel and C. M. Jensen, *Chem. Rev.*, 2007, **107**, 4111–4132.
34 Q. Lai, M. Paskevicius, D. A. Sheppard, C. E. Buckley, A. W. Thornton, M. R. Hill, Q. Gu, J. Mao, Z. Huang, H. K. Liu, Z. Guo, A. Banerjee, S. Chakraborty, R. Ahuja and K.-F. Aguey-Zinsou, *ChemSusChem*, 2015, **8**, 2789–2825.
35 U. Eberle, M. Felderhoff and F. Schuth, *Angew. Chem., Int. Ed.*, 2009, **48**, 6608–6630.
36 E. Callini, Z. Ö. K. Atakli, B. C. Hauback, S.-I. Orimo, C. Jensen, M. Dornheim, D. Grant, Y. W. Cho, P. Chen, B. Hjörvarsson, P. Jongh, C. Weidenthaler, M. Baricco, M. Paskevicius, T. R. Jensen, M. E. Bowden, T. S. Autrey and A. Züttel, *Appl. Phys. A: Mater. Sci. Process.*, 2016, **122**, 353.
37 G. Barkhordarian, T. Klassen, M. Dornheim and R. Bormann, *J. Alloys Compd.*, 2007, **440**, L18–L21.
38 J. J. Vajo, F. Mertens, C. C. Ahn, R. C. Bowman and B. Fultz, *J. Phys. Chem. B*, 2004, **108**, 13977–13983.
39 J. J. Vajo, S. L. Skeith and F. Mertens, *J. Phys. Chem. B*, 2005, **109**, 3719–3722.
40 U. Bösenberg, S. Doppiu, L. Mosegaard, G. Barkhordarian, N. Eigen, A. Borgschulte, T. R. Jensen, Y. Cerenius, O. Gutfleisch, T. Klassen, M. Dornheim and R. Bormann, *Acta Mater.*, 2007, **55**, 3951–3958.
41 S. V. Alapati, J. K. Johnson and D. S. Sholl, *J. Phys. Chem. B*, 2006, **110**, 8769–8776.
42 Y. W. Cho, J. H. Shim and B. J. Lee, *CALPHAD: Comput. Coupling Phase Diagrams Thermochem.*, 2006, **30**, 65–69.
43 J. Huot, *Handbook of Hydrogen Storage*, Wiley-VCH Verlag GmbH & Co. KGaA, 2010, ch. 4, pp. 81–116, DOI: 10.1002/9783527629800.
44 H. H. Van Mal, K. H. J. Buschow and A. R. Miedema, *J. Less-Common Met.*, 1974, **35**, 65–76.
45 M. Paskevicius, M. B. Ley, D. A. Sheppard, T. R. Jensen and C. E. Buckley, *Phys. Chem. Chem. Phys.*, 2013, **15**, 19774–19789.
46 Z. Zhao-Karger, R. Witter, E. G. Bardaji, D. Wang, D. Cossement and M. Fichtner, *J. Mater. Chem. A*, 2013, **1**, 3379–3386.
47 M. B. Ley, E. Roedern and T. R. Jensen, *Phys. Chem. Chem. Phys.*, 2014, **16**, 24194–24199.
48 E. Roedern, B. R. S. Hansen, M. B. Ley and T. R. Jensen, *J. Phys. Chem. C*, 2015, **119**, 25818–25825.
49 M. Matsuo and S.-i. Orimo, *Adv. Energy Mater.*, 2011, **1**, 161–172.
50 P. Schouwink, E. Didelot, Y.-S. Lee, T. Mazet and R. Černý, *J. Alloys Compd.*, 2016, **664**, 378–384.
51 A. Almenningen, G. Gundersen and A. Haaland, *Chem. Commun.*, 1967, 557–559.
52 J. Huot, D. B. Ravnsbæk, J. Zhang, F. Cuevas, M. Latroche and T. R. Jensen, *Prog. Mater. Sci.*, 2013, **58**, 30–75.
53 L. H. Jepsen, M. B. Ley, R. Černý, Y.-S. Lee, Y. W. Cho, D. Ravnsbæk, F. Besenbacher, J. Skibsted and T. R. Jensen, *Inorg. Chem.*, 2015, **54**, 7402–7414.
54 L. H. Jepsen, M. B. Ley, Y. Filinchuk, F. Besenbacher and T. R. Jensen, *ChemSusChem*, 2015, **8**, 1452–1463.
55 E. Wiberg and R. Bauer, *Z. Naturforsch., B: J. Chem. Sci.*, 1950, **5**, 397–398.
56 K. Chłopek, C. Frommen, A. Léon, O. Zabara and M. Fichtner, *J. Mater. Chem.*, 2007, **17**, 3496–3503.
57 P. Zanella, L. Crociani, N. Masciocchi and G. Giunchi, *Inorg. Chem.*, 2007, **46**, 9039–9041.
58 B. Richter, D. B. Ravnsbaek, N. Tumanov, Y. Filinchuk and T. R. Jensen, *Dalton Trans.*, 2015, **44**, 3988–3996.
59 V. I. Mikheeva and L. V. Titov, *Zh. Neorg. Khim.*, 1964, **9**, 789.
60 H. I. Schlesinger, R. T. Sanderson and A. B. Burg, *J. Am. Chem. Soc.*, 1939, **61**, 536.
61 N. A. Tumanov, D. A. Safin, B. Richter, Z. Lodziana, T. R. Jensen, Y. Garcia and Y. Filinchuk, *Dalton Trans.*, 2015, **44**, 6571–6580.
62 T. Jaroń, P. A. Orłowski, W. Wegner, K. J. Fijałkowski, P. J. Leszczyński and W. Grochala, *Angew. Chem., Int. Ed.*, 2015, **54**, 1236–1239.
63 T. Jaroń, W. Wegner, K. J. Fijałkowski, P. J. Leszczyński and W. Grochala, *Chem. – Eur. J.*, 2015, **21**, 5689–5692.
64 R. A. Varin, L. Zbroniec, M. Polanski, Y. Filinchuk and R. Černý, *Int. J. Hydrogen Energy*, 2012, **37**, 16056–16069.
65 R. Černý, N. Penin, V. D'Anna, H. Hagemann, E. Durand and J. Růžička, *Acta Mater.*, 2011, **59**, 5171–5180.
66 M. B. Ley, M. Paskevicius, P. Schouwink, B. Richter, D. A. Sheppard, C. E. Buckley and T. R. Jensen, *Dalton Trans.*, 2014, **43**, 13333–13342.
67 M. B. Ley, M. Jørgensen, R. Černý, Y. Filinchuk and T. R. Jensen, *Inorg. Chem.*, 2016, **55**, 9748–9756.
68 T. D. Humphries, M. B. Ley, C. Frommen, K. T. Munroe, T. R. Jensen and B. C. Hauback, *J. Mater. Chem. A*, 2015, **3**, 691–698.
69 A. R. West, *Solid State Chemistry and its Applications*, John Wiley and Sons Ltd, 1984.
70 D. B. Ravnsbæk, Y. Filinchuk, Y. Cerenius, H. J. Jakobsen, F. Besenbacher, J. Skibsted and T. R. Jensen, *Angew. Chem., Int. Ed.*, 2009, **48**, 6659–6663.
71 I. Llamas-Jansa, N. Aliouane, S. Deledda, J. E. Fonneløp, C. Frommen, T. Humphries, K. Lieutenant, S. Sartori, M. H. Sørby and B. C. Hauback, *J. Alloys Compd.*, 2012, **530**, 186–192.

 This journal is © The Royal Society of Chemistry 2017

72 J. E. Olsen, M. H. Sørby and B. C. Hauback, *J. Alloys Compd.*, 2011, **509**, L228–L231.
73 J. W. Kim, J.-H. Shim, J.-P. Ahn, Y. W. Cho, J.-H. Kim and K. H. Oh, *Mater. Lett.*, 2008, **62**, 2461–2464.
74 S. Doppiu, L. Schultz and O. Gutfleisch, *J. Alloys Compd.*, 2007, **427**, 204–208.
75 M. Fichtner, C. Frommen and O. Fuhr, *Inorg. Chem.*, 2005, **44**, 3479–3484.
76 H. W. Brinks, A. Istad-Lem and B. C. Hauback, *J. Phys. Chem. B*, 2006, **110**, 25833–25837.
77 P. Kuziora, M. Wyszyńska, M. Polanski and J. Bystrzycki, *Int. J. Hydrogen Energy*, 2014, **39**, 9883–9887.
78 Y. Sadikin, K. Stare, P. Schouwink, M. Brix Ley, T. R. Jensen, A. Meden and R. Černý, *J. Solid State Chem.*, 2015, **225**, 231–239.
79 V. N. Konoplev, *Russ. J. Inorg. Chem.*, 1980, **25**, 964–966.
80 R. Černý, G. Severa, D. B. Ravnsbæk, Y. Filinchuk, V. d'Anna, H. Hagemann, D. Haase, C. M. Jensen and T. R. Jensen, *J. Phys. Chem. C*, 2010, **114**, 1357–1364.
81 H. Hagemann, M. Longhini, J. W. Kaminski, T. A. Wesolowski, R. Černý, N. Penin, M. H. Sørby, B. C. Hauback, G. Severa and C. M. Jensen, *J. Phys. Chem. A*, 2008, **112**, 7551–7555.
82 I. Solinas and H. D. Lutz, *J. Solid State Chem.*, 1995, **117**, 34–38.
83 R. Černý, P. Schouwink, Y. Sadikin, K. Stare, L. Smrčok, B. Richter and T. R. Jensen, *Inorg. Chem.*, 2013, **52**, 9941–9947.
84 D. B. Ravnsbæk, L. H. Sørensen, Y. Filinchuk, D. Reed, D. Book, H. J. Jakobsen, F. Besenbacher, J. Skibsted and T. R. Jensen, *Eur. J. Inorg. Chem.*, 2010, 1608–1612.
85 R. Černý, D. B. Ravnsbæk, P. Schouwink, Y. Filinchuk, Y. Penin, J. Teyssier, L. Smrčok and T. R. Jensen, *J. Phys. Chem. C*, 2012, **116**, 1563–1571.
86 L. H. Rude, O. Zavorotynska, L. M. Arnbjerg, D. B. Ravnsbæk, R. A. Malmkjær, H. Grove, B. C. Hauback, M. Baricco, Y. Filinchuk, F. Besenbacher and T. R. Jensen, *Int. J. Hydrogen Energy*, 2011, **36**, 15664–15672.
87 D. B. Ravnsbæk, M. B. Ley, Y.-S. Lee, H. Hagemann, V. D'Anna, Y. W. Cho, Y. Filinchuk and T. R. Jensen, *Int. J. Hydrogen Energy*, 2012, **37**, 8428–8438.
88 M. B. Ley, S. Boulineau, R. Janot, Y. Filinchuk and T. R. Jensen, *J. Phys. Chem. C*, 2012, **116**, 21267–21276.
89 M. Matsuo, A. Remhof, P. Martelli, R. Caputo, M. Ernst, Y. Miura, T. Sato, H. Oguchi, H. Maekawa, H. Takamura, A. Borgschulte, A. Züttel and S. Orimo, *J. Am. Chem. Soc.*, 2009, **131**, 16389–16391.
90 T. Noritake, K. Miwa, M. Aoki, M. Matsumoto, S.-I. Towata, H.-W. Li and S.-I. Orimo, *Int. J. Hydrogen Energy*, 2013, **38**, 6730–6735.
91 M. Somer, S. Acar, C. Koz, I. Kokal, P. Höhn, R. Cardoso-Gil, U. Aydemir and L. Akselrud, *J. Alloys Compd.*, 2010, **491**, 98–105.
92 L. Tuan, C. K. Nguyen and T. D. Huan, *Phys. Status Solidi B*, 2014, **251**, 1539–1544.
93 S. R. H. Jensen, L. H. Jepsen, J. Skibsted and T. R. Jensen, *J. Phys. Chem. C*, 2015, **119**, 27919–27929.
94 E. Roedern and T. R. Jensen, *Inorg. Chem.*, 2015, **54**, 10477–10482.
95 O. Friedrichs, A. Borgschulte, S. Kato, F. Buchter, R. Gremaud, A. Remhof and A. Züttel, *Chem. – Eur. J.*, 2009, **15**, 5531–5534.
96 O. Friedrichs, J. W. Kim, A. Remhof, D. Wallacher, A. Hoser, Y. W. Cho, K. H. Oh and A. Zuttel, *Phys. Chem. Chem. Phys.*, 2010, **12**, 4600–4603.
97 O. Friedrichs, A. Remhof, A. Borgschulte, F. Buchter, S. I. Orimo and A. Zuttel, *Phys. Chem. Chem. Phys.*, 2010, **12**, 10919–10922.
98 A. Remhof, A. Borgschulte, O. Friedrichs, P. Mauron, Y. Yan and A. Züttel, *Scr. Mater.*, 2012, **66**, 280–283.
99 K. Park, H.-S. Lee, A. Remhof, Y.-S. Lee, Y. Yan, M.-Y. Kim, S. J. Kim, A. Züttel and Y. W. Cho, *Int. J. Hydrogen Energy*, 2013, **38**, 9263–9270.
100 Y. Yan, A. Remhof, D. Rentsch, Y.-S. Lee, Y. Whan Cho and A. Zuttel, *Chem. Commun.*, 2013, **49**, 5234–5236.
101 Y. Filinchuk, D. Chernyshov and R. Černý, *J. Phys. Chem. C*, 2008, **112**, 10579–10584.
102 D. Chernyshov, A. Bosak, V. Dmitriev, Y. Filinchuk and H. Hagemann, *Phys. Rev. B: Condens. Matter Mater. Phys.*, 2008, **78**, 172104.
103 Y. Filinchuk and H. Hagemann, *Eur. J. Inorg. Chem.*, 2008, 3127–3133.
104 R. L. Luck and E. J. Schelter, *Acta Crystallogr., Sect. C: Cryst. Struct. Commun.*, 1999, **55**, IUC9900151.
105 D. S. Marynick and W. N. Lipscomb, *Inorg. Chem.*, 1972, **11**, 820–823.
106 Y. Filinchuk, R. Černý and H. Hagemann, *Chem. Mater.*, 2009, **21**, 925–933.
107 S. Aldridge, A. J. Blake, A. J. Downs, R. O. Gould, S. Parsons and C. R. Pulham, *J. Chem. Soc., Dalton Trans.*, 1997, 1007–1012.
108 P. Schouwink, A. Ramel, E. Giannini and R. Černý, *CrystEngComm*, 2015, **17**, 2682–2689.
109 L. H. Rude, M. Corno, P. Ugliengo, M. Baricco, Y.-S. Lee, Y. W. Cho, F. Besenbacher, J. Overgaard and T. R. Jensen, *J. Phys. Chem. C*, 2012, **116**, 20239–20245.
110 B. Hilczer, M. Połomska, A. Pawłowski and J. Wolak, *Ferroelectrics*, 1994, **155**, 177–182.
111 R. Custelcean and J. E. Jackson, *Chem. Rev.*, 2001, **101**, 1963–1980.
112 H. Yamawaki, H. Fujihisa, Y. Gotoh and S. Nakano, *J. Alloys Compd.*, 2012, **541**, 111–114.
113 T. Noritake, M. Aoki, M. Matsumoto, K. Miwa, S. Towata, H. W. Li and S. Orimo, *J. Alloys Compd.*, 2010, **491**, 57–62.
114 H. Wu, W. Zhou, F. E. Pinkerton, M. S. Meyer, G. Srinivas, T. Yildirim, T. J. Udovic and J. J. Rush, *J. Mater. Chem.*, 2010, **20**, 6550–6556.
115 L. H. Jepsen, V. Ban, K. T. Møller, Y.-S. Lee, Y. W. Cho, F. Besenbacher, Y. Filinchuk, J. Skibsted and T. R. Jensen, *J. Phys. Chem. C*, 2014, **118**, 12141–12153.
116 I. Dovgaliuk, C. S. Le Duff, K. Robeyns, M. Devillers and Y. Filinchuk, *Chem. Mater.*, 2015, **27**, 768–777.
117 T. He, H. Wu, J. Chen, W. Zhou, G. Wu, Z. Xiong, T. Zhang and P. Chen, *Phys. Chem. Chem. Phys.*, 2013, **15**, 10487–10493.
118 T. He, H. Wu, G. Wu, J. Wang, W. Zhou, Z. Xiong, J. Chen, T. Zhang and P. Chen, *Energy Environ. Sci.*, 2012, **5**, 5686–5689.

119 A. B. E. Zirngieb, *W. Ger. Pat.*, 070148, 1959.
120 M. Mostajeran, D. J. Wolstenholme, C. Frazee, G. S. McGrady and R. T. Baker, *Chem. Commun.*, 2016, **52**, 2581–2584.
121 R. Černý and Y. Filinchuk, *Z. Kristallogr.*, 2011, **226**, 882–891.
122 D. B. Ravnsbæk, Y. Filinchuk, R. Černý and T. R. Jensen, *Z. Kristallogr.*, 2010, **225**, 557–569.
123 Y. Filinchuk, D. Chernyshov and V. Dmitriev, in *Boron hydrides, high potential hydrogen storage materials*, ed. U. B. Demirci and P. Miele, Nova publishers, 2010, pp. 138–164.
124 B. R. S. Hansen, K. T. Moller, M. Paskevicius, A.-C. Dippel, P. Walter, C. J. Webb, C. Pistidda, N. Bergemann, M. Dornheim, T. Klassen, J.-E. Jorgensen and T. R. Jensen, *J. Appl. Crystallogr.*, 2015, **48**, 1234–1241.
125 T. R. Jensen, T. K. Nielsen, Y. Filinchuk, J.-E. Jorgensen, Y. Cerenius, E. M. Gray and C. J. Webb, *J. Appl. Crystallogr.*, 2010, **43**, 1456–1463.
126 R. W. Broach, I. S. Chuang, T. J. Marks and J. M. Williams, *Inorg. Chem.*, 1983, **22**, 1081–1084.
127 P. H. Bird and M. R. Churchill, *Chem. Commun.*, 1967, 403.
128 J. H. Her, P. W. Stephens, Y. Gao, G. L. Soloveichik, J. Rijssenbeek, M. Andrus and J. C. Zhao, *Acta Crystallogr., Sect. B: Struct. Sci.*, 2007, **63**, 561.
129 R. Černý, Y. Filinchuk, H. Hagemann and K. Yvon, *Angew. Chem., Int. Ed.*, 2007, **46**, 5765–5767.
130 E. A. Nickels, M. O. Jones, W. I. F. David, S. R. Johnson, R. L. Lowton, M. Sommariva and P. P. Edwards, *Angew. Chem., Int. Ed.*, 2008, **47**, 2817–2819.
131 Y. Filinchuk, D. Chernyshov, A. Nevidomskyy and V. Dmitriev, *Angew. Chem., Int. Ed.*, 2008, **47**, 529–532.
132 O. A. Babanova, A. V. Soloninin, A. P. Stepanov, A. V. Skripov and Y. Filinchuk, *J. Phys. Chem. C*, 2010, **114**, 3712–3718.
133 Y. Filinchuk, A. V. Talyzin, D. Chernyshov and V. Dmitriev, *Phys. Rev. B: Condens. Matter Mater. Phys.*, 2007, **76**, 092104.
134 M. P. Pitt, C. J. Webb, M. Paskevicius, D. Sheptyakov, C. E. Buckley and E. M. Gray, *J. Phys. Chem. C*, 2011, **115**, 22669–22679.
135 G. Renaudin, S. Gomes, H. Hagemann, L. Keller and K. Yvon, *J. Alloys Compd.*, 2004, **375**, 98–106.
136 R. S. Kumar, E. Kim and A. L. Cornelius, *J. Phys. Chem. C*, 2008, **112**, 8452–8457.
137 Y. Filinchuk, E. Rönnebro and D. Chandra, *Acta Mater.*, 2009, **57**, 732–738.
138 F. Buchter, Z. Łodziana, A. Remhof, O. Friedrichs, A. Borgschulte, P. Mauron, A. Züttel, D. Sheptyakov, G. Barkhordarian, R. Bormann, K. Chlopek, M. Fichtner, M. H. Sorby, M. D. Riktor, B. C. Hauback and S. Orimo, *J. Phys. Chem. B*, 2008, **112**, 8042–8048.
139 F. Buchter, Z. Łodziana, A. Remhof, O. Friedrichs, A. Borgschulte, P. Mauron, A. Züttel, D. Sheptyakov, L. Palatinus, K. Chłopek, M. Fichtner, G. Barkhordarian, R. Bormann and B. C. Hauback, *J. Phys. Chem. C*, 2009, **113**, 17223–17230.
140 N. A. Tumanov, E. Roedern, Z. Łodziana, D. B. Nielsen, T. R. Jensen, A. V. Talyzin, R. Černý, D. Chernyshov, V. Dmitriev, T. Palasyuk and Y. Filinchuk, *Chem. Mater.*, 2016, **28**, 274–283.
141 Y. Filinchuk, A. V. Talyzin, H. Hagemann, V. Dmitriev, D. Chernyshov and B. Sundqvist, *Inorg. Chem.*, 2010, **49**, 5285–5292.
142 D. B. Ravnsbæk, E. A. Nickels, R. Černý, C. H. Olesen, W. I. F. David, P. P. Edwards, Y. Filinchuk and T. R. Jensen, *Inorg. Chem.*, 2013, **52**, 10877–10885.
143 M. Sharma, E. Didelot, A. Spyratou, L. M. L. Daku, R. Černý and H. Hagemann, *Inorg. Chem.*, 2016, **55**, 7090–7097.
144 T. Sato, K. Miwa, Y. Nakamori, K. Ohoyama, H.-W. Li, T. Noritake, M. Aoki, S.-I. Towata and S.-I. Orimo, *Phys. Rev. B: Condens. Matter Mater. Phys.*, 2008, **77**, 104114.
145 C. Frommen, N. Aliouane, S. Deledda, J. E. Fonneløp, H. Grove, K. Lieutenant, I. Llamas-Jansa, S. Sartori, M. H. Sørby and B. C. Hauback, *J. Alloys Compd.*, 2010, **496**, 710–716.
146 D. B. Ravnsbæk, L. H. Sørensen, Y. Filinchuk, F. Besenbacher and T. R. Jensen, *Angew. Chem., Int. Ed.*, 2012, **51**, 3582–3586.
147 J. E. Olsen, C. Frommen, T. R. Jensen, M. D. Riktor, M. H. Sorby and B. C. Hauback, *RSC Adv.*, 2014, **4**, 1570–1582.
148 W. Wegner, T. Jaroń and W. Grochala, *Int. J. Hydrogen Energy*, 2014, **39**, 20024–20030.
149 B. Richter, Aarhus University, Denmark, Personal Communication, 2016.
150 J. E. Olsen, C. Frommen, M. H. Sorby and B. C. Hauback, *RSC Adv.*, 2013, **3**, 10764–10774.
151 H. R. Hoekstra and J. J. Katz, *J. Am. Chem. Soc.*, 1949, **71**, 2488–2492.
152 A. C. Dunbar, PhD thesis, University of Illinois, Urbana-Champaign, USA, 2011.
153 E. R. Bernstein, W. C. Hamilton, T. A. Keiderling, S. J. La Placa, S. J. Lippard and J. J. Mayerle, *Inorg. Chem.*, 1972, **11**, 3009–3016.
154 P. Charpin, M. Nierlich, D. Vigner, M. Lance and D. Baudry, *Acta Crystallogr., Sect. C: Cryst. Struct. Commun.*, 1987, **43**, 1465–1467.
155 R. H. Banks, N. M. Edelstein, B. Spencer, D. H. Templeton and A. Zalkin, *J. Am. Chem. Soc.*, 1980, **102**, 620–623.
156 P. Schouwink, L. Smrcok and R. Černý, *Acta Crystallogr., Sect. B: Struct. Sci., Cryst. Eng. Mater.*, 2014, **70**, 871–878.
157 R. Černý, K. C. Kim, N. Penin, V. D'Anna, H. Hagemann and D. S. Sholl, *J. Phys. Chem. C*, 2010, **114**, 19127–19133.
158 D. B. Ravnsbæk, C. Frommen, D. Reed, Y. Filinchuk, M. Sørby, B. C. Hauback, H. J. Jakobsen, D. Book, F. Besenbacher, J. Skibsted and T. R. Jensen, *J. Alloys Compd.*, 2011, **509**, S698–S704.
159 I. Lindemann, R. Domènech Ferrer, L. Dunsch, Y. Filinchuk, R. Černý, H. Hagemann, V. D'Anna, L. M. Lawson Daku, L. Schultz and O. Gutfleisch, *Chem. – Eur. J.*, 2010, **16**, 8707–8712.
160 I. Dovgaliuk, *Synthesis, structure and properties of Al-based borohydrides for hydrogen storage*, PhD thesis, 2016, http://dial.uclouvain.be/handle/boreal:169194?site_name=UCL.
161 E. Roedern, Y.-S. Lee, M. B. Ley, K. Park, Y. W. Cho, J. Skibsted and T. R. Jensen, *J. Mater. Chem. A*, 2016, **4**, 8793–8802.
162 S. P. GharibDoust, M. Heere, M. H. Sørby, M. B. Ley, D. B. Ravnsbæk, C. H. Bjørn, R. Černý and T. R. Jensen, *Dalton Trans.*, 2016, **45**, 19002–19011.

 This journal is © The Royal Society of Chemistry 2017

163 W. Wegner, T. Jaroń and W. Grochala, *Acta Crystallogr., Sect. C: Cryst. Struct. Commun.*, 2013, **69**, 1289–1291.
164 P. Schouwink, V. D'Anna, M. B. Ley, L. M. Lawson Daku, B. Richter, T. R. Jensen, H. Hagemann and R. Černý, *J. Phys. Chem. C*, 2012, **116**, 10829–10840.
165 K. T. Møller, M. B. Ley, P. Schouwink, R. Černý and T. R. Jensen, *Dalton Trans.*, 2016, **45**, 831–840.
166 R. Černý, D. B. Ravnsbæk, G. Severa, Y. Filinchuk, V. D'Anna, H. Hagemann, D. Haase, J. Skibsted, C. M. Jensen and T. R. Jensen, *J. Phys. Chem. C*, 2010, **114**, 19540–19549.
167 T. Jaron and W. Grochala, *Dalton Trans.*, 2011, **40**, 12808–12817.
168 M. Brighi, P. Schouwink, Y. Sadikin and R. Černý, *J. Alloys Compd.*, 2016, **662**, 388–395.
169 I. Dovgaliuk, V. Ban, Y. Sadikin, R. Černý, L. Aranda, N. Casati, M. Devillers and Y. Filinchuk, *J. Phys. Chem. C*, 2014, **118**, 145–153.
170 W. Wegner, T. Jaron, M. A. Dobrowolski, L. Dobrzycki, M. K. Cyranski and W. Grochala, *Dalton Trans.*, 2016, **45**, 14370–14377.
171 T. Jaron, W. Wegner and W. Grochala, *Dalton Trans.*, 2013, **42**, 6886–6893.
172 P. Schouwink, M. B. Ley, T. R. Jensen, L. Smrcok and R. Černý, *Dalton Trans.*, 2014, **43**, 7726–7733.
173 N. Bindzus, F. Cargnoni, B. B. Iversen and C. Gatti, *J. Phys. Chem. C*, 2013, **117**, 2308–2316.
174 N. Bindzus, F. Cargnoni, C. Gatti, B. Richter, T. R. Jensen, M. Takata and B. B. Iversen, *Comput. Theor. Chem.*, 2015, **1053**, 245–253.
175 F. Buchter, Z. Lodziana, A. Remhof, P. Mauron, O. Friedrichs, A. Borgschulte, A. Züttel, Y. Filinchuk and L. Palatinus, *Phys. Rev. B: Condens. Matter Mater. Phys.*, 2011, **83**, 064107.
176 N. Bindzus, F. Cargnoni, B. B. Iversen and C. Gatti, *J. Phys. Chem. C*, 2015, **119**, 12109–12118.
177 M. R. Hartman, J. J. Rush, T. J. Udovic, R. C. Bowman and S. J. Hwang, *J. Solid State Chem.*, 2007, **180**, 1298–1305.
178 Y. Filinchuk and D. Chernyshov, *Acta Crystallogr., Sect. A: Found. Crystallogr.*, 2007, **63**, s240–s241.
179 Y. Yao and D. D. Klug, *Phys. Rev. B: Condens. Matter Mater. Phys.*, 2012, **86**, 064107.
180 S. Nakano, H. Fujihisa, H. Yamawaki and T. Kikegawa, *J. Phys. Chem. C*, 2015, **119**, 3911–3917.
181 V. Dmitriev, Y. Filinchuk, D. Chernyshov, A. V. Talyzin, A. Ilewski, O. Andersson, B. Sundqvist and A. Kurnosov, *Phys. Rev. B: Condens. Matter Mater. Phys.*, 2008, **77**, 174112.
182 P. Fischer and A. Züttel, *Mater. Sci. Forum*, 2004, **443–444**, 287–290.
183 M. D. Riktor, M. H. Sorby, K. Chlopek, M. Fichtner, F. Buchter, A. Zuttel and B. C. Hauback, *J. Mater. Chem.*, 2007, **17**, 4939–4942.
184 K. Miwa, M. Aoki, T. Noritake, N. Ohba, Y. Nakamori, S. Towata, A. Züttel and S. Orimo, *Phys. Rev. B: Condens. Matter Mater. Phys.*, 2006, **74**, 155122.
185 P. C. Aeberhard, K. Refson, P. P. Edwards and W. I. F. David, *Phys. Rev. B: Condens. Matter Mater. Phys.*, 2011, **83**, 174102.
186 M. Fichtner, K. Chłopek, M. Longhini and H. Hagemann, *J. Phys. Chem. C*, 2008, **112**, 11575–11581.
187 M. Paskevicius, M. P. Pitt, C. J. Webb, D. A. Sheppard, U. Filsø, E. M. Gray and C. E. Buckley, *J. Phys. Chem. C*, 2012, **116**, 15231–15240.
188 W. I. F. David, S. K. Callear, M. O. Jones, P. C. Aeberhard, S. D. Culligan, A. H. Pohl, S. R. Johnson, K. R. Ryan, J. E. Parker, P. P. Edwards, C. J. Nuttall and A. Amieiro-Fonseca, *Phys. Chem. Chem. Phys.*, 2012, **14**, 11800–11807.
189 A. Amieiro-Fonseca, S. R. Ellis, C. J. Nuttall, B. E. Hayden, S. Guerin, G. Purdy, J. P. Soulie, S. K. Callear, S. D. Culligan, W. I. F. David, P. P. Edwards, M. O. Jones, S. R. Johnson and A. H. Pohl, *Faraday Discuss.*, 2011, **151**, 369–384.
190 J.-H. Her, P. W. Stephens, Y. Gao, G. L. Soloveichik, J. Rijssenbeek, M. Andrus and J.-C. Zhao, *Acta Crystallogr., Sect. B: Struct. Sci.*, 2007, **63**, 561–568.
191 R. Černý, Y. Filinchuk, H. Hagemann and K. Yvon, *Angew. Chem.*, 2007, **119**, 5867–5869.
192 B. Dai, D. S. Sholl and J. K. Johnson, *J. Phys. Chem. C*, 2008, **112**, 4391–4395.
193 R. Černý and P. Schouwink, *Acta Crystallogr., Sect. B: Struct. Sci., Cryst. Eng. Mater.*, 2015, **71**, 619–640.
194 V. Ban, A. V. Soloninin, A. V. Skripov, J. Hadermann, A. Abakumov and Y. Filinchuk, *J. Phys. Chem. C*, 2014, **118**, 23402–23408.
195 L. George, V. Drozd, S. K. Saxena, E. G. Bardaji and M. Fichtner, *J. Phys. Chem. C*, 2009, **113**, 486–492.
196 T. Matsunaga, F. Buchter, P. Mauron, M. Bielman, Y. Nakamori, S. Orimo, N. Ohba, K. Miwa, S. Towata and A. Züttel, *J. Alloys Compd.*, 2008, **459**, 583–588.
197 D. B. Ravnsbæk, Y. Filinchuk, R. Černý, M. B. Ley, D. Haase, H. J. Jakobsen, J. Skibsted and T. R. Jensen, *Inorg. Chem.*, 2010, **49**, 3801–3809.
198 T. Jaron and W. Grochala, *Dalton Trans.*, 2010, **39**, 160–166.
199 Y.-S. Lee, J.-H. Shim and Y. W. Cho, *J. Phys. Chem. C*, 2010, **114**, 12833–12837.
200 H. Hagemann and R. Černý, *Dalton Trans.*, 2010, **39**, 6006–6012.
201 F. C. Gennari and M. R. Esquivel, *J. Alloys Compd.*, 2009, **485**, L47–L51.
202 B. J. Zhang, B. H. Liu and Z. P. Li, *J. Alloys Compd.*, 2011, **509**, 751–757.
203 J. Andrade-Gamboa, J. A. Puszkiel, L. Fernández-Albanesi and F. C. Gennari, *Int. J. Hydrogen Energy*, 2010, **35**, 10324–10328.
204 G. Wulfsberg, *Principles of Descriptive Inorganic Chemistry*, University Science Books, 1991.
205 D. A. Knight, R. Zidan, R. Lascola, R. Mohtadi, C. Ling, P. Sivasubramanian, J. A. Kaduk, S.-J. Hwang, D. Samanta and P. Jena, *J. Phys. Chem. C*, 2013, **117**, 19905–19915.
206 Z. Z. Fang, L. P. Ma, X. D. Kang, P. J. Wang, P. Wang and H. M. Cheng, *Appl. Phys. Lett.*, 2009, **94**, 044104.
207 A. Jarid, A. Lledos, Y. Jean and F. Volatron, *Inorg. Chem.*, 1993, **32**, 4695–4699.
208 R. G. Egdell and J. C. Green, *Inorg. Chim. Acta*, 2008, **361**, 462–466.

209 D. M. Goedde and G. S. Girolami, *Inorg. Chem.*, 2006, **45**, 1380–1388.
210 E. Callini, P. A. Szilagyi, M. Paskevicius, N. P. Stadie, J. Rehault, C. E. Buckley, A. Borgschulte and A. Zuttel, *Chem. Sci.*, 2016, **7**, 666–672.
211 L. Seballos, J. Z. Zhang, E. Rönnebro, J. L. Herberg and E. H. Majzoub, *J. Alloys Compd.*, 2009, **476**, 446–450.
212 J. Mullay, *J. Am. Chem. Soc.*, 1985, **107**, 7271–7275.
213 R. D. Shannon, *Acta Crystallogr., Sect. A: Cryst. Phys., Diffr., Theor. Gen. Crystallogr.*, 1976, **32**, 751–767.
214 I. Lindemann, R. D. Ferrer, L. Dunsch, R. Černý, H. Hagemann, V. D'Anna, Y. Filinchuk, L. Schultz and O. Gutfleisch, *Faraday Discuss.*, 2011, **151**, 231–242.
215 L. Pauling, *J. Am. Chem. Soc.*, 1929, **51**, 1010–1026.
216 Z. Łodziana and M. J. van Setten, *Phys. Rev. B: Condens. Matter Mater. Phys.*, 2010, **81**, 024117.
217 C. W. F. T. Pistorius, *Z. Phys. Chem.*, 1974, **88**, 253–263.
218 P. A. Madden and M. Wilson, *Chem. Soc. Rev.*, 1996, **25**, 339–350.
219 C. Frommen, M. H. Sørby, P. Ravindran, P. Vajeeston, H. Fjellvag and B. C. Hauback, *J. Phys. Chem. C*, 2011, **115**, 23591–23602.
220 E. Grube, C. H. Olesen, D. B. Ravnsbaek and T. R. Jensen, *Dalton Trans.*, 2016, **45**, 8291–8299.
221 L. H. Rude, E. Groppo, L. M. Arnbjerg, D. B. Ravnsbæk, R. A. Malmkjær, Y. Filinchuk, M. Baricco, F. Besenbacher and T. R. Jensen, *J. Alloys Compd.*, 2011, **509**, 8299–8305.
222 D. B. Ravnsbæk, L. H. Rude and T. R. Jensen, *J. Solid State Chem.*, 2011, **184**, 1858–1866.
223 L. H. Rude, U. Filso, V. D'Anna, A. Spyratou, B. Richter, S. Hino, O. Zavorotynska, M. Baricco, M. H. Sorby, B. C. Hauback, H. Hagemann, F. Besenbacher, J. Skibsted and T. R. Jensen, *Phys. Chem. Chem. Phys.*, 2013, **15**, 18185–18194.
224 R. H. Heyn, I. Saldan, M. H. Sorby, C. Frommen, B. Arstad, A. M. Bougza, H. Fjellvag and B. C. Hauback, *Phys. Chem. Chem. Phys.*, 2013, **15**, 11226–11230.
225 S. Hino, J. E. Fonneløp, M. Corno, O. Zavorotynska, A. Damin, B. Richter, M. Baricco, T. R. Jensen, M. H. Sørby and B. C. Hauback, *J. Phys. Chem. C*, 2012, **116**, 12482–12488.
226 H. Grove, L. H. Rude, T. R. Jensen, M. Corno, P. Ugliengo, M. Baricco, M. H. Sorby and B. C. Hauback, *RSC Adv.*, 2014, **4**, 4736–4742.
227 J. Y. Lee, Y.-S. Lee, J.-Y. Suh, J.-H. Shim and Y. W. Cho, *J. Alloys Compd.*, 2010, **506**, 721–727.
228 L. H. Rude, Y. Filinchuk, M. H. Sørby, B. C. Hauback, F. Besenbacher and T. R. Jensen, *J. Phys. Chem. C*, 2011, **115**, 7768–7777.
229 B. Brehler, *Z. Kristallogr.*, 1961, **115**, 373–402.
230 Y. Filinchuk, D. Chernyshov and V. Dmitriev, *Z. Kristallogr.*, 2008, **223**, 649–659.
231 T. W. Mak and F.-C. Mok, *J. Cryst. Mol. Struct.*, 1978, **8**, 183–191.
232 E. B. Brackett, T. E. Brackett and R. L. Sass, *J. Phys. Chem.*, 1963, **67**, 2132–2135.
233 A. Haase and G. Brauer, *Z. Anorg. Allg. Chem.*, 1978, **441**, 181–195.
234 L. M. Arnbjerg, D. B. Ravnsbæk, Y. Filinchuk, R. T. Vang, Y. Cerenius, F. Besenbacher, J.-E. Jørgensen, H. J. Jakobsen and T. R. Jensen, *Chem. Mater.*, 2009, **21**, 5772–5782.
235 M. Quilichini, P. Bernede, J. Lefebvre and P. Schweiss, *J. Phys.: Condens. Matter*, 1990, **2**, 4543–4558.
236 H. K. Roobottom, H. D. B. Jenkins, J. Passmore and L. Glasser, *J. Chem. Educ.*, 1999, **76**, 1570–1573.
237 O. Zavorotynska, M. Corno, E. Pinatel, L. H. Rude, P. Ugliengo, T. R. Jensen and M. Baricco, *Crystals*, 2012, **2**, 144–158.
238 H. W. Brinks, A. Fossdal and B. C. Hauback, *J. Phys. Chem. C*, 2008, **112**, 5658–5661.
239 N. Eigen, U. Bösenberg, J. Bellosta von Colbe, T. R. Jensen, Y. Cerenius, M. Dornheim, T. Klassen and R. Bormann, *J. Alloys Compd.*, 2009, **477**, 76–80.
240 D. A. Sheppard, C. Corgnale, B. Hardy, T. Motyka, R. Zidan, M. Paskevicius and C. E. Buckley, *RSC Adv.*, 2014, **4**, 26552–26562.
241 E. R. Pinatel, M. Corno, P. Ugliengo and M. Baricco, *J. Alloys Compd.*, 2014, **615**, S706–S710.
242 M. Corno, E. Pinatel, P. Ugliengo and M. Baricco, *J. Alloys Compd.*, 2011, **509**, S679–S683.
243 C. Pistidda, F. Karimi, S. Garroni, A. Rzeszutek, C. Bonatto Minella, C. Milanese, T. T. Le, L. H. Rude, J. Skibsted, T. R. Jensen, C. Horstmann, C. Gundlach, M. Tolkiehn, P. K. Pranzas, A. Schreyer, T. Klassen and M. Dornheim, *J. Phys. Chem. C*, 2014, **118**, 28409–28417.
244 K. S. Alcantara, J. M. Ramallo-Lopez, U. Boesenberg, I. Saldan, C. Pistidda, F. G. Requejo, T. Jensen, Y. Cerenius, M. Sørby, J. Avila, J. B. von Colbe, K. Taube, T. Klassen and M. Dornheim, *J. Phys. Chem. C*, 2012, **116**, 7207–7212.
245 J. Puszkiel, F. C. Gennari, P. Arneodo Larochette, H. E. Troiani, F. Karimi, C. Pistidda, R. Gosalawit–Utke, J. Jepsen, T. R. Jensen, C. Gundlach, M. Tolkiehn, J. Bellosta von Colbe, T. Klassen and M. Dornheim, *J. Power Sources*, 2014, **267**, 799–811.
246 I. Saldan, M. Schulze, C. Pistidda, R. Gosalawit-Utke, O. Zavorotynska, L. H. Rude, J. Skibsted, D. Haase, Y. Cerenius, T. R. Jensen, G. Spoto, M. Baricco, K. Taube and M. Dornheim, *J. Phys. Chem. C*, 2013, **117**, 17360–17366.
247 I. Saldan, R. Gosalawit-Utke, C. Pistidda, U. Bösenberg, M. Schulze, T. R. Jensen, K. Taube, M. Dornheim and T. Klassen, *J. Phys. Chem. C*, 2012, **116**, 7010–7015.
248 R. Gosalawit-Utke, K. Suarez, J. M. Bellosta von Colbe, U. Bösenberg, T. R. Jensen, Y. Cerenius, C. Bonatto Minella, C. Pistidda, G. Barkhordarian, M. Schulze, T. Klassen, R. Bormann and M. Dornheim, *J. Phys. Chem. C*, 2011, **115**, 3762–3768.
249 K. Suarez-Alcantara, M. H. Sørby, C. Pistidda, F. Karimi, I. Saldan, B. C. Hauback, T. Klassen and M. Dornheim, *J. Phys. Chem. C*, 2015, **119**, 11430–11437.
250 C. Bonatto Minella, S. Garroni, C. Pistidda, R. Gosalawit-Utke, G. Barkhordarian, C. Rongeat, I. Lindemann, O. Gutfleisch, T. R. Jensen, Y. Cerenius, J. Christensen, M. D. Baró, R. Bormann, T. Klassen and M. Dornheim, *J. Phys. Chem. C*, 2011, **115**, 2497–2504.

 This journal is © The Royal Society of Chemistry 2017

251 D. Blanchard, J. B. Marosson, M. D. Riktor, J. Kheres, D. Sveinbjörnsson, E. G. Bardaji, A. N. Leon, F. Juranyi, J. Wuttke and K. Lefmann, *J. Phys. Chem. C*, 2012, **116**, 2013–2023.

252 B. R. S. Hansen, M. Paskevicius, H.-W. Li, E. Akiba and T. R. Jensen, *Coord. Chem. Rev.*, 2016, **323**, 60–70.

253 O. A. Kanaeva, N. T. Kuznetsov and K. A. Solntsev, *Russ. J. Inorg. Chem.*, 1990, **35**, 1421.

254 I. Tiritiris, *Untersuchungen zu Reaktivität, Aufbau und struktureller Dynamik von salzartigen closo–Dodekaboraten*, Institut für Anorganische Chemie der Universität Stuttgart, 2003.

255 P. Schouwink, Y. Sadikin, W. van Beek and R. Černý, *Int. J. Hydrogen Energy*, 2015, **40**, 10902–10907.

256 Y. Sadikin, M. Brighi, P. Schouwink and R. Černý, *Adv. Energy Mater.*, 2015, **5**, 1501016.

257 F. E. Pinkerton, G. P. Meisner, M. S. Meyer, M. P. Balogh and M. D. Kundrat, *J. Phys. Chem. B*, 2005, **109**, 6–8.

258 X. B. Yu, Y. H. Guo, D. L. Sun, Z. X. Yang, A. Ranjbar, Z. P. Guo, H. K. Liu and S. X. Dou, *J. Phys. Chem. C*, 2010, **114**, 4733–4737.

259 H. Wu, W. Zhou, T. J. Udovic, J. J. Rush and T. Yildirim, *Chem. Mater.*, 2008, **20**, 1245–1247.

260 P. A. Chater, W. I. F. David and P. A. Anderson, *Chem. Commun.*, 2007, 4770–4772.

261 M. Aoki, K. Miwa, T. Noritake, G. Kitahara, Y. Nakamori, S. Orimo and S. Towata, *Appl. Phys. A: Mater. Sci. Process.*, 2005, **80**, 1409–1412.

262 G. P. Meisner, M. L. Scullin, M. P. Balogh, F. E. Pinkerton and M. S. Meyer, *J. Phys. Chem. B*, 2006, **110**, 4186–4192.

263 Y. E. Filinchuk, K. Yvon, G. P. Meisner, F. E. Pinkerton and M. P. Balogh, *Inorg. Chem.*, 2006, **45**, 1433–1435.

264 P. A. Chater, W. I. F. David, S. R. Johnson, P. P. Edwards and P. A. Anderson, *Chem. Commun.*, 2006, 2439–2441.

265 X. Y. Chen, Y. H. Guo and X. B. Yu, *J. Phys. Chem. C*, 2010, **114**, 17947–17953.

266 H. Chu, Z. Xiong, G. Wu, J. Guo, T. He and P. Chen, *Dalton Trans.*, 2010, **39**, 10585–10587.

267 X. B. Yu, Z. X. Yang, Y. H. Guo and S. G. Li, *J. Alloys Compd.*, 2011, **509**, S724–S727.

268 N. Poonyayant, V. Stavila, E. H. Majzoub, L. E. Klebanoff, R. Behrens, N. Angboonpong, M. Ulutagay-Kartin, P. Pakawatpanurut, E. S. Hecht and J. S. Breit, *J. Phys. Chem. C*, 2014, **118**, 14759–14769.

269 H. Chu, G. Wu, Y. Zhang, Z. Xiong, J. Guo, T. He and P. Chen, *J. Phys. Chem. C*, 2011, **115**, 18035–18041.

270 S. Higashi, K. Miwa, M. Aoki and K. Takechi, *Chem. Commun.*, 2014, **50**, 1320–1322.

271 S. R. Johnson, W. I. F. David, D. M. Royse, M. Sommariva, C. Y. Tang, F. P. A. Fabbiani, M. O. Jones and P. P. Edwards, *Chem. – Asian J.*, 2009, **4**, 849–854.

272 G. Soloveichik, J.-H. Her, P. W. Stephens, Y. Gao, J. Rijssenbeek, M. Andrus and J. C. Zhao, *Inorg. Chem.*, 2008, **47**, 4290–4298.

273 Y. Yang, Y. Liu, Y. Li, M. Gao and H. Pan, *Chem. – Asian J.*, 2013, **8**, 476–481.

274 Z. Tang, Y. Tan, Q. Gu and X. Yu, *J. Mater. Chem.*, 2012, **22**, 5312–5318.

275 H. Chu, G. Wu, Z. Xiong, J. Guo, T. He and P. Chen, *Chem. Mater.*, 2010, **22**, 6021–6028.

276 O. V. Kravchenko and S. E. S. Kravchencko, *Zh. Obshch. Khim.*, 1989, **59**, 1730–1734.

277 L. H. Jepsen, Y.-S. Lee, R. Černý, R. S. Sarusie, Y. W. Cho, F. Besenbacher and T. R. Jensen, *ChemSusChem*, 2015, **8**, 3472–3482.

278 A. Gradišek, L. H. Jepsen, T. R. Jensen and M. S. Conradi, *J. Phys. Chem. C*, 2016, **120**, 24646–24654.

279 Y. Guo, X. Yu, W. Sun, D. Sun and W. Yang, *Angew. Chem., Int. Ed.*, 2011, **50**, 1087–1091.

280 Y. Guo, Y. Jiang, G. Xia and X. Yu, *Chem. Commun.*, 2012, **48**, 4408–4410.

281 Z. Tang, Y. Tan, H. Wu, Q. Gu, W. Zhou, C. M. Jensen and X. Yu, *Acta Mater.*, 2013, **61**, 4787–4796.

282 Z. Tang, F. Yuan, Q. Gu, Y. Tan, X. Chen, C. M. Jensen and X. Yu, *Acta Mater.*, 2013, **61**, 3110–3119.

283 Q. Gu, L. Gao, Y. Guo, Y. Tan, Z. Tang, K. S. Wallwork, F. Zhang and X. Yu, *Energy Environ. Sci.*, 2012, **5**, 7590–7600.

284 J. Huang, Y. Tan, J. Su, Q. Gu, R. Černý, L. Ouyang, D. Sun, X. Yu and M. Zhu, *Chem. Commun.*, 2015, **51**, 2794–2797.

285 M. B. Ley, L. H. Jepsen, Y. S. Lee, M. Jørgensen, Y. W. Cho and T. R. Jensen, Personal communication, 2017.

286 W. Sun, X. P. Chen, Q. Gu, K. S. Wallwork, Y. Tan, Z. Tang and X. Yu, *Chem. – Eur. J.*, 2012, **18**, 6825–6834.

287 Y. Yang, Y. Liu, H. Wu, W. Zhou, M. Gao and H. Pan, *Phys. Chem. Chem. Phys.*, 2014, **16**, 135–143.

288 Y. Guo, H. Wu, W. Zhou and X. Yu, *J. Am. Chem. Soc.*, 2011, **133**, 4690–4693.

289 G. Xia, Q. Gu, Y. Guo and X. Yu, *J. Mater. Chem.*, 2012, **22**, 7300–7307.

290 E. B. Lobkovskii, A. L. Dorosinskii and K. N. Semenenko, *Zh. Strukt. Khim.*, 1974, **15**, 70–73.

291 F. Yuan, Q. Gu, Y. Guo, W. Sun, X. Chen and X. Yu, *J. Mater. Chem.*, 2012, **22**, 1061–1068.

292 D. B. Ravnsbaek, PhD dissertation, Aarhus University, 2011.

293 I. Olovsson and D. H. Templeton, *Acta Crystallogr.*, 1959, **12**, 832–836.

294 Z. Tang, Y. Tan, X. Chen, L. Ouyang, M. Zhu, D. Sun and X. Yu, *Angew. Chem., Int. Ed.*, 2013, **52**, 12659–12663.

295 X. Zheng, G. Wu, W. Li, Z. Xiong, T. He, J. Guo, H. Chen and P. Chen, *Energy Environ. Sci.*, 2011, **4**, 3593–3600.

296 C. H. Christensen, R. Z. Sørensen, T. Johannessen, U. J. Quaade, K. Honkala, T. D. Elmøe, R. Køhler and J. K. Nørskov, *J. Mater. Chem.*, 2005, **15**, 4106–4108.

297 H. Reardon, J. M. Hanlon, M. Grant, I. Fullbrook and D. H. Gregory, *Crystals*, 2012, **2**, 193–212.

298 L. H. Jepsen, J. Skibsted and T. R. Jensen, *J. Alloys Compd.*, 2013, **580**, S287–S290.

299 Y. Tan, Q. Gu, J. A. Kimpton, Q. Li, X. Chen, L. Ouyang, M. Zhu, D. Sun and X. Yu, *J. Mater. Chem. A*, 2013, **1**, 10155–10165.

300 X. Chen, F. Yuan, Q. Gu and X. Yu, *Dalton Trans.*, 2013, **42**, 14365–14368.
301 J. Luo, H. Wu, W. Zhou, X. Kang, Z. Fang and P. Wang, *Int. J. Hydrogen Energy*, 2012, **37**, 10750–10757.
302 P. Schouwink, F. Morelle, Y. Sadikin, Y. Filinchuk and R. Černý, *Energies*, 2015, **8**, 8286–8299.
303 G. Wolf, J. Baumann, F. Baitalow and F. P. Hoffmann, *Thermochim. Acta*, 2000, **343**, 19–25.
304 F. Baitalow, J. Baumann, G. Wolf, K. Jaenicke-Rößler and G. Leitner, *Thermochim. Acta*, 2002, **391**, 159–168.
305 A. Staubitz, A. P. M. Robertson and I. Manners, *Chem. Rev.*, 2010, **110**, 4079–4124.
306 A. C. Stowe, W. J. Shaw, J. C. Linehan, B. Schmid and T. Autrey, *Phys. Chem. Chem. Phys.*, 2007, **9**, 1831–1836.
307 Y. S. Chua, P. Chen, G. Wu and Z. Xiong, *Chem. Commun.*, 2011, **47**, 5116–5129.
308 H. Wu, W. Zhou and T. Yildirim, *J. Am. Chem. Soc.*, 2008, **130**, 14834–14839.
309 I. Dovgaliuk and Y. Filinchuk, *Int. J. Hydrogen Energy*, 2016, **41**, 15489–15504.
310 R. R. Rietz, A. Zalkin, D. H. Templeton, N. M. Edelstein and L. K. Templeton, *Inorg. Chem.*, 1978, **17**, 653–658.
311 M. Bremer, H. Nöth, M. Thomann and M. Schmidt, *Chem. Ber.*, 1995, **128**, 455–460.
312 F. Jaroschik, F. Bonnet, X.-F. Le Goff, L. Ricard, F. Nief and M. Visseaux, *Dalton Trans.*, 2010, **39**, 6761–6766.
313 S. Marks, J. G. Heck, M. H. Habicht, P. Oña-Burgos, C. Feldmann and P. W. Roesky, *J. Am. Chem. Soc.*, 2012, **134**, 16983–16986.
314 Q. Gu, Z. Wang, Y. Filinchuk, J. A. Kimpton, H. E. A. Brand, Q. Li and X. Yu, *J. Phys. Chem. C*, 2016, **120**, 10192–10198.
315 E. Roedern and T. R. Jensen, *ChemistrySelect*, 2016, **1**, 752–755.
316 L. Mosegaard, B. Møller, J.-E. Jørgensen, U. Bösenberg, M. Dornheim, J. C. Hanson, Y. Cerenius, G. Walker, H. J. Jakobsen, F. Besenbacher and T. R. Jensen, *J. Alloys Compd.*, 2007, **446–447**, 301–305.
317 *HSC Chemistry, Chemistry Software*, Outukumpu, Houston, 6.1 edn, 2006.
318 W. Adamczyk, P. Połczyński, A. Mika, T. Jaroń, Z. Mazej, K. J. Fijalkowski, R. Jurczakowski and W. Grochala, *J. Fluorine Chem.*, 2015, **174**, 22–29.
319 P. Nordlander, J. K. Norskov and F. Besenbacher, *J. Phys. F: Met. Phys.*, 1986, **16**, 1161–1171.
320 J. K. Nørskov and F. Besenbacher, *J. Less-Common Met.*, 1987, **130**, 475–490.
321 T. B. Flanagan and W. A. Oates, in *Hydrogen in Intermetallic Compounds I: Electronic, Thermodynamic, and Crystallographic Properties, Preparation*, ed. L. Schlapbach, Springer Berlin Heidelberg, Berlin, Heidelberg, 1988, pp. 49–85, DOI: 10.1007/3540183337_10.
322 E. H. Kisi, E. Mac, A. Gray and S. J. Kennedy, *J. Alloys Compd.*, 1994, **216**, 123–129.
323 M. Paskevicius, D. A. Sheppard and C. E. Buckley, *J. Am. Chem. Soc.*, 2010, **132**, 5077–5083.
324 D. P. Broom, *Int. J. Hydrogen Energy*, 2007, **32**, 4871–4888.
325 S. J. van der Molen, M. S. Welling and R. Griessen, *Phys. Rev. Lett.*, 2000, **85**, 3882–3885.
326 P. Mauron, F. Buchter, O. Friedrichs, A. Remhof, M. Bielmann, C. N. Zwicky and A. Zuttel, *J. Phys. Chem. B*, 2008, **112**, 906–910.
327 W. D. Davis, L. S. Mason and G. Stegeman, *J. Am. Chem. Soc.*, 1949, **71**, 2775–2781.
328 M. B. Smith and G. E. Bass, *J. Chem. Eng. Data*, 1963, **8**, 342–346.
329 A. Muller, F. Mathey and J. Bensoam, US4193978 A, 1980.
330 N. Ohba, K. Miwa, M. Aoki, T. Noritake, S. Towata, Y. Nakamori, S. Orimo and A. Züttel, *Phys. Rev. B: Condens. Matter Mater. Phys.*, 2006, **74**, 075110.
331 K. Miwa, N. Ohba, S.-I. Towata, Y. Nakamori and S.-I. Orimo, *Phys. Rev. B: Condens. Matter Mater. Phys.*, 2004, **69**, 245120.
332 P. Martelli, R. Caputo, A. Remhof, P. Mauron, A. Borgschulte and A. Züttel, *J. Phys. Chem. C*, 2010, **114**, 7173–7177.
333 H. W. Li, K. Kikuchi, Y. Nakamori, N. Ohba, K. Miwa, S. Towata and S. Orimo, *Acta Mater.*, 2008, **56**, 1342–1347.
334 Y. Yan, H.-W. Li, Y. Nakamori, N. Ohba, K. Miwa, S.-I. Towata and S.-I. Orimo, *Mater. Trans.*, 2008, **49**, 2751–2752.
335 E. R. Pinatel, E. Albanese, B. Civalleri and M. Baricco, *J. Alloys Compd.*, 2015, **645**, S64–S68.
336 M. J. van Setten, G. A. devWijs, M. Fichtner and G. Brocks, *Chem. Mater.*, 2008, **20**, 4952–4956.
337 J. Mao, Z. Guo, C. K. Poh, A. Ranjbar, Y. Guo, X. Yu and H. Liu, *J. Alloys Compd.*, 2010, **500**, 200–205.
338 Y. Kim, D. Reed, Y.-S. Lee, J. Y. Lee, J.-H. Shim, D. Book and Y. W. Cho, *J. Phys. Chem. C*, 2009, **113**, 5865–5871.
339 J. Kostka, W. Lohstroh, M. Fichtner and H. Hahn, *J. Phys. Chem. C*, 2007, **111**, 14026–14029.
340 S. Orimo, N. Nakamori, N. Ohba, K. Miwa, M. Aoki, S. Towata and A. Züttel, *Appl. Phys. Lett.*, 2006, **89**, 021920.
341 Y. Yan, A. Remhof, S.-J. Hwang, H.-W. Li, P. Mauron, S.-I. Orimo and A. Zuttel, *Phys. Chem. Chem. Phys.*, 2012, **14**, 6514–6519.
342 M. P. Pitt, M. Paskevicius, D. H. Brown, D. A. Sheppard and C. E. Buckley, *J. Am. Chem. Soc.*, 2013, **135**, 6930–6941.
343 O. Friedrichs, F. Buchter, A. Borgschulte, A. Remhof, C. N. Zwicky, P. Mauron, M. Bielmann and A. Züttel, *Acta Mater.*, 2008, **56**, 949–954.
344 A. Remhof, O. Friedrichs, F. Buchter, P. Mauron, A. Zuttel and D. Wallacher, *Phys. Chem. Chem. Phys.*, 2008, **10**, 5859–5862.
345 D. S. Stasinevich and G. A. Egorenko, *Russ. J. Inorg. Chem.*, 1968, **13**, 341–343.
346 J. Urgnani, F. J. Torres, M. Palumbo and M. Baricco, *Int. J. Hydrogen Energy*, 2008, **33**, 3111–3115.
347 M. M. Makansi, C. H. Muendel and W. A. Selke, *J. Phys. Chem.*, 1955, **59**, 40–42.
348 K. J. Bowles, *Vapor Pressure of Potassium to 2170 Degrees K*, National Aeronautics and Space Administration, TN D-4535, 1968.
349 D. N. Harries, M. Paskevicius, D. A. Sheppard, T. Price and C. E. Buckley, *Proc. IEEE*, 2012, **100**, 539–549.

 This journal is © The Royal Society of Chemistry 2017

350 M. Fellet, C. E. Buckley, M. Paskevicius and D. A. Sheppard, *MRS Bull.*, 2013, **38**, 1012–1013.

351 D. A. Sheppard, M. Paskevicius, T. D. Humphries, M. Felderhoff, G. Capurso, J. Bellosta von Colbe, M. Dornheim, T. Klassen, P. A. Ward, J. A. Teprovich, C. Corgnale, R. Zidan, D. M. Grant and C. E. Buckley, *Appl. Phys. A: Mater. Sci. Process.*, 2016, **122**, 395.

352 G. L. Soloveichik, Y. Gao, J. Rijssenbeek, M. Andrus, S. Kniajanski, R. C. Bowman Jr, S.-J. Hwang and J.-C. Zhao, *Int. J. Hydrogen Energy*, 2009, **34**, 916–928.

353 R. J. Newhouse, V. Stavila, S.-J. Hwang, L. E. Klebanoff and J. Z. Zhang, *J. Phys. Chem. C*, 2010, **114**, 5224–5232.

354 N. Hanada, K. Chlopek, C. Frommen, W. Lohstroh and M. Fichtner, *J. Mater. Chem.*, 2008, **18**, 2611–2614.

355 J. G. Vitillo, S. Bordiga and M. Baricco, *J. Phys. Chem. C*, 2015, **119**, 25340–25351.

356 Y. Yan, A. Remhof, D. Rentsch and A. Zuttel, *Chem. Commun.*, 2015, **51**, 700–702.

357 M. Chong, A. Karkamkar, T. Autrey, S.-I. Orimo, S. Jalisatgi and C. M. Jensen, *Chem. Commun.*, 2011, **47**, 1330–1332.

358 M. Chong, M. Matsuo, S.-I. Orimo, T. Autrey and C. M. Jensen, *Inorg. Chem.*, 2015, **54**, 4120–4125.

359 C. Pistidda, S. Garroni, F. Dolci, E. G. Bardají, A. Khandelwal, P. Nolis, M. Dornheim, R. Gosalawit, T. Jensen, Y. Cerenius, S. Suriñach, M. D. Baró, W. Lohstroh and M. Fichtner, *J. Alloys Compd.*, 2010, **508**, 212–215.

360 G. Severa, E. Ronnebro and C. M. Jensen, *Chem. Commun.*, 2010, **46**, 421–423.

361 Y. Kim, S.-J. Hwang, Y.-S. Lee, J.-Y. Suh, H. N. Han and Y. W. Cho, *J. Phys. Chem. C*, 2012, **116**, 25715–25720.

362 Y. Yan, A. Remhof, D. Rentsch, A. Zuttel, S. Giri and P. Jena, *Chem. Commun.*, 2015, **51**, 11008–11011.

363 M. D. Riktor, M. H. Sorby, K. Chlopek, M. Fichtner and B. C. Hauback, *J. Mater. Chem.*, 2009, **19**, 2754–2759.

364 Y. Yan, H.-W. Li, T. Sato, N. Umeda, K. Miwa, S.-I. Towata and S.-I. Orimo, *Int. J. Hydrogen Energy*, 2009, **34**, 5732–5736.

365 F. C. Gennari, L. Fernández Albanesi and I. J. Rios, *Inorg. Chim. Acta*, 2009, **362**, 3731–3737.

366 K. N. Semenenko, A. P. Chavgun and V. N. Surov, *Russ. J. Inorg. Chem.*, 1971, **16**, 271–273.

367 E. M. Dematteis, E. Roedern, E. R. Pinatel, M. Corno, T. R. Jensen and M. Baricco, *RSC Adv.*, 2016, **6**, 60101–60108.

368 E. G. Bardaji, Z. Zhao-Karger, N. Boucharat, A. Nale, M. J. van Setten, W. Lohstroh, E. Röhm, M. Catti and M. Fichtner, *J. Phys. Chem. C*, 2011, **115**, 6095–6101.

369 H.-S. Lee, Y.-S. Lee, J.-Y. Suh, M. Kim, J.-S. Yu and Y. W. Cho, *J. Phys. Chem. C*, 2011, **115**, 20027–20035.

370 M. B. Ley, E. Roedern, P. V. Thygesen and T. R. Jensen, *Energies*, 2015, **8**, 2701–2713.

371 J. Y. Lee, D. Ravnsbæk, Y.-S. Lee, Y. Kim, Y. Cerenius, J.-H. Shim, T. R. Jensen, N. H. Hur and Y. W. Cho, *J. Phys. Chem. C*, 2009, **113**, 15080–15086.

372 Z. Łodziana, P. Błoński, Y. Yan, D. Rentsch and A. Remhof, *J. Phys. Chem. C*, 2014, **118**, 6594–6603.

373 V. D'Anna, A. Spyratou, M. Sharma and H. Hagemann, *Spectrochim. Acta, Part A*, 2014, **128**, 902–906.

374 D. Reed and D. Book, *Curr. Opin. Solid State Mater. Sci.*, 2011, **15**, 62–72.

375 S. F. Parker, *Coord. Chem. Rev.*, 2010, **254**, 215–234.

376 M. Mancini, P. Bougeard, R. C. Burns, M. Mlekuz, B. G. Sayer, J. I. A. Thompson and M. J. McGlinchey, *Inorg. Chem.*, 1984, **23**, 1072–1078.

377 V. Stavila, J.-H. Her, W. Zhou, S.-J. Hwang, C. Kim, L. A. M. Ottley and T. J. Udovic, *J. Solid State Chem.*, 2010, **183**, 1133–1140.

378 I. Tiritiris, T. Schleid and K. Müller, *Appl. Magn. Reson.*, 2007, **32**, 459–481.

379 A. Remhof, Y. Yan, D. Rentsch, A. Borgschulte, C. M. Jensen and A. Zuttel, *J. Mater. Chem. A*, 2014, **2**, 7244–7249.

380 R. Černý, G. Severa, D. B. Ravnsbæk, Y. Filinchuk, V. D'Anna, H. Hagemann, D. R. Haase, C. M. Jensen and T. R. Jensen, *J. Phys. Chem. C*, 2009, **114**, 1357–1364.

381 G. N. Boiko, I. M. Yu and N. S. Kirill, *Russ. Chem. Rev.*, 1975, **44**, 1–8.

382 S. Narasimhan and R. Balakumar, *Aldrichimica Acta*, 1998, **31**, 19–26.

383 J. Andrieux, U. B. Demirci, J. Hannauer, C. Gervais, C. Goutaudier and P. Miele, *Int. J. Hydrogen Energy*, 2011, **36**, 224–233.

384 R. Caputo, S. Garroni, D. Olid, F. Teixidor, S. Surinach and M. D. Baro, *Phys. Chem. Chem. Phys.*, 2010, **12**, 15093–15100.

385 Z. P. Li, B. H. Liu, N. Morigasaki and S. Suda, *J. Alloys Compd.*, 2003, **354**, 243–247.

386 A. C. Dunbar, J. A. Macor and G. S. Girolami, *Inorg. Chem.*, 2013, **53**, 822–826.

387 D. F. Gaines, J. L. Walsh, J. H. Morris and D. F. Hillenbrand, *Inorg. Chem.*, 1978, **17**, 1516–1522.

388 T. A. Salupo, *Preparation of ytterbium and europium borides from Yb(II) and Eu(II) boron hydride precursors*, PhD thesis, Ohio State University, 1993.

389 M. Ehemann and H. Nöth, *Z. Anorg. Allg. Chem.*, 1971, **386**, 87–101.

390 T. J. Marks and J. R. Kolb, *Chem. Rev.*, 1977, **77**, 263–293.

391 G. N. Schrauzer, *Naturwissenschaften*, 1955, **42**, 438.

392 Y. Nakamori, K. Miwa, A. Ninomiya, H. Li, N. Ohba, S. Towata, A. Züttel and S. I. Orimo, *Phys. Rev. B: Condens. Matter Mater. Phys.*, 2006, **74**, 045126.

393 P. Błoński and Z. Łodziana, *Phys. Rev. B: Condens. Matter Mater. Phys.*, 2014, **90**, 054114.

394 B. Bogdanović and M. Schwickardi, *J. Alloys Compd.*, 1997, **253–254**, 1–9.

395 P. Chen, Z. Xiong, J. Luo, J. Lin and K. L. Tan, *Nature*, 2002, **420**, 302–304.

396 S. H. Bauer, A. Shepp and R. E. McCoy, *J. Am. Chem. Soc.*, 1953, **75**, 1003–1004.

397 W. I. F. David, J. W. Makepeace, S. K. Callear, H. M. A. Hunter, J. D. Taylor, T. J. Wood and M. O. Jones, *J. Am. Chem. Soc.*, 2014, **136**, 13082–13085.

398 L. H. Jepsen, P. Wang, G. Wu, Z. Xiong, F. Besenbacher, P. Chen and T. R. Jensen, *Phys. Chem. Chem. Phys.*, 2016, **18**, 25257–25264.

399 J. W. Turley and H. W. Rinn, *Inorg. Chem.*, 1969, **8**, 18–22.

400 L. Andrews and X. Wang, *Science*, 2003, **299**, 2049–2052.
401 M. Paskevicius, D. A. Sheppard and C. E. Buckley, *J. Alloys Compd.*, 2009, **487**, 370–376.
402 L. V. Dinh, D. A. Knight, M. Paskevicius, C. E. Buckley and R. Zidan, *Appl. Phys. A: Mater. Sci. Process.*, 2012, **107**, 173–181.
403 A. Remhof, Y. Yan, O. Friedrichs, J. W. Kim, M. Ph, A. Borgschulte, D. Wallacher, A. Buchsteiner, A. Hoser, K. H. Oh, Y. W. Cho and A. Züttel, *J. Phys.: Conf. Ser.*, 2012, **340**, 012111.
404 A. Borgschulte, E. Callini, B. Probst, A. Jain, S. Kato, O. Friedrichs, A. Remhof, M. Bielmann, A. J. Ramirez-Cuesta and A. Züttel, *J. Phys. Chem. C*, 2011, **115**, 17220–17226.
405 O. Friedrichs, A. Remhof, S. J. Hwang and A. Züttel, *Chem. Mater.*, 2010, **22**, 3265–3268.
406 S. H. Bauer, *J. Am. Chem. Soc.*, 1958, **80**, 294–298.
407 R. A. Varin, L. Zbroniec, M. Polanski and J. Bystrzycki, *Energies*, 2011, **4**, 1–25.
408 P. Jena, *J. Phys. Chem. Lett.*, 2011, **2**, 206–211.
409 H.-W. Li, Y. Yan, S.-I. Orimo, A. Züttel and C. M. Jensen, *Energies*, 2011, **4**, 185–214.
410 E. Callini, K.-F. Aguey-Zinsou, R. Ahuja, J. R. Ares, S. Bals, N. Biliškov, S. Chakraborty, G. Charalambopoulou, A.-L. Chaudhary, F. Cuevas, B. Dam, P. de Jongh, M. Dornheim, Y. Filinchuk, J. Grbović Novaković, M. Hirscher, T. R. Jensen, P. B. Jensen, N. Novaković, Q. Lai, F. Leardini, D. M. Gattia, L. Pasquini, T. Steriotis, S. Turner, T. Vegge, A. Züttel and A. Montone, *Int. J. Hydrogen Energy*, 2016, **41**, 14404–14428.
411 M. P. Pitt, M. Paskevicius, C. J. Webb, M. H. Sørby, S. Delleda, T. R. Jensen, B. C. Hauback, C. E. Buckley and E. M. Gray, *Int. J. Hydrogen Energy*, 2011, **36**, 8403–8411.
412 M. P. Pitt, P. E. Vullum, M. H. Sørby, H. Emerich, M. Paskevicius, C. E. Buckley, E. M. Gray, J. C. Walmsley, R. Holmestad and B. C. Hauback, *J. Alloys Compd.*, 2012, **527**, 16–24.
413 M. P. Pitt, P. E. Vullum, M. H. Sørby, H. Emerich, M. Paskevicius, C. E. Buckley, J. C. Walmsley, R. Holmestad and B. C. Hauback, *J. Phys. Chem. C*, 2012, **116**, 14205–14217.
414 A. Andreasen, M. B. Sørensen, R. Burkarl, B. Møller, A. M. Molenbroek, A. S. Pedersen, T. Vegge and T. R. Jensen, *Appl. Phys. A: Mater. Sci. Process.*, 2005, **82**, 515–521.
415 A. Andreasen, M. B. Sørensen, R. Burkarl, B. Møller, A. M. Molenbroek, A. S. Pedersen, J. W. Andreasen, M. M. Nielsen and T. R. Jensen, *J. Alloys Compd.*, 2005, **404–406**, 323–326.
416 L. Pasquini, E. Callini, M. Brighi, F. Boscherini, A. Montone, T. R. Jensen, C. Maurizio, M. Vittori Antisari and E. Bonetti, *J. Nanopart. Res.*, 2011, **13**, 5727–5737.
417 E. Callini, L. Pasquini, L. H. Rude, T. K. Nielsen, T. R. Jensen and E. Bonetti, *J. Appl. Phys.*, 2010, **108**, 073513.
418 E. Callini, L. Pasquini, T. R. Jensen and E. Bonetti, *Int. J. Hydrogen Energy*, 2013, **38**, 12207–12212.
419 M. Polanski, T. K. Nielsen, I. Kunce, M. Norek, T. Płociński, L. R. Jaroszewicz, C. Gundlach, T. R. Jensen and J. Bystrzycki, *Int. J. Hydrogen Energy*, 2013, **38**, 4003–4010.
420 R. A. Varin, Z. Zaranski, T. Czujko, M. Polanski and Z. S. Wronski, *Int. J. Hydrogen Energy*, 2011, **36**, 1177–1183.
421 J. Puszkiel, F. Gennari, P. A. Larochette, F. Karimi, C. Pistidda, R. Gosalawit-Utke, J. Jepsen, T. R. Jensen, C. Gundlach, J. B. von Colbe, T. Klassen and M. Dornheim, *Int. J. Hydrogen Energy*, 2013, **38**, 14618–14630.
422 C. Gosselin, S. Deledda, B. C. Hauback and J. Huot, *J. Alloys Compd.*, 2015, **645**, S304–S307.
423 M. Polanski, T. K. Nielsen, Y. Cerenius, J. Bystrzycki and T. R. Jensen, *Int. J. Hydrogen Energy*, 2010, **35**, 3578–3582.
424 M. Polanski, K. Witek, T. K. Nielsen, L. Jaroszewicz and J. Bystrzycki, *Int. J. Hydrogen Energy*, 2013, **38**, 2785–2789.
425 M. Polanski, J. Bystrzycki, R. A. Varin and T. Plocinski, *Int. J. Hydrogen Energy*, 2011, **36**, 1059–1065.
426 M. P. Pitt, M. Paskevicius, C. J. Webb, D. A. Sheppard, C. E. Buckley and E. M. Gray, *Int. J. Hydrogen Energy*, 2012, **37**, 4227–4237.
427 M. Dornheim, N. Eigen, G. Barkhordarian, T. Klassen and R. Bormann, *Adv. Eng. Mater.*, 2006, **8**, 377–385.
428 M. Dornheim and T. Klassen, in *Encyclopedia of Electrochemical Power Sources*, ed. C. K. Dyer, P. T. Moseley, Z. Ogumi, D. A. J. Rand, B. Scrosati and J. Garche, Elsevier Science, 2013.
429 M. Dornheim, S. Doppiu, G. Barkhordarian, U. Boesenberg, T. Klassen, O. Gutfleisch and R. Bormann, *Scr. Mater.*, 2007, **56**, 841–846.
430 C. J. Webb, *J. Phys. Chem. Solids*, 2015, **84**, 96–106.
431 J.-C. Crivello, B. Dam, R. V. Denys, M. Dornheim, D. M. Grant, J. Huot, T. R. Jensen, P. Jongh, M. Latroche, C. Milanese, D. Milčius, G. S. Walker, C. J. Webb, C. Zlotea and V. A. Yartys, *Appl. Phys. A: Mater. Sci. Process.*, 2016, **122**, 97.
432 J.-C. Crivello, R. V. Denys, M. Dornheim, M. Felderhoff, D. M. Grant, J. Huot, T. R. Jensen, P. Jongh, M. Latroche, G. S. Walker, C. J. Webb and V. A. Yartys, *Appl. Phys. A: Mater. Sci. Process.*, 2016, **122**, 85.
433 M. C. S. Escaño, E. Gyenge, R. L. Arevalo and H. Kasai, *J. Phys. Chem. C*, 2011, **115**, 19883–19889.
434 J. Yang, A. Sudik and C. Wolverton, *J. Phys. Chem. C*, 2007, **111**, 19134–19140.
435 F. Pendolino, P. Mauron, A. Borgschulte and A. Züttel, *J. Phys. Chem. C*, 2009, **113**, 17231–17234.
436 F. Pendolino, *J. Phys. Chem. C*, 2012, **116**, 1390–1394.
437 P. A. Berseth, A. G. Harter, R. Zidan, A. Blomqvist, C. M. Araújo, R. H. Scheicher, R. Ahuja and P. Jena, *Nano Lett.*, 2009, **9**, 1501–1505.
438 S. V. Alapati, J. K. Johnson and D. S. Sholl, *Phys. Chem. Chem. Phys.*, 2007, **9**, 1438–1452.
439 X. B. Yu, Z. Wu, Q. R. Chen, Z. L. Li, B. C. Weng and T. S. Huang, *Appl. Phys. Lett.*, 2007, **90**, 034106.
440 M. Paskevicius, B. Richter, M. Polanski, S. P. Thompson and T. R. Jensen, *Dalton Trans.*, 2016, **45**, 639–645.
441 D. A. Sheppard, L. H. Jepsen, T. R. Jensen, M. Paskevicius and C. E. Buckley, *J. Mater. Chem. A*, 2013, **1**, 12775–12781.
442 D. J. Siegel, C. Wolverton and V. Ozoliņš, *Phys. Rev. B: Condens. Matter Mater. Phys.*, 2007, **76**, 134102.
443 I. Saldan, C. Frommen, I. Llamas-Jansa, G. N. Kalantzopoulos, S. Hino, B. Arstad, R. H. Heyn, O. Zavorotynska, S. Deledda,

 This journal is © The Royal Society of Chemistry 2017

M. H. Sørby, H. Fjellvåg and B. C. Hauback, *Int. J. Hydrogen Energy*, 2015, **40**, 12286–12293.
444 X. B. Yu, D. M. Grant and G. S. Walker, *J. Phys. Chem. C*, 2008, **112**, 11059–11062.
445 M. Au, W. Spencer, A. Jurgensen and C. Zeigler, *J. Alloys Compd.*, 2008, **462**, 303–309.
446 X. B. Yu, D. M. Grant and G. S. Walker, *J. Phys. Chem. C*, 2009, **113**, 17945–17949.
447 I. Saldan, S. Hino, T. D. Humphries, O. Zavorotynska, M. Chong, C. M. Jensen, S. Deledda and B. C. Hauback, *J. Phys. Chem. C*, 2014, **118**, 23376–23384.
448 Y. H. Guo, X. B. Yu, L. Gao, G. L. Xia, Z. P. Guo and H. K. Liu, *Energy Environ. Sci.*, 2010, **3**, 464–469.
449 M. Au and A. Jurgensen, *J. Phys. Chem. B*, 2006, **110**, 7062–7067.
450 M. Au, A. Jurgensen and K. Zeigler, *J. Phys. Chem. B*, 2006, **110**, 26482–26487.
451 H.-W. Li, D. Matsumura, Y. Nishihata, E. Akiba and S.-I. Orimo, *J. Jpn. Inst. Met. Mater.*, 2013, **77**, 627–630.
452 B. R. S. Hansen, D. B. Ravnsbæk, D. Reed, D. Book, C. Gundlach, J. Skibsted and T. R. Jensen, *J. Phys. Chem. C*, 2013, **117**, 7423–7432.
453 U. Bösenberg, J. W. Kim, D. Gosslar, N. Eigen, T. R. Jensen, J. M. Bellosta von Colbe, Y. Zhou, M. Dahms, D. H. Kim, R. Günther, Y. W. Cho, K. H. Oh, T. Klassen, R. Bormann and M. Dornheim, *Acta Mater.*, 2010, **58**, 3381–3389.
454 O. Zavorotynska, I. Saldan, S. Hino, T. D. Humphries, S. Deledda and B. C. Hauback, *J. Mater. Chem. A*, 2015, **3**, 6592–6602.
455 U. Bösenberg, U. Vainio, P. K. Pranzas, J. M. Bellosta von Colbe, G. Goerigk, E. Welter, M. Dornheim, A. Schreyer and R. Bormann, *Nanotechnology*, 2009, **20**, 204003.
456 Z. Xiong, G. Wu, J. Hu and P. Chen, *Adv. Mater.*, 2004, **16**, 1522–1525.
457 G. Barkhordarian, T. Klassen and R. Bormann, *Int. Pat.* WO2006063627, 2006.
458 T. D. Humphries, G. N. Kalantzopoulos, I. Llamas-Jansa, J. E. Olsen and B. C. Hauback, *J. Phys. Chem. C*, 2013, **117**, 6060–6065.
459 S. Garroni, C. Pistidda, M. Brunelli, G. B. M. Vaughan, S. Surinach and M. D. Baro, *Scr. Mater.*, 2009, **60**, 1129–1132.
460 C. Pistidda, G. Barkhordarian, A. Rzeszutek, S. Garroni, C. B. Minella, M. D. Baró, P. Nolis, R. Bormann, T. Klassen and M. Dornheim, *Scr. Mater.*, 2011, **64**, 1035–1038.
461 C. Milanese, S. Garroni, A. Girella, G. Mulas, V. Berbenni, G. Bruni, S. Suriñach, M. D. Baró and A. Marini, *J. Phys. Chem. C*, 2011, **115**, 3151–3162.
462 S. Kato, A. Borgschulte, M. Bielmann and A. Zuttel, *Phys. Chem. Chem. Phys.*, 2012, **14**, 8360–8368.
463 F. Karimi, P. Klaus Pranzas, C. Pistidda, J. A. Puszkiel, C. Milanese, U. Vainio, M. Paskevicius, T. Emmler, A. Santoru, R. Utke, M. Tolkiehn, C. B. Minella, A.-L. Chaudhary, S. Boerries, C. E. Buckley, S. Enzo, A. Schreyer, T. Klassen and M. Dornheim, *Phys. Chem. Chem. Phys.*, 2015, **17**, 27328–27342.
464 K. T. Møller, A. S. Fogh, M. Paskevicius, J. Skibsted and T. R. Jensen, *Phys. Chem. Chem. Phys.*, 2016, **18**, 27545–27553.
465 B. R. S. Hansen, D. B. Ravnsbaek, J. Skibsted and T. R. Jensen, *Phys. Chem. Chem. Phys.*, 2014, **16**, 8970–8980.
466 P. de la Mora, M. Castro and G. Tavizon, *J. Solid State Chem.*, 2002, **169**, 168–175.
467 U. Bösenberg, D. B. Ravnsbæk, H. Hagemann, V. D'Anna, C. B. Minella, C. Pistidda, W. van Beek, T. R. Jensen, R. Bormann and M. Dornheim, *J. Phys. Chem. C*, 2010, **114**, 15212–15217.
468 J.-H. Shim, J.-H. Lim, S.-U. Rather, Y.-S. Lee, D. Reed, Y. Kim, D. Book and Y. W. Cho, *J. Phys. Chem. Lett.*, 2010, **1**, 59–63.
469 F. Cova, E. C. E. Rönnebro, Y. J. Choi, F. C. Gennari and P. A. Larochette, *J. Phys. Chem. C*, 2015, **119**, 15816–15822.
470 T. E. C. Price, D. M. Grant, D. Weston, T. Hansen, L. M. Arnbjerg, D. B. Ravnsbæk, T. R. Jensen and G. S. Walker, *J. Am. Chem. Soc.*, 2011, **133**, 13534–13538.
471 O. Friedrichs, J. W. Kim, A. Remhof, F. Buchter, A. Borgschulte, D. Wallacher, Y. W. Cho, M. Fichtner, K. H. Oh and A. Zuttel, *Phys. Chem. Chem. Phys.*, 2009, **11**, 1515–1520.
472 X. B. Yu, D. M. Grant and G. S. Walker, *Chem. Commun.*, 2006, 3906–3908.
473 E. Deprez, M. A. Muñoz-Márquez, M. A. Roldán, C. Prestipino, F. J. Palomares, C. B. Minella, U. Bösenberg, M. Dornheim, R. Bormann and A. Fernández, *J. Phys. Chem. C*, 2010, **114**, 3309–3317.
474 J. Hu, R. Witter, H. Shao, M. Felderhoff and M. Fichtner, *J. Mater. Chem. A*, 2014, **2**, 66–72.
475 C. Pistidda, S. Garroni, C. B. Minella, F. Dolci, T. R. Jensen, P. Nolis, U. Bösenberg, Y. Cerenius, W. Lohstroh, M. Fichtner, M. D. Baró, R. Bormann and M. Dornheim, *J. Phys. Chem. C*, 2010, **114**, 21816–21823.
476 D. Pottmaier, C. Pistidda, E. Groppo, S. Bordiga, G. Spoto, M. Dornheim and M. Baricco, *Int. J. Hydrogen Energy*, 2011, **36**, 7891–7896.
477 G. Barkhordarian, T. R. Jensen, S. Doppiu, U. Bösenberg, A. Borgschulte, R. Gremaud, Y. Cerenius, M. Dornheim, T. Klassen and R. Bormann, *J. Phys. Chem. C*, 2008, **112**, 2743–2749.
478 Y. Kim, D. Reed, Y.-S. Lee, J.-H. Shim, H. N. Han, D. Book and Y. W. Cho, *J. Alloys Compd.*, 2010, **492**, 597–600.
479 M. Gonzalez-Silveira, R. Gremaud, H. Schreuders, M. J. V. Setten, E. Batyrev, A. Rougier, L. Dupont, E. G. Bardají, W. Lohstroh and B. Dam, *J. Phys. Chem. C*, 2010, **114**, 13895–13901.
480 X.-D. Kang, P. Wang, L.-P. Ma and H.-M. Cheng, *Appl. Phys. A: Mater. Sci. Process.*, 2007, **89**, 963–966.
481 S. A. Jin, J. H. Shim, Y. W. Cho, K. W. Yi, O. Zabara and M. Fichtner, *Scr. Mater.*, 2008, **58**, 963–965.
482 Y. Zhang, Q. Tian, J. Zhang, S.-S. Liu and L.-X. Sun, *J. Phys. Chem. C*, 2009, **113**, 18424–18430.
483 A. Remhof, O. Friedrichs, F. Buchter, P. Mauron, J. W. Kim, K. H. Oh, A. Buchsteiner, D. Wallacher and A. Züttel, *J. Alloys Compd.*, 2009, **484**, 654–659.

484 D. B. Ravnsbæk and T. R. Jensen, *J. Phys. Chem. Solids*, 2010, **71**, 1144–1149.
485 D. B. Ravnsbæk and T. R. Jensen, *J. Appl. Phys.*, 2012, **111**, 112621.
486 M. J. van Setten and M. Fichtner, *J. Alloys Compd.*, 2009, **477**, L11–L12.
487 Q. Shi, X. Yu, R. Feidenhans'l and T. Vegge, *J. Phys. Chem. C*, 2008, **112**, 18244–18248.
488 R. Liu, D. Reed and D. Book, *J. Alloys Compd.*, 2012, **515**, 32–38.
489 E. Roedern and T. R. Jensen, *J. Phys. Chem. C*, 2014, **118**, 23567–23574.
490 J. J. Vajo, W. Li and P. Liu, *Chem. Commun.*, 2010, **46**, 6687–6689.
491 K. Yvon and G. Renaudin, in *Encyclopedia of Inorganic-Chemistry*, ed. R. B. King, John Wiley & Sons, Ltd, 2006, DOI: 10.1002/0470862106.ia087.
492 M. Norek, T. K. Nielsen, M. Polanski, I. Kunce, T. Płociński, L. R. Jaroszewicz, Y. Cerenius, T. R. Jensen and J. Bystrzycki, *Int. J. Hydrogen Energy*, 2011, **36**, 10760–10770.
493 M. R. Ghaani, M. Catti and A. Nale, *J. Phys. Chem. C*, 2012, **116**, 26694–26699.
494 K.-B. Kim, J.-H. Shim, Y. W. Cho and K. H. Oh, *Chem. Commun.*, 2011, **47**, 9831–9833.
495 F. C. Gennari, *Int. J. Hydrogen Energy*, 2011, **36**, 15231–15238.
496 P. Mauron, M. Bielmann, A. Remhof, A. Züttel, J.-H. Shim and Y. W. Cho, *J. Phys. Chem. C*, 2010, **114**, 16801–16805.
497 M. B. Ley, M. Meggouh, R. Moury, K. Peinecke and M. Felderhoff, *Materials*, 2015, **8**, 5891–5921.
498 S. C. Amendola, S. L. Sharp-Goldman, M. S. Janjua, N. C. Spencer, M. T. Kelly, P. J. Petillo and M. Binder, *Int. J. Hydrogen Energy*, 2000, **25**, 969–975.
499 J.-H. Wee, *J. Power Sources*, 2006, **155**, 329–339.
500 H. C. Brown and C. A. Brown, *J. Am. Chem. Soc.*, 1962, **84**, 1493–1494.
501 Y. Shang and R. Chen, *Energy Fuels*, 2006, **20**, 2142–2148.
502 C.-j. Liu, U. Burghaus, F. Besenbacher and Z. L. Wang, *ACS Nano*, 2010, **4**, 5517–5526.
503 V. Berube, G. Chen and M. S. Dresselhaus, *Int. J. Hydrogen Energy*, 2008, **33**, 4122–4131.
504 S. Cheung, W. Q. Deng, A. C. T. van Duin and W. A. Goddard, *J. Phys. Chem. A*, 2005, **109**, 851–859.
505 J. J. Liang, *Appl. Phys. A: Mater. Sci. Process.*, 2005, **80**, 173–178.
506 R. W. P. Wagemans, J. H. van Lenthe, P. E. de Jongh, A. J. van Dillen and K. P. de Jong, *J. Am. Chem. Soc.*, 2005, **127**, 16675–16680.
507 X. Yao and G. Lu, *Chin. Sci. Bull.*, 2008, **53**, 2421–2431.
508 V. Bérubé, G. Radtke, M. Dresselhaus and G. Chen, *Int. J. Energy Res.*, 2007, **31**, 637–663.
509 C. Weidenthaler, *Nanoscale*, 2011, **3**, 792–810.
510 S. Cahen, J. B. Eymery, R. Janot and J. M. Tarascon, *J. Power Sources*, 2009, **189**, 902–908.
511 T. K. Nielsen, F. Besenbacher and T. R. Jensen, *Nanoscale*, 2011, **3**, 2086–2098.
512 F. E. Pinkerton, *J. Alloys Compd.*, 2011, **509**, 8958–8964.
513 J. J. Vajo, *Curr. Opin. Solid State Mater. Sci.*, 2011, **15**, 52–61.
514 M. Fichtner, *Nanotechnology*, 2009, **20**, 204009.
515 P. E. de Jongh and P. Adelhelm, *ChemSusChem*, 2010, **3**, 1332–1348.
516 P. Ngene, P. Adelhelm, A. M. Beale, K. P. de Jong and P. E. de Jongh, *J. Phys. Chem. C*, 2010, **114**, 6163–6168.
517 S. Zhang, A. F. Gross, S. L. Van Atta, M. Lopez, P. Liu, C. C. Ahn, J. J. Vajo and C. M. Jensen, *Nanotechnology*, 2009, **20**, 204027.
518 Z. Zhao-Karger, J. Hu, A. Roth, D. Wang, C. Kübel, W. Lohstroh and M. Fichtner, *Chem. Commun.*, 2010, **46**, 8353–8355.
519 R. Bogerd, P. Adelhelm, J. H. Meeldijk, K. P. de Jong and P. E. de Jongh, *Nanotechnology*, 2009, **20**, 204019.
520 X. Liu, D. Peaslee, C. Z. Jost, T. F. Baumann and E. H. Majzoub, *Chem. Mater.*, 2011, **23**, 1331–1336.
521 P. Ngene, R. van den Berg, M. H. W. Verkuijlen, K. P. de Jong and P. E. de Jongh, *Energy Environ. Sci.*, 2011, **4**, 4108–4115.
522 M. L. Christian and K.-F. Aguey-Zinsou, *ACS Nano*, 2012, **6**, 7739–7751.
523 Y. Yan, Y. S. Au, D. Rentsch, A. Remhof, P. E. de Jongh and A. Zuttel, *J. Mater. Chem. A*, 2013, **1**, 11177–11183.
524 M. A. Wahab, Y. Jia, D. Yang, H. Zhao and X. Yao, *J. Mater. Chem. A*, 2013, **1**, 3471–3478.
525 S. Sartori, K. D. Knudsen, F. S. Hage, R. H. Heyn, E. G. Bardaji, Z. Zhao-Karger, M. Fichtner and B. C. Hauback, *Nanotechnology*, 2012, **23**, 255704.
526 A. Ampoumogli, G. Charalambopoulou, P. Javadian, B. Richter, T. R. Jensen and T. Steriotis, *J. Alloys Compd.*, 2015, **645**, S480–S484.
527 P. Javadian, D. A. Sheppard, C. E. Buckley and T. R. Jensen, *Nano Energy*, 2015, **11**, 96–103.
528 Y. Yan, A. Remhof, P. Mauron, D. Rentsch, Z. Łodziana, Y.-S. Lee, H.-S. Lee, Y. W. Cho and A. Züttel, *J. Phys. Chem. C*, 2013, **117**, 8878–8886.
529 T. K. Nielsen, U. Bösenberg, R. Gosalawit, M. Dornheim, Y. Cerenius, F. Besenbacher and T. R. Jensen, *ACS Nano*, 2010, **4**, 3903–3908.
530 R. Gosalawit-Utke, C. Milanese, T. K. Nielsen, F. Karimi, I. Saldan, K. Pranzas, T. R. Jensen, A. Marini, T. Klassen and M. Dornheim, *Int. J. Hydrogen Energy*, 2013, **38**, 1932–1942.
531 R. Gosalawit−Utke, T. K. Nielsen, K. Pranzas, I. Saldan, C. Pistidda, F. Karimi, D. Laipple, J. Skibsted, T. R. Jensen, T. Klassen and M. Dornheim, *J. Phys. Chem. C*, 2011, **116**, 1526–1534.
532 G. Xia, Y. Tan, F. Wu, F. Fang, D. Sun, Z. Guo, Z. Huang and X. Yu, *Nano Energy*, 2016, **26**, 488–495.
533 R. Gosalawit-Utke, C. Milanese, P. Javadian, J. Jepsen, D. Laipple, F. Karmi, J. Puszkiel, T. R. Jensen, A. Marini, T. Klassen and M. Dornheim, *Int. J. Hydrogen Energy*, 2013, **38**, 3275–3282.
534 R. Gosalawit-Utke, C. Milanese, P. Javadian, A. Girella, D. Laipple, J. Puszkiel, A. S. Cattaneo, C. Ferrara, J. Wittayakhun, J. Skibsted, T. R. Jensen, A. Marini,

 This journal is © The Royal Society of Chemistry 2017

T. Klassen and M. Dornheim, *J. Alloys Compd.*, 2014, **599**, 78–86.
535 R. Utke, S. Thiangviriya, P. Javadian, T. R. Jensen, C. Milanese, T. Klassen and M. Dornheim, *Mater. Chem. Phys.*, 2016, **169**, 136–141.
536 S. Thiangviriya, P. Plerdsranoy, N. Wiset, P. Javadian, T. R. Jensen and R. Utke, *J. Alloys Compd.*, 2015, **633**, 484–493.
537 P. Javadian, C. Zlotea, C. M. Ghimbeu, M. Latroche and T. R. Jensen, *J. Phys. Chem. C*, 2015, **119**, 5819–5826.
538 P. Javadian, D. A. Sheppard, C. E. Buckley and T. R. Jensen, *Int. J. Hydrogen Energy*, 2015, **40**, 14916–14924.
539 B. Schmitz, U. Müller, N. Trukhan, M. Schubert, G. Férey and M. Hirscher, *ChemPhysChem*, 2008, **9**, 2181–2184.
540 A. Phan, C. J. Doonan, F. J. Uribe-Romo, C. B. Knobler, M. O'Keeffe and O. M. Yaghi, *Acc. Chem. Res.*, 2010, **43**, 58–67.
541 Y. Oumellal, A. Rougier, G. A. Nazri, J. M. Tarascon and L. Aymard, *Nat. Mater.*, 2008, **7**, 916–921.
542 V. Yartys, D. Noreus and M. Latroche, *Appl. Phys. A: Mater. Sci. Process.*, 2016, **122**, 43.
543 S. Sartori, F. Cuevas and M. Latroche, *Appl. Phys. A: Mater. Sci. Process.*, 2016, **122**, 135.
544 T. H. Mason, X. Liu, J. Hong, J. Graetz and E. H. Majzoub, *J. Phys. Chem. C*, 2011, **115**, 16681–16687.
545 M. Matsuo, Y. Nakamori, S.-I. Orimo, H. Maekawa and H. Takamura, *Appl. Phys. Lett.*, 2007, **91**, 224103.
546 T. J. Udovic, M. Matsuo, A. Unemoto, N. Verdal, V. Stavila, A. V. Skripov, J. J. Rush, H. Takamura and S.-I. Orimo, *Chem. Commun.*, 2014, **50**, 3750–3752.
547 L. He, H.-W. Li, H. Nakajima, N. Tumanov, Y. Filinchuk, S.-J. Hwang, M. Sharma, H. Hagemann and E. Akiba, *Chem. Mater.*, 2015, **27**, 5483–5486.
548 N. Kamaya, K. Homma, Y. Yamakawa, M. Hirayama, R. Kanno, M. Yonemura, T. Kamiyama, Y. Kato, S. Hama, K. Kawamoto and A. Mitsui, *Nat. Mater.*, 2011, **10**, 682–686.
549 W. S. Tang, A. Unemoto, W. Zhou, V. Stavila, M. Matsuo, H. Wu, S.-I. Orimo and T. J. Udovic, *Energy Environ. Sci.*, 2015, **8**, 3637–3645.
550 H. Maekawa, M. Matsuo, H. Takamura, M. Ando, Y. Noda, T. Karahashi and S.-I. Orimo, *J. Am. Chem. Soc.*, 2009, **131**, 894–895.
551 H. Oguchi, M. Matsuo, J. S. Hummelshøj, T. Vegge, J. K. Nørskov, T. Sato, Y. Miura, H. Takamura, H. Maekawa and S. Orimo, *Appl. Phys. Lett.*, 2009, **94**, 141912.
552 B. A. Boukamp and R. A. Huggins, *Phys. Lett. A*, 1979, **72**, 464–466.
553 M. Matsuo, S. Kuromoto, T. Sato, H. Oguchi, H. Takamura and S.-I. Orimo, *Appl. Phys. Lett.*, 2012, **100**, 203904.
554 V. Thangadurai, D. Pinzaru, S. Narayanan and A. K. Baral, *J. Phys. Chem. Lett.*, 2015, **6**, 292–299.
555 T. J. Udovic, M. Matsuo, W. S. Tang, H. Wu, V. Stavila, A. V. Soloninin, R. V. Skoryunov, O. A. Babanova, A. V. Skripov, J. J. Rush, A. Unemoto, H. Takamura and S.-I. Orimo, *Adv. Mater.*, 2014, **26**, 7622–7626.
556 M. Jansen, *Angew. Chem., Int. Ed.*, 1991, **30**, 1547–1558.
557 P. Martelli, A. Remhof, A. Borgschulte, R. Ackermann, T. Strässle, J. P. Embs, M. Ernst, M. Matsuo, S.-I. Orimo and A. Züttel, *J. Phys. Chem. A*, 2011, **115**, 5329–5334.
558 N. Verdal, T. J. Udovic, J. J. Rush, H. Wu and A. V. Skripov, *J. Phys. Chem. C*, 2013, **117**, 12010–12018.
559 A. V. Skripov, A. V. Soloninin, M. B. Ley, T. R. Jensen and Y. Filinchuk, *J. Phys. Chem. C*, 2013, **117**, 14965–14972.
560 A. V. Skripov, O. A. Babanova, A. V. Soloninin, V. Stavila, N. Verdal, T. J. Udovic and J. J. Rush, *J. Phys. Chem. C*, 2013, **117**, 25961–25968.
561 N. Verdal, T. J. Udovic, V. Stavila, W. S. Tang, J. J. Rush and A. V. Skripov, *J. Phys. Chem. C*, 2014, **118**, 17483–17489.
562 M. Paskevicius, B. R. S. Hansen, M. Jørgensen, B. Richter and T. R. Jensen, *Nat. Commun.*, 2017, accepted.
563 M. Paskevicius, M. P. Pitt, D. H. Brown, D. A. Sheppard, S. Chumphongphan and C. E. Buckley, *Phys. Chem. Chem. Phys.*, 2013, **15**, 15825–15828.
564 N. Verdal, J.-H. Her, V. Stavila, A. V. Soloninin, O. A. Babanova, A. V. Skripov, T. J. Udovic and J. J. Rush, *J. Solid State Chem.*, 2014, **212**, 81–91.
565 N. Verdal, H. Wu, T. J. Udovic, V. Stavila, W. Zhou and J. J. Rush, *J. Solid State Chem.*, 2011, **184**, 3110–3116.
566 N. Verdal, M. R. Hartman, T. Jenkins, D. J. DeVries, J. J. Rush and T. J. Udovic, *J. Phys. Chem. C*, 2010, **114**, 10027–10033.
567 V. V. Volkov, M. Khikmatov, U. Mirsaidov, S. P. Gabuda and S. G. Kozlova, *J. Struct. Chem.*, 1988, **29**, 58–61.
568 D. J. Huettner, J. L. Ragle, L. Sherk, T. R. Stengle and H. J. C. Yeh, *J. Chem. Phys.*, 1968, **48**, 1739–1744.
569 E. C. Reynhardt and J. A. J. Lourens, *J. Phys. C: Solid State Phys.*, 1980, **13**, 2765–2779.
570 E. C. Reynhardt and J. A. J. Lourens, *J. Chem. Phys.*, 1984, **80**, 6240–6244.
571 N. Verdal, T. J. Udovic, W. Zhou, J. J. Rush, D. J. De Vries and M. R. Hartman, *J. Phys. Chem. C*, 2013, **117**, 876–883.
572 H. Wu, W. S. Tang, V. Stavila, W. Zhou, J. J. Rush and T. J. Udovic, *J. Phys. Chem. C*, 2015, **119**, 6481–6487.
573 N. Kunkel, H. Kohlmann, A. Sayede and M. Springborg, *Inorg. Chem.*, 2011, **50**, 5873–5875.
574 N. Kunkel, A. Meijerink, M. Springborg and H. Kohlmann, *J. Mater. Chem. C*, 2014, **2**, 4799–4804.
575 B. Daudin, R. Lagnier and B. Salce, *J. Magn. Magn. Mater.*, 1982, **27**, 315–322.
576 A. M. Tishin and Y. I. Spichkin, *The Magnetocaloric Effect and its Applications*, Institute of Physics, Bristol, 2003.
577 J.-L. Liu, Y.-C. Chen, F.-S. Guo and M.-L. Tong, *Coord. Chem. Rev.*, 2014, **281**, 26–49.
578 B. Sundqvist and O. Andersson, *Phys. Rev. B: Condens. Matter Mater. Phys.*, 2006, **73**, 092102.
579 B. Sundqvist and O. Andersson, *Int. J. Thermophys.*, 2009, **30**, 1118–1129.
580 T. Hayashi, K. Tobita, Y. Nakamori and S. Orimo, *J. Nucl. Mater.*, 2009, **386–388**, 119–121.
581 H. I. Schlesinger, H. C. Brown, A. E. Finholt, J. R. Gilbreath, H. R. Hoekstra and E. K. Hyde, *J. Am. Chem. Soc.*, 1953, **75**, 215–219.

582 J. Ma, N. A. Choudhury and Y. Sahai, *Renewable Sustainable Energy Rev.*, 2010, **14**, 183–199.
583 A. S. Tayi, A. Kaeser, M. Matsumoto, T. Aida and S. I. Stupp, *Nat. Chem.*, 2015, **7**, 281–294.
584 J. Echeverría, G. Aullón, D. Danovich, S. Shaik and S. Alvarez, *Nat. Chem.*, 2011, **3**, 323–330.
585 I. Dovgaliuk, H. Hagemann, T. Leyssens, M. Devillers and Y. Filinchuk, *Int. J. Hydrogen Energy*, 2014, **39**, 19603–19608.
586 J. G. Vitillo, E. Groppo, E. G. Bardaji, M. Baricco and S. Bordiga, *Phys. Chem. Chem. Phys.*, 2014, **16**, 22482–22486.
587 C. V. Picasso, D. A. Safin, I. Dovgaliuk, F. Devred, D. Debecker, H.-W. Li, J. Proost and Y. Filinchuk, *Int. J. Hydrogen Energy*, 2016, **41**, 14377–14386.
588 S. Pylypko, E. Petit, P. G. Yot, F. Salles, M. Cretin, P. Miele and U. B. Demirci, *Inorg. Chem.*, 2015, **54**, 4574–4583.

 This journal is © The Royal Society of Chemistry 2017